Effect of metal oxide nano-particles on the properties and degradation behaviour of polycarbonate and poly(methyl methacrylate)

by

TSHWAFO ELIAS MOTAUNG (M.Sc.)

Submitted in accordance with the requirements for the degree of

Philosophiae Doctor (Ph.D.) in Polymer Science

Department of Chemistry

Faculty of Natural and Agricultural Sciences

at the

UNIVERSITY OF THE FREE STATE (QWAQWA CAMPUS)

SUPERVISOR: PROF A.S. LUYT

October 2012

DECLARATION

I declare that the dissertation hereby submitted by me for the degree Philosophiae Doctor at the University of the Free State is my own independent work and has not previously been submitted by me at another university/faculty. I furthermore cede copyright of the dissertation in favour of the University of the Free State.

_____ _____

Motaung T.E. (Mr) Luyt A.S. (Prof)

DEDICATIONS

To my late father John Letsatsi Motaung and my constantly supporting mother Madinkeng Motaung. Special dedication to my grandmother, Makilibone Motaung, who has recently celebrated her 93rd birthday. This Ph.D. is for you. I love all of you forever.

To my sister Dinkeng Motaung. I really do not have the words that will express my appreciation for all sacrifices you have made to keep the family going during the hard times. I love you.

To my brothers and sisters Modiehi, Mathasi, Khauhelo (and his son Katleho), Thato and Tumi. Thank you for your love and support. You are my world. I love you all.

To my nephews and nieces. You are so special to me and life is so enjoyable around you.

ACKNOWLEDGEMENTS

First of all I would like to thank God who gave me strength, blessing, and courage during this study and during all of my life.

I would like to express my deepest and profound gratitude to my supervisor, Prof. Adriaan Stephanus Luyt, for his guidance, encouragement, and endless support during my Ph.D. study. I learned a lot throughout your supervision. I really feel that words will not express my appreciation to whatever you have done for me.

A big thank you to Dr Maria Luisa Saladino for a very fruitful collaboration. I learned a lot from our discussions during my visits to Palermo.

I would also like to thank:

- ♥ The colleagues in Prof. Massimo Messori's research group (Maria Elena Darecchio, Davide Morselli, Federica Bondioli and Paola Fabbri) at the University of Modena and Reggio Emilia, Italy.
- ♥ The colleagues in Prof. Eugenio Caponetti's research group (Alberto Spinella and Giorgio Nasillo) at the Università degli Studi di Palermo, Italy.
- ♥ All my former and present colleagues in Prof. Luyt's research group (Mr. Mfiso Mngomezulu, Mr. Thabang Mokhothu, Mr. Sibusiso Ndlovu, Mr. Mokgaotsa Mochane, Mr. Teboho Mokhena, Dr Stephen Ochigbo, Miss Motshabi Sibeko,Dr Spirit Molefi, Mr. Teboho Motsoeneng, Dr. Nagi Greesh, Mr. Tankiso Mokoena, Ms. Cheryl-Ann Clarke, Dr. He Wei, Mr. Bongane Msibi, Mr. Lucky Dlamini, Ms. Nomadlosi Nhlapo, Mr. Tladi Mofokeng, Mrs. Moipone Malimabe, Dr. Essa Ahmad, Mr. Lulu Mohomane, Mr. Tsietsi Tsotetsi, Mrs. Doreen Mosiangaoko, Mr. Shale Sefadi, Ntate Moji).
- ♥ Julia Puseletso Mofokeng for her help, support, and kindness (Julita thank you).
- ♥ Mrs. Marlize Jackson for her kind support.
- ♥ Universitá di Palermo funded by P.O.R. Sicilia and MIUR for supporting this research through the COOPERLINK 2009 Prot. CII098ZQLT "Sintesie caratterizzazione di

compositi polimetilmetacrilato e nano-TiO_2/-ZrO_2", as well as the National Research Foundation in South Africa and the University of the Free State.

♥ All my brothers, friends and colleagues in the Faculty of Natural and Agricultural Sciences.

ABSTRACT

Melt compounding was used to prepare polycarbonate (PC) and poly(methyl methacrylate) (PMMA) nanocomposites with different amounts of metal-oxide fillers (silica, zirconia and titania). Zirconia and two types of titania were prepared by a sol-gel method, whereas a commercial hydrophobic silica having chemically surface bonded methyl groups was used. Titania nanoparticles were annealed at 200 and 600 °C to obtain the anatase and rutile phases, respectively. The effect of filler amount, in the range 1-5 wt.%, on the morphology, mechanical properties and thermal degradation kinetics was investigated by means of transmission electron microscopy (TEM), X-ray diffractometry (XRD), small-angle X-ray scattering (SAXS), dynamic mechanical analysis (DMA), thermogravimetric analyses (TGA), Fourier-transform infrared spectroscopy (FTIR), ^{13}C cross-polarization magic-angle spinning nuclear magnetic resonance spectroscopy ($^{13}C\{^{1}H\}$CP-MAS NMR) and measures of proton spin-lattice relaxation time in the rotating frame ($T_{1\rho}(H)$), in the laboratory frame ($T_1(H)$) and cross polarization times (T_{CH}).

Results showed that the nanoparticles were well dispersed in the polymers whose structure remained amorphous, except for zirconia in a PC matrix, which showed the appearance of a local lamellar order around the nanoparticles. The silica, titania and zirconia nanopaticles increased the thermal stability of the polymers, except for the highest silica and zirconia contents in the PC system which showed a decrease. A similar trend in the activation energies of thermal degradation was observed. The presence of zirconia and silica showed a decrease in the storage and loss moduli at lower temperatures, probably due to a plasticization effect. The two types of titania nanoparticles influenced the rigidity of the polymers in different ways because of their different carbon contents, particle sizes and crystal structures. NMR results suggested that, in the presence of a metal oxide, the observations in the PMMA systems could be related to heteronuclear dipolar interactions between the carbonyl carbons and the surrounding hydrogen nuclei, and in the PC systems to intermolecular interactions involving the carbonyl groups.

TABLE OF CONTENTS

LIST OF TABLES

LIST OF FIGURES

LIST OF SYMBOLS AND ABBREVIATIONS

^{13}C {^{1}H} CP-MAS NMR	^{13}C cross-polarization magic-angle spinning nuclear magnetic resonance
AFM	Atomic force microscopy
CHC	Cyclohexene carbonate units
DMA	Dynamic mechanical analysis
DSC	Differential scanning calorimetry
E_a	Activation energy
EDS	Energy dispersive spectroscopy
EDX	Energy dispersive X-ray
FTIR	Fourier-transform infrared spectroscopy
HEBM	High energy ball milling
KAS	Kissinger-Akahira-Sunose
LOI	Limiting oxygen index
MA	Methacrylic acid
MMA	Methyl methacrylate
MPS	Methacryloxypropyltrimethoxysilane
NMR	Nuclear magnetic resonance
OFE	Oriented finite element analysis
OFW	Ozawa–Flynn-Wall
PC	Polycarbonate
PMMA	Poly(methyl methacrylate)
Q	Momentum transfer
SAXS	Small angle X-ray scattering
SEM	Scanning electron microscopy
$T_1(H)$	Proton spin-lattice relaxation time in the laboratory frame
$T_1\rho(H)$	Proton spin-lattice relaxation time in the rotating frame
T_{CH}	Proton spin-lattice cross polarization times
TEM	Transmission electron microscopy
TEOS	Tetraethyl orthosilicate

TEOT	Tetraethyl orthotitanate
T_g	Glass transition temperature.
TGA	Thermogravimetric analysis
UV	Ultraviolet
VCT	Variable contact time
VSL	Variable spin lock
XRD	X-ray diffraction

Chapter 1

Introduction and literature review

1.1 Introduction

A broad range of elegant polymer materials has been developed for practical applications such as challenges in advanced aerospace, mechanical, automotive, bionics and medical technologies [1-4]. Meanwhile nanotechnology has developed rapidly, permitting manipulation of polymers and nanofillers that form the building blocks of desired materials [5-7]. The use of nanofiller particles as reinforcement in the polymer composites is an important area of research. Unlike larger reinforcement particles, the effects of the smaller particles on composites are unpredictable i.e. sometimes enhancing the composite properties [8-10], but other times diminishing them [11-15]. The enhancements in properties were mainly observed to be motivated by the small size effect, surface chemistry, interaction at the interface, filler loading, quantum size effect and macroscopic quantum tunnel effect [16-20].

There is an increased interest in the application of thermoplastics due to their toughness, resistance to chemical attack and recyclability [21-25]. It was further found that the addition of nanofillers in the thermoplastics give superior impact and damage resistance properties, especially at very low filler loadings (1-5%) [26-28]. Thermoplastic polymers used in thermoplastic nanocomposites can be divided into two classes: high temperature thermoplastics and engineering thermoplastics. The classification is based on the maximum service temperature of the polymers, which in turn is based on the glass transition temperature (T_g). Engineering thermoplastics are dominating industrial applications due to their outstanding mechanical properties such as stiffness, toughness, and low creep that make them valuable in the manufacture of structural products like gears, food containers, bearings and electronic devices [29-33]. Poly(methyl methacrylate) (PMMA) and polycarbonate (PC) attracted attention due to their inexpensiveness and fascinating properties (i.e. optical, mechanical, viscoelastic and thermal degradation kinetics). PMMA is mostly applied in medical technologies and implants, while PC is applied mostly in electronic components and construction materials [33-36].

Although their properties were found satisfactory in different applications, there were still important properties that need to be enhanced in order to extend the applications of these engineering polymers. For instance, microbial adhesion onto PMMA has been a long-standing drawback. Moreover, PC and PMMA have poor fatigue resistance, poor resistance to solvents, low thermal stability and high moisture sorption. In a bid to improve these drawbacks different nanofillers incorporated into these matrices were investigated [33-40]. PMMA and PC nanocomposites were of interest for improved thermal and mechanical properties, i.e, reduced flammability, reduced gas permeability, as well as their good potential to maintain excellent optical clarity. Different preparation methods for the nanocomposites have been studied, including solution mixing and *in situ* polymerization [35-40].

Thermoplastic nanocomposites containing different types (organic and inorganic) and shapes (nanofibres, nanotubes, nanowires and nanorods) of nanofillers were prepared for potential applications such as solid state lubricants, catalysts and components of magnetic devices. Amongst the nanofillers the oxides nanoparicles were mostly used in the preparation of the nanocomposites, mainly due to their abundance and inexpensiveness [41-43]. *In situ* synthesis of the particles was found to be the better method to produce small nanoparticles [44,45]. A number of methods were used to synthesize oxides nanoparticles including sol-gel, microemulsion and solution combustion [44-48].

The gel combustion process, belonging to the solution combustion synthesis, has been extensively used for the synthesis of nanoparticles of several metal oxides [45-50]. The sol-gel method has also been widely used in preparing materials as nanoparticles, films, and bulk forms [44-46]. This method is based on a colloidal solution (sol) that acts as a precursor for an integrated network (or gel) of discrete particles. Typical precursors are metal alkoxides and metal salts (such as chlorides, nitrates and acetates), which undergo various forms of hydrolysis and polycondensation reactions.

1.1.1 Oxides nanoparticles

Metal and non-metal oxides are a large and important class of chemical compounds in which oxygen was combined with a metal or non-metal. Some metal oxides are used as pigments in the painting industry, for cosmetics and for magnetic purposes (e.g. FeO, TiO_2). In recent years, the application of metal oxides for environmental remediation had become another active field for research [51-57]. Aluminum oxide was mostly used for the manufacturing of laboratory instrument tubes and sample holders. Zirconia is a multi-use synthetic gem often used as a replacement for diamonds and rubies in laser technology. Instead of diamonds, rings, necklaces, bracelets and earrings featured cubic zirconia because it is much cheaper than diamonds. Non-metal oxides also have a number of commercial and industrial uses. Silica and arsenic trioxide are famous non-metal oxides due to its commercial usage and medical applications. As nanosized particles, oxides can exhibit unique physical and chemical properties due to their small size and a high density of corner or edge surface sites. Investigations have shown that these properties would likely optimize ultraviolet (UV) absorption and enhance the stiffness, toughness, and service life of polymeric materials when the nanoparticles are incorporated into a polymer matrix [51-54].

1.1.2 Properties of nanoparticulated oxides

There are various factors which could affect the performance of particular oxide nanoparticles for specific applications. These factors include the chemical composition, physical, electrical, mechanical, thermal properties, and the synthesis route [51-54]. Transition-metal oxides are mostly used as nanofillers due to their fascinating properties at nanometre scale (magnets, prized as materials for electronics) and abundance. The nature of the transition metal or non metal oxide, as well as the surface modification, determine the final properties of the nanoparticles [55]. Titanium dioxide (TiO_2), zirconium dioxide (ZrO_2) and silicon dioxide (SiO_2) nanoparticles are amongst the oxides which attracted a lot of attention due to the ease of synthesis and their abundance.

1.1.2.1 Titanium dioxide

Titanium dioxide (titanium(IV)oxide or titania), chemical formula TiO_2, is a naturally occurring oxide of titanium covalently bonded to oxygen. It occurs in nature as polymorphs - rutile, anatase and brookite - mostly used industrially in catalysis, white pigments and photovoltaic based applications. The most common form is the rutile phase, which is also the equilibrium phase at all temperatures. [18-20,56,57].

In bulk titania the rutile phase is the thermodynamic stable phase. However, at sizes close to 15 nm (and below) the surface free energy and stress contributions stabilize the anatase phase. Around 35 nm the rutile phase seems to be more stable, despite the fact that brookite has free energy values close to that of rutile [57,56,18]. From a first principles analysis of surface energy, it was suggested that the average surface energy of an anatase crystal may be lower than that of a rutile crystal [20]. However, the principle contradicted experimental measurements of the surface stress contribution for a similar particle size where a larger value for the anatase phase was found [58]. In these nano-TiO_2 materials, surface energy was related to the presence of under-coordinated Ti cations; the surfaces with four-fold-coordinated centers having larger energy than those with five-fold coordination, and the surface energy approximately increases with the number of under-coordinated positions.

It is well known that the metastable anatase and brookite phases both convert to rutile upon heating. In addition, studies indicated that a smaller average primary particle size decreased the onset and the rate of the phase transformation (adjusting thermal stability), thus displaying a broader range of coexistence between anatase and rutile with decreasing particle size. These advantages of TiO_2 nanostructured materials provoked the current technological application of the material in electronics for higher temperature use [59].

1.1.2.2 Zirconium dioxide

Zirconium dioxide (ZrO_2), or zirconia, is a crystalline oxide of zirconium. It is commonly found as a stable mineral with a monoclinic crystalline structure called baddeleyite. The high

temperature cubic crystalline form is rarely found in nature as the mineral tazheranite $(Zr,Ti,Ca)O_2$), or cubic zirconia. The monoclinic structure transforms to unquenchable tetragonal and cubic (fluorite) structures at approximately 1400 and 2700 K (up to the melting point of ca. 2950 K) [61-62].

A decrease in the size of pure zirconia to less than 30 nm was found to significantly stabilize the tetragonal phase. The characteristics of the tetragonal-monoclinic transition in the nanoparticles were affected by a number of intrinsic or extrinsic factors like the particle size, the pressure, potential mismatch between local and long range order, or the presence of phase stabilizers either in the bulk (dopants) or at the surface. It was further established that the tetragonal-monoclinic transformation in nanosized pure zirconia was favoured when increasing the particle size or decreasing the pressure [17,63,64]. Particles smaller than 100 nm showed an increase in the band gap energy, except for particles smaller than approximately 10 nm. This observation was attributed to quantum confinement effects. The deviation for the very small particles was attributed to a crystallinity transition. However, surface modification of the nanocrystalline metal oxide particles with enediol ligands was found to be another approach for the modification of the optical and electrical properties, resulting in red shifts of the optical absorption with respect to the unmodified nanocrystallite [65].

1.1.2.3 Silicon dioxide

Silicon dioxide (silica) is an oxide of silicon with the chemical formula SiO_2. It is known for its hardness and three crystalline forms (quartz, tridymite and cristobalite). Often it would occur as a non-crystalline oxidation product. Silica is one of the most abundant oxide materials in the earth's crust and occurs commonly in nature as sandstone, silica sand quartzite. This precursor of silicate glasses and ceramics can exist in an amorphous form (vitreous silica) or in a variety of crystalline forms [66,67].

Silica generally has good abrasion resistance, electrical insulation and good thermal stability. It had been found that adsorption of water enhances the surface electrical conductivity of silica [68]. It is insoluble in all acids with the exception of hydrogen fluoride (HF). A fused silica is

mainly used where good dielectric and insulating properties are required, though it may also be used as refractory materials or investment casting. Quartz is an insulator with band gaps in excess of 6 eV commonly used as substrates for supported catalysts. Upon heating the quartz to higher temperatures, its thermal expansion decreases and it will transform to tridymite and crystobalite [69].

The electrical and optical properties of silica are strongly dependent on size, especially when formed into nanotubes, nanowires and nanoparticles due to their quantum confinement effect. Their different applications are also shape dependent. Silica nanotubes are ideal for application in the biological separation of estrone *via* a molecular imprinting technique, because they are easy to make, have a cross-linked structure, and are very suitable for the formation of a delicate recognition site. Recently, sub wavelength-diameter silica nanowires have been demonstrated for guiding light within the visible and near infrared spectral ranges. The large surface areas of the nanoparticles have the ability to affect a large volume fraction of a matrix polymer [70-72].

1.1.3 Synthesis of the oxide nanoparticles

An essential area of research in nanotechnology is the manufacturing of nanoparticles of different chemical compositions, sizes, shapes and performance for the different desired applications. Many preparation methods of oxide nanoparticles have been developed, including physical methods (mechanical milling; pulsed electrodeposition, gas-to-particle routes, inert gas condensation, flame pyrolysis and chemical vapor synthesis), as well as wet chemical techniques (sol-gel, micro-emulsions, co-precipitation and solution combustion). However, there is no general strategy to make nanoparticles with narrow size distributions, tailored properties, and desired morphologies, which could be universally applied to different materials [44-47].

In many investigations chemical methods were preferred over physical methods due to expensive equipment, sample contamination and safety reasons. In a sol-gel process metal oxides are prepared *via* hydrolysis of precursors, usually alkoxides in alcoholic solutions, resulting in the corresponding oxo-hydroxide. Condensation of molecules leads to the formation of a network of the metal hydroxide. Hydroxyl-species undergo polymerization by condensation and form a

dense porous gel. Appropriate drying and calcination lead to ultrafine porous oxides. In a study where SiO_2 and TiO_2 were prepared by the hydrolysis and condensation of TEOS (tetraethyl orthosilicate) and TEOT (tetraethyl orthotitanate) it was shown that the properties of the nanoparticles could be controlled by varying the ratio of water to ethanol and the reaction time [73-75]. The microemulsion technique is based on the formation of micro/nano-reaction vessels under a ternary mixture containing water, a surfactant and oil, which are isotropic liquid media with nano-sized water droplets dispersed in an oil phase. An inorganic phase (metal oxide precursor) is then dispersed in the mixture. The surfactant molecule stabilizes the water droplets because they have polar head groups and non-polar organic tails. The organic portion faces towards the oil phase and polar group towards the water. These micro-water droplets then form nano-reactors for the formation of nanoparticles [76,77]. In the co-precipitation method a salt precursor (chloride, nitrate, etc.) was dissolved in water (or another solvent) to precipitate the oxo-hydroxide form with the help of a base. In this technique it is difficult to control the size and chemical homogeneity of mixed-metal oxides [78,79].

Among these techniques, the sol-gel combustion process is the best method to prepare highly crystalline and ultrafine particles characterized by large specific surface areas. The process developed at the beginning of the nineties is a combination of the combustion process and the chemical gelation process and used the heat energy released by the redox exothermic reaction between a fuel (i.e. citric acid, urea, glycine or glycol) and an oxidizer (i.e. nitrates) at a relatively low igniting temperature to give a nanostructured powder. The powder usually slightly bonds into soft and very porous agglomerates which could be easily ground by a mortar and pestle. The process is not only safe but also time and energy saving exploiting the advantages of inexpensive precursors, mixing of compositions at the level of atoms or molecules, and synthesizing of ultrafine, highly homogeneous powder. This method has been used successfully for the synthesis of several oxide nanoparticles such as CeO_2, SnO_2, Fe_2O_3, NiO and TiO_2 [80-82]. However, only few studies have shown interest in investigating the method for the preparation of titania for incorporation in a polymer matrix [83-85].

1.2 Engineering thermoplastics

1.2.1 Poly(methyl methacrylate)

Poly(methyl methacrylate) or poly(methyl-2-methylpropanoate) is a transparent, odourless, tasteless, and nontoxic thermoplastic exhibiting excellent mechanical strength, high Young's modulus, corrosion resistant properties and good dimensional stability and hardness. It can be used in many fields, such as in aircraft glazing, signs, lighting, dentures, food-handling equipment, and contact lenses. Unfortunately, its low conductivity (less than 10 -14 S cm^{-1}), poor flame retardancy, thermal stability and abrasion resistance, and low elongation at break limit its applications in some fields [21-23]. A possible method to improve the performance is compounding the polymer with special nanofillers. It was shown that the mechanical, viscoelastic, thermal, abrasion and hardness properties of the PMMA matrix were influenced by the presence, quantity and dispersion of nanofillers, and interactions at the interface [8,28,24,86].

The thermal degradation of PMMA is an important property that may be influenced by the presence of nanofiller. PMMA degrades through two possible mechanisms, depending on the number of weak links emanating from the preparation [29,30]. A literature survey indicated that if there is a large number of weak links, TGA would show multiple steps related to the formation of a random distribution of products. The first step was related to the initial scission of PMMA, which includes homolytic scission of the methoxycarbonyl side groups ($-COOCH_3$). The second step was related to the random scission of C−C bonds in the main-chain. However, other authors claimed that the mechanism changes if there is a negligible number of weak links in the PMMA chains. In this case, TGA shows a single step which is associated with the release of the monomer. They found that, though the propagation of radicals to form MMA dominates over random chain scission in the backbone, the scission dominates at relatively high temperatures [29-31].

1.2.2 PMMA nanocomposites

1.2.2.1 Morphology

There were a number of investigations on nanocomposites of PMMA containing either non-metal or metal oxides (e.g. Zno, NiO, CuO). In most cases Scanning electron microscopy (SEM), Transmission electron microscopy (TEM), X-ray powder diffraction (XRD), Atomic force microscopy(AFM) and Fourier transform infrared spectroscopy (FTIR) were used to characterize the morphology. In *in situ* prepared nanocomposites with TiO_2 and Fe_2O_3 as fillers in PMMA, the final product showed improved surface hydrophilicity, PMMA porosity and colour [87,88]. In other studies where ZnO/PMMA nanocomposites were synthesized by chain polymerisation of MMA in bulk between two glass plates, ZnO particles were homogeneously dispersed in the PMMA matrix with few agglomerates [26,27]. The dispersability of the fillers within the matrix was related to interactions at the polymer-filler interface. Another study showed that surface roughness increased with an increase in metal oxide content [58]. In most of the PMMA nanocomposites containing oxide nanoparticles it was possible to improve the dispersion of the filler through decreasing the size and quantity of the particles, and through surface modification [26,27].

1.2.2.2 Thermal properties

The thermal properties of PMMA containing either non-metal or metal oxides have been studied by a number of researchers using thermogravimetric analysis (TGA) and differential scanning calorimetry (DSC). The results of the weight loss of PMMA containing either non-metal or metal oxide as a function of temperature could be summarized as follows: The number of degradation steps in most cases was controlled by the type of PMMA used. Most PMMA nanocomposites thermally degrade between 250 and 450 °C, regardless of preparation route. The presence of oxides generally increased the thermal stability without affecting the thermal degradation mechanism of PMMA. The increase in thermal stability was attributed to interaction between the surface of the particles and segments of the PMMA chains which reduced segmental mobility [86,26]. However, some reported results indicated a decrease in thermal stability in the presence

of oxides. The authors attributed this observation to the surface modification of the particles and to poor dispersibility [12,13].

The glass transition temperature (T_g) of PMMA/alumina nanocomposites, prepared via *in situ* polymerization, was studied by DSC in two similar studies [8,25]. At smaller weight fractions (<1.0 wt % of 38 nm fillers, or < 0.5 wt % of 17 nm fillers) it was found that there were no changes in the composite T_g [8]. However, at greater filler concentrations, the T_g was observed to decrease precipitously compared to that of the neat polymer. The decrease was attributed to a threshold at which a significant volume fraction of the polymer has higher mobility. The T_g depression was suppressed by coating the nanoparticles to make them compatible with the matrix. Another study, however, showed decreasing T_g values at smaller weight fractions in PMMA, and related it to a decrease in molecular weight and/or a decrease in syndiotacticity of the synthesized PMMA [25].

1.2.2.3 Mechanical and viscoelastic properties

Dynamic mechanical analysis (DMA) and tensile testing were mostly used to get information on the mechanical properties of PMMA-(non)metal dioxide nanocomposites [8,25,89]. The presence the nanoparticles (Al_2O_3, ZnO_2, and Ta_2O_5) in PMMA matrix generally showed a significant increase in Young's modulus, storage modulus, loss modulus and glass transition temperature, especially at a low filler loadings [61]. However, there are some investigations which showed a reduction in the mechanical properties [8,25]. The differences in the influence of these nanoparticles on the mechanical properties were attributed mainly to the degree of dispersion of the filler nanoparticles in the PMMA matrix.

1.2.3 PMMA-silica nanocomposites

1.2.3.1 Morphology

In previous investigations of poly(methylmethacrylate)/silica (PMMA-SiO_2) nanocomposites AFM, SEM, TEM and FTIR techniques were used to investigate the morphology. The

preparation of PMMA-SiO_2 nanocomposites *via in situ* emulsion polymerization in the presence of an initiator was investigated [90-98]. Generally, homogeneous dispersion of silica in PMMA was obtained, even though there were some noticeable agglomerates and a framework of small pores. The dispersion of silica was attributed to the interaction at the silica-PMMA interface. In most cases modified silica nanoparticles showed a better dispersion in the PMMA matrix which led to better transparency and stronger interaction at the interface. If the interaction was too strong, nanocomposites with core-shell morphology formed. AFM results indicated that the surface roughness increased in the presence of silica. Similar morphological results were found in separate studies where PMMA-SiO_2 nanocomposites were prepared by single screw extrusion, melt compounding and *in situ* radical polymerization [99]. However, the *in situ* radical polymerization prepared nanocomposites showed exceptional dispersion of silica in PMMA compared to the *in situ* emulsion polymerization prepared PMMA-SiO_2 nanocomposites [60]. In the sol-gel prepared nanocomposites, the morphology images and FTIR results showed that nano-scale SiO_2 particles were uniformly distributed in and covalently bonded to the PMMA host matrix without macroscopic organic-inorganic phase separation [90,41,100,101]. The preparation of PMMA-SiO_2 nanocomposites *via* solution mixture of PMMA and silica was also investigated [34,101-103]. A good dispersion of silica in the PMMA matrix and small clusters were observed. The silica showed a better dispersion when it was annealed at a low temperature for longer times or when the PMMA was grafted. The dispersion was attributed to the size and shape of the nanoparticles which influenced the interfacial interaction.

Some studies prepared nanocomposites of PMMA-SiO_2 by high energy ball milling (HEBM) [35,104,105]. There were no specific interactions observed between the PMMA matrix and the silica. The FTIR results showed that HEBM had no significant influence on the structure of PMMA. In contrast, Benito *et al*. [104] showed that HEBM induced particular conformational changes on both the ester group and the backbone of the PMMA, which seemed to be the cause of a specific polymer chain packing appearing at the interface. The change in the PMMA chain configuration was attributed to the long milling time.

1.2.3.2 Thermal properties

The thermal behaviour in most PMMA-SiO_2 nanocomposites was investigated by TGA and DSC. For most of the PMMA-SiO_2 nanocomposites prepared *via in situ* emulsion polymerization the presence of silica retarded the thermal decomposition of the polymer chains, which was attributed to the large silica surface area and radicals that were probably trapped by the silica during degradation [91-93]. However, the opposite trend where the presence of silica in PMMA did not enhance the thermal stability was also observed [12,103]. From the thermal degradation kinetics in another study of PMMA-SiO_2 nanocomposites it was apparent that the addition of silica could lead to decreased activation energy of degradation [35]. The observations were related to weak interaction at the polymer- filler interface.

The thermal stability of most PMMA-SiO_2 nanocomposites was governed by the modification of the silica surface. For instance, Hu *et al.* [97] increased the thermal stability of the nanocomposites *via in situ* polymerization by introducing methyl groups on the silica surface. In another study, where a core-shell morphology was formed, the increase in thermal stability of the PMMA-silica nanocomposites was attributed to the presence of silica and uncondensed residual of the precursor which needed a large amount of heat to decompose [91].

Other studies, where the nanocomposites were prepared by single screw extrusion and melt compounding, found an increase in the thermal stability in the presence of silica [95,96,99]. This was attributed to good interaction at the PMMA-silica interface. The presence of silica in studies on *in situ* radical polymerization prepared nanocomposites showed slightly reduced thermal stability of the nanocomposites and slightly delayed random initiation along the polymer backbone. However, it appeared that the overall PMMA degradation mechanism was not significantly modified by the addition of nano silica particles.

In sol-gel prepared nanocomposites the increase in silica content shifted the degradation of the matrix to higher temperatures [41,90,101]. This was attributed to the organic chains which were trapped in the inorganic silica matrix. In another study on sol-gel prepared PMMA-silica nanocomposites the presence of silica in air and nitrogen atmospheres showed increased thermal

stability and much higher stability in air. The increase in thermal stability was attributed to the formation of an inorganic-organic network. In the air atmosphere the thermal stability was attributed to the ability of inorganic components to stabilize the free radicals generated at high temperature.

In the nanocomposites prepared by high energy ball milling (HEBM) the PMMA showed a new thermal degradation step at a lower temperature [35,104,108]. The kinetic analysis of the thermal degradation of the PMMA also showed a lower activation energy. These observations were attributed to a high concentration of end chains due to the milling process. It was further observed that after adding silica nanoparticles, the effect of milling on the thermal degradation and the kinetic analysis was even more pronounced. However, the opposite effect was found when the amount of nanoparticles was further increased. These results were attributed to more chain scission when the silica nanoparticles were mixed with PMMA up to the threshold.

Li *et al*. [106], in their DSC analysis of *in situ* polymerized PMMA in the presence of silica nanoparticles, indicated that unconverted monomers trapped in the pores of silica could polymerize during the first scan and lead to multiple exotherms of PMMA. Chan *et al.* [107], however, related the multiple exotherms of PMMA to the incomplete condensation during silica nanoparticles synthesis. Lui *et al.* [12], on the other hand, did not observe an exotherm for PMMA/silica nanocomposites prepared in a similar way. Castrillo *et al*. [108] found a decrease in the glass transition temperature for PMMA, and two glass transitions for PMMA-silica nanocomposites when milling times were longer than 6 hours. These observations were related to a higher extent of chain scission that occurred during the mixing of the two components.

1.2.3.3 Mechanical and thermomechanical properties

Many PMMA-SiO_2 nanocomposites studies investigated the mechanical and viscoelastic properties of the nanocomposites through tensile testing and DMA. In most cases the DMA results of these nanocomposites prepared *via in situ* emulsion polymerization showed higher storage and loss moduli, glass transition temperatures and elastic moduli than PMMA [90-98]. The glass transition temperature of these nanocomposites increased with increasing silica

content. However, other authors found a decrease in the glass transition temperature of PMMA with nanosilica addition [13,105]. Kashiwagi *et al.* [13] attributed the decrease to residual solvent in the sample, and Hub *et al.* [102] attributed it to non-equilibrium trapped voids in the sample. The stiffness and loss modulus of the nanocomposites with modified silica nanoparticles were even higher, and so were the glass transition temperatures. The apparent hardness, tensile strength, impact strength and flexural strength increased in the presence of silica. Those were related to physical bonding, at polymer filler interface, between silica and PMMA that acted as restriction sites for the movement of polymer chains [92,96]. Fu *et al.* [109] added hydroxyppropyl acrylate as a catalyst to the tetramethyl othosilicate (TEOS) precursor during the *in situ* polymerization of PMMA-SiO_2 nanocomposites. The hardness, elasticity modulus, and wear of the materials increased in the presence of the catalyst. The increase was related to covalent bonds formed between the organic matrix and the silica.

Some studies revealed that the mechanical performance of PMMA-SiO_2 nanocomposites could be correlated with the pore structure of the silica nanocomposites [109,110]. Silica with the largest pore size and pore volume showed the greatest enhancement in mechanical properties. In general, 3D framework structures and large mesopore sizes were preferred over smaller and lower dimensional pore structures, because they provided a greater degree of polymer confinement and interfacial interactions that led to improved mechanical properties.

Similar improvements in the mechanical properties (storage and loss moduli, damping factor, hardness and tensile strength) were found in the sol-gel and melt compounding prepared PMMA-SiO_2 nanocomposites, and all these observations were attributed to PMMA-silica interfacial interaction [41,90,100]. Yeh *et al.* [100] found that the addition of silica showed a decrease in impact strength of PMMA-SiO_2 nanocomposites, but they did not offer a clear explanation.

1.2.4 PMMA-zirconia nanocomposites

1.2.4.1 Morphology

In studies of the morphology of PMMA-ZrO_2 nanocomposites prepared by *in situ* polymerization [112-116] it was found that single, non-agglomerated ZrO_2 nanoparticles were homogeneously dispersed in the polymer matrix. The good dispersion of the particles at nanometre level gave rise to the transparency observed for these nanocomposites. No obvious optical difference could be seen with the naked eye between the highly filled and pristine PMMA samples. At higher zirconia content the reduction in transparency of the nanocomposites was related agglomeration of the zirconia particles. In studies where surface modified nanoparticles were used, the good dispersion of the nanoparticles was associated with the existence of hydrogen bonds [87,90]. Wang *et al*. [41] found that, in the absence of surface modification, the nanoparticles could covalently bond to PMMA, and there was no obvious macroscopic organic-inorganic phase separation.

For sol-gel prepared nanocomposites it was also found that the nano-scaled ZrO_2 particles were uniformly distributed in the host matrix without changing the PMMA structure, and it was related to interaction between the components [116,117]. The results were confirmed by FTIR, which showed a shift in the carbonyl absorption to a lower wavenumber in the presence of the zirconia nanoparticles. Similar results were found by Shang *et al.* [118] where PMMA-ZrO_2 composites were prepared by solution mixing. Unfortunately they offered no explanation for their observation.

1.2.4.2 Thermal properties

In most of the *in situ* polymerized nanocomposites, TGA results showed a clear increase in thermal stability with increasing zirconia content [112-115]. These studies related the improvement in thermal stability to the formation of networks between the polymer and the inorganic moieties, which led to the restrained movement of free radicals generated by the thermal decomposition of the PMMA matrix. Hu *et al.* [112] showed that functionalised ZrO_2

exhibited better thermal stability than non-functionalised ZrO_2 at 200 ºC. However, beyond 200 ºC there was a clear decrease in thermal stability. The increase in thermal stability of the functionalized nanoparticles was attributed to the organic components of the attached methacryloxypropyltrimethoxysilane (MPS). Unfortunately it was not explained how those organic components improved the thermal stability and why the thermal stability suddenly decreased beyond 200 ºC.

Investigation of the thermal stability and degradation kinetics of PMMA-zirconia hybrids prepared by a sol-gel method in air and nitrogen [116,117], showed that the PMMA and nanocomposites degraded in three steps and that the thermal stability of PMMA increase in the presence of zirconia. However, in the second step in nitrogen and the third step in air the thermal stability of the nanocomposites was lower. This was related to different mechanisms of thermal degradation in air and nitrogen. The kinetic results showed that the activation energy (E_a) values for the degradation of the nanocomposites were higher than that of pure PMMA in air. In nitrogen the E_a values for the first and last stage were larger than those of PMMA. This increase was associated with the nanoparticles inhibiting the formation of free radicals and reaction with oxygen in air. Wang *et al.* [119] observed a significantly higher thermal stability and lower heat release rate in air than in nitrogen when zirconia was present in PMMA. They related this observation to the formation of char compacted around the zirconia nanoparticles, which protected the material from further burning.

1.2.4.3 Mechanical and thermomechanical properties

For PMMA-ZrO_2 nanocomposites prepared *via in situ* emulsion polymerization the storage and loss moduli, glass transition and elastic modulus were significantly higher in the glassy state than those of PMMA [112-115]. These were related to the reinforcing effect of the zirconia nanoparticles. However, in the rubbery state the PMMA modulus was independent of the filler content and this was attributed to the weak interaction between the polymer and filler at higher temperatures. A quick increase in pendulum hardness of PMMA-ZrO_2 nanocomposites was observed at extremely low ZrO_2 contents and there was a steady increase in scratch resistance with increasing zirconia content. These were attributed to the increased crosslinking density of

the PMMA in the presence of zirconia nanoparticles. Their viscosity measurements confirmed that zirconia nanoparticles played a cross-linking role in PMMA.

Hu *et al.* [115] found, from tensile results, that for PMMA-ZrO_2 nanocomposites the reinforcement of ZrO_2, though not remarkable, enhanced rigidity without loss of toughness. This was attributed to bonding between the polymer and the functionalized zirconia. These results were in line with a study of Hu *et al.* [112] where the elastic modulus of the nanocomposites was determined from indentation tests.

1.2.5 PMMA-titania nanocomposites

1.2.5.1 Morphology

A fair amount of work has been done to characterize the morphology of PMMA-TiO_2 nanocomposites prepared using different methods [15,120-128]. In most cases the PMMA-TiO_2 nanocomposites were transparent with the refractive index increasing with the addition of the filler. *In situ* polymerization of these nanocomposites yielded materials with the nanoparticles appearing to be nearly spherical and well dispersed, although agglomerates were visible. The surface modified nanoparticles appeared to disperse better than the unmodified nanoparticles. The structure of PMMA did not appear to be changed by the presence of the nanoparticles. A change in the absorption peak position of TiO_2 was generally attributed to a particular functional group grafted onto the TiO_2 surface before polymerization. The presence of pores was significant, and they were similar to those in PMMA-TiO_2 nanocomposites prepared by solution mixing. Ahmad *et al*. [87] found that the virgin PMMA exhibited porous structure, while the pores disappeared in the PMMA-TiO_2 nanocomposites. That was related to the ability of the hydrophilic filler to intercalate within the PMMA matrix.

In melt mixed and twin extruded PMMA-TiO_2 nanocomposites a uniform dispersion of modified and unmodified titania was observed with the existence of few agglomerates smaller than 0.2 μm in the modified system, and bigger in the unmodified system [40,124]. The titania was modified by addition of the coupling agent 3-acryloxypropyl trimethoxysilane. The TiO_2 agglomerate sizes

were controlled by increasing the number of extrusions and the melt mixing time during the preparation of the PMMA-TiO_2 nanocomposites. For nanopaticle loadings above 2% there was a non-uniform distribution of the filler in the PMMA matrix, independent of the number of extrusions and the melt mixing time.

Khaled *et al*. [126] used methacrylic acid (MA) to modify the surface of fibril and spherical titania nanoparticles. The MA was then copolymerized with methyl methacrylate (MMA) to form a TiO_2-PMMA nanocomposites. TEM and SEM results showed that generally the functionalized titania in was better dispersed in PMMA than the corresponding unfunctionalised system. It was observed that while there were several individual functionalized nanofibre particles distributed, most were clumped together in nano bundles uniformly dispersed in the polymer matrix. The functionalized TiO_2 nanospheres were uniformly dispersed throughout PMMA. These results were confirmed by FTIR, where chemical bonding between the modified fillers and PMMA was observed.

Inkyo *et al*. [124] used a beads assisted mill to form suspensions of modified and unmodified titania nanoparticles in methyl methacrylate, followed by polymerization. The beads milling successfully broke up the titania nanoparticle agglomerates when the coupling agent 3-acryloxypropyl trimethoxysilane to was added to the PMMA-titania suspension. Agglomerated particles were broken up into primary particles as small as 10 nm in suspensions with nanoparticle mass fractions up to 0.05. The well-dispersed titania nanoparticles had very little effect on the transmittance of visible light through MMA, but they reduced the UV absorbing properties of MMA. TEM images showed that the milled nanoparticles remained well dispersed in the nanocomposites. The results were related to the effectiveness of the milling process to disperse the nanoparticles into the organic solvent.

1.2.5.2 Thermal properties

The influence of the TiO_2 in on the thermal properties of most *in situ* polymerization prepared PMMA-TiO_2 nanocomposites was investigated by TGA and DSC [120-123]. Some TGA studies were done in nitrogen and in air [120,121,124]. The char content increased with increasing

titania content. The nanocomposites generally exhibited better thermal stability than pristine PMMA, and those containing modified nanoparticles prior to polymerization showed the best thermal stability. This effect was more obvious during thermo-oxidative degradation. The increase in decomposition temperatures was attributed to the interfacial interaction between titania and PMMA.

In some studies PMMA and PMMA/TiO_2 nanocomposites showed respectively three and two degradation steps [120,121]. The lack of a third peak, attributed to head to head linkage, in the nanocomposites was the result of the nanoparticles that reacted as radical scavengers and/or chain-transfer agents during the polymerization. The same systems showed respectively two and one degradation steps in oxygen [120]. The two degradation steps were attributed to free radicals suppressed by oxygen, and the one degradation step was attributed to an inhibiting effect by the nanoparticles. Some studies, where the nanocomposites were prepared through *in situ* polymerization, showed the decreased thermal stability of PMMA in the presence of the TiO_2 nanoparticles [13,125]. This was attributed to physisorbed water evaporating at lower temperatures.

An increase in thermal stability of PMMA-TiO_2 nanocomposites was also shown for melt mixed, twin-screw extruded, beads assisted mill and sol-gel prepared nanocomposite [15,30,124]. This was attributed to the large specific surface area of the nanoparticles giving more interaction sites. In the sol-gel study they attributed this increase to trapped inorganic moieties that impeded the polymer chain segment motions. Chatterjee *et al*. [40] and Laachaci *et al.* [125] prepared PMMA-TiO_2 nanocomposites by twin screw extrusion and melt blending respectively, and studied the thermal degradation kinetics of the nanocomposites. In both studies the activation energy increased with an increase in the filler content, decreased at higher filler contents. The increase in the activation energy compared to that of pure PMMA was related to a stabilizing effect, and the decrease at higher contents to a catalytic effect, of the agglomerated nanoparticles.

Some DSC studies showed an increase in T_g with an increase in the nanoparticles loading, and the effect was more pronounced where functionalized TiO_2 nanoparticles were used [15,125,127]. This was attributed to the strong interfacial bonding between the functionalized

nanofiller and the polymer matrix. However, a decrease in glass transition was also observed for some PMMA-TiO_2 nanocomposites, which was attributed to the plasticization effect of the presence of lower molar mass components. Ling *et al*. [15] studied PMMA-TiO_2 nanocomposites, synthesized through *in* situ polymerization, using differential thermal analysis (DTA) in air. They did not only find an increase in T_g with increasing nanoparticles loading, but also a separation of the endothermic melting peak of the nanocomposites into two peaks. This was related to a physical and chemical intercross of the polymer matrix chains and the polymer chains grafted onto the nanoparticles.

1.2.5.3 Mechanical and thermomechanical properties

Many studies have shown little interest in the characterization of the mechanical properties of PMMA-TiO_2 nanocomposites. In the studies where the mechanical properties were investigated, the storage and loss moduli increased and tan δ shifted to higher temperatures relative to those of the neat polymer [39,124-126]. The increase was more pronounced at lower TiO_2 volume fractions. The increase was attributed to the improved interfacial adhesion between the nanoparticles and the polymer as a result of physiochemical interaction. The stronger interfacial surface absorbed stress imposed on the nanocomposites. In the studies where the nanocomposites were prepared through twin screw extrusion, the tensile modulus, dimensional stability and glass transition increased with an increase in TiO_2 nanoparticles content. This was explained as being the result of possible chemical and physical interactions that formed a crosslinked structure.

Hamming *et al.* [127] prepared PMMA-TiO_2 nanocomposites by mixing a solution of PMMA with certain amounts of modified and unmodified TiO_2. The TiO_2 was modified by adsorbing biomimetic initiator on the surface from an aqueous solution. The sample of 2 wt% unmodified TiO_2 in PMMA showed a broadening of the damping factor (tan δ) peak towards lower temperatures. In contrast, the sample of 2 wt% modified TiO_2 in PMMA showed a tan δ peak shift towards higher temperatures. In the first case, the early onset of relaxation was related to an indication of a weak interaction between the nanoparticles and the surrounding polymer, while in the second case the observation was related to indirect evidence that the interphase region had

percolated through the entire composite. It was also attributed to strong interaction between the modified nanoparticles and the surrounding polymer.

The results of Khaled *et al*. [126] confirmed that, regardless of weight percentage and shape of nanofiller in the composite, chemical bonding between the functionalized titania nanoparticles and the PMMA matrix produced significantly higher values of dynamic elastic moduli compared to the composites with nonfunctionalized titania nanoparticles. They went on to compare the mechanical properties of titania nanofibers and nanospheres in the composite, and observed that the TiO_2 nanofibers generally were better reinforcers than the TiO_2 nanospheres.

1.3 Polycarbonate

Polycarbonate (PC), mainly bisphenol A polycarbonate, show very good physical and chemical properties, such as good mechanical strength, good thermal stability and high heat distortion temperature. PC is a condensation polymer that forms a bulky stiff molecule, which promotes rigidity, strength, creep resistance and high heat deflection temperature. PC is typically amorphous and exhibit good transparency. The bulk amorphous chains produce considerable free volume, resulting in a polymer with high ductility, impact resistance and low scratch-resistance. PC is applied in many areas such as construction, electrical, automotive, aircraft, medical and packaging applications and recently in car lights and laser optical data storage (compact disks). The price of PC is between that of commodity thermoplastics and special engineering thermoplastics, which makes it the largest volume engineering thermoplastic [33-36,130-132]. PC also has a high limiting oxygen index (LOI) and produces a large fraction of char upon combustion when subjected to thermogravimetric analysis. It is usually processed at higher temperatures (over 300 °C) by an injection molding process.

Several investigations, by means of various analytical techniques such as pyrolysis-mass spectroscopy, pyrolysis-gas chromatography, assisted laser desorption ionization, and TGA-FTIR, were performed on the thermal decomposition of PC and the many structures formed in PC chains during thermal degradation [132-138]. There are some of controversies about the true chemical reaction occurring during the thermal degradation of bisphenol-A polycarbonate. Some

authors [33,139] reported that the degradation starts at carbonate linkages (< 400 □C), while at higher temperatures the isopropylidene group starts to be susceptible to loss of methyl radicals. Other studies [136,137,140] revealed that the carbonate linkages undergo rearrangement at lower temperatures by intramolecular ester exchange and disproportionation of isopropylidene linkages. In an attempt to suggest a mechanism, Jang *et al.* [36] reported that the main thermal degradation pathways followed chain scission of the isopropylidene linkage, and hydrolysis/alcoholysis and rearrangements of carbonate linkages. In the case of chain scission, they proposed that methyl scission of isopropylidene occurs first. However, McNeill *et al.* [140] suggested that polycarbonate follows a homolytic chain scission mechanism during the thermal degradation of PC.

These controversies were also obvious in studies reported on the air atmosphere degradation of PC, with TGA results showing multiple step degradation [30,33,133]. For example, Jang *et al.* [33] found two TGA steps and attributed the first step to oxidative hydrogen cleavage of the isopropylidene linkage, followed by hydrolysis and alcoholysis of the carbonate. Li *et al.* [133] observed three steps and attributed the first stage to decarboxylation, dehydration, dealkylation and hydrogen abstraction, together with crosslinking between the residual aromatic carbon atoms. The second and third stages were attributed to the degradation of aromatic carbons.

1.3.1 PC nanocomposites

1.3.1.1 Morphology

Polycarbonate-γ-Fe_2O_3 and polycarbonate-CuO composite films were prepared by a solvent casting method [37]. In other studies PC-zinc oxide (ZnO) nanocomposites containing 0.1, 0.5, 1 or 5 wt. % nanoparticles were prepared by milling and injection molding [38,43]. Intense XRD peaks were found for the PC nanocomposites which showed the development of crystallinity in the PC matrix. This was related to the complexation of γ-Fe_2O_3 and CuO nanomaterials with the polycarbonate matrix. In the PC-ZnO nanocomposites non-uniform distribution of the ZnO particles was observed from TEM, while SEM and energy dispersive spectroscopy (EDS) showed the formation of micron-sized nano-ZnO agglomerates or clusters in the PC matrix. The

MgO particles in a flame retardant PC-magnesium oxide (MgO) nanocomposite were nanodispersed in the PC matrix [134]. The composites were further burned in oxygen and micrographs were taken. No obvious difference was observed between the micrographs of PC and the PC/MgO nanocomposite, and this was attributed to failure of the filler to influence the final morphology of the char.

1.3.1.2 Thermal properties

Simultaneous TGA/DTA of PC, PC/γ-Fe_2O_3 and PC/CuO nanocomposites were undertaken [37], while PC-ZnO nanocomposites were investigated using DSC [38,43]. The presence of CuO and γ-Fe_2O_3 nanoparticles in PC showed an increase in thermal stability, and all the samples showed a two-step mass loss. The first step was attributed to the partial decomposition of the surface-oxygenated PC and the second step to complete PC decomposition.

Other studies found a decrease in thermal stability of all the composites compared to that of PC, and a decrease in residual content in the presence of a metal oxide (CuO, Al_2O_3, MoO_3 ,CeO_3, and MgO) as additive in PC [132,134]. They related the lower thermal stability to the catalysis of the thermal degradation by the metal oxides, and the decreased residual content to a possible reaction occurring between the metal oxides and PC during heating. Dong *et al.* [134] showed that small amounts of MgO led to increased LOI values, which they related to the nanodispersion of MgO in the PC matrix.

DSC analyses showed that the presence of ZnO gave rise to a decrease in the glass transition temperature of the nanocomposites [38,43]. A significant decrease was observed when ionic liquid was added [43]. The observations were related to a plasticizing effect by the fillers.

1.3.1.3 Mechanical and thermomechanical properties

The presence of nano-filler generally increased the stiffness and reduced the ductility of PC [37-39]. Carrión et *al*. [38] found that 1 wt.% ZnO nanoparticles significantly reduced both the tensile strength and the elongation at break of PC, and that the presence of 0.5% ZnO in PC

increased its hardness, while 1% ZnO reduced its hardness. They related the observations to the more homogeneous dispersion of the filler at lower contents. In another study [43] an ionic liquid (IL) of 1-hexyl-3-methylimidazolium hexafluorophosphate had been added to a PC+0.5 wt.% ZnO nanocomposite. The presence of IL reduced friction and wear compared to IL-free PC+0.5 wt.% ZnO nanocomposite. These were related to the formation of a more homogeneous dispersion in the presence of IL.

In another study the abrasive wear resistance of injection molded PC and PC/ZnO nanocomposites containing 0.5 wt% ZnO nanoparticles were determined as a function of the sliding direction with respect to injection flow [141]. The neat PC showed anisotropic behaviour with instantaneous penetration depth more than 50% higher in the direction parallel to the melt injection flow than in the transverse direction. The addition of ZnO nanoparticles reduced the instantaneous penetration depth in the longitudinal direction and lowered the viscoelastic recovery which led to large residual depth. The addition of 0.5 wt % of ZnO nanoparticles increased the storage modulus and reduced the glass transition temperature of PC. The observations were related to interactions between the nanoparticles and the polymer network.

1.3.2 PC-silica nanocomposites

1.3.2.1 Morphology

The morphology of PC after incorporating silica nanoparticles into the PC matrix had been investigated by several authors. A couple of studies showed that PC-silica nanocomposites prepared by a simple one-step injection moulding process contained nanopowders aggregated into small nano-clusters, and these nano-clusters were well dispersed in the polymer matrix [142,143]. FTIR confirmed that the dispersion was promoted by chemical bonding between the organic and inorganic phases. However, good dispersion of silica particles inside the polymer matrix was not observed in some other studies [144,145]. Chau et *al*. [144] found that the size of the SiO_2 domains generally increased with increasing amount of TEOS in sol-gel prepared nanocomposites. There was no explanation given for the enlargement.

1.3.2.2 Thermal properties

The thermal properties of the nanocomposites were investigated by DSC. The T_g of the polycarbonate increased after the addition of 5 wt% silica nanopowder functionalized with a silane coupling agent. DSC results showed that the incorporation of silica nanopowders increased the T_g of PC in PC-silica nanocomposites [142]. This was related to the restriction of polymer chain segments motion by the interfacial interactions between the surface functionalized silica nanopowders and the polymer molecules. Other studies found that an increase in silica content in a PC matrix, prepared through sol-gel, led to a decrease in both the glass transition and thermal degradation temperatures [144,145]. The decrease was related to an increase in free volume and catalysis by silica, or to the presence of a large fraction of the rigid structure of cyclohexene carbonate units (CHC). The presence of silica nanoparticles in a PC matrix prepared by melt mixing showed an improvement in thermal stability. This was related to hydrogen bonding interaction between the hydroxide groups on the silica surface and carbonyl groups in the PC [50,143].

1.3.2.3 Mechanical and thermomechanical properties

PC-nano silica prepared by melt-mixing in an internal mixer showed an increased storage modulus for lower loadings of hydrophobic silica, which contained chemically surface-bonded methyl groups [50,143]. The nanocomposites showed strongly enhanced scratch resistance, impact property and hardness. This was related to the presence of the modified silica which strengthened the material, mainly through hydrogen bonding. A similar reason was given for the increased storage modulus of the nanocomposites prepared by solution mixing [146]. However, in this case the storage modulus did not differ significantly for the samples containing modified and unmodified silica. This observation was related to the fairly strong interaction that already existed between the hydroxide groups on the silica and the carbonyl groups in PC. The volumetric strain at the cross-section where necking dominates was also studied. The results showed that the filler caused significant differences in the onset and propagation of necking, and it was related to the disruption of the molecular structure of the polymer by the filler.

1.3.3 PC-zirconia nanocomposites

1.3.3.1 Morphology

PC-zirconia nanocomposites were studied by several authors and they used TEM, SEM, FTIR and XRD to investigate the morphology [147-149]. Homogeneously dispersed nanoparticles were observed for the solution mixing prepared nanocomposites. The efficient dispersion of the nanoparticles and the absence of crystallization resulted in highly transparent nanocomposites with up to 50 wt % ZrO_2 nanoparticles. The refractive indices of the nanocomposites increased with increasing amount of nanoparticles. This was related to the efficient dispersion of the nanoparticles, which have a higher refractive index than the matrix. Xu *et al*. [148] used AFM in their study and found a marginal influence of the nanoparticles on the surface smoothness of the nanocomposites. The low surface roughness of the nanocomposite film was attributed to the homogenous dispersion and small size of the ZrO_2 nanoparticles.

1.3.3.2 Thermal properties

Only a few studies reported on the thermal characterisation of PC-ZrO_2 nanocomposites [147-149]. The TGA results of the nanocomposites showed that most of the transparent nanocomposites a higher thermal stability than the matrix polymer, although further increase of the filler content led to reduced thermal stability [147,148]. The decreased thermal stability at the higher filler content was related to the evaporation of the entrapped organic solvent and/or the unreacted monomer in the ZrO_2 agglomerates. Imai *et al*. [147] further modified the PC by sulfonic acid. The introduction of the sulfonic acid moiety reduced the thermal stability of the matrix polymer.

1.3.3.3 Mechanical and thermomechanical properties

The same researchers [147-149] reported on the mechanical and thermomechanical properties of PC and its zirconia nanocomposites**.** DMA analysis showed that both the hardness and elastic modulus increased with increasing ZrO_2 content up to 20 wt%, and this was linked to the

reinforcing role of the ZrO_2 nanoparticles. However, the hardness of the nanocomposite film decreased considerably for 25 wt% of ZrO_2. This was related to agglomeration of ZrO_2 nanoparticles in the polymer matrix.

1.3.4 PC-titania nanocomposites

1.3.4.1 Morphology

The morphology of PC-titania nanocomposites after the incorporation of low levels of filler was investigated with the help of SEM, energy dispersive X-ray (EDX), XRD, AFM and TEM [42,147,150]. The results showed that TiO_2 was well dispersed inside the matrix, with no agglomeration, even at higher contents (6-11%). Imai *et al*. [147] modified both the nanoparticles and the matrix polymer. The nanoparticle surfaces were modified with phosphoric acid 2-ethylhexyl esters, while a sulfonic acid moiety was introduced into the PC. Further dispersion of the nanoparticles and the absence of crystallization resulted in highly transparent nanocomposites with up to 42 wt% TiO_2 nanoparticles. That was attributed to the modification of the components which led to a better interfacial interaction.

In another study where the nanocomposites were prepared *via* extrusion, the fractured material showed areas of apparent densification around the notch edge [42]. These areas appeared as circular crater-like areas in the SEM photographs. EDX analysis of these areas showed an extremely high concentration of titanium dioxide at the centre of the crater. It seems as if the TiO_2 generated sites of nucleation for the growth of a densified form of PC.

1.3.4.2 Thermal properties

Not much work has been done on the thermal properties of the nanocomposites. Imai *et al*. [147] found that the presence of titania deteriorated the thermal stability of the nanocomposites. The same results were found by Gupta *et al*. [131], who related the results to a catalytic effect by the nanoparticles. Imai *et al*. [147] related the behaviour to the state of dispersion of the nanoparticles within the matrix polymer and the preparation conditions. They also investigated

the thermal degradation kinetics of the nanocomposites. Based on their calculations, they suggested that the degradation of the PC and the nanocomposites respectively followed second and first order kinetics. In the case of PC, the observations were related to crosslinking and branching resulting from the degradation. However, the observations for the PC nanocomposites were related to a predominance of chain scission.

Blackwood *et al.* [42] analysed PC-titania nanocomposites prepared by twin screw extrusion to investigate possible nucleation effects by the filler. They did, however, not observe any nucleation effect.

1.3.4.3 Mechanical and thermomechanical properties

The incorporation of titania into PC led to a reduction in the fracture energy and changes in the failure mechanism of injection molded test samples [42]. Electron microscopic examination of the fracture surfaces indicated that changes in the failure mechanism resulted from the occurrence of large areas of densified polymer around the filler particles. The densification reduced the extent of segmental motion within the polymer matrix.

Rouabah *et al.* [150] studied the effect of quenching temperature on the mechanical properties of PC-TiO_2 nanocomposites at 0 °C, at room temperature and at 40 °C. The values of density, elongation at break, modulus of elasticity and yield stress were lower after quenched at 0 °C, wereas the modulus increased for those cooled at room temperature. An increase in Izod impact strength, elongation at break, minimum density and decreased modulus were observed for quenching at 40 °C. The results were associated with the amount of free volume. For instance, in the fast cooling case, the macromolecular chains had less time to reorganize which induced an increase in the free volume that led to the observed reduced properties.

1.4 Solid state NMR investigations of polymer-filler interactions

Before 1940 studies of solid polymers had been limited to bulk mechanical techniques (tensile testing, impact testing, and DMA), from which the molecular characteristics were indirectly inferred. Only around 1970, after the introduction of neutron scattering and solid state NMR techniques, have scientists been able to directly investigate the molecular characteristics of polymers in the solid state. The NMR's advantage to measure motional frequency in different ranges makes it an excellent tool for studying molecular motions in solid polymers [151-155]. For example, previous studies, where pure PMMA, PC, polypropylene and epoxy were analysed *via* NMR, showed that spin lattice relaxation in the laboratory frame (MHz) values are particularly sensitive to side chain motions, whereas spin lattice relaxation in the rotating frame is sensitive to molecular motions that occur in the kHz range. The density of molecular motion (cross polarization) in a polymer system can be used to determine the extent of motional heterogeneity and phase separation in a polymer system.

The use of high resolution NMR in studies of polymer blends has been shown to be a valuable tool for the characterization of polymer-polymer miscibility and the forces that drive miscibility. For example, in a review article by Guo et *al*. [156] it was shown that, for polymer blends, NMR has the ability to give information on the phase diagrams, on phase separation and redissolution, kinetics, and on blends containing crystalline polymers. The development of NMR as applied in blends escalated to polymer-filler nanocomposites in recent studies, due to the ability to study the interaction at the polymer-filler interface and the effect of the interaction on the mobility of polymer chains [153-155].

Mansencal *et al.* [155] studied high resolution solid-state NMR of the carbon black filler-1,2-polybutadiene rubber interaction. They found that the presence of the nanofiller brought a reduction in the mean relaxation time, and related it to the 1,2-polybutadiene moieties' affinity towards the carbon black surface and an increase in rigidity. Gurovich *et al.* [153] made similar observations in the investigation of polyisoprene-silica composites. Saladino *et al.* [157] studied the ^{13}C cross-polarization magic-angle spinning nuclear magnetic resonance of a Ce:YAG-poly(methyl methacrylate) composite prepared by *in situ* polymerization. The presence of the

filler showed no modification in the chemical shift and increased the spin-lattice relaxation time in the rotating frame and in the laboratory frame. The increases in the values were related to the increase in polymer stiffness. However the cross-polarization time values decreased in the presence of the filler and this was related to a decrease in the dipolar interactions of the carbonyl carbon.

1.4 References

1. P.B. Willis, C. Hsieh. Space applications of polymeric materials. Jet Propulsion Laboratory. California Institute of Technology (1999).
2. M.A.C. Stuart, W.T.S. Huck, J. Genzer, M. Muller, C. Ober, M. Stamm, G.B. Sukhorukov, I. Szleifer, V.V. Tsukruk, M. Urban, F. Winnik, S. Zauscher, I. Luzinov, S. Minko. Emerging applications of stimuli-responsive polymer materials. Nature Materials 2010; 9:101-113.
   DOI: 10.1038/nmat2614
3. S. Bourbigot, S. Duquesne, C. Jama. Polymer nanocomposites: How to reach low flammability? Macromolecular Symposia 2006; 233:180-190.
   DOI: 10.1002/masy.200650123
4. V. Quaglini, P. Dubini, D. Ferroni, C. Poggi. Influence of counterface roughness on friction properties of engineering plastics for bearing applications. Materials and Design 2009; 30:1650-1658.
   DOI: 10.1016/j.matdes.2008.07.025
5. W.E. Gacitua, A.A. Ballerini, J. Zhang. Polymer nanocomposites: Synthetic and natural fillers, a review. Maderas. Cienciay Tecnología 2005; 7:159-178.
   DOI: 10.4067/S0718-221X2005000300002
6. A. Lagashetty, A. Venkataraman. Polymer nanocomposites. Resonance 2005; 10:49-60.
   DOI: 10.1080/00914031003760642
7. E. Manias, J. Zhang, J.Y. Huh, K. Manokruang, P. Songtipya, M.M.J. Gasco. Polyethylene nanocomposites heat-sealants with a versatile peelable character. Macromolecular Rapid Communications 2009; 30:17-23.
   DOI: 10.1002/marc.200800553

8. B.J. Ash, L.S. Schadler, R.W. Siegel. Glass transition behavior of alumina/ polymethylmethacrylate nanocomposites. Materials Letters 2002; 55:83-87.
DOI: 10.1016/S0167-577X (01)00626-7
9. S. Srivastava, M. Haridas, K.J. Basu. Optical properties of polymer nanocomposites. Bulletin Materials Science 2008; 31:213-217.
10. N. Hu, Z. Masunda, C. Yan, G. Yamamoto, H. Fukunaga, T. Hashida. The electrical properties of polymer nanocomposites with carbon nanotube fillers. Nanotechnology 2008; 19:1-10.
DOI: 10.1088/0957-4484/19/21/215701
11. D.R. Paul, L.M. Robeson. Polymer nanotechnology: Nanocomposites. Polymer 2008; 49:3187-3204.
DOI: 10.1016/polymer.2008.04.017
12. Y.L. Liu, C.Y. Hsu, K.Y. Hsu. Poly(methylmethacrylate)-silica nanocomposites confirmed films from surface-functionalized silica nanoparticles. Polymer 2005; 46:1851-1856.
DOI: 10.1016/j.polymer.2005.01.009
13. T. Kashiwagi, A.B. Morgan, J.M. Antonucci, M.R. Van Landingham, R.H. Harris, W.H. Awad, J.R. Shields. Thermal and flammability properties of silica-poly(methylmethacrylate) nanocomposites. Journal of Applied Polymer Science 2003; 89:2072-2078.
DOI: 10.1002/app.12307
14. P. Ruben, G.B. Javier. Structure and thermostability of PMMA in PMMA/silica nanocomposites: Effect of high-energy ball milling and the amount of nanofiller. Polymer Composites 2010; 31:1585-1592.
DOI: 10.1002/pc.20946
15. Z. Ling, L. Zhongshi, F.A. Wenjun, P. Tianyou. A novel polymethyl methacrylate (PMMA)-TiO_2 nanocomposite and its thermal and photic stability. Wuhan University Journal of Natural Sciences 2006; 11:415-418.
DOI: 10.1007/BF02832134
16. A. Anžlovar, K. Kogej, Z.C. Orel, M. Žigon. Polyol mediated nano size zinc oxide and nanocomposites with poly(methyl methacrylate). eXPRESS Polymer Letters 2011; 5:604-619.

DOI: 10.3144/expresspolymlett.2011.59

17. T. Pagnier, M. Boulova, N. Sergent, P. Bouvier, G. Lucazeau. Nanopowders and nanostructured oxides: Phase transitions and surface reactivity. Journal of Raman Spectroscopy 2007; 38:756-761.
DOI: 10.1002/jrs.1687

18. S.N. Karthick, K.V. Hemalatha, H. Seo, D. Ludeman , J.K. Kim , K. Prabakar, H.J. Kim. Titanium oxide prepared by polymer gel assisted combustion method for dye-sensitized solar cell. Current Applied Physics 2011; 11:127-130.
DOI: 10.1016/j.cap.2010.11.088

19. M.S.P. Francisco, V.R. Mastelaro. Inhibition of the anatase-rutile phase transformation with addition of CeO_2 to CuO-TiO_2 system: Raman spectroscopy, x-ray diffraction, and textural studies. Journal of Materials Chemistry 2002; 14:2514-2518.
DOI: 10.1021/cm011520b

20. H. Zhang, J.F. Banfield. Understanding polymorphic phase transformation behavior during growth of nanocrystalline aggregates: Insights from TiO_2. Journal of Materials Chemistry 2000; 104:3481-3487.
DOI: 10.1021/jp000499j

21. X. Ma, B. Zhou, Y. Deng, Y. Sheng, C. Wang, Y. Pan, Z. Wang. Study on $CaCO_3$/PMMA nanocomposites microspheres by soapless emulsion polymerization. Colloids and Surfaces A: Physicochemical and Engineering Aspects 2008; 312:190-194.
DOI: 10.1016/j.colsurfa.2007.06.058

22. L. Katsikas, M. Avramović, R.D.B. Cortés, M. Milovanović, M.T.K. Krušić, I.G. Popović. The thermal stability of poly(methyl methacrylate) prepared by RAFT polymerization. Journal of Serbian Chemical Society 2008; 73:915-921.
DOI: 10.2298/JSC0809915K

23. F. Sava, R. Cristescu, G. Socol, R. Radvan, R. Savastru, D. Savastru. Structure of bulk and thin films of poly-methylmethacrylate (PMMA) polymer prepared by pulsed laser deposition. Journal of Optoelectronics and Advanced Materials 2002; 4:965-970.
DOI: 10.1016/S0169-4332(02)01415- 0

24. M.C. Costache, D. Wang, M.J. Heidecker, E. Manias, C.A. Wilkie. The thermal degradation of poly(methyl methacrylate) nanocomposites with montmorillonite, layered

double hydroxides and carbon nanotubes. Polymers for Advanced Technologies 2006; 17:272-280.
DOI: 10.1002/pat.697

25. B.J. Ash, R.W. Siegel, L.S. Schadler. Glass-transition temperature behavior of alumina/PMMA nanocomposites. Journal of Polymer Science: Part B: Polymer Physics 2004; 42:4371-4383.
DOI: 10.1002/polb.20297
26. A. Anžlovar, K. Kogej, Z.C. Orel, M. Žigon. Polyol mediated nano size zinc oxide and nanocomposites with poly(methyl methacrylate). eXPRESS Polymer Letters 2011; 5:604-619.
DOI: 10.3144/expresspolymlett.2011.59
27. M. Sato, A. Kawata, S. Morito, Y. Sato, I. Yamaguchi. Preparation and properties of polymer/zinc oxide nanocomposites using functionalized zinc oxide quantum dots. European Polymer Journal 2008; 44:3430-3438.
DOI: 10.1016/j.eurpolymj.2008.08.014
28. G.C. Singh, N.L. Singh, D. Shah, S. Tripathi, A. Avasthi. Study of dielectrical properties of swift heavy ion induced modifications in metal oxide/PMMA nanocomposites. Microsystem Technologies 2010; 117:76-84.
DOI: 10.1080/10584587.2010.489427
29. B.J. Holland, J.N. Hay. The value and limitations of non-isothermal kinetics in the study of polymer degradation. Thermochimica Acta 2002; 388:253-273.
DOI: 10.1016/S0040-6031(02)00034-5
30. Z. Gao, T. Kaneko, D. Hou, M. Nakada. Kinetics of thermal degradation of poly(methyl methacrylate) studied with the assistance of the fractionation conversion at the maximum reaction rate. Polymer Degradation and Stability 2004; 84:399-403.
DOI: 10.1016/j.polymdegradstab.2003.11.015
31. T.L. Tsai, C.C. Lin, G.L. Guo, T.C. Chu. Chemical kinetics of polymethyl methacrylate (PMMA) decomposition assessed by a microwave-assisted digestion system. Industrial & Engineering Chemistry Research 2008; 47:2554-2560.
DOI: 10.1021/ie0714246

32. S. Liu, H. Ye, Y. Zhou, J. He, Z. Jiang, J. Zhao, X. Huang. Study on flame-retardant mechanism of polycarbonate containing sulfonate-silsesquioxane-fluoro retardants by TGA and FTIR. Polymer Degradation and Stability 2006; 91:1808-1814.
DOI: 10.1016/j.polymdegradstab.2005.11.013
33. B.N. Jang, C.A. Wilkie. The thermal degradation of bisphenol A polycarbonate in air. Thermochimica Acta 2005; 426:73-84.
DOI: 10.1016/j.tca.2004.07.023
34. B. Zhang, F.D. Blum. Thermogravimetric study of ultrathin PMMA films on silica: Effect of tacticity. Thermochimica Acta 2003; 396: 211-217.
DOI: 10.1016/s0040-6031(02)00518-X
35. R. Pantaleón, G.B. Javier. Structure and thermostability of PMMA in PMMA/silica nanocomposites: Effect of high-energy ball milling and the amount of nanofiller. Polymer Composites 2010; 31:1585-1592.
DOI: 10.1002/pc.20946
36. B.N. Jang, C.A. Wilkie. A TGA/FTIR and mass spectral study on the thermal degradation of bisphenol A polycarbonate. Polymer Degradation and Stability 2004; 86:419-430.
DOI: 10.1016/j.polymdegradstab.2004.05.009
37. A. Lagashetty, H. Vijayanand, S. Basavaraja, M.D. Bedre, A. Venkataraman. Preparation, characteristics, and thermal studies of γ-Fe_2O_3 and CuO dispersed polycarbonate nanocomposites. Journal of Thermal Analysis and Calorimetry 2010; 99:577-581.
DOI: 10.1007/s10973-009-0475-8
38. F.J. Carrión, J. Sanes, M.D. Bermudez. Influence of ZnO nanoparticles filler on the properties and wear resistance of polycarbonate. Wear 2007; 262:1504-1510.
DOI: 10.1016/j.wear.2007.01.016
39. A. Chatterjee. Effect of nanoTiO_2 addition on poly(methyl methacrylate): An exciting nanocomposite. Journal of Applied Polymer Science 2010; 116:3396-3407.
DOI: 10.1002/app.31883
40. A. Chatterjee. Properties improvement of PMMA using nano TiO_2. Journal of Applied Polymer Science 2010; 118:2890-2897.
DOI: 10.1002/app.32567

41. H. Wang, P. Xu, W. Zhong, L. Shen, Q. Du. Transparent poly(methylmethacrylate)/silica/ zirconia nanocomposites with excellent thermal stabilities. Polymer Degradation and Stability 2005; 87:319-327.
DOI: 10.1016/j.polymdegradstab.2004.08.015
42. K.M. Blackwood, R.A. Pethrick, F.I. Simpson. Titanium dioxide induced failure in polycarbonate. Journal of Materials Science 1995; 30:4435-4445.
DOI: 10.1007/BF00361529
43. F.J. Carrión, J. Sanes, M.D. Bermudez. Effect of ionic liquid on the structure and tribological properties of polycarbonate-zinc oxide nanodispersion. Materials Letters 2007; 61:4531-4535.
DOI: 10.1016/j.matlet.2007.02.044
44. Y. Bao, A.B. Pakhomov, K.M. Krishnan. A general approach to synthesis of nanoparticles with controlled morphologies and magnetic properties. Journal of Applied Physics 2005; 97:1-3.
DOI: 10.1063/1.1853991
45. J. Lodhia, G. Mandarano, N.J. Ferris, P. Eu, S.F. Cowell. Development and use of iron oxide nanoparticles (Part 1): Synthesis of iron oxide nanoparticles for MRI. Biomedical Imaging and Intervention Journal 2010; 6:1-10.
DOI: 10.2349/biij.6.2.e1
46. L. Zhou, J. Xu, X. Li, F. Wang. Metal oxide nanoparticles from inorganic sources via a simple and general method. Materials Chemistry and Physics 2006; 97:137-142.
DOI: 10.1016/j.matchemphys.2005.07.062
47. G. Oskam. Metal oxide nanoparticles: Synthesis, characterization and application. Journal of Sol-Gel Science and Technology 2006; 37:161-164.
DOI: 10.1007/s10971-005-6621-2
48. F. Bondioli, V. Cannillo, E. Fabbri, M. Messori. Preparation and characterization of epoxy resins filled with submicron spherical zirconia particles. Polymer 2006; 51:11-12.
DOI: 10.1111/j.1551-2916.2008.02666.x
49. R. Zhang, J.Y. Lee, Z.L. Liu. Pechini process-derived tin oxide and tin oxide-graphite composites for lithium-ion batteries. Journal of Power Sources 2002; 122:596-605.
DOI: 10.1016/S0378-7753(02)00483-4

50. A.S. Luyt, M. Messori, P. Fabbri, J.P. Mofokeng, R. Taurion, T. Zanasi, F. Pilati. Polycarbonate reinforced with silica nanoparticles. Polymer Bulletin 2011; 66:991-1004. DOI: 10.1007/s00289-010-0408-5
51. X. Qiu, C. Burda. Chemically synthesized nitrogen-doped metal oxide nanoparticles. Chemical Physics 2007; 339:1-10. DOI: 10.1016/j.chemphys.2007.06.039
52. L.P. Sung, S. Scierka, M.B. Anaraki, D.L. Ho. Characterization of metal-oxide nanoparticles: Synthesis and dispersion in polymeric coatings. Materials Research Society Symposium Proceedings 2003; 740:1541-1546. DOI: 10.100.2/ADP014258
53. J.P. Jolivet. S. Cassaignon, C. Chanéac, D. Chiche, O. Durupthy, D. Portehault. Design of metal oxide nanoparticles: Control of size, shape, crystalline structure and functionalization by aqueous chemistry. C.R. Chimie 2010; 13:40-51. DOI: 10.1016/j.crci.2009.09.012
54. L.S.A. Torres, L.M.L. Marin, R.E.N. Anita, G.H. Pardon, V.M. Castano. Biocompartible metal-oxide nanoparticles: Nanotechnology improvement of conventional prosthetic acrylic resins. Journal of Nanomaterials 2010; 2011:1-8. DOI: 10.1155/2011/941561
55. G.S. Rohrer. The anisotropy of metal oxide surface properties. In: D.P Woodruff (Ed.). The Chemical Physics of Solid Surfaces. Elsevier: United State of America (2007) p.485-513.
56. M.F. Garcia, J.A. Rodriguez. Metal oxide nanoparticles. http://www.bnl.gov/isd/documents.pdf (Accessed on 12 September 2012)
57. A.S. Barnard, P. Zapol. Predicting the energetics, phase stability, and morphology evolution of faceted and spherical anatase nanocrystals. Journal of Physical Chemistry 2004; 108:18435-18440. DOI: ORG/10.1021/JP0472459
58. D.R. Coronado, G.R. Gattorno, M.E.E. Pesqueira, C. Cab, R. Coss, G. Oskam. Phase-pure TiO_2 nanoparticles: Anatase, brookite and rutile. Nanotechnology 2008; 19:1-10. DOI: 10.1088/0957-4484/19/14/145605
59. K. Thamaphat, P. Limsuwan, B. Ngotawornchai. Phase characterization of TiO_2. Kasetsart Journal: Natural Science 2008; 42: 357 – 361.

DOI:10.1002/ppsc

60. A.D. Brailsford, E.M. Logothetis. Selected aspects of gas sensing. Sensors and Actuators B: Chemical 1998; 52:195-203.
DOI: 10.1016/S0925-4005(98)00273-1

61. S.I. Somov, G. Reinhardt, U. Guth, W. Göpel. Multi-electrode zirconia electrolyte amperometric sensors. Solid State Ionics 2000; 136:543-547.
DOI: 10.1016/S0167-2738(00)00412-4

62. Y.D. Tretyakov, E.A. Goodilin. Chemical principles of preparation of metal-oxide superconductor. Russian Chemical Reviews 2000; 69:1-34.
DOI: 10.1070/RC2000v069n01ABEH000526

63. G. Pacheco, J.J. Fripiat. Physical chemistry of the thermal transformation of mesoporous and microporous zirconia. The Journal of Physical Chemistry 2000; 104:11906–11911.
DOI: 10.1021/jp001455d

64. P.A. Deshpande, S. Polisetti, G. Madras. Rapid synthesis of ultrahigh adsorption capacity zirconia by a solution combustion technique. Langmuir 2011; 27: 3578-3587.
DOI: 10.1021/la104674k

65. T. Rajh, L.X. Chen, K. Lukas, T. Liu, M.C. Thurnauer, D.M. Tiede. Surface restructuring of nanoparticles: An efficient route for ligand-metal oxide crosstalk. The Journal of Physical Chemistry B 2002; 106:10543-10552.
DOI: 10.1021/jp021235v

66. P.M. Schneider, W.B. Fowler. Band structure and optical properties of silicon dioxide. Physical Review Letters 1976; 36:425-428.
DOI: 10.1103/PhysRevLett.36.425

67. N.V. Rumak, V.V. Khatko. Structure and properties of silicon dioxide thermal films. II. 110 nm thick SiO_2 films. Physica Status Solidi (A) 1984; 86:477-484.
DOI: 10.1002/pssa.2210860203

68. J.H. Anderson, G.A. Parks. The electrical conductivity of silica gel in the presence of adsorbed water. The Journal of Physical Chemistry 1998; 72:3662-3668.
DOI: 10.1021/j100856a051

69. V.G. Panteleev, N.V. Klocheva, A.V. Strui, K.S. Ramm. Mechanical properties of quartz ceramics at their service temperature. Chemistry and Materials Science 1990; 46:414-417.

DOI: 10.1007/BF00678950

70. C. Li, Brian, C. Benicewicz. Synthesis of well-defined polymer brushes grafted onto silica nanoparticles via surface reversible addition-fragmentation chain transfer polymerization. Macromolecules 2005; 38:5929-5936.
DOI: 10.1021/ma050216r

71. H. Yang, S. Zhang, W. Yang, X. Chen, Z. Zhuang, J. Xu, X. Wang. Molecularly imprinted sol-gel nanotubes membrane for biochemical separations. Journal of the American Chemical Society 2004; 126:4054-4055.
DOI: 10.1021/ja0389570

72. H. Guo, H. Qian, S. Sun, D. Sun, H. Yin, X. Cai, Z. Liu, J. Wu, T. Jiang, X. Liu. Hollow mesoporous silica nanoparticles for intracellular delivery of fluorescent dye. Chemistry Central Journal 2011; 5:1-10.
DOI: 10.1186/1752-153X-5-1

73. H.L. Castricum, A. Sah, J.A.J. Geenevasen, R. Kreiter, D.H.A. Blank, J.F. Vente, J.E. Elshof. Structure of hybrid organic–inorganic sols for the preparation of hydrothermally stable membranes. Journal of Sol-Gel Science and Technology 2008; 48:11–17.
DOI: 10.1007/s10971-008-1742-z

74. S. Choi, B. Chu, S.G. Lee, S.W. Lee, S.S. Im, S.H. Kim, J.K. Park. Titania-doped silica fibers prepared by electrospinning and sol-gel process. Journal of Sol-Gel Science and Technology 2004; 30:215-221.

75. G. Debora, G. Yoshitaka, M. Celso, C. Tania, B. Edilson. The effects of temperature of condensation on the thermal stability and morphology of 1,4-phenylenediamine-1-propylsilica xerogels. Journal of Sol-Gel Science and Technology 2005; 34: 189-195.
DOI: 10.1007/s10971-005-1365-6

76. E. Kockrick, P. Krawiec, U. Petasch, H.P. Martin, M. Herrmann, S. Kaskel. Porous CeO_x/SiC nanocomposites prepared from reverse polycarbosilane-based microemulsions. Journal of Materials Chemistry 2008; 20:77–83.
DOI: 10.1021/cm071657n

77. H.E. Nasr, W.S. Mohamed. In situ emulsion polymerization of terpolymer/montmorillonite nanocomposites using redox initiation system. Journal of American Science 2010; 6:1195-1201.

78. B. Tang, L. Yuan, T. Shi, L. Yu, Y. Zhu. Preparation of nano-sized magnetic particles from spent pickling liquors by ultrasonic-assisted chemical co-precipitation. Journal of Hazardous Materials 2009; 163:1173-1178.
DOI:10.1016/j.jhazmat.2008.07.095

79. Z. Ding, C. An, Q. Li, Z. Hou, J. Wang, H. Qi, F. Qi. Preparation of ITO nanoparticles by liquid phase coprecipitation method. Journal of Nanomaterials 2009; 2010:1-5.
DOI: 10.1155/2010/543601

80. G.E. Lascalea, D.G. Lamas, L. Pérez, E.D. Cabanillas, N.E. Walsöe de Reca. Synthesis of ZrO_2-15 mol% CeO_2 nanopowders by a pH-controlled nitrate–glycine process. Materials Letters 2004; 58:2456-2460.
DOI: 10.1016/j.matlet.2004.02.036

81. J.S. Lian, X.Y. Zhang, H.P. Zhang, Z.H. Jiang, J. Zhang. Synthesis of nanocrystalline NiO/doped CeO_2 compound powders through combustion of citrate/nitrate gel. Materials Letters 2004; 58:1183-1188.
DOI: 10.1016/j.matlet.2003.08.032

82. A.S. Mukasyan, P. Epstein, P. Dinka. Solution combustion synthesis of nanomaterials. Proceedings of the Combustion Institute 2007; 31:1789-1795.
DOI: 10.1016/j.proci.2006.07.052

83. K. Nagaveni, G. Sivalingam, M.S. Hegde, G. Madras. Solar photocatalytic degradation of dyes: High activity of combustion synthesized nano TiO_2. Applied Catalysis B: Environmental 2004; 48:83-93.
DOI: 10.1016/j.apcatb.2003.09.013

84. H. Hassan. Synthesis of titanium carbide by the combustion of TiO_2-2Mg-C and 3TiO_2-4Al-3C systems in a tubular furnace. Iranian Journal of Chemistry & Chemical Engineering 2009; 28:1-6.
DOI: 1021-9986/09/1/71

85. Q. Xia, Z. Si, Z. Yu, G. Qiu. Sol-gel auto-combustion synthesis of samarium-doped TiO_2 nanoparticles and their photocatalytic activity under visible light irradiation. Materials Science and Engineering B 2007; 137:189-194.
DOI: 10.1016/j.mseb.2006.11.011

86. M.M. Demir, M. Memesa, P. Castignolles, G. Wegner. PMMA/zinc oxide nanocomposites prepared by in-situ bulk polymerization. Macromolecular Rapid Communications 2006; 27:763–770.
DOI: 10.1002/marc.200500870

87. S. Ahmad, S. Ahmad, S.A. Agnihotry. Synthesis and characterization of in situ prepared poly(methyl methacrylate) nanocomposites. Bulletin of Materials Science 2007; 30:31-35.
DOI: 10.1007/s12034-007-0006-9

88. S. Schlabach, R. Ochs, T. Hanemann, D.V. Szabo. Nanoparticles in polymer-matrix composites. Microsystem Technologies 2011; 17:183-193.
DOI: 10.1007/s00542-010-1176-8

89. M. Agrawal, S. Gupta, N.E. Zafeiropoulos, U. Oertel, R. Häßler, M. Stamm. Nano-level mixing of ZnO into poly(methyl methacrylate). Macromolecular Chemistry and Physics 2010; 211:1925-1932.
DOI: 10.1002/macp.201000191

90. J.L.H. Chau, C.C. Hsieh, Y.M. Lin, A.K. Li. Preparation of transparent silica-PMMA nanocomposites hard coatings. Progress in Organic Coatings 2008; 62:436-439.
DOI: 10.1016/j.porgcoat.2008.02.005

91. C. Barthet, A.J. Hickey, D.B. Cairns, S.P. Armes. Synthesis of novel polymer-silica colloidal nanocomposites via free-radical polymerization of vinyl monomers. Advanced Materials 1999; 11:408-410.
DOI: 10.1002/(SICI)1521-4095(199903)11:5<408::AID-ADMA408>3.0.CO;2-Y

92. X.L. Xie, Q.X. Liu, R.K.Y. Li, X.P. Zhou, Q.X. Zhang, Z.Z. Yu, Y.W. Mai. Rheological and mechanical properties of PVC/$CaCO_3$ nanocomposites prepared by *in situ* polymerization. Polymer 2004; 45:6665-6673.
DOI: 10.1016/j.polymer.2004.07.045

93. T. Mizetani, K. Arai, M. Miyamoto, Y. Kimura. Preparation of spherical nanocomposites consisting of silica core and polyacrylate shell by emulsion polymerization. Journal of Applied Science 2006; 99:659–669.
DOI: 10.1002/app.22503

94. F. Yang, R. Yngard, A. Hernberg, G.L. Nelson. Thermal stability and flammability of polymer-silica nanocomposites prepared via extrusion. ACS Symposium Series 2005; 922:144-154.
DOI: 10.1021/bk-2006-0922.ch012

95. F. Yang, G.L. Nelson. Polymer/silica nanocomposites prepared via extrusion. Polymers for Advanced Technologies 2006; 17:320-326.
DOI: 10.1002/pat.695

96. H.P. Fu, R.Y. Hong, Y.J. Zhang, H.Z. Li, B. Xu, Y. Zheng, D.G. Wei. Preparation and properties investigation of PMMA/silica composites derived from silicic acid. Polymers for Advanced Technologies 2009; 20:84-91.
DOI: 10.1002/pat.1226

97. Y.H. Hu, C.Y. Chen, C.C. Wang. Viscoelastic properties and thermal degradation kinetics of silica/PMMA nanocomposites. Polymer Degradation and Stability 2004; 84:545-553.
DOI: 10.1016/j.polymdegradstab.2004.02.001

98. X. Ding, Z. Wang, D. Han, Y. Zhang, Y. Shen, Z. Wang, L. Niu. An effective approach to synthesis of poly(methyl methacrylate)/silica nanocomposites. Nanotechnology 2006; 17:4796-4801.
DOI: 10.1088/0957-4484/17/19/002

99. S. Etienne, C. Becker, D. Ruch, B. Grignard, G. Cartigny, C. Detrembleur, C. Calberg, R. Jerome. Effects of incorporation of modified silica nanoparticles on the mechanical and thermal properties of PMMA. Journal of Thermal Analysis and Calorimetry 2007; 87:101-104.
DOI: 10.1007/s10973-006-7827-4

100. J.M. Yeh, C.J. Weng, K.Y. Huang, C.C. Lin. Effect of baking treatment and material composition on the properties of bulky PMMA-silica hybrid sol-gel material with low volume shrinkage. Journal of Applied Science 2006; 101:1151-1159.
DOI: 10.1002/app.24211

101. R. Saito, S. Kobayashi, T. Shimo, H. Hayashi. Surface hardness of organic polymer-silica nanocomposites prepared with perhydropolysilazane. Proceedings of the 8th Polymer for Advanced Technologies International Symposium, Budapest, Hungary (2005).

102. C. Hub, S.E. Harton, M.A. Hunt, R. Fink, H. Ade. Influence of sample preparation and processing on observed glass transition temperatures of polymer nanocomposites. Journal of Polymer Science: Part B: Polymer Physics 2007; 45:2270-2276.
DOI: 10.1002/polb.21249

103. Y. Kobayashi, Y.W.M. Sarata, H. Hamada, K. Yamada, M. Kotaki, K. Yoshinaga, H. Karakawa, H. Ito, K. Kamaza, T. Kikutani. Mechanical and thermal properties of micro- and nano-silica-filled PMMA micro injection moldings. 16th International Conference on Composite Materials, Kyoto, Japan (2007).

104. J.G. Benito, D. Olmos. Efficient dispersion of nanoparticles in thermoplastic polymers. Society of Plastics Engineers 2010; 41:1-3.
DOI: 10.1002/spepro.002566

105. J.G. Benito, G.G. Gaitano. Interfacial conformations and molecular structure of PMMA in PMMA/silica nanocomposites. Effect of high-energy ball milling. Macromolecules 2008; 41:4777-4785.
DOI: 10.1021/ma800260k

106. M.C. Li, X. Deng, U.R. Cho. Study on the structure, thermal properties, and mechanical properties of PMMA-grafted SBR/clay nanocomposites. Journal of Composite Materials 2010; 44:1279-1288.
DOI: 10.1177/0021998309353964

107. C.K. Chana, S.L. Peng, I.M. Chua, S.C. Ni. Effects of heat treatment on the properties of poly(methyl methacrylate)/silica hybrid materials prepared by sol-gel process. Polymer 2001; 42:4189-4196.
DOI: 10.1016/s0032-3861(00)00817-x

108. P.D. Castrillo, D. Olmos, D.R. Amador, J. González-Benito. Real dispersion of isolated fumed silica nanoparticles in highly filled PMMA prepared by high energy ball milling. Journal of Colloid and Interface Science 2007; 308:318–324.
DOI: 10.1016/j.jcis.2007.01.022

109. Y. Fu, Q.Q. Ni, K. Ken, I. Masaharu. Development of PMMA/silica hybrid and its material properties. Journal of Society of Material Science 2003; 52:992-997.
DOI: 10.1016/S0032-3861(00)00817-X

110. F.A. Zhang, D.K. Lee, T.J. Pinnavaia. PMMA–mesocellular foam silica nanocomposites prepared through batch emulsion polymerization and compression molding. Polymer 2009; 50:4768-4774.
DOI: 10.1016/j.polymer.2009.08.007

111. F.A. Zhang, D.K. Lee, T.J. Pinnavaia. PMMA/mesoporous silica nanocomposites: Effect of framework structure and pore size on thermomechanical properties. Polymer Chemistry 2010; 1:107-113.
DOI: 10.1039/b9py00232d

112. Y. Hu, S. Zhou, L. Wu. Surface mechanical properties of transparent poly(methyl methacrylate)/zirconia nanocomposites prepared by in situ bulk polymerization. Polymer 2009; 50:3609-3616.
DOI: 10.1016/j.polymer.2009.03.02

113. Y. Wang, D. Zhang, L. Shi, L. Li, J. Zhang. Novel transparent ternary nanocomposites films of trialkoxysilane-capped poly(methyl methacrylate)/zirconia/titania with incorporating networks. Materials Chemistry and Physics 2008; 110:463-470.
DOI:10.1016/jmetchemphys.2008.03.006

114. M. Atik, F.P. Luna, S.H. Messaddeq, M.A. Aegerter. Ormocer (ZrO_2-PMMA) films for stainless steel corrosion protection. Journal of Sol-Gel Science and Technology 1997; 8:517-522.
DOI: 10.1007/bf02436892

115. Y. Hu, G. Gu, S. Zhou, L. Wu. Preparation and properties of transparent PMMA/ZrO_2 nanocomposites using 2-hydroxyethyl methacraylate as a coupling agent. Polymer 2011; 52:122-129.
DOI: 101016/j.polymer.2010.11.020

116. S.H. Messaddeq, S.H. Pulcinelli, C.V. Santilli, A.C. Guastaldi, Y. Massaddeq. Macrostructure and corrosion resistance of inorganic-organic (ZrO_2-PMMA) hybrid coating on stainless steel. Journal of Non-Crystalliane Solids 1999; 247:164-170. DOI: 10.1016/S0022-3093(99)00058-7

117. X. Wang, L. Wu, J. Li. Influence of nanozirconia on the thermal stability of poly(methyl methacrylate) prepared by in situ bulk polymerization. Journal of Applied Polymer Science 2010; 117:163-170.

DOI 10.1002/app.31970

118. L. Shang, M. Liu, D. Tu, G. Liu, X. Liu, Z. Ji. Low -voltage organic-field-effect transistor with PMMA/ZrO_2 bilayer dielectric. IEEE Transactions on Electron Devices 2009; 56:370-376.
DOI: 10.1016/j.eurpolymj.2006.12.012
119. X. Wang, L. Wu, J. Li. Synergistic flame retarded poly(methyl methacrylate) by nano-ZrO_2 and triphenylphosphate. Journal of Thermal Analysis and Calorimetry 2011; 103:741-746.
DOI: 10.1007/s10973-010-1050-z
120. E. Džunuzović, M.M. Cincović, J. Vuković, K. Jeremić, J.M. Nedeljković. Thermal properties of PMMA/TiO_2 nanocomposites prepared by *in-situ* bulk polymerization. Polymer Composites 2009; 30:737-742.
DOI: 10.1002/pc.20606
121. E. Džunuzović, K. Jeremić, J.M. Nedeljković. In situ radical polymerization of methyl methacrylate in a solution of surface modified TiO_2 and nanoparticles. European Polymer Journal 2007; 43:3719-3726.
DOI: 10.1016/j.eurpolymer.2007.06.026
122. B. Hojjati, P.A. Charpentier. Synthesis and kinetics of graft polymerization of methyl methacrylate from the RAFT coordinated surface of nano-TiO_2. Journal of Polymer Science: Part A: Polymer Chemistry 2008; 46:3926-3937.
DOI: 10.1002/pola.22724
123. S. Yamada, E. Mouri, K. Yoshinaga. Incorporation of titanium dioxide particles into polymer matrix using block copolymer micelles for fabrication of high refractive and transparent organic-inorganic hybrid materials. Journal of Polymer Science: Part A: Polymer Chemistry 2011; 49:712-718.
DOI:10.1002/pola.24483
124. M. Inkyo, Y. Tokunaga, T. Tahara, T. Iwaki, F. Iskandar, C.J. Hogan, K. Okuyama. Beads mill-assisted synthesis of polymethyl methacrylate (PMMA)-TiO_2 nanoparticle composites. Industrial and Engineering Chemistry Research 2008; 47:2597-2604.
DOI:10.1021/ie07069j

125. A. Laachachi, M. Ferriol, M. Cochez, D. Ruch, J.M.L. Cuesta. The catalytic role of oxide in the thermooxidative degradation of poly(methyl methacrylate)-TiO_2 nanocomposites. Polymer Degradation and Stability 2008; 93:1131-1137.
DOI: 10.1016/j.polymdegradstab.2008.03.006

126. S.M. Khaled, R. Sui, P.A. Charpentier, A.S. Rizkalla. Synthesis of TiO_2-PMMA nanocomposites: Using methacrylic acid as a coupling agent. Langmuir 2007; 23:3988-3995.
DOI: 10.1021/la062879n

127. L.M. Hamming, R. Qiao, P.B. Messersmith, L.C. Brinson. Effect of dispersion and interfacial modification on the macroscale properties of TiO_2 polymer-matrix nanocomposites. Composites Science and Technology 2009; 69:1880-1886.
DOI: 10.1016/j.compositech.2009.04.005

128. J.M. Yeh, C.J. Weng, K.Y. Huang, H.Y. Huang, Y.H. Yu, C.H. Yin. Thermal and optical properties of PMMA-titania hybrid materials prepared by sol-gel approach with HEMA as coupling agent. Journal of Applied Polymer Science 2004; 94:400-405.
DOI: 10.1002/app.20909

129. X. Sun, X. Chen, X. Liu, S. Qu. Optical properties of poly(methyl methacrylate)-titania nanostructure thin films containing ellipsoid-shaped titania nanoparticles from ex-situ sol-gel method at low growth temperature. Applied Physics B 2010; 103:391-398.
DOI: 10.1007/s00340-010-4265-6

130. R. Zong, Y. Hu, N. Liu, S. Wang, G. Liao. Evaluation of the thermal degradation of PC/ABS/montmorillonite nanocomposite. Polymers for Advanced Technologies 2005; 16:725-731.
DOI: 10.1002/pat.51

131. M.C. Gupta, S.G. Viswanath. Role of metal oxide in the thermal degradation of bisphenol A polycarbonate. Journal of Thermal Analysis 1996; 46:1671-1679.
DOI: 10.1021/ie9700167

132. H. Polli, L.A.M. Pontes, A.S. Araujo. Application of model-free kinetics to the study of thermal degradation of polycarbonate. Journal of Thermal Analysis and Calorimetry 2005; 79:383-387.
DOI: 10.1007/s10973-005-0070-6

133. X.G. Li, M.R. Huang. Thermal degradation of bisphenol A polycarbonate by high-resolution thermogravimetry. Polymer International 1999; 48:387-391.
DOI: 10.1002/(sici)1097-0126(199905)

134. Q. Dong, C. Gao, Y. Ding, F. Wang, B. Wen, S. Zhang, T. Wang, M. Yang. A polycarbonate/magnesium oxide nanocomposite with high flame retardancy. Journal of Applied Polymer Science 2011; 123:1085-1093.
DOI: 10.1002/app.34574

135. Q. Dong, C. Gao, Y. Ding, F. Wang, B. Wen, S. Zhang, T. Wang, M. Yang. Thermal properties and flame retardancy of polycarbonate/hydroxyapatite nanocomposite. Journal of Applied Polymer Science 2008; 109:659-663.
DOI: 10.1002/app.28053

136. C. Montaudo, S. Carroccio, C. Puglisi. Thermal and thermooxidative degradation process in poly(bisphenol A carbonate). Journal of Analytical and Applied Pyrolysis 2002; 64:229-247.
DOI: 10.1016/s0165-2370(02)00034-7

137. C. Montaudo, S. Carroccio, C. Puglisi. Mechanism of thermal oxidation of poly(bisphenol A carbonate). Macromolecules 2002; 35:4297-4305.
DOI: 10.1021/ma012077

138. K. Oba, H. Ohtani, S. Tsuge. Confirmation of the xanthone structure in thermally treated polycarbonates by reactive pyrolysis-gas chromatography/mass spectrometry. Polymer Degradation and Stability 2001; 74:171-176.
DOI:10.1016/S0141-3910(01)00153-7

139. A. Davis, J.H. Golden. Thermal degradation of polycarbonate. Journal of the Chemistry Society (B) 1968; 180:45-47.
DOI: 10.1039/j29680000045

140. I.C. McNeill. Degradation studies of some polyesters and polycarbonates: 3-Polyglycollide. Polymer Degradation and Stability 1985; 12:373-385.
DOI:10.1016/0141-3910(85)90127-2

141. B.M. Dolores, B.W.C. Vilches, F.S. José. Scratch resistance of polycarbonate containing ZnO nanoparticles: Effect of sliding direction. Journal of Nanoscience and Nanotechnology 2010; 10:6683-6689.

DOI: 10.1166/jnn.2010.2513

142. J.L.H. Chau, S.L.C. Hsu, Y.M. Chen, C.C. Yang, P.C.F. Hsu. A simple route towards polycarbonate-silica nanocomposites. Advanced Powder Technology 2010; 21:341-343.
DOI: 10.1016/j.apt.2010.02.005
143. A. Christman, P. Lenny, J.C. Quantin, A.S. Caro-Bretelle, J.M.L. Cuesta. Mechanical behavior at large strain of polycarbonate nanocomposites during uniaxial tensile test. Journal of the European Ceramic Society 2011; 52:4033-4044.
DOI: 10.106/j.polymer.2011.06.056
144. C.S. Tan, T.W. Kuo. Synthesis of polycarbonate-silica nanocomposites from copolymerization of CO_2 with allyl glycidyl ether, cyclohexene oxide, and sol-gel. Journal of Applied Polymer Science 2005; 98:750-757.
DOI: 10.1002/app.22126
145. N. Suzuki, Y. Yamauchi. Fabrication of mesostructured silica titania rods on substrates by using polycarbonate membranes. Journal of Nanomaterials 2010; 2010:1-4.
DOI: 10.1155/2010/382043
146. R. Poręba, M. Špírková, Z. Hrdlička. Mechanical and thermochemical properties of polycarbonate-based polyurethane-silica nanocomposites. Processing and Application of Ceramics 2011; 5:155-159.
DOI: 10.10Sl/jp4:20030687
147. Y. Imai, A. Terahara, Y. Hakuta, K. Matsui, H. Hayashi, N. Ueno. Transparent poly(bisphenol A carbonate)-based nanocomposites with high refractive index nanoparticles. European Polymer Journal 2009; 45:630-638.
DOI: 10.1016/J.europolyj.2008.12.013
148. K. Xu, S. Zhou, L. Wu. Effect of highly dispersible zirconia nanoparticles on the properties of UV-curable poly(urethane-acrylate) coatings. Journal of Materials Science 2009; 44:1613-1621.
DOI: 10.1007/s10853-008-3231-8
149. K. Luo, S. Zhou, L. Wu, B. You. Preparation and properties of cross-linked zirconia nanoparticles films on polycarbonate. Thin Solid Films 2010; 518: 6804-6810.
DOI: 10.1016/j.tsf.2010.06.035

150. F. Rouabah, M. Fois, L. Ibos, A. Boudenne, D. Dadache, N. Haddaoui, P. Ausset. Mechanical and thermal properties of polycarbonate. II. Influence of titanium dioxide content and quenching on pigmented polycarbonate. Journal of Applied Polymer Science 2007; 106:2710-2717.
DOI: 10.1002/app.26807

151. A.A. Parker. Soild state NMR of polymers: A review of molecular motions and morphology. Consulting and Product Development 2004; 1-24.

152. W. Kolodziejski, A. Corma, K. Wozniak, J. Klinowski. ^{13}C-^{1}H cross-polarization NMR in solid at natural ^{13}C abundance. Journal of Physical Chemistry 1996; 100:7345-7351.
DOI:10.1021/jp953750h

153. D. Gurovich, C.W. Macosko, M. Tirrell. The influence of filler-filler and filler-polymer interaction on the physical properties of silica-filled liquid polyisoprene. Rubber Chemistry and Technology 2003; 76:1-12.
DOI: http://dx.doi.org/10.5254/1.3538492

154. D.G. Cory, W.M. Ritchey. Inversion recovery cross-polarization NMR in solid semicrystalline polymers. Macromolecules 1989; 22:1611-1615.
DOI: 10.1021/ma00194a018

155. R. Mansencal, B. Haidar, A. Vidal, L. Delmotte, J.M. Chezeau. High resolution solid-state NMR investigation of the filler-rubber interaction: 2. High-speed [^{1}H] magic-angle spinning NMR spectroscopy in carbon-black-filled polybutadiene. Polymer International 2001; 50:387-394.
DOI:10.1002/pi.640/pdf

156. M. Guo. Solid-state high resolution NMR on miscibility of polymer blends. Trip 1996; 4:238-244.

Chapter 2

The effect of silica nanoparticles on the morphology, mechanical properties and thermal degradation kinetics of PMMA

This chapter has been published as:

(1) M.L. Saladino, T.E. Motaung, A.S. Luyt, A. Spinella, G. Nasillo, E. Caponetti. The effect of silica nanoparticles on the morphology, mechanical properties and thermal degradation kinetics of PMMA. Polymer Degradation and Stability 2012; 97:452-459

(2) M.L. Saladino, T.E. Motaung, A.S. Luyt, A. Spinella, G. Nasillo, E. Caponetti. Corrigendum to "The effect of silica nanoparticles on the morphology, mechanical properties and thermal degradation kinetics of PMMA. Polymer Degradation and Stability 2012; 97:2477.

Abstract

Silica-PMMA nanocomposites with different silica quantities were prepared by a melt compounding method. The effect of silica amount, in the range 1-5 wt.%, on the morphology, mechanical properties and thermal degradation kinetics of PMMA was investigated by means of transmission electron microscopy (TEM), X-ray diffractometry (XRD), dynamic mechanical analysis (DMA), thermogravimetric analyses (TGA), Fourier-transform infrared spectroscopy (FTIR), ^{13}C cross-polarization magic-angle spinning nuclear magnetic resonance spectroscopy ($^{13}C\{^{1}H\}$CP-MASNMR) and measures of proton spin-lattice relaxation time in the rotating frame ($T_{1\rho}(H)$), in the laboratory frame ($T_1(H)$) and cross polarization times (T_{CH}). Results showed that silica nanoparticles are well dispersed in the polymeric matrix whose structure remains amorphous. The degradation of the polymer occurs at higher temperature in the presence of silica because of the interaction between the two components.

Keywords: PMMA; silica; $^{13}C\{^{1}H\}$CP-MAS NMR; degradation kinetics.

2.1 Introduction

The use of inorganic nanoparticles as additives to improve polymer performance has received industrial and academic interest in recent years. Among the nanocomposite materials, one of the most widely studied is silica-poly(methylmethacrylate) (PMMA) because of its optical and mechanical properties [1-5]. In fact, the silica nanoparticles incorporated into the polymer matrix can improve the strength, the abrasion-resistance and the ageing-resistance of the polymer. The nanocomposite properties are strongly dependent on "molecular" properties, and in particular on the nature and dimensions of the organic–inorganic interfaces, on the mechanisms of interaction between the organic and inorganic components, and on the structural and dynamic properties of either the organic or inorganic phases. However, the incomplete condensation and poor thermal stability of PMMA has a negative influence on the optical and thermal properties of the composites, even if properties like the surface hardness increases with an increase in the amount of silica [4].

Several methods have been used to prepare nanocomposites: solution mixing, physical mixing, *in situ* polymerization and single screw extrusion [6-8]. Ma *et al.* [9] prepared polyacrylate–silica nanocomposites by a sol–gel process *via in situ* emulsion polymerization. Yu *et al.* [10] synthesized surface-modified silica particles and copolymerized the obtained nanoparticles with MMA monomers. Freris e*t al.* [11] performed the polymer encapsulation of submicrometer-sized silica particles by the synthesis of the polymer shell, poly(methyl methacrylate), under static conditions in a reaction medium free of surfactants and stabilizing agents. Preparation of SiO_2-PMMA nanocomposites *via in situ* emulsion polymerization in the presence of an initiator was investigated [12-15]. It was found that the presence of silica retarded the thermal decomposition of the polymer chains, which was related to the large silica surface area, to radicals probably trapped by silica during degradation and to uncondensed residue of the precursor which needed a large amount of heat to decompose. The storage and loss modulus, glass transition temperature (T_g) and activation energy of all the composites increased with the amount of silica. An increase in the thermal stability and activation energy with chain length of the organic molecules was observed when organically modified silica was used [15]. However, the opposite trend where the presence of silica in PMMA did not enhance the thermal stability was also observed [16,17].

Some authors, studying the thermal degradation kinetics, have reported that the addition of silica could also lead to a decreased activation energy of degradation [18].

An improvement in thermal stability with an increase in silica content was observed in silica-PMMA nanocomposites prepared by using single-screw extrusion [19,20]. The nanocomposites showed significant improvement in the mechanical performance and thermal stabilities, although they were not strictly flame retardant when subjected to fire tests like limiting oxygen index or horizontal Bunsen burner tests.

The purpose of this study was to prepare silica-PMMA nanocomposites through a melt compounding method by using chemically modified SiO_2 nanoparticles. Both nanoparticles and composites were characterized using transmission electron microscopy (TEM), X-ray diffractometry (XRD), dynamic mechanical analysis (DMA) thermogravimetric analyses (TGA), FT-IR spectroscopy and ^{13}C cross-polarization magic-angle spinning nuclear magnetic resonance ($^{13}C\{^{1}H\}$ CP-MAS NMR) and measures of proton spin-lattice relaxation time in the rotating frame ($T_{1\rho}(H)$), in the laboratory frame ($T_1(H)$) and cross polarization times (T_{CH}). The effect of the presence and amount of silica nanoparticles on the thermal and mechanical properties and on thermal degradation kinetics of the PMMA will be discussed.

2.2 Experimental

2.2.1 Materials

AEROSIL® R972 (R972, Degussa, Germany) is a hydrophobic silica having chemically surface bonded methyl groups, based on a hydrophilic fumed silica with a specific surface area of 130 $m^2\ g^{-1}$ and an average primary particle size of 16 nm. Silica was dried at 120 °C under static vacuum for a minimum of 16 hours before further use.

Commercial grade poly(methyl methacrylate) (PMMA, Altuglas® V920T) produced by Bayer Materials Science, Italy and having a melt flow rate at 230 °C/3.8 kg of 1g/10 min, and an M_w =

350 000, was used in pellet form. The polymer was dried at 120 °C overnight under static vacuum before processing.

2.2.2 Preparation of composites

PMMA was thoroughly mixed with 1, 2 and 5 wt.% silica for 10 min at 200 °C and 30 rpm in the 50 mL internal mixer of a Brabender Plastograph from Duisburg, Germany. The mixed samples were melt-pressed into 1 mm thick sheets at 200 °C for 5 min.

2.2.3 Analysis methods

Transmission electron microscopy (TEM) micrographs were acquired by using a JEM-2100 (JEOL, Japan) electron microscope, equipped with an X-ray energy dispersive spectrometer (EDS, Oxford, model INCA ENERGY-200T) for analysis of elements, operating at a 200 kV accelerating voltage. A few tens of a milligram of the powders were dispersed in 2 mL of isopropanol and a small drop of the dispersion was deposited on a 300 mesh carbon-coated copper grid, which was introduced into the TEM analysis chamber after complete solvent evaporation. Thin nanocomposite samples of about 50 nm in thickness were cutted using a Leica EM UC6 ultramicrotome equipped with a Leica EMFC6 cryocamera and a diamond blade. The thin samples thus obtained were deposited onto the cupper grids.

The dynamic mechanical analysis (DMA) of the blends and composites were investigated from 40 to 180 ºC in the bending mode at a heating rate of 5 ºC min^{-1} and a frequency of 1 Hz using a Perkin Elmer Diamond DMA from Waltham, Massachusetts, U.S.A.

Thermogravimetric analysis (TGA) was performed in a Perkin Elmer TGA7 from Waltham, Massachusetts, U.S.A. The analyses were done under flowing nitrogen at a constant flow rate of 20 mL min^{-1}. Samples (5-10 mg) were heated from 25 to 600 °C at different heating rates. The degradation kinetic analysis was done using the following two methods:

Ozawa-Flynn-Wall method

This is a conversional linear method based on the equation:

$$\ln \beta = c - 1.052 \frac{E_a}{RT} \qquad (1)$$

where $\ln \beta$ = heating rate in K min^{-1}, T = temperature in K, E_a = activation energy in kJ mol^{-1}, and R = universal gas constant. The plot $\log \beta$ vs. $\frac{1}{T}$, obtained from TGA curves recorded at several heating rates, should be a straight line. The activation energy can be evaluated from its slope.

Kissinger-Akahira-Sunose method

$$\ln(\frac{\beta}{T^2}) = \ln(\frac{AR}{E_a \bullet g(\alpha)}) - \frac{E_a}{RT} \qquad (2)$$

where α = fraction of conversion, A = pre-exponential factor and $g(\alpha)$ = algebraic expression for integral methods. From the TGA curves recorded at different heating rates β, temperatures T were determined at the conversions α = 10% ~ 90%. The activation energies were calculated from the slope of the straight lines $\ln(\frac{\beta}{T^2})$ versus $\frac{1}{T}$.

The thermogravimetric analysis-Fourier-transform infrared (TGA-FTIR) analyses were performed in a Perkin Elmer STA6000 simultaneous thermal analyser from Waltham, Massachusetts, U.S.A. The analyses were done under flowing nitrogen at a constant flow rate of 20 mL min^{-1}. Samples (20-25 mg) were heated from 30 to 600 °C at 10° C min^{-1} and held for 4 min at 600 °C. The furnace was linked to the FTIR (Perkin Elmer Spectrum 100, Massachusetts, U.S.A.) with a gas transfer line. The volatiles were scanned over a 400 – 4000 cm^{-1} wavenumber range at a resolution of 4 cm^{-1}. The FTIR spectra were recorded in the transmittance mode at different temperatures during the thermal degradation process.

X-ray powder diffraction (XRD) patterns were recorded in the 2-70° 2θ range at steps of 0.05° and a counting time of 5 s/step on a Philips PW 1050 diffractometer, equipped with a Cu tube and a scintillation detector beam. The X-ray generator worked at 40 kV and 30 mA. The

instrument resolution (divergent and antiscatter slits of 0.5°) was determined using standards free from the effect of reduced crystallite size and lattice defects.

The $^{13}C\{^{1}H\}$ CP-MAS NMR spectra were obtained at room temperature with a Bruker Avance II 400 MHz (9.4 T) spectrometer operating at 100.63 MHz for the ^{13}C nucleus with a MAS rate of 13 kHz, 400 scans, a contact time of 1.5 s and a repetition delay of 2 sec. The optimization of the Hartmann-Hahn condition [21] was obtained using an adamantine sample. Each sample was placed in a 4 mm zirconia rotor with KEL-F cap using silica as filler to avoid inhomogeneities inside the rotor. The proton spin–lattice relaxation time in the rotating frame $T_{1\rho}(H)$ was indirectly determined, with the variable spin lock (VSL) pulse sequence, by the carbon nucleus observation using a 90°–τ–spin-lock pulse sequence prior to cross-polarization [22]. The data acquisition was performed by ^{1}H decoupling with spin lock durations, τ, ranging from 0.1 to 7.5 ms and a contact time of 1.5 ms. The T_{CH} values for all carbon signals of PMMA were obtained through variable contact time (VCT) experiments [23]. The contact times used in the VCT experiments were 0.05, 0.1, 0.2, 0.3, 0.4, 0.5, 0.6, 0.8, 1.0, 1.2, 1.5, 2.0, 2.5, 3.0, 3.5, 4.0, 4.5, 5.0, 6.0 and 7.0 ms. The proton spin–lattice relaxation time in the laboratory frame $T_1(H)$ was determined, with the saturation recovery pulse sequence [24], by the carbon nucleus observation using a 90°–τ–90° pulse sequence prior to cross polarization with a delay time τ ranging from 0.01 to 3 s.

2.3 Results and discussion

The TEM micrographs of the SiO_2 powder are shown in Figure 2.1. Aggregates of size between 1 and 3 μm and composed by a large number of nanoparticles (more than 500) of rounded morphology are observed. The histogram, also shown in Figure 2.1, was obtained after analysing several micrographs and depicts a relatively uniform and narrow particle size distribution which mean size is 20 nm.

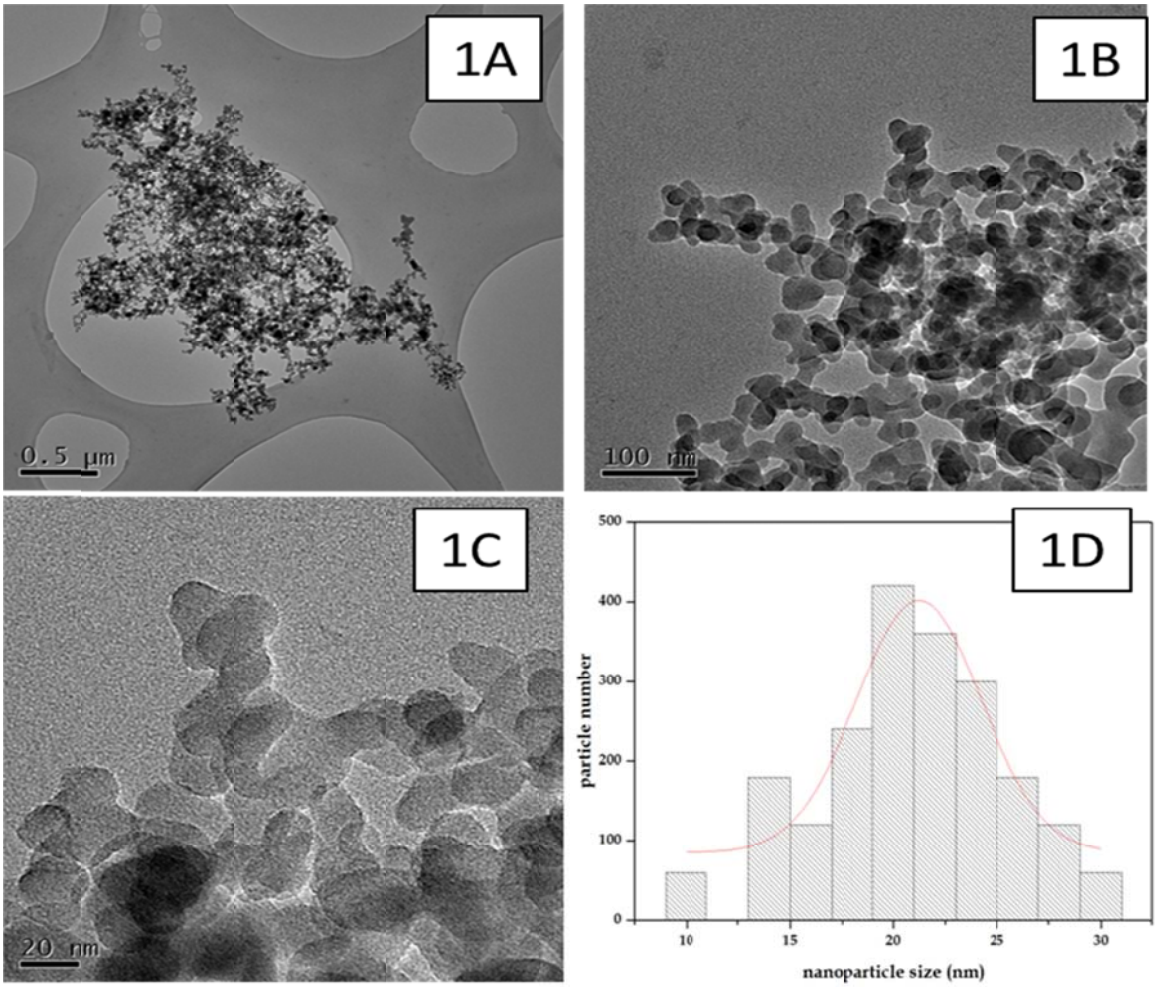

Figure 2.1 TEM micrographs of the SiO_2 powder. A careful statistical analysis of the particle size (histogram) supplies an average value of 20 nm

The TEM micrographs of the PMMA-silica composite having 5 wt.% of SiO2 are shown in Figure 2.2. The SiO_2 particles maintain the same mean size of those of the powder. They form clusters uniformly dispersed in the composite. Each aggregate is constituted by ca 20 nanoparticles.

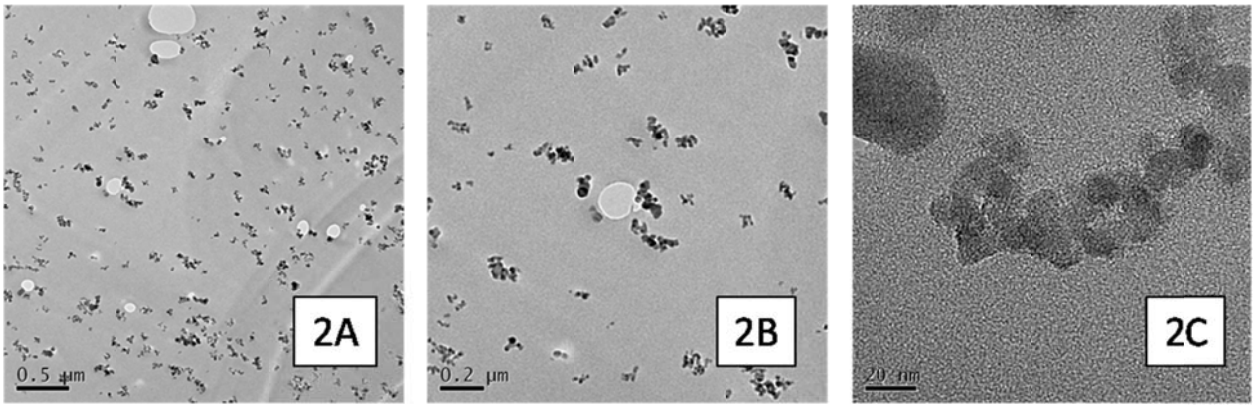

Figure 2.2 TEM micrographs of silica-PMMA composite having 5 wt.% of SiO_2

The storage modulus of the pure PMMA and of PMMA-silica composites having 1, 2 and 5 wt.% of SiO_2 are reported in Figure 2.3A. Below the glass transition temperature the storage modulus of all the nanocomposites is lower than that of PMMA, probably because of a plasticizing effect of the silica nanoparticles on the PMMA matrix. Above the glass transition temperature the 1 and 2% silica containing nanocomposites still have storage moduli below that of PMMA, but the 5% containing nanocomposite has higher storage modulus values. It seems as if effective immobilization of the polymer chains only takes place at the higher silica quantities. The loss modulus of the composites, shown in Figure 2.3B, follows the same trend as the storage modulus. In this case, however, the glass transition temperatures for both the 2% and 5% silica containing composites are higher than that of pure PMMA, indicating that effective immobilization already starts when 2% nanoparticles are introduced into the polymer. The tan δ curves, shown in Figure 2.3C, confirm the observation from the loss modulus curves.

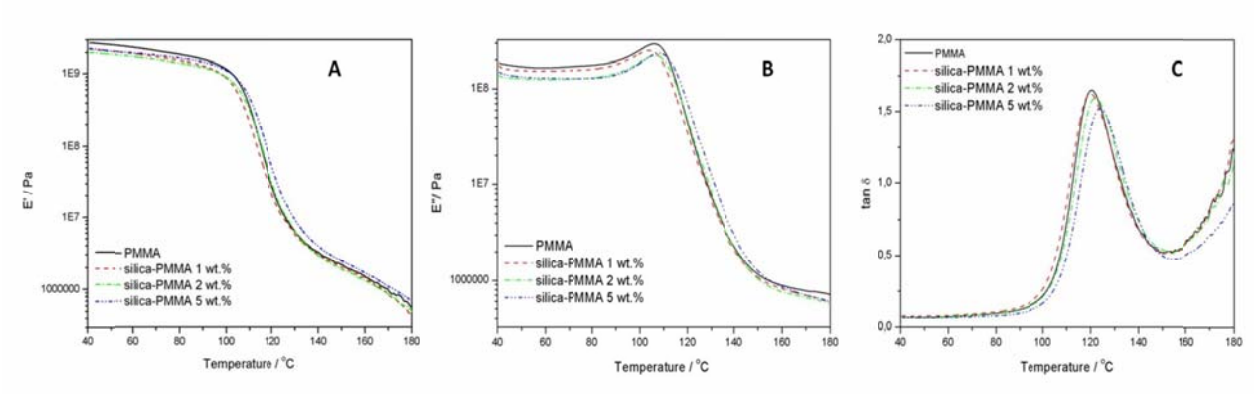

Figure 2.3 (A) Storage modulus, (B) loss modulus and (C) tan δ curves of PMMA and silica-PMMA nanocomposites

The TGA curves of the pure PMMA and of PMMA-silica composites having 1, 2 and 5 wt.% of SiO_2 performed at a heating rate of 10 ºC min^{-1} are reported in Figure 2.4. All the samples show a single-step degradation, and this degradation step clearly moves to higher temperatures with increasing silica amount, with that for the 5% silica containing sample significantly (about 10 °C) higher than those for the other samples.

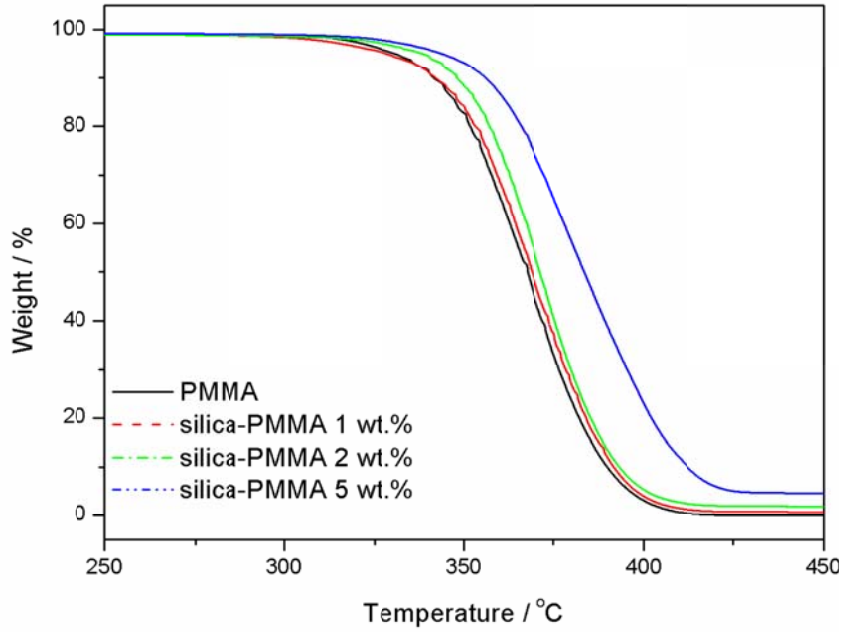

Figure 2.4 TGA curves of PMMA and the silica-PMMA nanocomposites, recorded at a heating rate of 10 ºC min^{-1}

The most commonly used approaches to determine the apparent kinetic parameters are the Ozawa-Flynn-Wall (OFW) and the Freidman and Kissinger-Akahira-Sunose (KAS) methods for polymer degradation [25-27]. Burnham *et al.* [28] recommend the KAS method for accuracy of activation energy values. In this work the KAS and OFW methods were used. From the dynamic TGA curves of PMMA, PMMA-silika (2 and 5 wt.%) at heating rates of 3, 5, 7 and 9 °C min^{-1} the isoconversional graphs of ln β *versus* 1/*T* according to Equation 1 were plotted (Figures 2.5 and 2.6), as well as ln (β/T^2) *versus* 1/T according to Equation 2 (Figures 2.7 and 2.8).

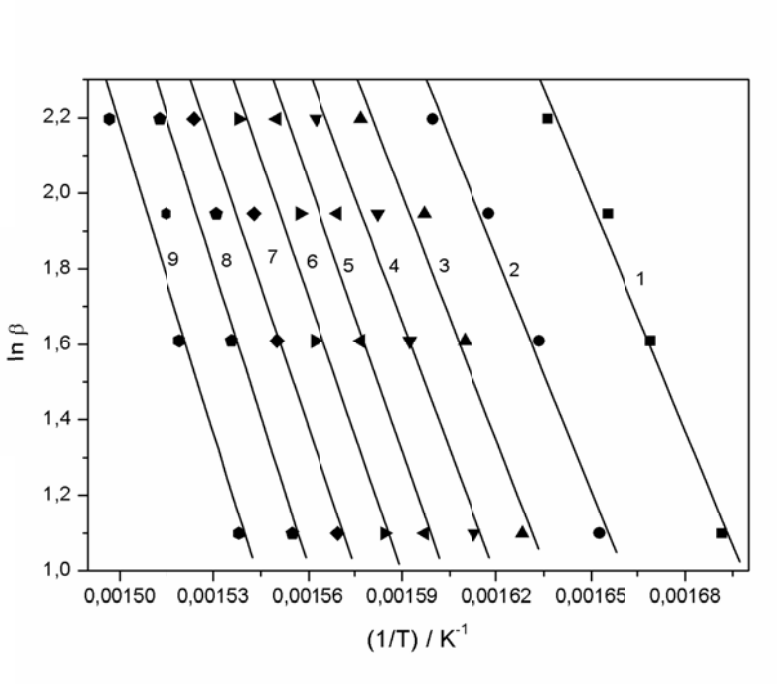

Figure 2.5 Ozawa –Flynn-Wall plots for PMMA for the following degrees of conversion: 1) α = 0.1, 2) α = 0.2, 3) α = 0.3, 4) α = 0.4, 5) α = 0.5, 6) α = 0.6, 7) α = 0.7, 8) α = 0.8, 9) α = 0.9

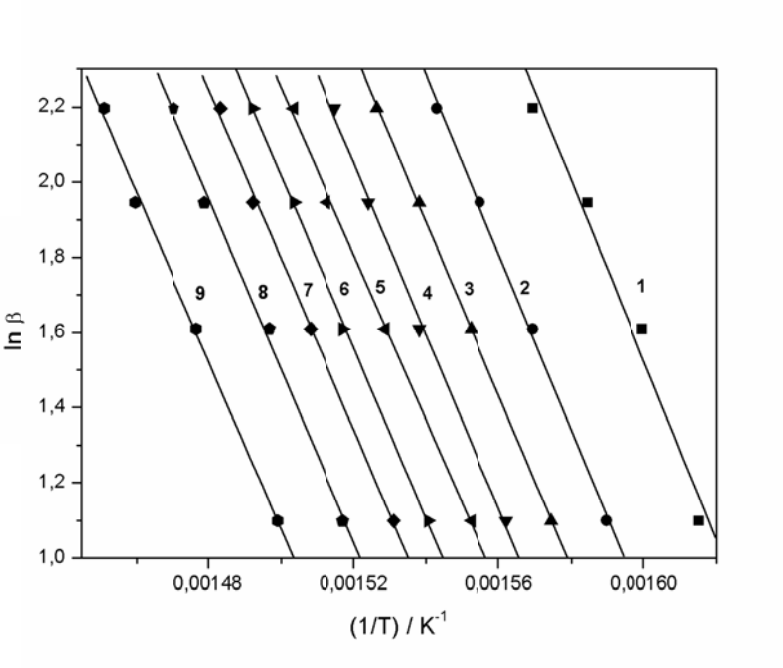

Figure 2.6 Ozawa –Flynn-Wall plots for PMMA-SiO_2 (5 wt.%) for the following degrees of conversion: 1) α = 0.1, 2) α = 0.2, 3) α = 0.3, 4) α = 0.4, 5) α = 0.5, 6) α = 0.6, 7) α = 0.7, 8) α = 0.8, 9) α = 0.9

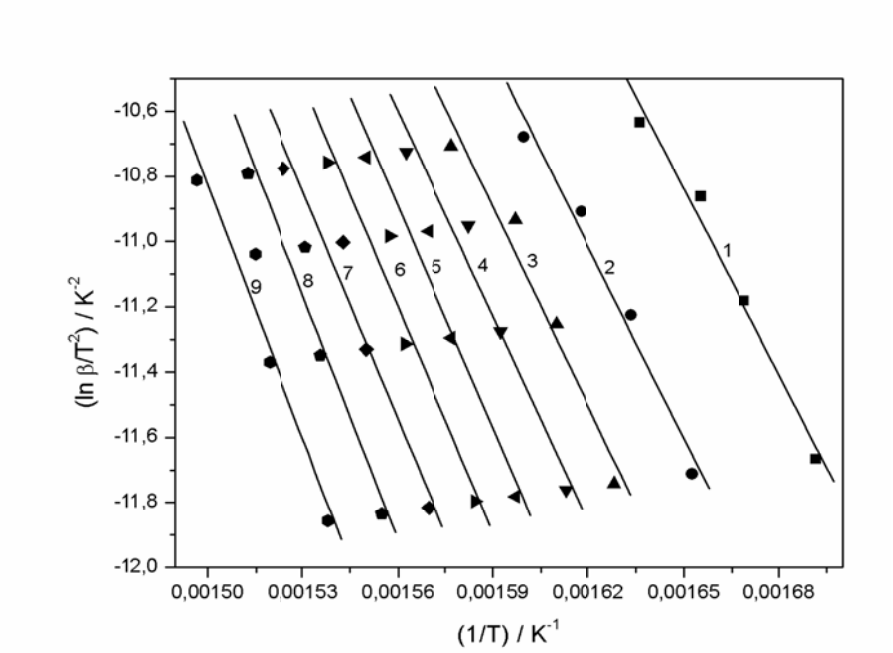

Figure 2.7 Kissinger-Akahira-Sunose plots for PMMA for the following degrees of conversion: 1) α = 0.1, 2) α = 0.2, 3) α = 0.3, 4) α = 0.4, 5) α = 0.5, 6) α = 0.6, 7) α = 0.7, 8) α = 0.8, 9) α = 0.9

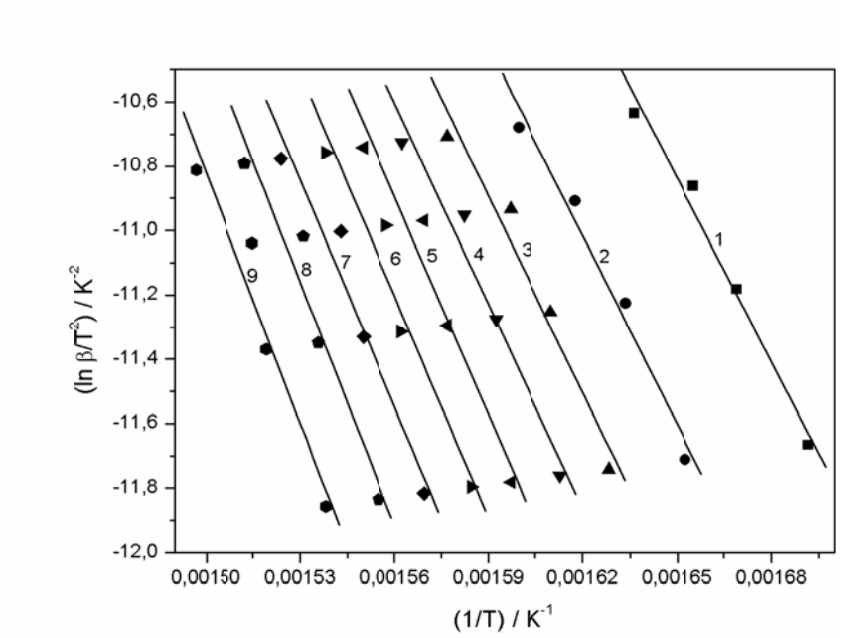

Figure 2.8 Kissinger-Akahira-Sunose plots for PMMA-silica (5 wt.%) for the following degrees of conversion: 1) α = 0.1, 2) α = 0.2, 3) α = 0.3, 4) α = 0.4, 5) α = 0.5, 6) α = 0.6, 7) α = 0.7, 8) α = 0.8, 9) α = 0.9

The activation energy values were calculated from the slopes of the isoconversional plots. Both isoconversional methods give similar values of the activation energies within experimental uncertainty. Figure 2.9 illustrates the relationship between the activation energies and the degree of conversion. The activation energies of degradation of PMMA increased with an increase in the degree of conversion, while those of PMMA-silica (5 wt.%) decreased. The PMMA-silica (5 wt.%) shows higher activation energies of degradation up to around 40% mass loss (Figure 2.9), while at higher degrees of conversion those of PMMA-silica (5 wt.%) are lower. In the case of pure PMMA the increase in activation energy has been explained by Gao *et al.* [28] as a change in degradation mechanism from unzipping to random chain scission. In the presence of the nanoparticles, however, the activation energies of degradation at lower degrees of conversion are significantly higher than those of pure PMMA, and these activation energies slightly decrease with increasing degree of conversion and were lower than those for pure PMMA at degrees of conversion above 0.4. It is possible that strong interaction between PMMA and the silica nanoparticles retarded the diffusion of the volatile degradation products from the sample, which led to unnaturally high activation energy values at low degrees of conversion. According to several authors [28-32], the presence of silica seems to catalyze the degradation process by giving an alternative degradation route. In the presence of silica, certain intermediates are apparently formed with increasing α, that decompose first and require a lower E_a. This is an acceptable explanation for our own observations at higher degrees of conversion.

TGA-FTIR analyses were done to establish the nature of the degradation product(s), and to confirm the observations from the kinetic analysis of the thermal degradation process of PMMA and PMMA-silica (5 wt.%). Figure 2.10 shows the FTIR spectra of the degradation products of pure PMMA at different temperatures during the degradation process.

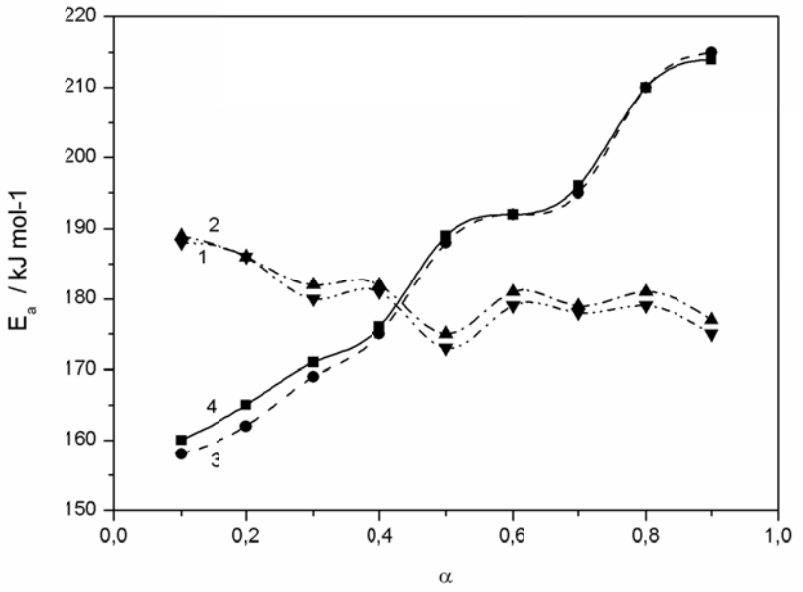

Figure 2.9 E_a values obtained by the OFW and KAS methods: (1) PMMA (KAS), (2) PMMA (OFW), (3) PMMA-silica (5 wt.%) (KAS), (4) PMMA-silica (5 wt.%) (OFW)

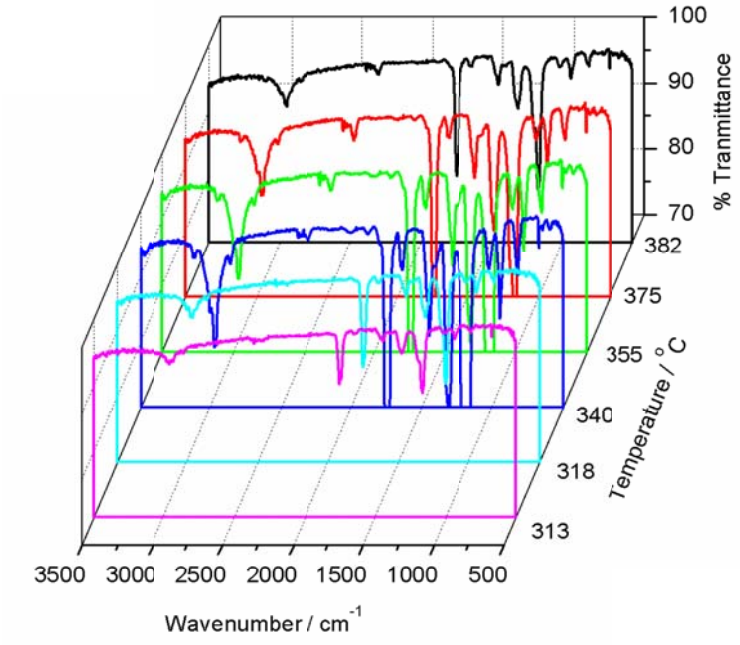

Figure 2.10 FTIR curves at different temperatures during the thermal degradation of PMMA in a TGA at a heating rate of 10 °C min^{-1}

All the spectra almost perfectly match the known spectrum of methyl metacrylate (MMA), which confirms the primary degradation as that of de-polymerization. The peak around 2966 cm^{-1} is assigned to the CH_3 and CH_2 stretching vibrations, whereas their bending vibration appeared around 1451 cm^{-1} for CH_2 and 1314 cm^{-1} for CH_3. In addition, the carbonyl absorption vibration appeared around 1744 cm^{-1} and the stretching vibration for C-O was around 1167 cm^{-1}. No new peaks or peak shifts were observed for the nanocomposite samples. There is a clear increase in peak intensity for all the characteristic peaks with increasing temperature, it reaches a maximum, and decreases again with further increase in temperature. The PMMA-silica (5 wt.%) sample shows the same spectra and a similar trend (Figure 2.11).

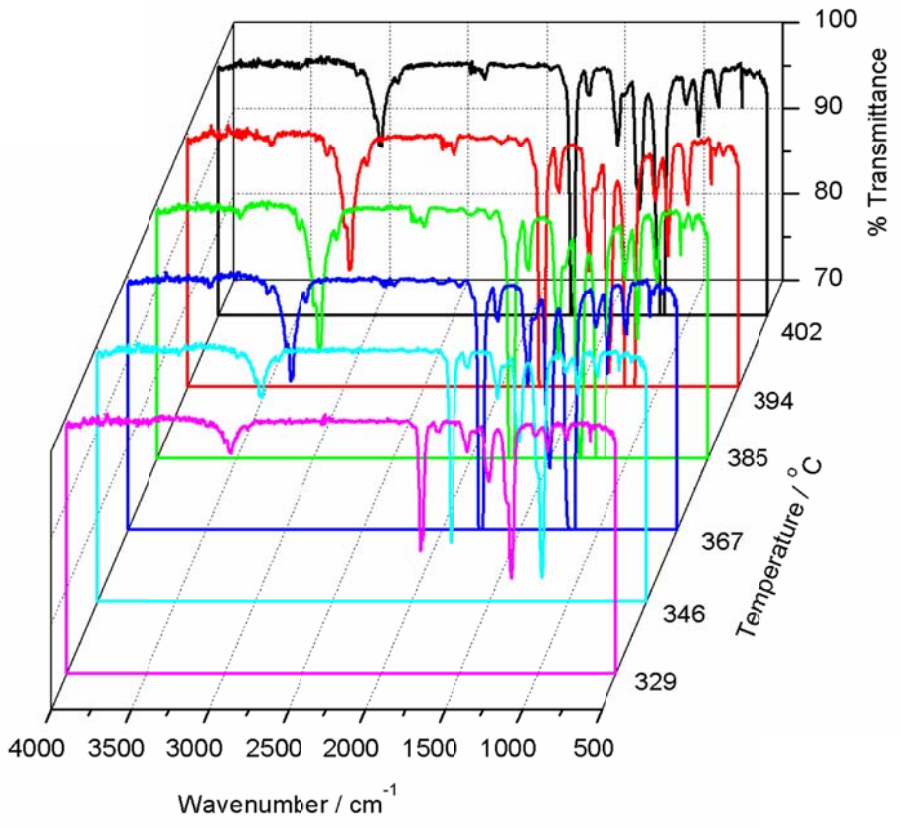

Figure 2.11 FTIR curves at different temperatures during the thermal degradation of PMMA-silica (5 wt.%) in a TGA at a heating rate of 10 °C min^{-1}

When the spectra of PMMA, PMMA-silica (2 and 5 wt.%), obtained at the same temperature, are compared (Figure 2.12), it is clear that there is a decrease in peak intensity with increasing

amount of silica. Although the presence of silica nanoparticles clearly did not change the degradation mechanism, it clearly had an influence on either the temperature range during which depolymerisation occurs, and/or on the ease with which the volatile MMA monomer is released during the degradation process. Whatever the reason for the delayed mass loss, the interaction between PMMA or MMA and the silica nanoparticles could play a significant role in changing the degradation kinetics.

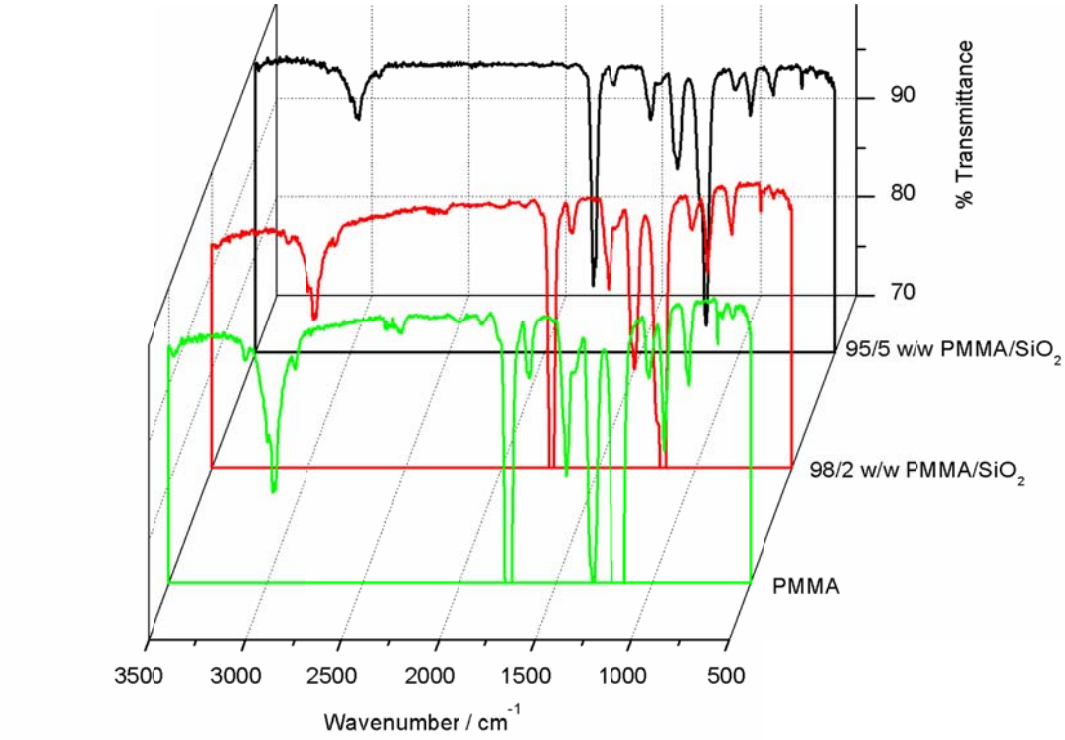

Figure 2.12 FTIR curves obtained at 340 °C during the degradation of PMMA and PMMA-silica (2 and 5 wt.%) in a TGA at a heating rate of 10 °C min^{-1}

Thus, XRD and ^{13}C {^{1}H} CP-MAS NMR measurements were performed in order to attempt a correlation between the mechanical properties and the structure of the nanocomposites. The XRD patterns of the silica powder, pure PMMA and the silica-PMMA (5 wt.%) are shown in Figure 2.13. The diffraction pattern of silica powder shows a broad band around 2θ = 21.2, typical of an amorphous material. The diffraction pattern of PMMA shows a broad diffraction

peak at 2θ = 14, typical of an amorphous material, together with two bands of lower intensities centred at 29.7 and 41.7 [33]. The diffraction pattern of the PMMA-silica (5 wt.%) sample shows the same three bands observed in the pure PMMA, indicating that neither the orientation of the PMMA chains nor the amorphous structure of the silica was influenced during the preparation process.

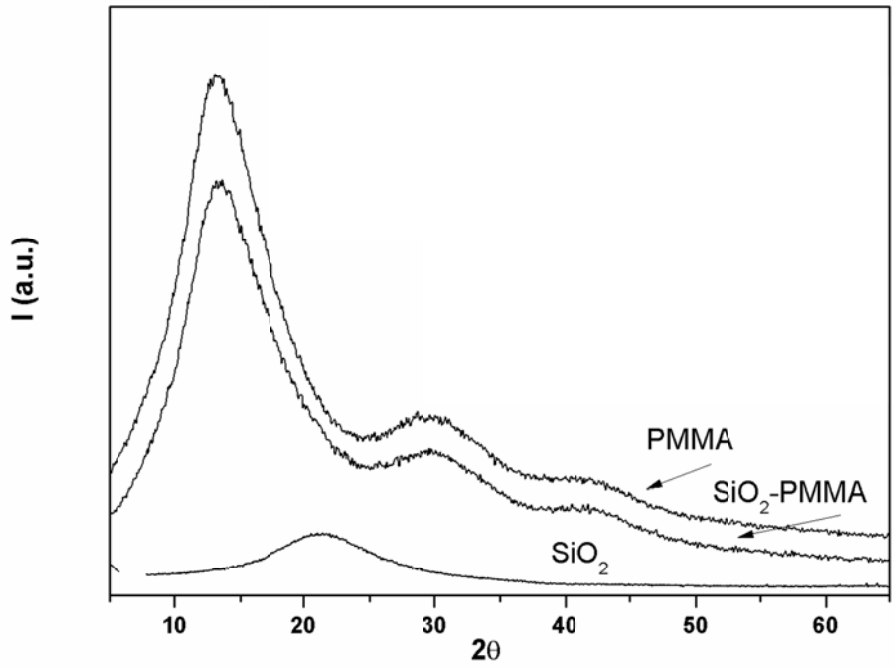

Figure 2.13 XRD patterns of silica powder, pure PMMA and the PMMA-silica (5 wt.%) nanocomposite

However, detailed information on the physical-chemical environment of each component (nanoparticles and polymer) could not be obtained by the above experiment. To gain insight into the organization of the polymer molecules in contact with the nanoparticle surface, ^{13}C $\{^{1}H\}$ CP-MAS NMR experiments were performed. The ^{13}C $\{^{1}H\}$ CP-MAS NMR spectra of PMMA and of the PMMA-silica (5 wt.%) are shown in Figure 2.14. Five peaks are present in all the spectra: peak 1 at 17 ppm is related to the methyl group, peak 2 at 45 ppm to the methylene group, peak 3 at 52 ppm to the quaternary carbon of the polymeric chain, peak 4 at 56 ppm to the methoxyl group and peak 5 at 177 ppm to the carbonyl carbon, according to literature [34]. No

modification in the chemical shift and in the band shape is observed after composite formation, indicating that no chemical modification occurred in the polymer.

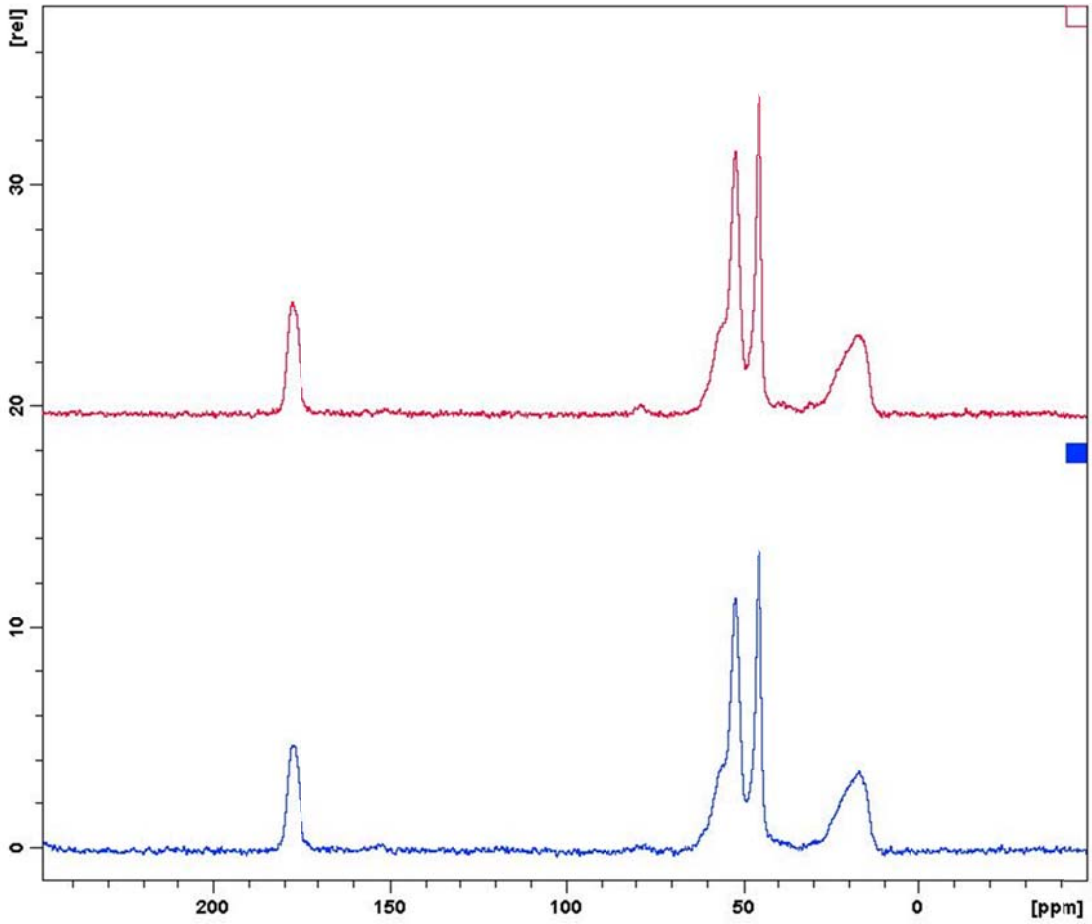

Figure 2.14 ^{13}C {^{1}H} CP-MAS NMR spectra of PMMA (lower spectrum) and of PMMA-silica (5 wt.%) (upper spectrum).

Thus, the spin-lattice relaxation time, in the laboratory frame $T_1(H)$ and in the rotating frame $T_{1\rho}(H)$, and the cross-polarization time T_{CH} were determined through solid-state NMR measurements in order to evaluate the dynamic modifications occurring in the polymeric chain of the PMMA matrix after composite formation. The $T_1(H)$, $T_{1\rho}(H)$, and T_{CH} values obtained from each peak in the ^{13}C spectra of all the samples are reported in Table 2.1.

Table 2.1 Relaxation time values for all the peaks in the ^{13}C spectra of PMMA and of the PMMA-silica (5 wt.%) nanocomposite

ppm	PMMA			PMMA-silica (5 wt.%)		
	T_1H (s)	$T_{1\rho}H$ (ms)	T_{CH} (µs)	T_1H (s)	$T_{1\rho}H$ (ms)	T_{CH} (µs)
178	0.70 ± 0.02	18.1 ± 0.5	1306 ± 167	0.76 ± 0.03	22.9 ± 0.8	1080 ± 95
56	0.71 ± 0.03	20.4 ± 0.9	254 ± 79	0.75 ± 0.05	23.0 ± 1.0	236 ± 41
52	0.71 ± 0.01	16.2 ± 0.2	339 ± 42	0.70 ± 0.01	19.1 ± 0.2	319 ± 30
45	0.71 ± 0.01	17.0 ± 0.2	614 ± 33	0.69 ± 0.01	19.5 ± 0.3	401 ± 25
17	0.71 ± 0.01	19.3 ± 0.4	320 ± 36	0.73 ± 0.03	22.9 ± 0.3	305 ± 24

The PMMA-silica composite shows larger T_1H values for the carbonyl carbon. This is evidence that the interaction between the silica filler and the polymer matrix is principally localized in this nucleus environment. The $T_{1\rho}$ is sensitive to molecular motions which occur in the kHz region. In particular, it is inversely proportional to the spectral density of motion in the kHz frequency region. These motions reflect the dynamic behaviour of a polymeric chain in a range of a few nanometres. Larger $T_{1\rho}$ values result in an increase in polymer rigidity. A homogeneous $T_{1\rho}H$ increase was observed for the PMMA-silica composite, suggesting an increase of the polymer stiffness and that the silica is well dispersed into the PMMA matrix, thus confirming that the filler has an observable effect on the polymer chain mobility.

The T_{CH} value decrease for the signal at 178 ppm indicates that there is an increase in the heteronuclear dipolar interactions between the carbonyl carbon and the surrounding hydrogen nuclei. This is an evidence that the presence of the silica into the PMMA matrix makes the polymer structure more rigid. This rigidity increase favours the cross polarization mechanism yielding shorter T_{CH} values. The interactions between silica and PMMA led to a restriction of the PMMA chain mobility, and/or hindering of the diffusion of volatile decomposition products as hypothesized by the DMA and TGA measurements.

2.4 Conclusions

PMMA-silica nanocomposites were prepared by melt compounding and were systematically investigated as a function of silica amount from 1 to 5 wt.%. The silica is well dispersed into the PMMA matrix and does not change the amorphous structure of PMMA. The filler has an observable effect on the polymer chain mobility, even if the effective immobilization of the polymer chains only takes place at the higher silica contents. The nanoparticles act as catalysts of the degradation process, but do not change the polymerization mechanism. The degradation of the polymer occurs at higher temperatures in the presence of silica and moves to higher temperature with increasing silica content. This is due to the interaction between the two components which occurred at the interface through the carbonylic groups of the polymer, as proven by solid-state NMR measurements.

2.5 References

1. F. Yang, G.L. Nelson. PMMA/silica nanocomposites studies: Synthesis and properties. Journal of Applied Polymer Science 2004; 91:3844-3850.
   DOI: 10.1002/app.13573
2. A.Z. Muhammad, A.W. Muhammad, N. Hilal. Preparation and characterization of novel porous PMMA-SiO_2 hybrid membranes. Desalination 2006; 192:262-270.
   DOI: 10.1016/j.desal.2005.09.022
3. Y.H. Hu, C.Y. Chen, C.C. Wang. Viscoelastic properties and thermal degradation kinetics of silica/PMMA nanocomposites. Polymer Degradation and Stability 2004; 84:545-553.
   DOI:10.1016/j.polymdegradstab.2004.02.001
4. N. García, T. Corrales, J. Guzmán, P. Tiemblo. Understanding the role of nanosilica particle surfaces in the thermal degradation of nanosilica–poly(methyl methacrylate) solution-blended nanocomposites: From low to high silica concentration. Polymer Degradation and Stability 2007, 92: 635-643.
   DOI: 10.1016/j.polymdegradstab.2007.01.006
5. N. Cinausero, N. Azema, J.-M. Lopez-Cuesta, M. Cochez, M. Ferriol. Synergistic effect between hydrophobic oxide nanoparticles and ammonium polyphosphate on fire properties

of poly(methyl methacrylate) and polystyrene. Polymer Degradation and Stability 2011; 96:1445:1454
DOI:10.1016/j.polymdegradstab.2011.05.008

6. C. Barthet, A.J. Hickey, D.B. Cairns, S.P. Armes. Synthesis of novel polymer-silica colloidal nanocomposites via free-radical polymerization of vinyl monomers. Advanced Materials 1999; 11:408-410.
DOI: 10.1002/(SICI)1521-4095(199903)11:5<408::AID-ADMA408>3.0.CO;2-Y
7. X.L. Xie, Q.X. Liu, R.K.Y. Li, X.P. Zhou, Q.X. Zhang, Z.Z. Yu, Y.W. Mai. Rheological and mechanical properties of PVC/$CaCO_3$ nanocomposites prepared by *in situ* polymerization. Polymer 2004; 45:6665-6673.
DOI:10.1016/j.polymer.2004.07.045
8. T. Mizutani, K. Arai, M. Miyamoto, Y. Kimura. Preparation of spherical nanocomposites consisting of silica core and polyacrylate shell by emulsion polymerization. Journal of Applied Polymer Science 2006; 99:659–669.
DOI: 10.1002/app.22503
9. J.Z. Ma, J. Hu, Z.J. Zhang. Polyacrylate/silica nanocomposites materials prepared by sol-gel process. European Polymer Journal 2007; 43: 4169–4177.
DOI:10.1016/j.eurpolymj.2007.06.051
10. Y.Y. Yu, C.Y. Chen, W.C. Chen. Synthesis and characterization of organic-inorganic hybrid thin films from poly(acrylic) and monodispersed colloidal silica. Polymer 2003; 44:593-601.
DOI: 10.1016/S0032-3861(02)00824-8
11. I. Freris, D. Cristofori, P. Riello, A. Benedetti. Encapsulation of submicrometer-sized silica particles by a thin shell of poly(methyl methacrylate). Journal of Colloid and Interface Science 2009; 331:351-355.
DOI:10.1016/j.jcis.2008.11.052
12. X. Ding, Z. Wang, D. Han, Y. Zhang, Y. Shen, Z. Wang, L. Niu. An effective approach to synthesis of poly(methyl methacrylate)/silica nanocomposites. Nanotechnology 2006; 17:4796-4801.
DOI:10.1088/0957-4484/17/19/002

13. F.P. Viras, X. Li, T.A. King. Thermal analysis of PMMA/gel silica glass composites. Journal of Sol-Gel Science and Technology 1996; 7:203-209.
DOI:10.1007/BF00401038
14. H.P. Fu, R.Y. Hong, Y.J. Zhang, H.Z. Li, B. Xu, Y. Zheng, D.G. Wei. Preparation and properties investigation of PMMA/silica composites derived from silicic acid. Polymers for Advanced Technologies 2009; 20:84-91.
DOI:10.1002/pat.1226
15. Y.H. Hu, C.Y. Chen, C.C. Wang. Viscoelastic properties and thermal degradation kinetics of silica/PMMA nanocomposites. Polymer Degradation and Stability 2004; 84:545-553.
DOI:10.1016/j.polymdegradstab.2004.02.001
16. Y.L. Liu, C.Y. Hsu, K.Y. Hsu. Poly(methyl methacrylate)-silica nanocomposites films from surface-functionalized silica nanoparticles. Polymer 2005; 46:1851-1856.
DOI:10.1016/j.polymer.2005.01.009
17. T. Kashiwagi, A.B. Morgan, J.M. Antonucci, M.R. Van Landingham, R.H. Harris, Jr., W.H. Awad, J.R. Shields. Thermal and flammability properties of a silica-poly(methyl methacrylate) nanocomposite. Journal of Applied Polymer Science 2003; 89:2072-2078.
DOI:10.1002/app.12307
18. P. Ruben, G.B. Javier. Structure and thermostability of PMMA in PMMA/silica nanocomposites: Effect of high-energy ball milling and the amount of nanofiller. Polymer Composites 2010; 31:1585-1592.
DOI:10.1002/pc.20946
19. F. Yang, R. Yngard, A. Hernberg, G.L. Nelson. Thermal stability and flammability of polymer-silica nanocomposites prepared via extrusion. ACS symposium Series 2005; 922:144-154.
DOI: 10.1021/bk-2006-0922.ch012
20. F. Yang, G. L. Nelson. Polymer/silica nanocomposites prepared via extrusion. Polymers for Advanced Technologies 2006; 17: 320-326.
DOI: 10.1002/pat.695
21. S.R. Hartmann, E.L. Hahn. Nuclear double resonance in the rotating frame. Physical Review Online Archive 1962; 128:2042-2053.
DOI: 10.1103/PhysRev.128.2042

22. C. Lau, Y. Mi. A study of blending and complexation of poly(acrylic acid)/poly(vinyl pyrrolidone). Polymer 2002; 43:823-829.
DOI: 10.1016/S0032-3861(01)00641-3

23. P. Conte, R. Spaccini, A. Piccolo. State of art of CPMAS ^{13}C-NMR spectroscopy applied to natural organic matter. Progress in Nuclear Magnetic Resonance Spectroscopy 2004; 44:215-223.
DOI:10.1016/j.pnmrs.2004.02.002

24. R.G. Alamo, J.A. Blanco, I. Carrilero. Measurement of the ^{13}C spin-lattice relaxation time of the non-crystalline regions of semicrystalline polymers by a CP-MAS-based method. Polymer 2002; 43:1857-1865.
DOI: 10.1016/S0032-3861(01)00761-3

25. H. Wang, X. Tao, E. Newton. Thermal degradation kinetics and lifetime prediction of a luminescent conducting polymer. Polymer International 2004; 53:20-26.
DOI:10.1002/Pi.1279

26. W. Kim, S.D. Kim, S.B. Lee, I.K. Hong. Kinetic characterization of thermal degradation process for commercial rubbers. Journal of Industrial and Engineering Chemistry 2000; 6:348-355.

27. K. Chrissafis. Kinetics of thermal degradation of polymers. Journal of Thermal Analysis and Calorimetry 2009; 95: 273-283.
DOI: 10.1007/s10973-008-9041-z

28. Z. Gao, T. Kaneko, D. Hou. M. Nakada. Kinetics of thermal degradation of poly(methyl methacrylate) studied with the assistance of the fractionation conversion at the maximum reaction rate. Polymer Degradation and Stability 2004; 84: 399-403.
DOI:10.1016/j.polymdegradstab.2003.11.015.

29. S. Vyazovkin, A.K. Burnham, J.M. Criado, L.A.P. Maqueda, C. Popescu, N. Sbirrazzuoli. ICTAC Kinetics Committee recommendations for performing kinetic computations on thermal analysis data. Thermochimica Acta 2011;520:1-19.
DOI:10.1016/j.tca.2011.03.034

30. B.J. Holland, J.N. Hay. The value and limitations of non-isothermal kinetics in the study of polymer degradation. Thermochimica Acta 2002; 253-273.
DOI: 10.1016/S0040-6031(02)00034-5

31. P.K. Roy, P. Surekha, C. Rajagopal, V. Chouldhary. Thermal degradation studies of LDPE containing cobalt stearate as pro-oxidant. eXPRESS Polymer Letters 2007; 1:208-216. DOI:10.3144/expresspolymlett.2007.32

32. S. Vyazovkin. A unified approach to kinetic processing of nonisothermal data. International Journal of Chemical kinetics 1996; 28:95-101. DOI: 10.1002/(SICI)1097-4601(1996)28:2<95::AID-KIN4>3.0.CO;2-G

33. M.L. Saladino, A. Zanotto, M.D. Chillura, A. Spinella, G. Nasillo, E. Caponetti. Ce:YAG nanoparticles embedded in a PMMA matrix: Preparation and characterization. Langmuir 2010; 26:13442-13449. DOI:10.1021/la9042809

34. A.P.A.M. Eijkelenboom, W.E.J.R. Maas, W.S. Veeman, G.H.W. Buning, J.M.J. Vankan. Triple-resonance fluorine-19, proton, and carbon-13 CP-MAS NMR study of the influence of PMMA tacticity on the miscibility in PMMA/poly(vinylidene fluoride) (PVF2) blends. Macromolecules 1992;25:4511-4518. DOI: 10.1021/ma00044a009

Chapter 3

PMMA-titania nanocomposites: Properties and thermal degradation behavior

This chapter has been published as:
T.E. Motaung, A.S. Luyt, F. Bondioli, M. Messori, M.L. Saladino, A. Spinella, G. Nasillo, E. Caponetti. PMMA-titania nanocomposites: Properties and thermal degradation behaviour. Polymer Degradation and Stability 2012; 97:1325-1333

Abstract

Titania nanoparticles were prepared using a sol-gel method and calcination at 200 and 600 °C in order to obtain anatase and rutile phases, respectively. The obtained powders were used to prepare PMMA-titania nanocomposites by the melt compounding method. The effect of the crystalline phase and the amount of titania, in the range 1-5 wt.%, on the morphology, mechanical properties and thermal degradation kinetics of PMMA was investigated by means of X-ray diffractometry (XRD), transmission electron microscopy (TEM), ^{13}C cross-polarization magic-angle spinning nuclear magnetic resonance spectroscopy ($^{13}C\{^{1}H\}$CP-MAS NMR), including the measurement of proton spin-lattice relaxation time in the rotating frame ($T_{1\rho}(H)$), in the laboratory frame ($T_1(H)$) and cross polarization times (T_{CH}), and dynamic mechanical analysis (DMA), thermogravimetric analysis (TGA), and Fourier-transform infrared (FTIR) spectroscopy. Results showed that both types of titania were well dispersed in the polymeric matrix, whose structure remained amorphous. The two types of nanoparticles influenced the degradation of the polymer in different ways because of their different carbon content, particle size and crystal structures.

Keywords: PMMA; titania; nanocomposites; interfacial interaction; properties; degradation kinetics.

3.1 Introduction

Incorporation of inorganic nanoparticles into a polymer matrix has led to composites with improved thermal and mechanical properties [1-3]. There are a number of recent papers reporting on thermal degradation studies on poly(methyl methacrylate) (PMMA) containing boehmite, alumina, iron oxide and different clays [4-9]. It was found that metal oxides have a pronounced effect on the morphology, as well as mechanical and thermal behaviour of PMMA. Some authors found that the well dispersed metal oxide nanoparticles in PMMA improved its mechanical properties, and increased its thermal stability and activation energy of thermal degradation [5-8]. These observations were attributed to strong interfacial interaction and stabilization of the free radicals by the inorganic compounds. However, Laachachi *et* al., in their investigation of PMMA nanocomposites with organically modified clays, found a decrease in the thermal stability of PMMA and attributed it to a catalytic effect of the clays on PMMA degradation [9].

The introduction of titania (TiO_2) into a PMMA matrix received much attention due to improvements in the glass transition and thermal stability of the composites. Several methods have been used to prepare poly(methyl methacrylate)-titania (PMMA-TiO_2) nanocomposites, including *ex-situ* sol-gel polymerization, radical polymerization and solution mixing [2,3,10]. For nanocomposites prepared *via in situ* bulk polymerization it was found that the presence of TiO_2 retarded the thermal decomposition of the polymer [11]. This was attributed to the excellent interaction of the polymer chains with the TiO_2 nanoparticles and the barrier effect to the evaporation of small molecules generated during the thermal decomposition of the PMMA matrix. The opposite trend, where the presence of TiO_2 in a PMMA matrix did not enhance the thermal stability, was also observed and it was associated with the evaporation of physisorbed water [12]. Storage and loss modulus, glass transition temperature (T_g), pendulum hardness and activation energy of the thermal degradation of the nanocomposites increased with increasing TiO_2 content in PMMA-TiO_2 nanocomposites [13]. It was also found that the presence of TiO_2 in the PMMA matrix could lead to a decrease in T_g [2]. The decrease in this case was associated with significant formation of agglomerates and poor interaction. In another study the decrease in T_g was attributed to the increased length of the polymer chains grown from the nanoparticles due to increased polymerization time [14].

PMMA-TiO_2 nanocomposites prepared *via* solution mixing were also investigated [15,16]. The nanocomposites showed significant improvement in mechanical performance, thermal stability, glass transition temperature and activation energy of thermal degradation of the PMMA. Similar results were found for PMMA-TiO_2 nanocomposites prepared through extrusion and rheometer mixing [17-19]. In these cases the titania was synthesized and modified by pure catechol. The improvement in the properties was attributed to good interfacial interaction and nanoparticles dispersion, which led to immobilization of the polymer chains. In contrast, the unmodified nanoparticles showed a decrease in glass transition which was linked to repulsive interaction with the surrounding polymer chains [15].

A review paper on the photoinduced reactivity of titanium dioxide [20] discusses the differences between anatase and rutile titania, all of which may cause the nanoparticles of these two titania phases to interact differently when incorporated into a polymer matrix. First of all the exposed planes of these nanoparticles are different because, although both anatase and rutile titania have octahedral structures, anatase titania can be regarded to be built up from octahedrals that are connected by their vertices, while in rutile titania the edges are connected. Further it was found that the anatase phase has a different oxygen vacancy than the rutile phase, as well as higher electron mobility, lower dielectric constant, lower density, lower deposition temperature and lower surface energy. Both these titania phases were found to have catalytic properties.

Most of the reported studies concentrated on commercial anatase titania incorporated in PMMA, while little information was provided regarding incorporation of the rutile phase into PMMA. No systematic comparison of the properties of PMMA-TiO_2 nanocomposites, containing respectively anatase and rutile titania, has been reported in literature. The purpose of this study was to prepare PMMA-TiO_2 nanocomposites, containing anatase and rutile titania respectively, through melt compounding, and analysing the sample morphologies as well as their degradation and thermomechanical behaviour. The fillers were prepared by using sol-gel combustion methods. The nanoparticles and the composites were characterized using oriented finite element analysis (OFE), X-ray diffractometry (XRD), transmission electron microscopy (TEM), ^{13}C cross-polarization magic-angle spinning nuclear magnetic resonance spectrometry ($^{13}C\{^1H\}$ CP-

MAS NMR), including the measurement of proton spin-lattice relaxation time in the rotating frame ($T_{1\rho}(H)$), in the laboratory frame ($T_1(H)$) and cross polarization times (T_{CH}), dynamic mechanical analysis (DMA), thermogravimetric analyses (TGA), and TGA-Fourier-transform infrared spectroscopy (TGA-FTIR).

3.2 Experimental

3.2.1 Materials

Titanium isopropoxide ($Ti(i\text{-}OPr)_4$, Sigma Aldrich), nitric acid (Sigma Aldrich), and glycine (Sigma Aldrich) were used as received. Conductivity grade water (resistance = 18.1 MΩ) was used. Commercial grade poly(methyl methacrylate) (PMMA, Altuglas® V920T) produced by Bayer Materials Science, Italy, having a melt flow rate at 230 °C/3.8 kg of 1g/10 min, and an M_w = 350 000, was used in pellet form. The polymer was dried at 120 °C overnight under static vacuum before processing.

3.2.2 Titania preparation

Titania was prepared by the sol-gel combustion of aqueous solutions containing $TiO(NO_3)_2$, as precursor, and glycine as fuel. Titanium isopropoxide, $Ti(i\text{-}OPr)_4$, was hydrolyzed for 1 hour under magnetic stirring to obtain titanyl hydroxide, $TiO(OH)_2$. The obtained titanyl hydroxide was reacted with nitric acid (1 h) to produce an aqueous solution of titanyl nitrate [$TiO(NO_3)_2$] that was used as the precursor for the synthesis of titania. The molar ratio $Ti(i\text{-}OPr)_4$:H_2O and of $TiO(OH)_2$:HNO_3 was fixed at 1:4. The aqueous solution of titanyl nitrate was mixed with glycine (glycine:titanyl nitrate molar ratio = 2) and ammonium nitrate (glycine:NH_4NO_3 molar ratio = 0.5) followed by heating in an oven at 80 °C until complete dehydration. The obtained gel was ignited in an electric furnace at 450 °C. Once ignited, the combustion process was completed in a very short time (5 min) with the appearance of flame. After the synthesis, the slightly agglomerated titania powder was divided in two parts that were thermally treated in air for two hours at 200 °C and at 600 °C in order to crystallize the anatase and rutile phases, respectively. After the treatment, the colours of the powders were black and white, respectively.

3.2.3 Preparation of the nanocomposites

The PMMA pellets were thoroughly mixed with 1, 2 and 5 wt.% titania for 10 min at 200 °C and 30 rpm in a 50 mL internal mixer of a Brabender Plastograph (Duisburg, Germany). The mixed samples were melt-pressed into 1 mm thick sheets at 200 °C for 5 min.

3.2.4 Analysis methods

Oriented finite element analysis (OFE) was carried out on a Carlo Erba EA 1110 apparatus in order to determine the residual carbon content in the titania particles.

Transmission electron microscopy (TEM) micrographs were acquired by using a JEM-2100 (JEOL, Japan) electron microscope, equipped with an X-ray energy dispersive spectrometer (EDS, Oxford, model INCA ENERGY-200T) for analysis of elements, operating at a 200 kV accelerating voltage. A few tens of a milligram of the powders were dispersed in 2 mL of isopropanol and a small drop of the dispersion was deposited on a 300 mesh carbon-coated copper grid, which was introduced into the TEM analysis chamber after complete solvent evaporation. Thin nanocomposite samples of about 50 nm in thickness were cut using a Leica EM UC6 ultramicrotome equipped with a Leica EMFC6 cryocamera and a diamond blade. The thin samples thus obtained were deposited onto the copper grids.

X-ray powder diffraction (XRD) patterns were recorded in the 2-70° 2θ range at steps of 0.05° and a counting time of 5 s/step on a Philips PW 1050 diffractometer, equipped with a Cu tube and a scintillation detector beam. The X-ray generator worked at 40 kV and 30 mA. The instrument resolution (divergent and antiscatter slits of 0.5°) was determined using standards free from the effect of reduced crystallite size and lattice defects. Diffraction patterns were analyzed according to the Rietveld method [21] using the programme MAUD [22].

The $^{13}C\{^{1}H\}$ CP-MAS NMR spectra were obtained at room temperature with a Bruker Avance II 400 MHz (9.4 T) spectrometer operating at 100.63 MHz for the ^{13}C nucleus with a MAS rate

of 10 kHz, 400 scans, a contact time of 1.5 s and a repetition delay of 2 s. Optimization of the Hartmann-Hahn condition [23] was obtained using an adamantine sample. Each sample was placed in a 4 mm zirconia rotor with KEL-F caps using silica as filler to avoid inhomogeneities inside the rotor. The proton spin–lattice relaxation time in the rotating frame $T_{1\rho}(H)$ was indirectly determined, with the *variable spin lock (VSL)* pulse sequence, by carbon nucleus observation using a 90°–τ–spin-lock pulse sequence prior to cross-polarization [24]. The data acquisition was performed by ^{1}H decoupling with a delay time, τ, ranging from 0.1 to 7.5 ms and a contact time of 1.5 ms. The T_{CH} values for all the carbon signals of PMMA were obtained through *variable contact time (VCT)* experiments [25]. The contact times used in the (VCT) experiments were 0.05, 0.1, 0.2, 0.3, 0.4, 0.5, 0.6, 0.8, 1.0, 1.2, 1.5, 2.0, 2.5, 3.0, 3.5, 4.0, 4.5, 5.0, 6.0 and 7.0 ms. The proton spin–lattice relaxation time in the laboratory frame $T_1(H)$ was determined, with the *saturation recovery pulse* sequence [26], by the carbon nucleus observation using a 90°–τ–90° pulse sequence prior to cross polarization with a delay time τ ranging from 0.01 to 3 s.

The dynamic mechanical analysis (DMA) of the composites were performed from 40 to 180 ºC in the bending mode at a heating rate of 5 ºC min^{-1} and a frequency of 1 Hz using a Perkin Elmer Diamond DMA (Waltham, Massachusetts, U.S.A.).

Thermogravimetric analysis (TGA) was performed in a Perkin Elmer TGA7 (Waltham, Massachusetts, U.S.A.). The analyses were done under flowing nitrogen at a constant flow rate of 20 mL min^{-1}. Samples (5-10 mg) were heated from 25 to 600 °C at heating rates of 3, 5, 7 and 9 °C min^{-1}. The degradation kinetics analyses were done using the following two methods [27]. The *Ozawa-Flynn-Wall method* is an isoconversional linear method based on the equation:

$$\ln \beta = c - 1.052 \frac{E_a}{RT} \qquad (1)$$

where β = heating rate in K min^{-1}, c is a constant, E_a = activation energy in kJ mol^{-1}, R = universal gas constant, and T = temperature in K. The plot of $\log \beta$ vs. $\frac{1}{T}$, obtained from the TGA curves recorded at several heating rates, should be a straight line. The activation energy can

be evaluated from its slope. The second method is *Kissinger-Akahira-Sunose* which it is based on the equation

$$\ln(\frac{\beta}{T^2}) = \ln(\frac{AR}{E_a \bullet g(\alpha)}) - \frac{E_a}{RT} \qquad (2)$$

where α = fraction of conversion (defined as mass loss at respective temperature), A = pre-exponential factor and $g(\alpha)$ = algebraic expression for integral methods. From the TGA curves recorded at different heating rates β, temperatures T were determined at the conversions α = 10% - 90%. The activation energies were calculated from the slope of the straight lines of $\ln(\frac{\beta}{T^2})$ versus $\frac{1}{T}$.

The TGA-FTIR analyses were performed in a Perkin Elmer STA6000 simultaneous thermal analyzer (Waltham, Massachusetts, U.S.A.). The analyses were done under flowing nitrogen at a constant flow rate of 20 mL min^{-1}. Samples (20-25 mg) were heated from 30 to 600 °C at 10° C min^{-1} and held for 4 min at 600 °C. The furnace was linked to the FTIR (Perkin Elmer Spectrum 100, Waltham, Massachusetts, U.S.A.) with a gas transfer line. The volatiles were analyzed over a 400-4000 cm^{-1} wavenumber range at a resolution of 4 cm^{-1}. The FTIR spectra of the volatiles emitted at different temperatures during the degradation process were recorded in the transmittance mode.

3.3 Results and discussion

3.3.1 Elemental analysis

The elemental analysis performed on the powders show that nitrogen, carbon and hydrogen were present in the powders due to an incomplete combustion reaction between the glycine and the nitrate (Table 3.1). Their quantities were low and decreased at higher temperatures. The presence of carbon explains the black color of the powders treated at 200 °C.

Table 3.1 Elemental analysis of calcined powders

Sample	Nitrogen / wt%	Carbon / wt%	Hydrogen / wt%
Un-calcined	1.05	1.57	0.86
Titania treated at 200 °C	1.08	0.92	1.02
Titania treated at 600 °C	0.28	0.15	_

3.2.2 X-ray diffraction (XRD)

The XRD patterns of the TiO_2 powder treated at 200 °C and 600 °C, pure PMMA, and their respective composites containing 2 and 5 wt.% of fillers are shown in Figure 3.1. The peak profile of the TiO_2 powder treated at 200 °C is very broad, thus accounting for the nanocrystalline condition of the materials with, probably, a large lattice disorder. Rietveld analysis [21] of the spectrum has been performed on the XRD patterns of the two powders. The sample treated at 200°C is constituted of a pure anatase phase [S.G. $I4_1/amd$, a = 3.771(±1) Å and c = 9.484(±1) Å, Z = 4] with an average crystallite size of ca 640±20 Å, while the powder treated at 600 °C is described in terms of two crystalline phases: 99±1 wt.% of tetragonal rutile [S.G. P42/mnm, a = 4.5933 (±1) Å and c = 2.9592±1 Å, average crystallite size 1070±20 Å and 2±1 wt.% of orthorhombic brookite [S.G. Pcab, a = 5.4558 (±1) Å, b = 9.1819 (±1) Å and c = 5.1429 (±1) Å, average crystallite size 200±10 Å]. In both powders a small quantity of amorphous carbon is present.

The diffraction pattern of PMMA shows a broad diffraction peak at 2θ = 14°, typical of an amorphous material, together with two bands of lower intensities centred at 29.7° and 41.7°. The XRD spectrum of the nanocomposites shows the bands observed in PMMA together with the peaks of the fillers, the intensity of which increases with increasing quantity. This confirms that the filler maintained its structure in the composite, and that the orientation of the PMMA chains was also not influenced during the nanocomposite preparation process as occurred in other composites [28].

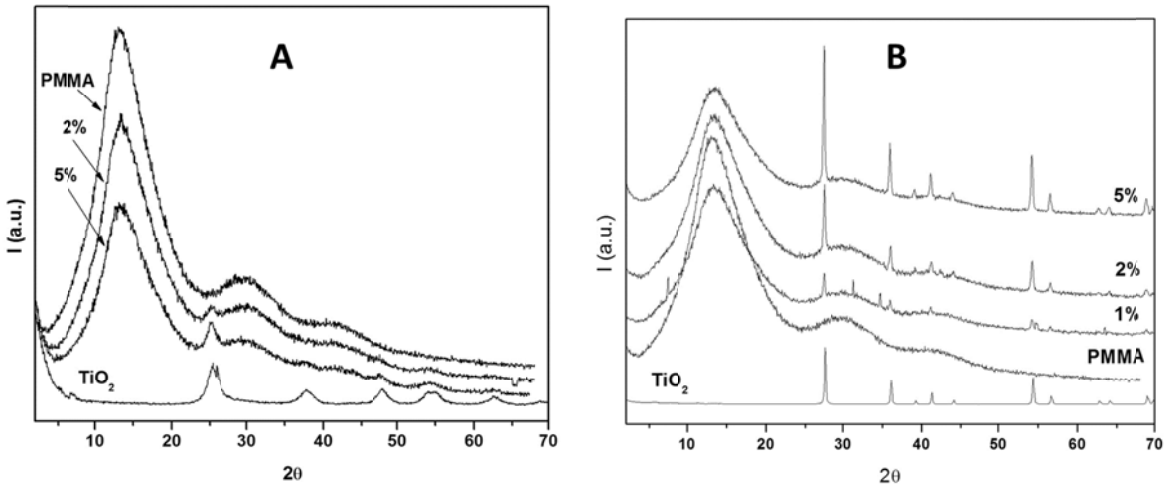

Figure 3.1 (a) XRD patterns of TiO_2 powder treated at 200 °C, pure PMMA, and PMMA-TiO_2 nanocomposites containing 2 and 5 wt.% of TiO_2, and (b) XRD patterns of TiO_2 powder treated at 600°C, pure PMMA, and PMMA-TiO_2 nanocomposites containing 2 and 5 wt.% of TiO_2

3.3.3 Transmission electron microscopy (TEM)

Some TEM micrographs of the anatase and rutile titania powders are reported in Figures 3.2 and 3.3, respectively. The anatase titania is constituted of aggregates with sizes between 0.5 and 1 micron. The aggregates are formed by several particles of about 20 nm diameter very densely packed. The EDS spectrum of anatase titania, in Figure 3.2, show the characteristic peaks of Ti and O of the sample, together with copper of the grid. The rutile titania is constituted of particles with sizes between 1 and 2 micron. The particles were formed by several irregular smaller particles of about 50-100 nm diameter very densely packed.

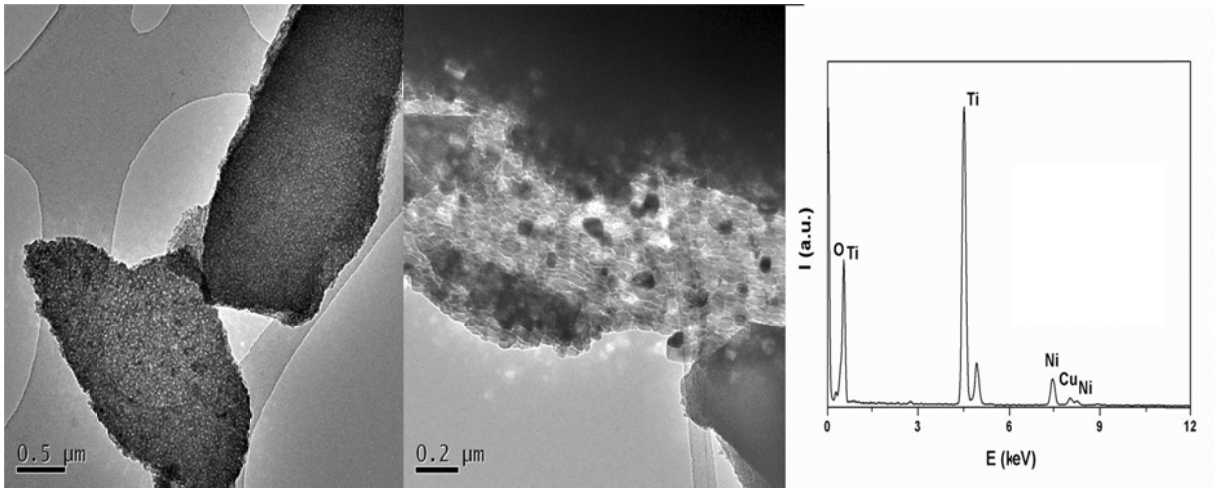

Figure 3.2 TEM micrographs of the TiO_2 (anatase) powder

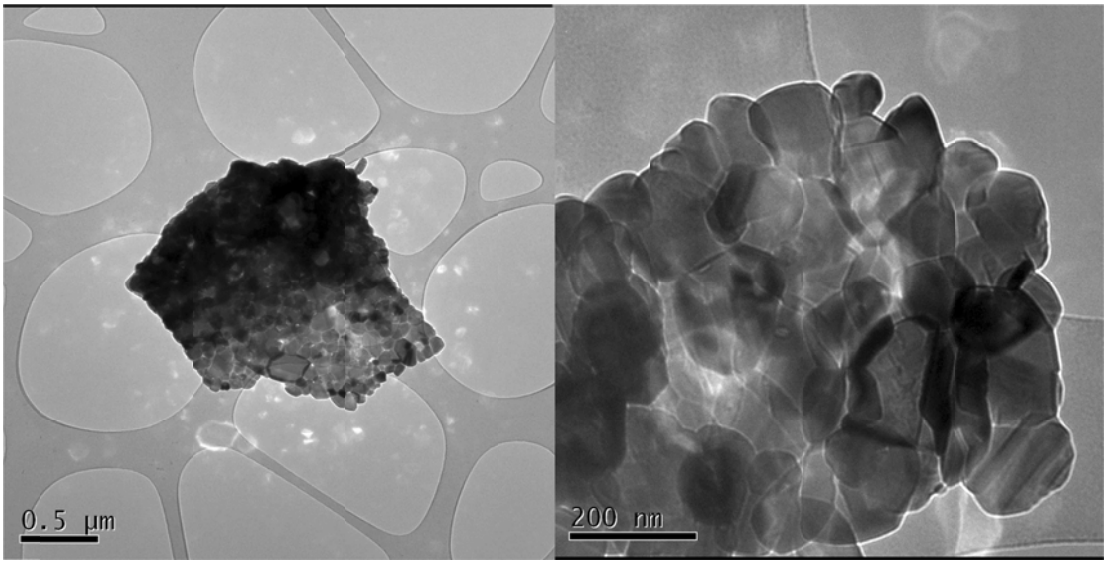

Figure 3.3 TEM micrographs of the TiO_2 (rutile) powder

The TEM micrographs of the 95/5 w/w PMMA-TiO_2 (anatase) and 95/5 w/w PMMA-TiO_2 (rutile) nanocomposites are reported in Figures 3.4 and 3.5, respectively. The PMMA-TiO_2 (anatase) nanocomposite is constituted of spongy aggregates of about 0.5 microns composed of smaller particles of TiO_2. The PMMA-TiO_2 (rutile) nanocomposite is constituted of particles of about 100 nm that form aggregates irregular in shape like that observed in the powder. The observed nanoparticles are similar in size to those of the used powder. In both cases the particles

were well dispersed, but there were clear indications of nanoparticle agglomeration which are smaller in the rutile titania containing PMMA.

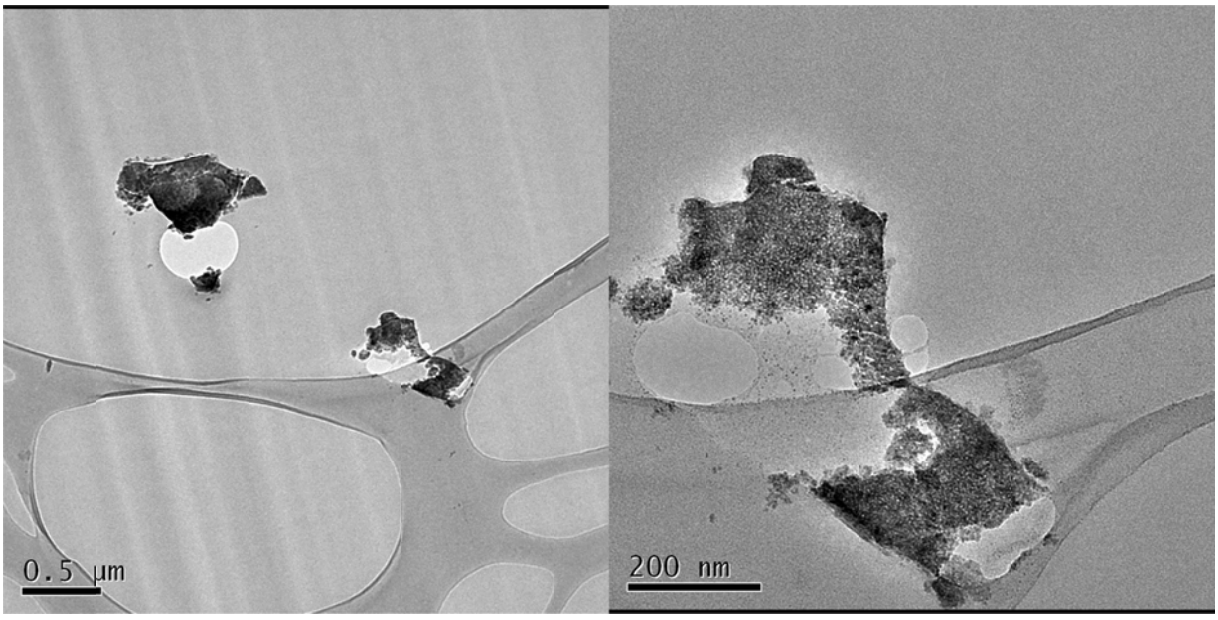

Figure 3.4 TEM micrographs of the 95/5 w/w PMMA-TiO_2 (anatase) composite

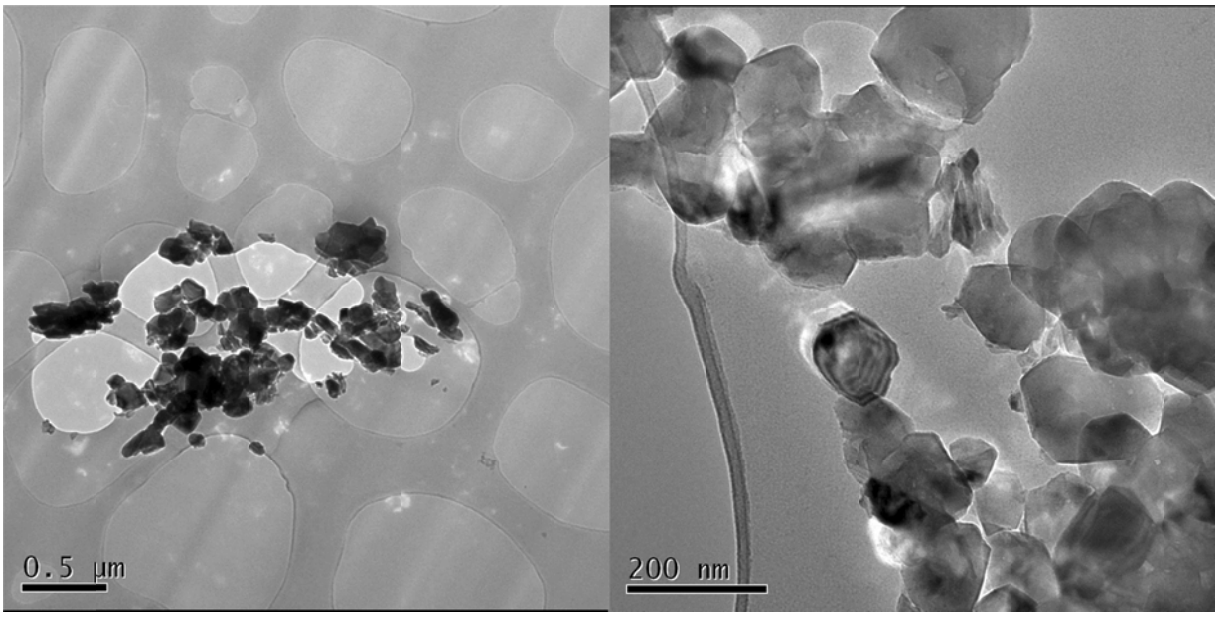

Figure 3.5 TEM micrographs of the 95/5 w/w PMMA-TiO_2 (rutile) composite

3.3.4 Nuclear magnetic resonance (NMR) spectroscopy

^{13}C $\{^{1}H\}$ CP-MAS NMR spectra of PMMA and of the composites having 5 wt.% of filler are reported in Figure 3.6. Five peaks are present in all the spectra. According to literature [29] peak 1 at 17 ppm is related to the methyl group, peak 2 at 45 ppm is related to the methylene group, peak 3 at 52 ppm is related to the quaternary carbon of the polymeric chain, peak 4 at 56 ppm is related to the methoxyl group and peak 5 at 177 ppm is related to the carbonyl carbon. No modification in the chemical shift and in the band shape is observed after composite formation, indicating that no chemical modification occurred in the polymer.

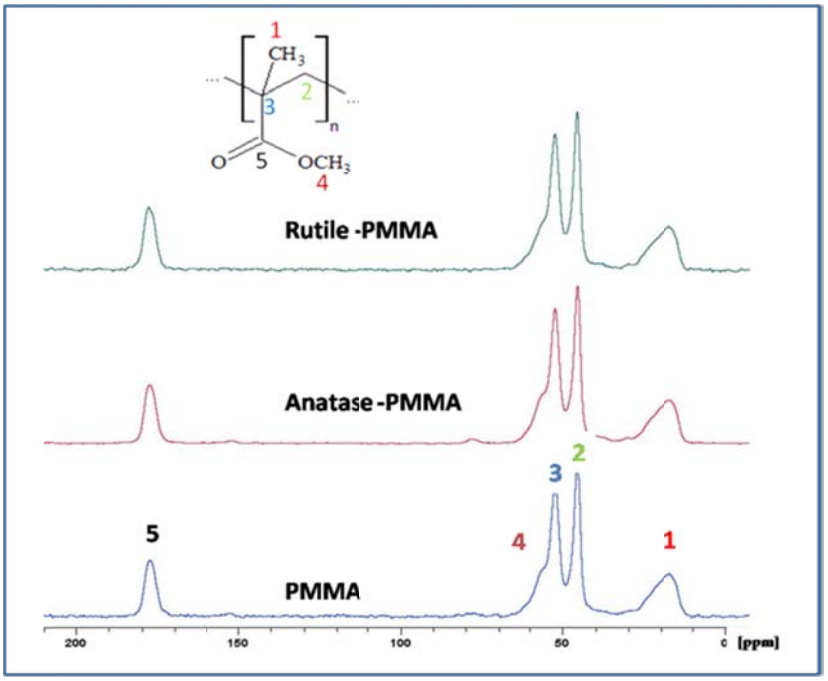

Figure 3.6 ^{13}C $\{^{1}H\}$ CP-MAS NMR spectra of PMMA, PMMA-TiO_2 (anatase) and PMMA-TiO_2 (rutile)

The spin-lattice relaxation time in the laboratory frame $T_1(H)$ and in the rotating frame $T_{1\rho}(H)$ and the cross-polarization time T_{CH} were determined through solid-state NMR measurements in order to evaluate the dynamic modifications occurring in the polymeric chain of the PMMA matrix after composite formation. The $T_1(H)$, $T_{1\rho}(H)$, and T_{CH} values obtained from each peak in the ^{13}C spectra of all the samples are reported in Table 3.2.

Table 3.2 Relaxation time values for all the peaks in the ^{13}C spectra of the PMMA and the two composites having 5 wt% of filler

	T_1H (s)			$T_{1\rho}H$ (ms)			T_{CH} (μs)		
ppm	**PMMA**	**Anatase-PMMA**	**Rutile-PMMA**	**PMMA**	**Anatase-PMMA**	**Rutile-PMMA**	**PMMA**	**Anatase-PMMA**	**Rutile-PMMA**
178	0.70 ± 0.02	0.67 ± 0.01	0.74 ± 0.01	18.1 ± 0.5	24.7 ± 0.6	17.2 ± 0.6	1306 ± 167	971 ± 95	1053 ± 95
56	0.71 ± 0.03	0.68 ± 0.02	0.72 ± 0.02	20.4 ± 0.9	24.1 ± 0.9	20.3 ± 0.9	254 ± 79	126 ± 14	112 ± 20
52	0.71 ± 0.01	0.68 ± 0.01	0.70 ± 0.01	16.2 ± 0.2	19.8 ± 0.1	20.4 ± 0.1	339 ± 42	275 ± 27	285 ± 21
45	0.71 ± 0.01	0.67 ± 0.01	0.69 ± 0.01	17.0 ± 0.2	20.1 ± 0.1	19.2 ± 0.1	614 ± 33	375 ± 22	652 ± 17
17	0.71 ± 0.01	0.66 ± 0.01	0.69 ± 0.01	19.3 ± 0.4	22.7 ± 0.3	17.1 ± 0.3	320 ± 36	269 ± 21	328 ± 16

The presence of the fillers in the PMMA matrix slightly modifies only the $T_1(H)$ values for the PMMA-TiO_2 (rutile) having 5 wt.% of TiO_2. This indicates that the materials were dynamically homogeneous in a range from tens to hundreds of nanometres. An increase in $T_{1\rho}(H)$ values was observed for the PMMA-TiO_2 (anatase) composite. In particular, the bigger effect involved the carbonyl carbons. The presence of rutile TiO_2 did not significantly affect the $T_{1\rho}(H)$ values. The $T_{1\rho}(H)$ parameter is inversely proportional to the spectral density of motion in the kHz frequency region which reflects the dynamic behaviour of a polymeric chain in a range of a few nanometres. Larger $T_{1\rho}(H)$ values result from an increase in the stiffness of a polymer.

The decrease in T_{CH} values for the PMMA-TiO_2 (anatase) composite indicates that there is an increase in the heteronuclear dipolar interactions between the carbons and the surrounding hydrogen nuclei. This is evidence that the presence of the anatase TiO_2 into the PMMA matrix made the polymer structure more rigid. This rigidity increase favoured the cross polarization mechanism yielding smaller T_{CH} values. The presence of rutile TiO_2 in PMMA gave rise to similar, but less intense, effects.

3.3.5 Dynamic mechanical analysis (DMA)

The storage modulus of the pure PMMA, as well as those of PMMA-TiO_2 (anatase) and PMMA-TiO_2 (rutile) composites having 1, 2 and 5 wt.% of TiO_2, are reported in Figures 3.7 and 3.8. The presence of anatase TiO_2 does not show much influence on the storage and loss modulus at lower temperatures, but these values are observably higher above the glass transition (Figures 3.7a and 3.7b). This suggests that the particles immobilized the polymer chains at higher temperatures, probably due to the increase in rigidity (as observed from the NMR results), although the higher carbon content in the particles could also have played a role. Figure 3.8a shows that 1 and 2% rutile TiO_2 reduced the storage modulus values between 40 and 90 °C, probably because of a plasticizing effect of the titania nanoparticles on the PMMA matrix (the TEM results show less agglomeration in the case of the rutile titania nanoparticles), while 5 wt.% rutile TiO_2 increased the storage modulus above the glass transition. It seems as if effective immobilization of the polymer chains only takes place at higher rutile titania content, which is in line with the NMR results that indicated less intense interaction between PMMA and rutile titania. The loss modulus curves follow the same trend (Figure 3.8b). Whatever the reason for the increased storage modulus, the difference in carbon content between the rutile and anatase phases, as confirmed through elemental analysis, could also have contributed to the differences in modulus.

The glass transition temperature of PMMA generally increased in the anatase titania containing nanocomposites (Figure 3.7c). In the nanocomposites containing rutile titania, only the composite with 5% rutile titania showed a significant increase in the glass transition temperature. These results were unexpected compared to the NMR results, which suggested strong interaction between anatase titania and PMMA. Although these results and the T_{CH} values obtained by NMR do not seem to support each other, it should be realized that the T_{CH} values reflect the dipolar interactions within a nanometer scale and can therefore not be strictly correlated with the bulk thermal mechanical properties. On the other hand, the T_1H relaxation time values, which describe the dynamic behaviour of macromolecules within a larger scale, are slightly higher for the 95/5 w/w PMMA-TiO_2 (rutile) than for those of the neat PMMA and the PMMA-TiO_2 (anatase) samples, suggesting an increase in matrix stiffness which is in line with the DMA results.

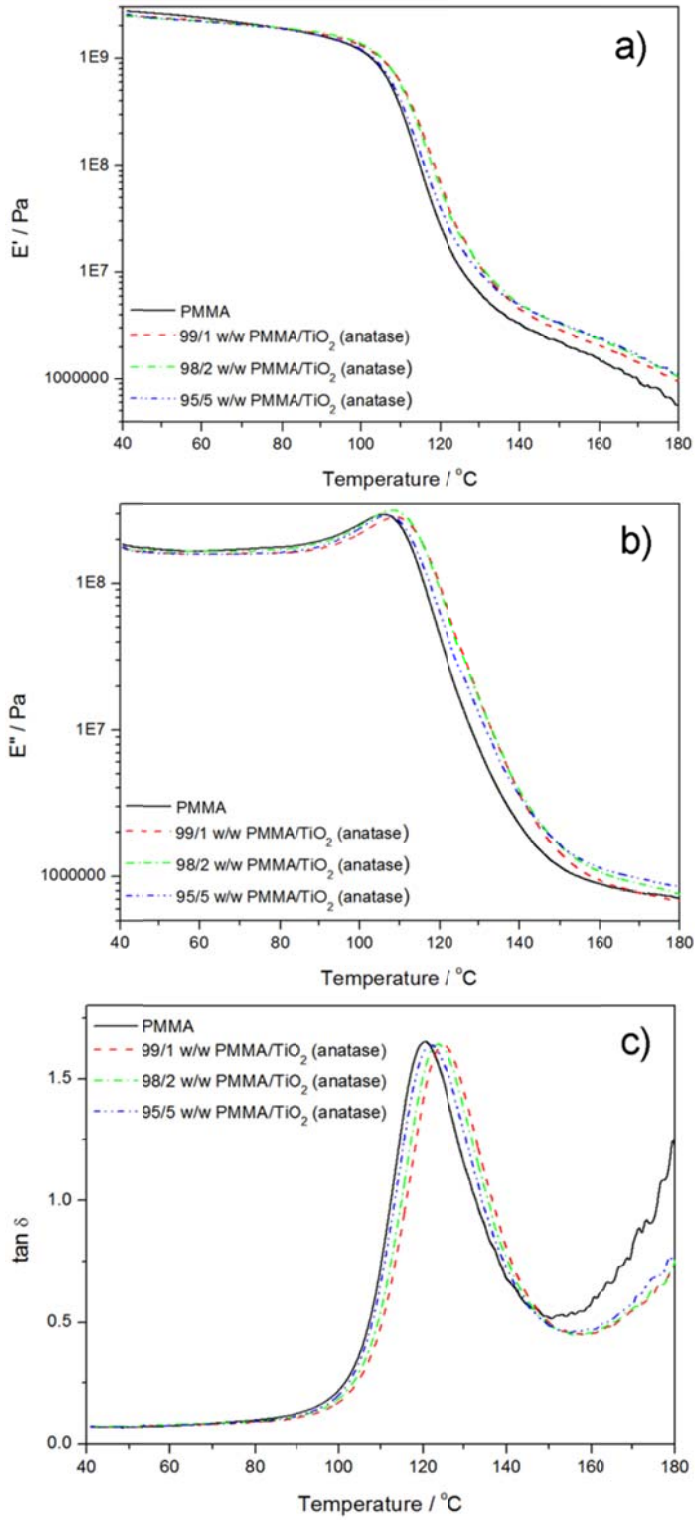

Figure 3.7 (a) Storage modulus, (b) loss modulus and (c) tan δ curves of PMMA and PMMA-TiO_2 (anatase) nanocomposites

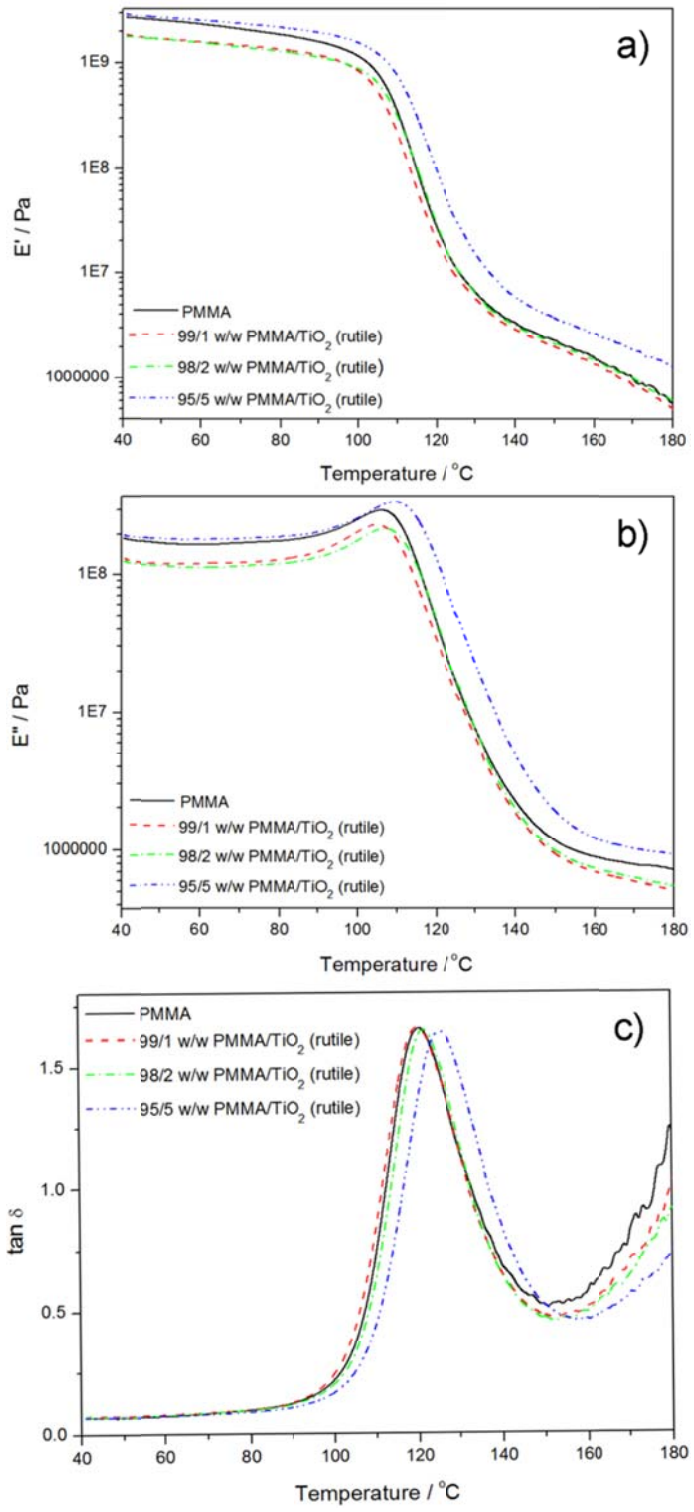

Figure 3.8 (a) Storage modulus, (b) loss modulus and (c) tan δ curves of PMMA and PMMA-TiO_2 (rutile) nanocomposites

3.3.6 Thermogravimetric analysis (TGA)

The TGA curves of all the samples are reported in Figure 3.9. They all show a single-step degradation and an increase in char content with an increase in the titania amount. The degradation temperatures for the anatase titania system slightly moves to higher values with increasing nanoparticle content, whereas there was no significant change for the rutile titania system. This could be related to the interaction between the anatase titania and PMMA, according to NMR findings, which led to immobilization of free radical chains formed during degradation and/or hindering of the diffusion of volatile decomposition products. The results support the NMR observation in which the presence of anatase titania showed a more significant influence on polymer chain mobility than the rutile titania. Different authors suggested different mechanisms for the thermal stability improvement. Wang *et al.* [1], in their study of PMMA-silica/zirconia nanocomposites, explained the improvement in thermal stability as being the result of the formation of networks of polymer chains and inorganic moieties which may restrain the movement of free radicals. In another study on PMMA-titania nanocomposites [30] they confirmed their view of radical trapping being the main degradation stabilization mechanism. However, Laachachi *et al.* [31] proposed the restriction of polymer chain mobility as the mechanism for improvement in thermal stability. It therefore seems as if the issue has not been resolved yet, and it is quite possible that the improvement in thermal stability may be the result of a combination of radical trapping and polymer chain immobilization.

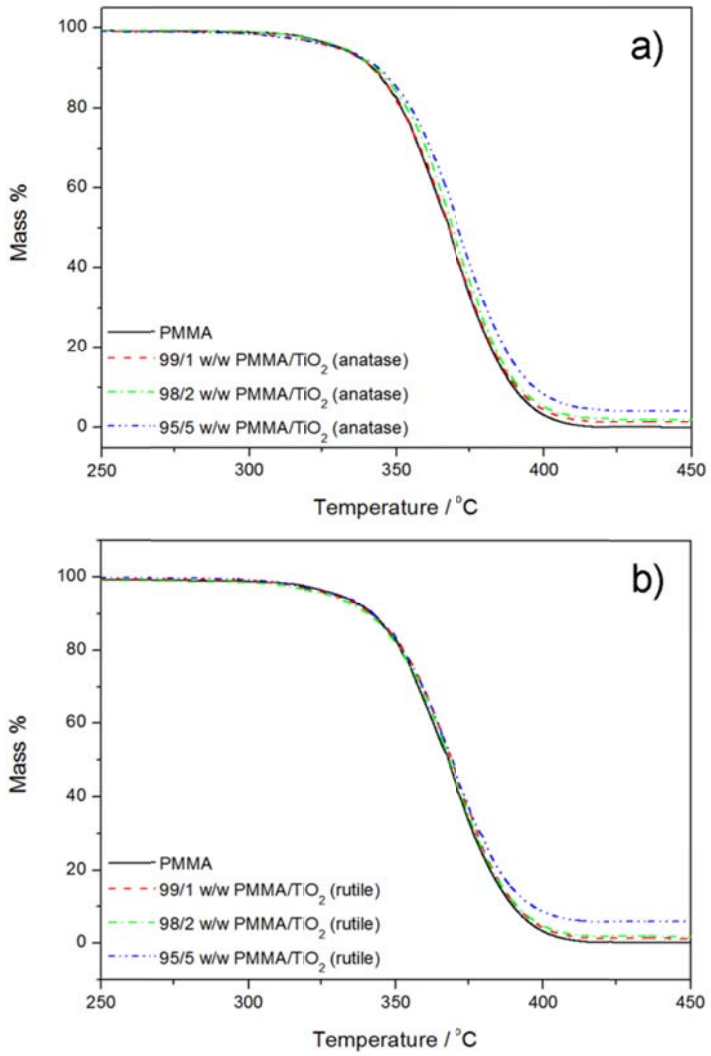

Figure 3.9 TGA curves of PMMA, and of (a) PMMA-TiO_2 (anatase) and (b) PMMA-TiO_2 (rutile) nanocomposites

The isoconversional graphs of ln β *versus* 1/*T* and ln (β/T^2) *versus* 1/T were plotted from the TGA curves of PMMA, 95/5 w/w PMMA-titania (anatase) and 95/5 w/w PMMA- titania (rutile) at heating rates of 3, 5, 7 and 9 °C min^{-1}. The activation energy values were calculated from the slopes of the isoconversional plots according to Equations 1 and 2. Both isoconversional methods gave similar values of the activation energies within experimental uncertainty. The relationship between the activation energies and the degree of conversion is reported in Figure 3.10.

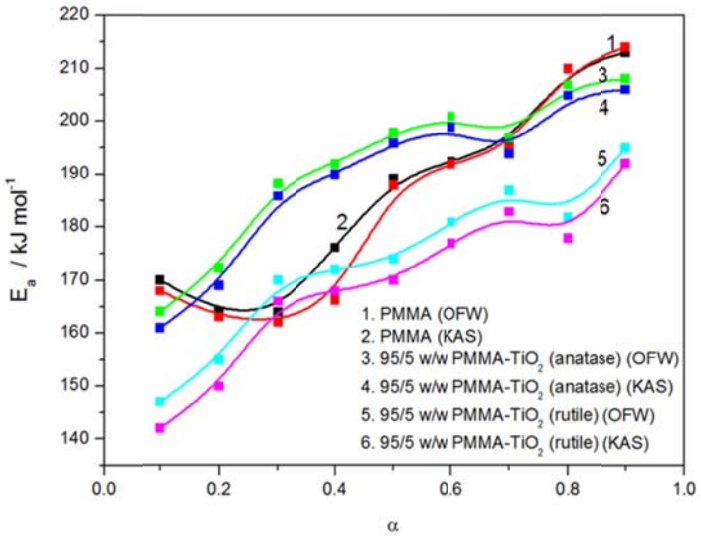

Figure 3.10 E_a values as function of extent of degradation obtained by the OFW and KAS methods

These values fall within the range of activation energies for PMMA degradation reported previously [32,33]. The activation energy values of pure PMMA and its nanocomposites generally showed an increase with the degree of conversion. The increase in activation energy with an increase in degree of conversion during the degradation of polymers was observed and explained in several papers [32-34]. Gao *et al.* [33] gave an acceptable explanation for the change in activation energy with increasing degree of degradation for PMMA. They linked this observation to a change in reaction order which may have been brought about by a change in degradation mechanism from a first-order unzipping reaction to a higher order chain scission reaction.

The presence of anatase titania show higher activation energy of degradation values between 20 and 70% weight loss than those of PMMA. The observation supports the increase in thermal stability of the PMMA-TiO_2 (anatase) nanocomposites observed in TGA. However, the presence of the rutile phase generally shows lower activation energy of degradation values. The decreased activation energy suggests that rutile titania may have acted as a catalyst for the thermal decomposition of the composites. Although the differences between the anatase and rutile titania phases (summarized in the 'Introduction' section) indicate that the anatase phase should have had a more significant catalytic effect, the differences in carbon contents in the two phases as

well as the lower extent of agglomeration in the case of rutile titania may have contributed to the latter having a more significant catalytic effect.

TGA-FTIR analyses were done to establish the nature of the degradation product(s), and to confirm the observations from the kinetic analysis of the thermal degradation process of PMMA and 95/5 w/w PMMA-titania. All the spectra almost perfectly match the known spectrum of methyl methacrylate (MMA), which confirms the primary degradation as that of de-polymerization (Figures 3.11 to 3.14).

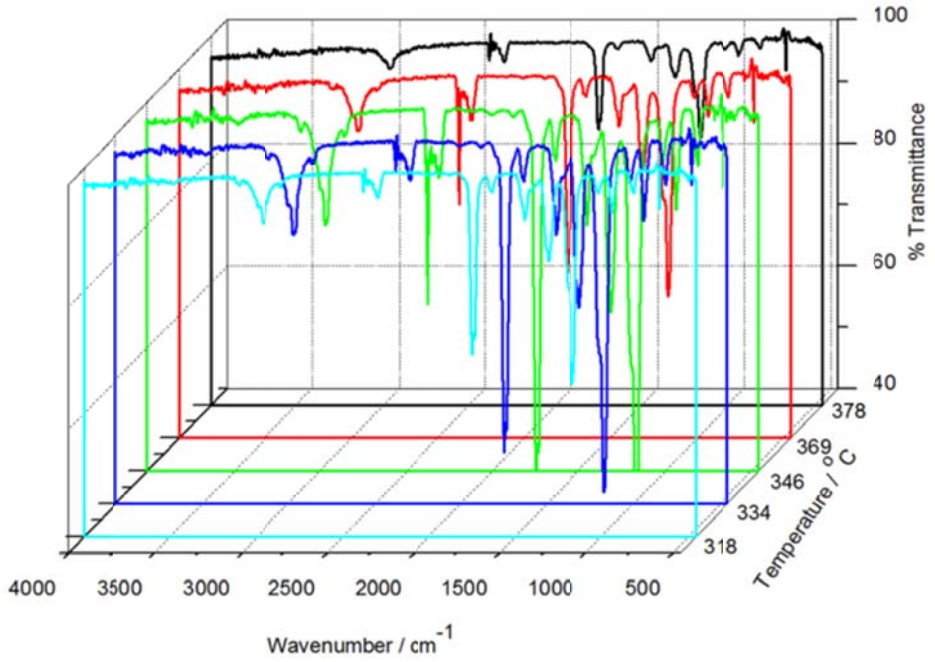

Figure 3.11 FTIR curves at different temperatures during the thermal degradation of PMMA

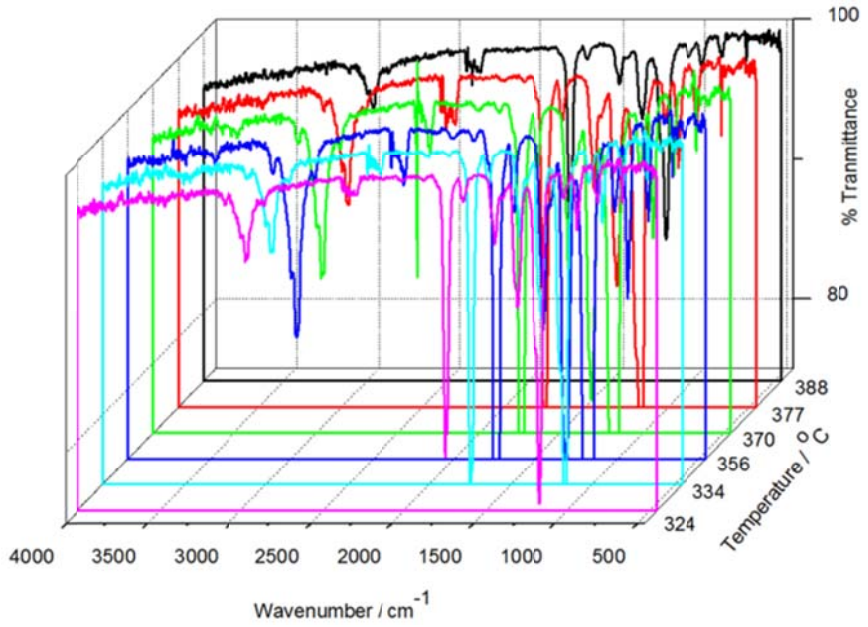

Figure 3.12 FTIR curves at different temperatures during the thermal degradation of 95/5 w/w PMMA-TiO_2 (anatase)

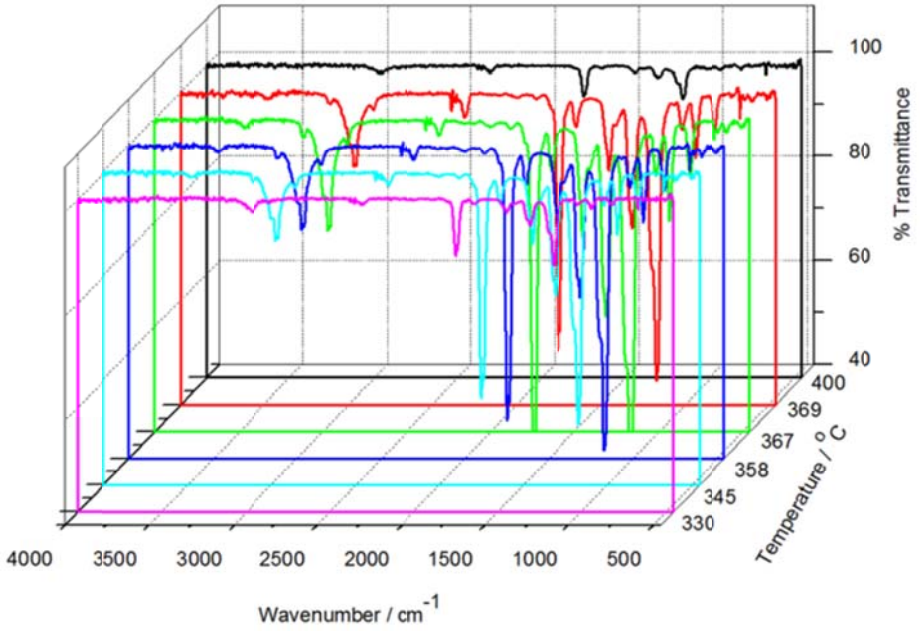

Figure 3.13 FTIR curves at different temperatures during the thermal degradation of 95/5 w/w PMMA-TiO_2 (rutile)

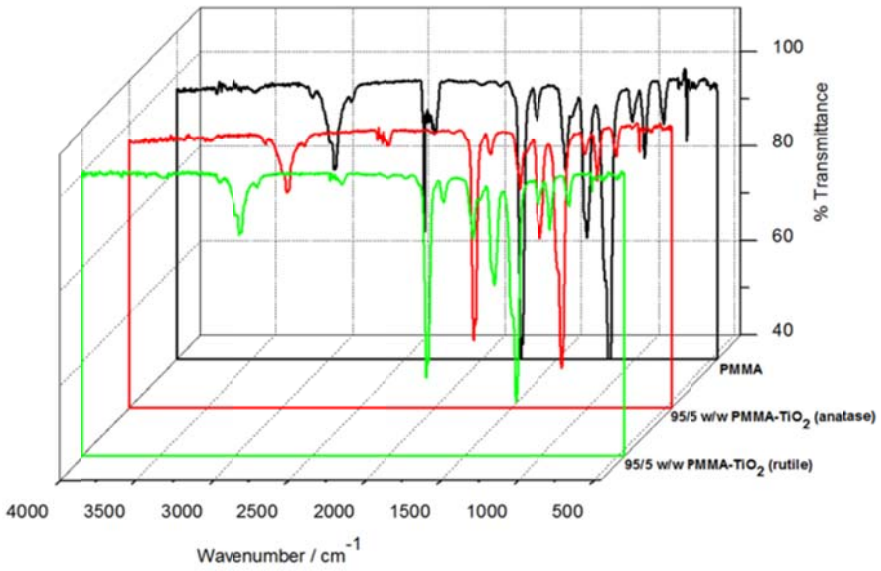

Figure 3.14 FTIR curves obtained at 346 °C during the degradation of PMMA, 95/5 w/w PMMA-TiO_2 (anatase) and 95/5 w/w PMMA-TiO_2 (rutile)

The peak around 2966 cm^{-1} is assigned to the CH_3 and CH_2 stretching vibrations, whereas their bending vibration appeared around 1451 cm^{-1} for CH_2 and 1314 cm^{-1} for CH_3. The carbonyl absorption vibration appears around 1744 cm^{-1} and the stretching vibration for C-O is around 1167 cm^{-1}. The peak at around 2336 cm^{-1} is related to the asymmetric stretching mode of CO_2. No new peaks or peak shifts were observed for the nanocomposite samples. There is a clear increase in peak intensity for all the characteristic peaks with increasing temperature, it reaches a maximum, and decreases again with further increase in temperature. It can be observed that at around 400°C the peaks of PMMA and the PMMA-TiO_2 (rutile) nanocomposite start to disappear, while that of the PMMA-TiO_2 (anatase) nanocomposite are still intense. It seems as if the volatilization of the degradation products is slower for the PMMA-TiO_2 (anatase) nanocomposite, which implies more intimate contact between PMMA or MMA and anatase titania (Figure 3.14). This supports the improved thermal stability and higher activation energy of the PMMA-TiO_2 (anatase) nanocomposite compared to the PMMA-TiO_2 (rutile) nanocomposite.

3.4 Conclusions

Two types of titania, anatase and rutile, were successfully prepared and their structures were confirmed by XRD. Elemental analysis evidenced the presence of different carbon contents in these two types of nanoparticles. PMMA-titania nanocomposites with both types of nanoparticles were prepared. TEM analysis showed that both rutile and anatase titania were well dispersed into the PMMA matrix (although that of rutile titania was slightly better) and did not change the amorphous structure of the PMMA. The fillers had different effects on the polymer chain mobility. NMR results showed different extents of interaction between PMMA and the two different types of titania. The two types of titania nanoparticles had slightly different influences on the thermomechanical properties of PMMA, as well as its degradation kinetics. These were probably the result of differences in particle size, extent of agglomeration, crystalline structure and carbon content. The quantification of the influence of these differences on the respective properties of the PMMA nanocomposites will be the subject of a separate study.

3.5 References

1. H. Wang, P. Xu, W. Zhong, L. Shen, Q. Du. Transparent poly(methyl methacrylate)/silica/zirconia nanocomposites with excellent thermal stabilities. Polymer Degradation and Stability 2005; 87:319-327. DOI:10.1016/j.polymdegradstab.2004.08.015
2. Y. Hu, G. Gu, S. Zhou, L. Wu. Preparation and properties of transparent PMMA/ZrO_2 nanocomposites using 2-hydroxyethyl methacrylate as a coupling agent. Polymer 2011; 52:122-129. DOI:10.1016/j.polymer.2010.11.020
3. H. Wang, P. Xu, S. Meng, W. Zhong, W. Du, Q. Du. Poly(methyl methacrylate)/silica/zirconia nanocomposites with greatly improved thermal and ultraviolet-shielding properties. Polymer Degradation and Stability 2006; 91:1455-1461. DOI:10.1016/j.polymdegradstab.2005.10.008

4. T. Orban, N.A. Isitman, J. Hacaloglu, C. Kaynak. Thermal degradation of organophosphorus flame-retardant poly(methyl methacrylate) nanocomposites containing nanoclay and carbon nanotubes. Polymer Degradation and Stability 2012; 97:273-280. DOI:10.1016/j.polymdegradstab.2011.12.020
5. E. Džunuzović, M. Marinović-Cinović, K. Jeremić, J. Nedeljković. Influence of cubic α-Fe_2O_3 particles on the thermal stability of poly(methyl methacrylate) synthesized by *in situ* bulk polymerization. Polymer Degradation and Stability 2009; 97:701-704. DOI: 10.1016/j.polymdegradstab.2008.12.018
6. S. Majoni, S. Su, J.M. Hossenlopp. The effect of baron-containing layered hydroxyl salt (LHS) on the thermal stability and degradation kinetics of poly(methyl methacrylate). Polymer Degradation and Stability 2010; 95:1593-1604. DOI: 10.1016/j.polymdegradstab.2010.05.033
7. A. Laachachi, M. Ferriol, M. Cochez, J.-M.L. Cuesta, D. Ruch. A comparison of the role boehmite (AlOOH) and alumina (Al_2O_3) in the thermal stability and flammability of poly(methyl methacrylate). Polymer Degradation Stability 2004; 94:1373-1378. DOI: 10.1016/j.polymdegradstab.2009.05.014
8. T. Orhan, N.A. Isitman, J. Hacaloglu, C. Kaynak. Thermal degradation mechanisms of aluminium phosphate, melamine polyphosphate and zinc borate in poly(methyl methacrylate). Polymer Degradation Stability 2011; 96:1780-1787. DOI: 10.1016/j.oplymdegradstab.2011.07.019
9. A. Laachachi, D. Ruch, F. Addiego, M. Ferriol, M. Cochez, J.-M.L. Cuesta. Effect of ZnO and organo-modified montmorillonite on thermal degradation of poly(methyl methacrylate) nanocomposites. Polymer Degradation and Stability 2009; 94:670-678. DOI: 10.1016/j.polymdegradstab.2008.12.002
10. X. Sun, X. Chen, X. Liu, S. Qu. Optical properties of poly (methyl methacrylate)-titania nanostructure thin films containing ellipsoid-shaped titania nanoparticles from ex-situ sol-gel method at low growth temperature. Applied Physics B 2011; 103:391-398. DOI 10.1007/s00340-010-4265-6
11. S.M. Khaled, R. Sui, P.A. Charpentier, A.S. Rizkalla. Synthesis of TiO_2-PMMA nanocomposite: Using methacrylic acid as a coupling agent. Langmuir 2007; 23:3988-3995.

DOI: 10.1021/la062879n

12. S. Ahmad, S. Ahmad, S.A. Agnihotry. Synthesis and characterization of in situ prepared poly(methyl methacrylate) nanocomposites. Bulletin of Materials Science 2007; 30:31-35. DOI: 10.1007/s12034-007-0006-9
13. Z. Ling, L. Zhongshi, F.A. Wenjun, P. Tianyou. A novel polymethyl methacrylate (PMMA)-TiO_2 nanocomposite and its thermal and photic stability. Wuhan University Journal of Natural Sciences 2006; 11:415-418. DOI: 10.1007/BF02832134
14. B. Hojjati, P.A. Charpentier. Synthesis and kinetics of graft polymerization of methyl methacrylate from the RAFT coordinated surface of nano-TiO_2. Journal of Polymer Science Part A: Polymer Chemistry 2008; 46:3926-3937. DOI: 10.1002/pola.22724
15. L.M. Hamming, R. Qiao, P.B. Messersmith, L.C. Brinson. Effects of dispersion and interfacial modification on the macroscale properties of TiO_2 polymer–matrix nanocomposites. Composites Science and Technology 2009; 69:1880-1886. DOI:10.1016/j.compscitech.2009.04.005
16. N. Patra, M. Salerno, M. Malerba, P.D. Cozzoli, A. Athanassiou. Improvement of thermal stability of poly (methyl methacrylate) by incorporation of colloidal TiO_2 nanorods. Polymer Degradation Stability 2011; 96:1377-1381. DOI: 10.1016/j.polymdegradstab.2011.03.020
17. A. Laachachi, M. Ferriol, M. Cochez, D. Ruch, J.M.L. Cuesta. The catalytic role of oxide in the thermooxidative degradation of poly (methyl methacrylate)-TiO_2 nanocomposites. Polymer Degradation and Stability 2008; 93:1131-1137. DOI:10.1016/j.polymdegradstab.2008.03.006
18. A. Chatterjee. Effect of nano TiO_2 addition on poly (methyl methacrylate): An exciting nanocomposite. Journal of Applied Polymer Science 2010; 116:3396-3407. DOI:10.1002/app.31883
19. A. Chatterjee. Properties improvement of PMMA using nano TiO_2. Journal of Applied Polymer Science 2010; 118:2890-2897. DOI:10.1002/app.32567

20. O. Carp, C.L. Huisman, A. Reller. Photoinduced reactivity of titanium dioxide. Progress in Solid State Chemistry 2004; 32:33-177.
DOI: 10.1016/j.progsolidstchem.2004.08.001
21. R.A. Young (Ed.). The Rietveld Method. Oxford University Press: Oxford (1993).
22. L. Lutterotti, S. Gialanella. X-ray diffraction characterization of heavily deformed metallic specimens. Acta Metallurgica 1998; 46:101-110.
DOI: 10.1016/S1359-6454(97)00222-X
23. S.R. Hartmann, E.L. Hahn. Nuclear double resonance in the rotating frame. Physical Review Online Archive 1962; 128:2042-2053.
DOI: 10.1103/PhysRev.128.2042
24. C. Lau, Y. Mi. A. Study of blending and complexation of poly (acrylic acid)/poly (vinyl pyrrolidone). Polymer 2002; 43:823-829.
DOI: 10.1016/S0032-3861(01)00641-3
25. P. Conte, R. Spaccini, A. Piccolo. State of art of CPMAS ^{13}C-NMR spectroscopy applied to natural organic matter. Progress in Nuclear Magnetic Resonance Spectroscopy 2004; 44:215-223.
DOI:10.1016/j.pnmrs.2004.02.002
26. R.G. Alamo, J.A. Blanco, I. Carrilero. Measurement of the ^{13}C spin-lattice relaxation time of the non-crystalline regions of semicrystalline polymers by a CP-MAS-based method. Polymer 2002; 43:1857-1865.
DOI: 10.1016/S0032-3861(01)00761-3
27. S. Vyazovkin, A.K. Burnham, J.M. Criado, L.A.P. Maqueda, C. Popescu, N. Sbirrazzuoli. ICTAC Kinetics Committee recommendations for performing kinetic computations on thermal analysis data. Thermochimica Acta 2011; 520:1-19.
DOI:10.1016/j.tca.2011.03.034
28. M.L. Saladino, A. Zanotto, D. Chillura Martino, A. Spinella, G. Nasillo, E. Caponetti. Ce:YAG nanoparticles embedded in a PMMA matrix: Preparation and characterization. Langmuir 2010; 26:13442-13449.
DOI: 10.1021/la9042809
29. A.P.A.M. Eijkelenboom, W.E.J.R. Maas, W.S. Veeman, G.H.W, Buning, J.M.J. Vankan. Triple-resonance fluorine-19, proton, and carbon-13 CP-MAS NMR study of the influence

of PMMA tacticity on the miscibility in PMMA/poly (vinylidene fluoride) (PVF2) blends. Macromolecules 1992; 25:4511-4518.
DOI: 10.1021/ma00044a009

30. H. Wang, S. Meng, P. Xu, W. Zhong, Q. Du. Effect of traces of inorganic content on thermal stability of poly(methylmethacrylate) nanocomposites. Polymer Engineering and Science 2007; 47:302-307.
DOI; 10.1002/pen.20708

31. A. Lachaachi, M. Cochez, M Ferriol, J.M. Lopez-Cuesta, E. Leroy. Influence of TiO_2 and Fe_2O_3 fillers on the thermal properties of poly(methyl methacrylate) (PMMA). Materials Letters 2005; 59:36-39.

32. B.J. Holland, J.N. Hay. The value and limitations of non-isothermal kinetics in the study of polymer degradation. Thermochimica Acta 2002; 388:253-273.
DOI: 10.1016/S0040-6031(02)00034-5

33. Z. Gao, T. Kaneko, D. Hou, M. Nakada. Kinetics of thermal degradation of poly (methyl methacrylate) studied with the assistance of the fractionation conversion at the maximum reaction rate. Polymer Degradation and Stability 2004; 84:399-403.
DOI:10.1016/j.polymdegradstab.2003.11.015

34. S. Vyazovkin. A unified approach to kinetic processing of nonisothermal data. International. Journal of Chemical kinetics 1996; 28:95-101.
DOI: 10.1002/(sici)1097-4601(1996)28:2<95::aid-kin4>3.0.co;2-g

Chapter 4

Morphology, mechanical properties and thermal degradation kinetics of PMMA-zirconia nanocomposites prepared by melt compounding

This chapter has been published as:
T.E. Motaung, A.S. Luyt, M.L. Saladino, D.C. Martino, E. Caponetti. Morphology, mechanical properties and thermal degradation kinetics of PMMA-zirconia composites prepared by melt compounding. eXPRESS Polymer Letters 2012; 6:871-881

Abstract

Zirconia nanoparticles were synthesized by means of a sol-gel method and embedded in poly(methyl methacrylate) (PMMA) by melt compounding. The zirconia was well dispersed in the PMMA matrix, with only a few clusters, especially for the highest investigated zirconia content. NMR results showed heteronuclear dipolar interactions involving the carbons and the surrounding hydrogen nuclei. The effect of the amount of zirconia, in the range of 1-5 wt.%, on the thermomechanical properties and thermal degradation kinetics of PMMA was also investigated by means of dynamic mechanical analysis (DMA), thermogravimetric analyses (TGA), and Fourier-transform infrared spectroscopy (FTIR). The presence of zirconia showed a decrease in the storage and loss moduli at lower temperatures, probably due to a plasticization effect. The presence of zirconia in PMMA slightly increased its thermal stability, but the activation energies of thermal degradation for the nanocomposites were significantly lower, at degrees of conversion higher than 0.3, than those of pure PMMA.

Keywords: PMMA; zirconia; nanocomposites; morphology; dynamic mechanical analysis; thermal degradation

4.1 Introduction

Nanocomposite materials, based on a polymer matrix and inorganic nanoparticle fillers, have drawn considerable attention in recent years, due to improvements in various properties including electrical, thermal, optical and other mechanical properties [1-5]. Poly(methyl methacrylate)/zirconia (PMMA-ZrO_2) is one of the most important nanocomposites that has been applied for the increasing demands of optical waveguides, ophthalmic lenses, antireflection coatings and adhesives for optical components. Several methods including *in situ* polymerization, sol-gel methods for the preparation of nanoparticles, and *in situ* emulsion polymerization have been used to prepare the nanocomposites. FTIR, TEM and UV investigations showed that zirconia nanoparticles were generally homogeneously dispersed in the polymer matrix at primary particle size level and that the composites were transparent [6-12].

TGA analyses of PMMA-ZrO_2 nanocomposites in air and nitrogen atmospheres, where a sol-gel method was used for the preparation of the nanocomposites, showed three degradation steps with the thermal stability increasing in the presence of zirconia [10,11]. However, the onset temperatures of the second step in nitrogen and of the third step in air of the nanocomposites were lower. This was related to different mechanisms of thermal degradation in air and nitrogen atmospheres. The kinetic results showed that the values of activation energy (E_a) for the degradation of the nanocomposites in air were higher than that of pure PMMA. In nitrogen the E_a values of thermal degradation for first and the last stages were larger than that of PMMA. The increase was associated with the action of the nanoparticles to inhibit the formation of free radicals. A similar reason was given by Wang *et al.* [13] in a study of synergistic flame-retarded systems consisting of nano-ZrO_2 and triphenylphosphate for PMMA prepared by a solution mixing process. They observed more significant increases in the thermal stability of the PMMA-ZrO_2 nanocomposites in air than in nitrogen.

DMA analysis of PMMA-ZrO_2 nanocomposites prepared *via in situ* emulsion polymerization, showed higher storage and loss moduli, glass transition (T_g) and elastic modulus than PMMA in the glassy state [6-8,12]. This was related to the reinforcing effect of the zirconia nanoparticles. However, in the rubbery state, the PMMA modulus was independent of the filler content, which

was attributed to the weak interaction between the polymer and filler at high temperatures. It was found that the pendulum hardness of PMMA-ZrO_2 nanocomposites quickly increased with increasing ZrO_2 content, even for low content, and that there was steady increment of scratch resistance with increasing zirconia content. The hardness and abrasion behaviour was attributed to the gel effect on PMMA-ZrO_2 nanocomposites by ZrO_2 nanoparticles during polymerization.

Hu *et al.* [10] prepared PMMA-ZrO_2 nanocomposites by modifying non-aqueous synthesized ZrO_2 nanoparticles with methacryloxypropyltrimethoxysilane (MPS) in tetrahydrofuran, dispersing MPS-functionalized ZrO_2 nanoparticles in MMA and performing *in situ* bulk polymerization with controlled pre-polymerization time. They found that the ZrO_2 enhanced rigidity without loss of toughness, though not remarkable. This was attributed to bonding between the polymer and the functionalized zirconia. The results were in line with the study of Hu *et al.* [6], where an increase in elastic modulus was observed.

The purpose of this study was to prepare PMMA-ZrO_2 nanocomposites through a melt compounding method. Zirconia was prepared using a sol-gel method. Both nanoparticles and composites were characterized using X-ray diffractometry (XRD), transmission electron microscopy (TEM), ^{13}C cross-polarization magic-angle spinning nuclear magnetic resonance ($^{13}C\{^1H\}$ CP-MAS NMR), dynamic mechanical analysis (DMA), thermogravimetric analyses (TGA), and Fourier-transform infrared (FTIR) spectroscopy. The effect of the presence and amount of zirconia nanoparticles on the thermal and mechanical properties, as well as the thermal degradation kinetics, of the PMMA will be discussed.

4.2 Experimental

4.2.1 Materials

Tetra-*n*-propylzirconate (TPZ, Aldrich), capronic acid (Aldrich), ethanol (Eurobase), ammonium hydroxide (NH_4OH, Aldrich) were used as received without further purification. Commercial grade poly(methyl methacrylate) (PMMA, Altuglas® V920T) produced by Bayer Materials Science, Italy and having a melt flow rate at 230 °C/3.8 kg of 1g/10 min, and an M_w = 350 000,

was used in pellet form. The polymer was dried at 120 °C overnight under static vacuum before processing.

2.2.2 Zirconia preparation

The ZrO_2 nanoparticles were prepared according to the sol-gel method reported by Bondioli *et al.* [14].

4.2.2 Preparation of the composites

The PMMA pellets were thoroughly mixed with 1, 2 and 5 wt.% zirconia for 10 min at 200 °C and 30 rpm in a 50 mL internal mixer of a Brabender Plastograph from Duisburg, Germany. The mixed samples were melt-pressed into 1 mm thick sheets at 200 °C for 5 min.

4.2.3 Analysis methods

Oriented finite element analysis (OFE) was carried out on a Carlo Erba EA 1110 apparatus in order to determine the residual carbon content in the zirconia particles.

TEM micrographs were acquired by using a JEM-2100 (JEOL, Japan) electron microscope operating at 200 kV accelerating voltage equipped with an X-ray energy dispersive spectrometer (EDS, Oxford, model INCA ENERGY-200T) for analysis of elements. Few tens of milligrams of powders were dispersed in 2 mL of isopropanol and a small drop of the dispersion was deposited on a 300 mesh carbon-coated copper grid, which was introduced into the TEM chamber analysis after the complete solvent evaporation. Nanocomposite thin samples of about 50 nm in thickness were cut using a Leica EM UC6 ultramicrotome equipped with a Leica EMFC6 cryocamera and a diamond blade. The thin samples thus obtained were deposited onto copper grids.

XRD patterns were recorded in the 2-70° 2θ range at steps of 0.05° and a counting time of 5 s/step on a Philips PW 1050 diffractometer, equipped with a Cu tube and a scintillation detector beam. The X-ray generator worked at 40 kV and 30 mA. The instrument resolution (divergent

and antiscatter slits of 0.5°) was determined using standards free from the effect of reduced crystallite size and lattice defects. Diffraction patterns were analyzed according to the Rietveld method [15] using the programme MAUD [16].

The ^{13}C {^{1}H} CP-MAS NMR spectra were obtained at room temperature with a Bruker Avance II 400 MHz (9.4 T) spectrometer operating at 100.63 MHz for the ^{13}C nucleus with a MAS rate of 10 kHz, 400 scans, a contact time of 1.5 s and a repetition delay of 2 sec. The optimization of the Hartmann-Hahn condition [17] was obtained using an adamantine sample. Each sample was placed in a 4 mm zirconia rotor with KEL-F caps using silica as filler to avoid inhomogeneities inside the rotor. The proton spin–lattice relaxation time in the rotating frame $T_{1\rho}(H)$ was indirectly determined, with the *variable spin lock* (VSL) pulse sequence, by the carbon nucleus observation using a 90°–τ–spin-lock pulse sequence prior to cross-polarization [18]. The data acquisition was performed by ^{1}H decoupling with a delay time, τ, ranging from 0.1 to 7.5 ms and a contact time of 1.5 ms. The T_{CH} values for all carbon signals of PMMA were obtained through variable contact time (VCT) experiments [19]. The contact times used in the (VCT) experiments were 0.05, 0.1, 0.2, 0.3, 0.4, 0.5, 0.6, 0.8, 1.0, 1.2, 1.5, 2.0, 2.5, 3.0, 3.5, 4.0, 4.5, 5.0, 6.0 and 7.0 ms. The proton spin–lattice relaxation time in the laboratory frame $T_1(H)$ was determined, with the saturation recovery pulse sequence [20], by the carbon nucleus observation using a 90°–τ–90° pulse sequence prior to cross polarization with a delay time τ ranging from 0.01 to 3 s.

The dynamic mechanical analysis (DMA) of the blends and composites was performed from 40 to 180 ºC in the bending mode at a heating rate of 5 ºC min^{-1} and a frequency of 1 Hz using a Perkin Elmer Diamond DMA from Waltham, Massachusetts, U.S.A.

Thermogravimetric analysis (TGA) was performed in a Perkin Elmer TGA7 from Waltham, Massachusetts, U.S.A. The analyses were done under flowing nitrogen at a constant flow rate of 20 mL min^{-1}. Samples (5-10 mg) were heated from 25 to 600 °C at different heating rates. The degradation kinetic analysis was done using the following two methods. The Ozawa-Flynn-Wall method is an isoconversional linear method based on the equation:

$$\ln \beta = c - 1.052 \frac{E_a}{RT} \qquad (1)$$

where β = heating rate in K min^{-1}, c is constant, E_a = activation energy in kJ mol^{-1}, R = universal gas constant, and T = temperature in K. The plot of $\log\beta$ vs. $\frac{1}{T}$, obtained from the TGA curves recorded at several heating rates, should be a straight line. The activation energy can be evaluated from its slope. The second method is Kissinger-Akahira-Sunose which it is based on the equation

$$\ln(\frac{\beta}{T^2}) = \ln(\frac{AR}{E_a \bullet g(\alpha)}) - \frac{E_a}{RT} \qquad (2)$$

where β, E_a, R and T were defined before, α = fraction of conversion, A = pre-exponential factor and $g(\alpha)$ = algebraic expression for integral methods. From the TGA curves recorded at different heating rates β, temperatures T were determined at the conversions α = 10% ~ 90%. The activation energies were calculated from the slope of the straight lines of $\ln(\frac{\beta}{T^2})$ versus $\frac{1}{T}$.

The thermogravimetric analysis-Fourier-transform infrared (TGA-FTIR) analyses were performed in a Perkin Elmer STA6000 simultaneous thermal analyzer from Waltham, Massachusetts, U.S.A. The analyses were done under flowing nitrogen at a constant flow rate of 20 mL min^{-1}. Samples (20-25 mg) were heated from 30 to 600 °C at 10° C min^{-1} and held for 4 min at 600 °C. The furnace was linked to the FTIR (Perkin Elmer Spectrum 100, Massachusetts, U.S.A.) with a gas transfer line. The volatiles were scanned over a 400 – 4000 cm^{-1} wavenumber range at a resolution of 4 cm^{-1}. The FTIR spectra were recorded in the transmittance mode at different temperatures during the thermal degradation process.

4.3 Results and discussion

The elemental analysis of zirconia particles shows a significantly carbon content of 7.2 % and a hydrogen content of 4.4 %. These residues can be attributed to an incomplete sol-gel reaction of the zirconia precursor tetra-*n*-propylzirconate (TPZ).

The XRD patterns of the ZrO_2 powder, pure PMMA and of the composites are reported in Figure 4.1. The analysis of the XRD patterns was performed using the Rietveld method [15]. The pattern of zirconia powder is described in terms of two crystalline phases: 80 (± 3) wt.% of

tetragonal [S.G. P42/mnm, a = 3.6205 (± 1) Å and c = 5.14245 (± 1) Å, average crystallite size 180 Å (±3)] and 20 (± 3) wt.% of monoclinic [S.G. P21/c, a = 5.03 (± 1) Å, b = 5.06 (± 1) Å, c = 5.04 (± 1) Å and β =98.7°, average crystallite size 500 (± 30) Å] Baddeleyite. The diffraction pattern of PMMA shows a broad diffraction peak at 2θ = 14°, typical of an amorphous material, together with two bands of lower intensities centred at 29.7° and 41.7°. The XRD patterns of the PMMA-ZrO_2 nanocomposites having 1, 2 and 5 wt.% of ZrO_2 show the bands of PMMA together with the peaks of the zirconia in which the intensity increases with zirconia quantity. This suggests that zirconia maintains its structure in the composite and that the orientation of the PMMA chains is not influenced by the filler.

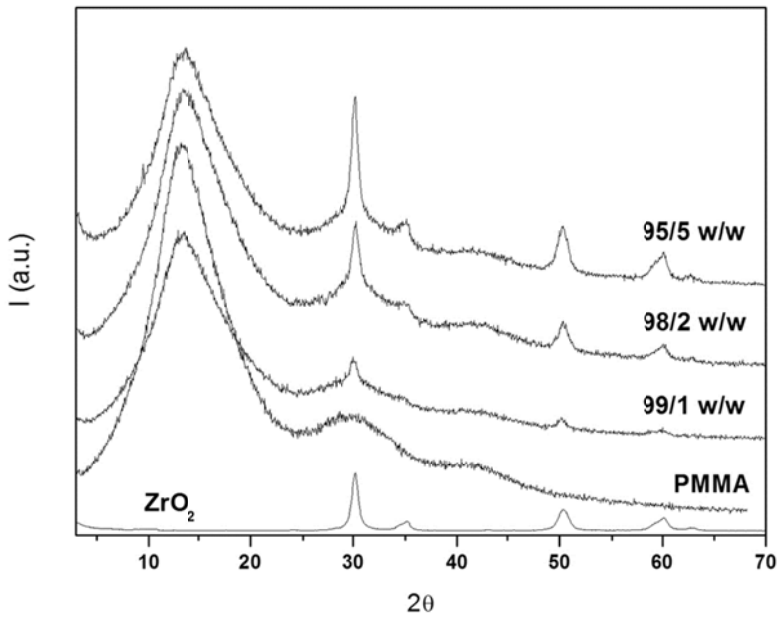

Figure 4.1 XRD patterns of zirconia powder, pure PMMA and of the PMMA-ZrO_2 nanocomposites

Some TEM micrographs and the EDS spectrum of zirconia powder are reported in Figure 4.2. Aggregates with a large number of particles (more than 30) of different sizes are observed. In each aggregate bigger, quite thick particles (around 200-400 nm) are surrounded by smaller spongy particles (50-100 nm). The EDS spectrum shows the characteristic peaks of Zr and O in the sample, together with nickel and the copper of the grid. The TEM micrographs of the PMMA-ZrO_2 nanocomposite having 5 wt.% of zirconia, reported in Figure 4.3, show aggregates

constituted of many small particles of 100 and 200 nm in size having spongy surfaces dispersed in the polymer.

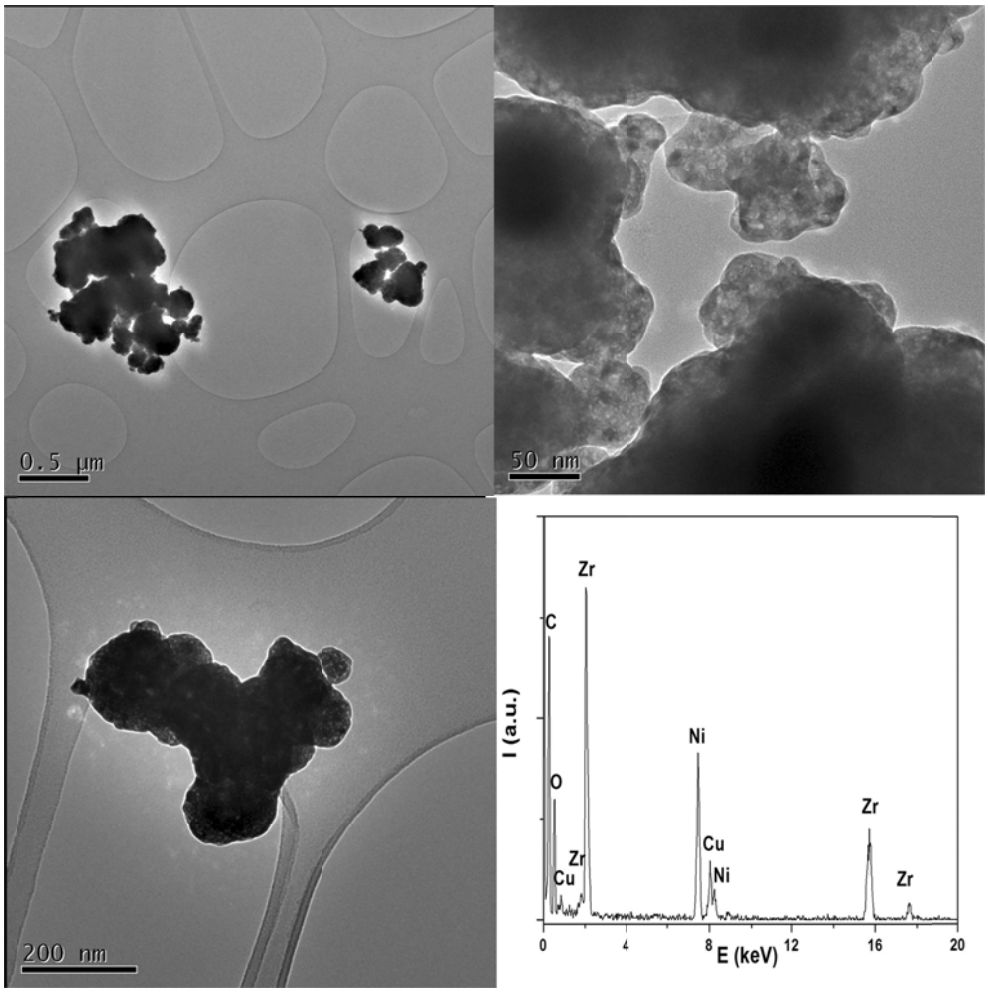

Figure 4.2 TEM micrographs and EDS spectrum of zirconia powder

The TEM micrographs of the PMMA-ZrO_2 nanocomposites having 1 and 2 wt.% of zirconia still show some aggregation, but to a lower extent, and the nanoparticle dispersion looks better (Figures 4.4 and 4.5).

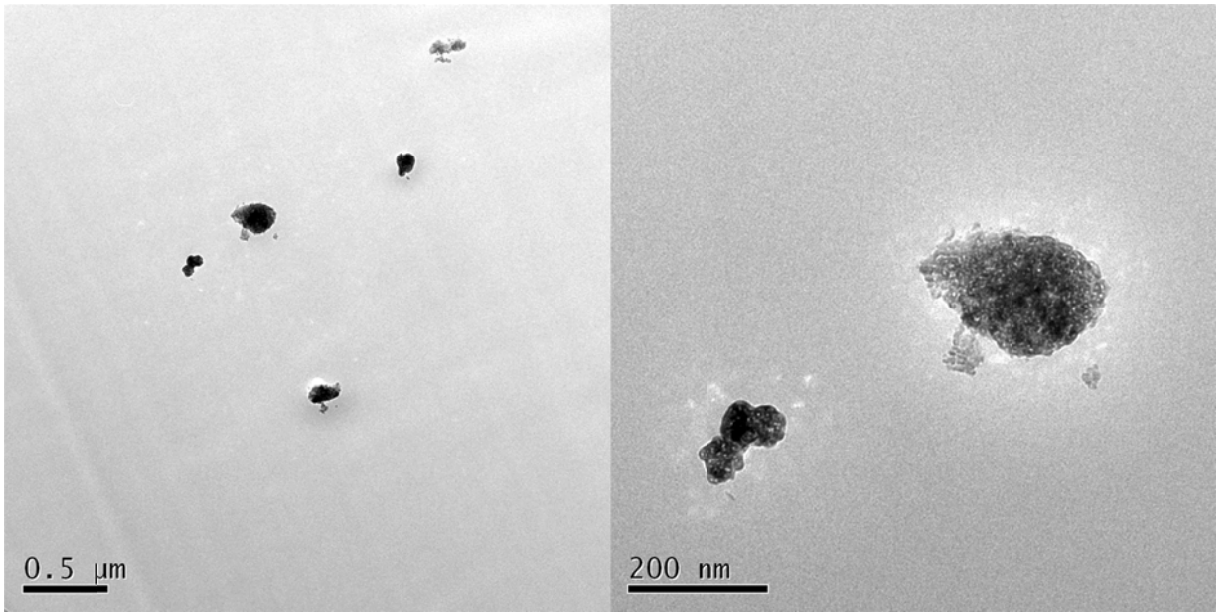

Figure 4.3 TEM micrographs of the 5 wt.% PMMA-ZrO_2 nanocomposite

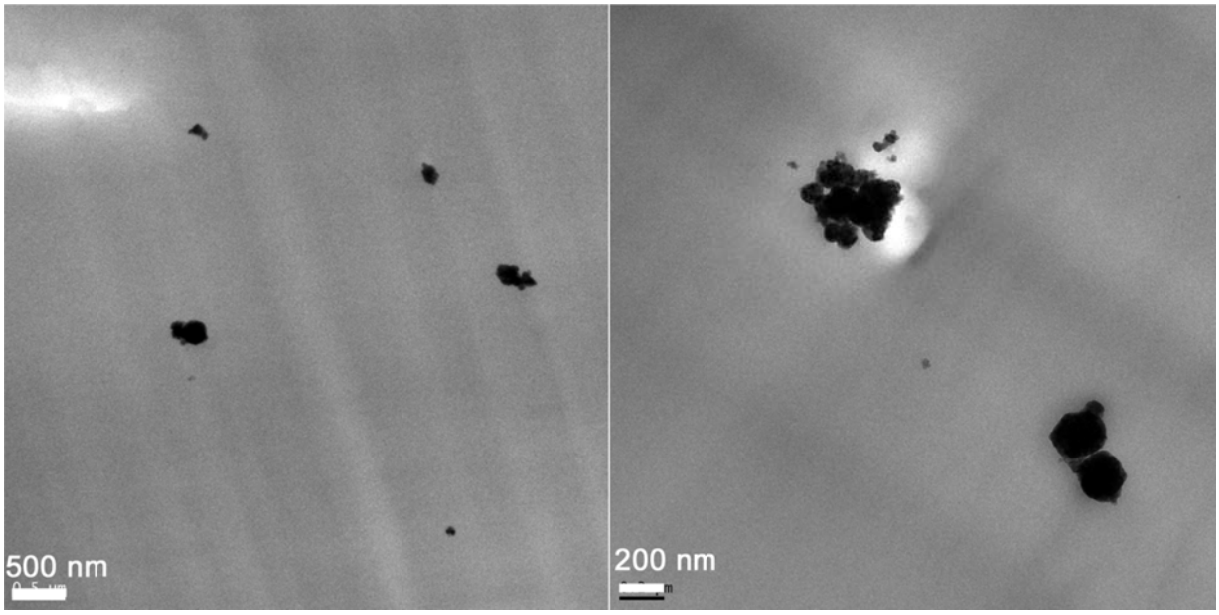

Figure 4.4 TEM micrographs of the 1 wt.% PMMA-ZrO_2 nanocomposite

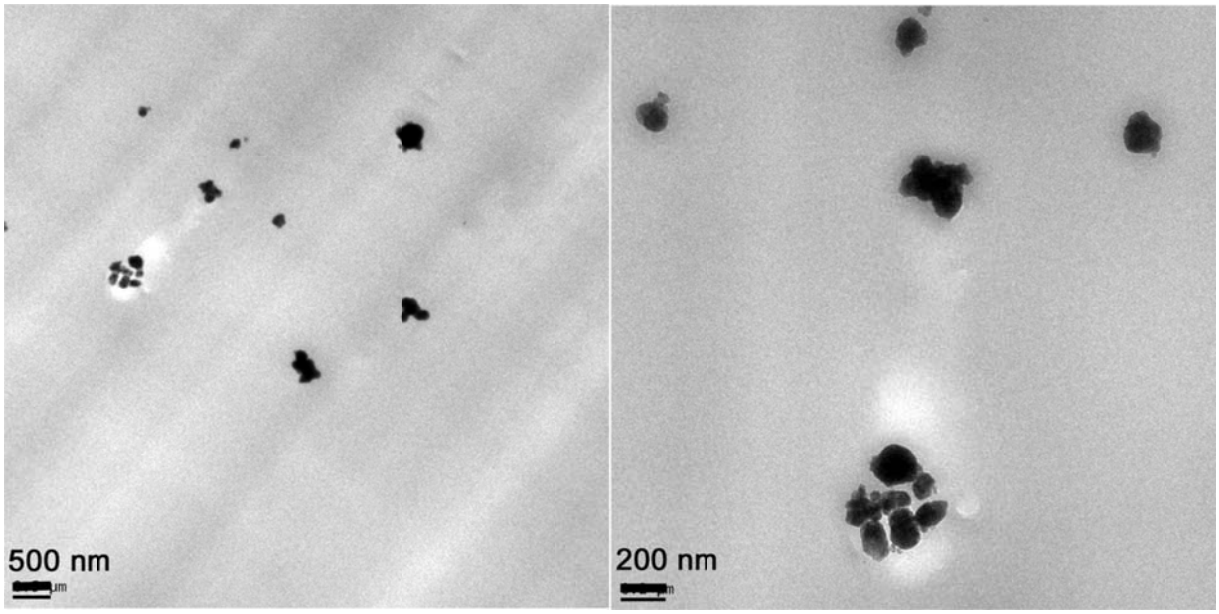

Figure 4.5 TEM micrographs of the 2 wt.% PMMA-ZrO_2 nanocomposite

The DMA curves of the pure PMMA, and the PMMA composites having 1, 2 and 5 wt.% of zirconia are shown in Figure 4.6. The presence of zirconia shows a decrease in the storage and loss moduli at lower temperatures, which could be the result of more free space for molecular vibration in the presence of the inorganic (nano)particles. Above the glass transition temperature the 2 and 5% zirconia containing nanocomposites have storage moduli similar to PMMA, but the 1% containing nanocomposite has higher storage modulus values. It seems as if effective immobilization of the polymer chains only takes place at the lower zirconia content. The tan δ curves, shown in Figure 4.6C, confirm that the presence of zirconia did not have a significant influence, except for the nanocomposite containing 1 wt.% ZiO_2, which shows a little increase in the glass transition temperature. These results are surprising because a rigidity increase of the polymer chains is generally observed at higher filler content [21]. They could, however, be explained by considering the aggregation of particles at higher filler quantity. Aggregation would reduce the exposed surface area of the nanoparticles and decrease the extent of interaction of these particles with the polymer, thereby reducing the immobilization of the polymer chains by the nanoparticles.

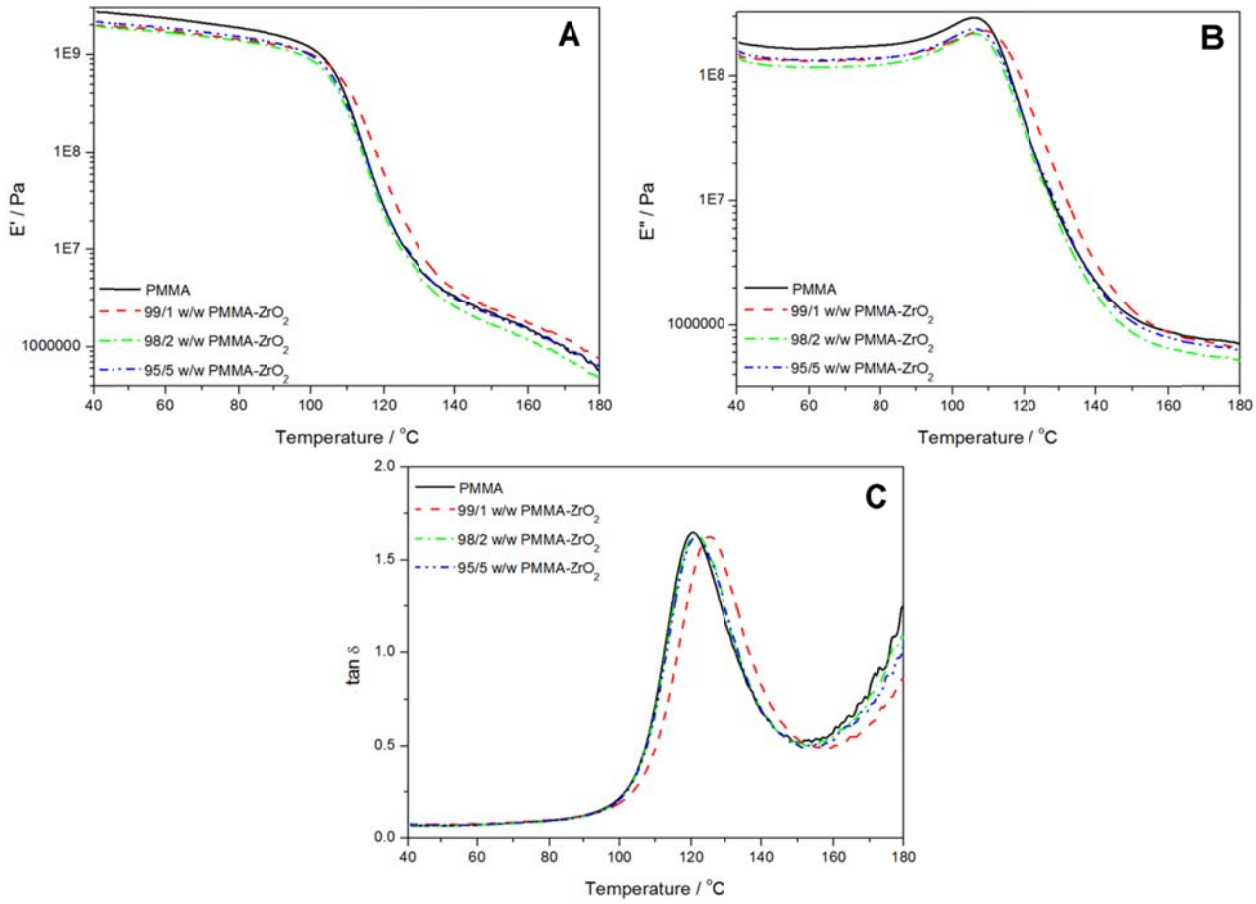

Figure 4.6 (A) Storage modulus, (B) loss modulus and (C) tan δ curves of PMMA and PMMA-ZrO_2 nanocomposites

The TGA curves of the pure PMMA and of the composites having 1, 2 and 5 wt.% of zirconia are reported in Figure 4.7. All the samples show single-step degradation and an increase in char content with an increase in the zirconia content. The amount of char is in line with the amount of zirconia initially mixed into the sample (Table 4.1).

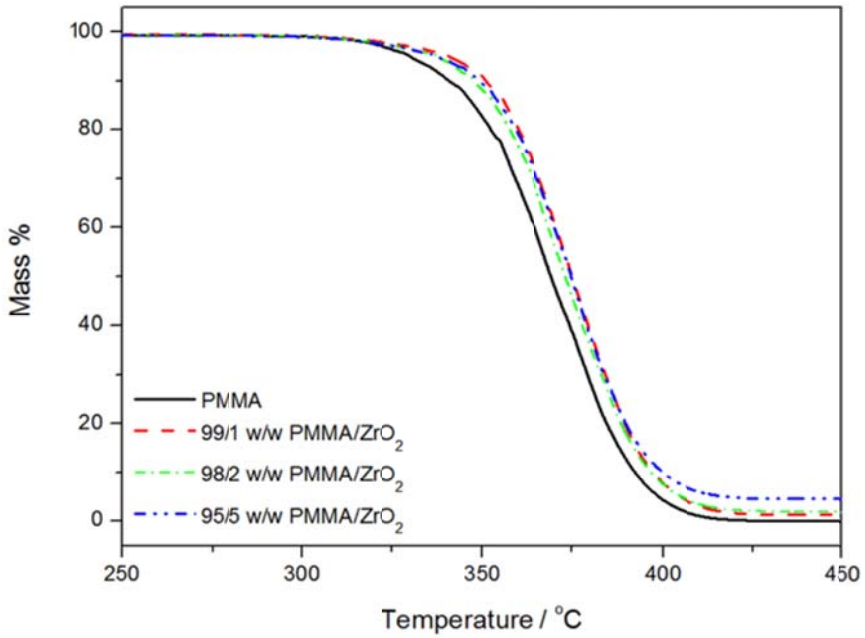

Figure 4.7 TGA curves of PMMA and PMMA-ZrO_2 nanocomposites

Table 4.1 Char content values for all PMMA-zirconia nanocomposites

Sample	Char content / %
98/1 w/w PMMA-ZrO_2	1.33 ± 0.11
98/2 w/w PMMA-ZrO_2	2.10 ± 0.13
98/5 w/w PMMA-ZrO_2	4.88 ± 1.11

The standard deviation values suggest that the nanoparticles dispersion in the polymer matrix was fairly homogeneous, except for the 5% zirconia containing sample which has a very high standard deviation value. This is probably the result of a large number of aggregates formed in this nanocomposite, as observed from the TEM micrographs and according to the hypothesis made when discussing the tan δ data. The presence of zirconia in PMMA slightly increased its thermal stability, but the thermal stability does not increase with increasing amount of zirconia. This is probably due to interactions between the zirconia and the free radical formed during degradation which immobilized the free radicals and retarded the degradation process. It is

possible that the nanoparticles also interacted with the volatile decomposition products and in the process retarded its diffusion out of the sample.

From the TGA curves of PMMA and PMMA-zirconia (5 wt.%) at heating rates of 3, 5, 7 and 9 °C min^{-1} the isoconversional graphs of ln β *versus* 1/*T* according to Equation 1 were plotted, and of ln (β/T^2) *versus* 1/T according to Equation 2. The activation energy values were calculated from the slopes of the isoconversional plots. Both isoconversional methods give similar values of the activation energies within experimental uncertainty. Figure 4.8 illustrates the relationship between the activation energies and the degree of conversion. The activation energy values of pure PMMA and its nanocomposites generally show an increase with the degree of conversion. However, those of the nanocomposites slightly decrease after 80% mass loss. The activation energy values of the nanocomposite are slightly higher than those of pure PMMA up to about 30 % mass loss, which is in line with the higher thermal stabilities observed in Figure 4.7. However, the differences between the two sets of values increase with increasing degree of conversion. The lower activation energy values for the nanocomposite at higher conversions may be related to strong interactions between zirconia and the free radicals formed during degradation, giving rise to the nanoparticles having a catalytic effect on the PMMA degradation during the more advanced stages of degradation [22,23].

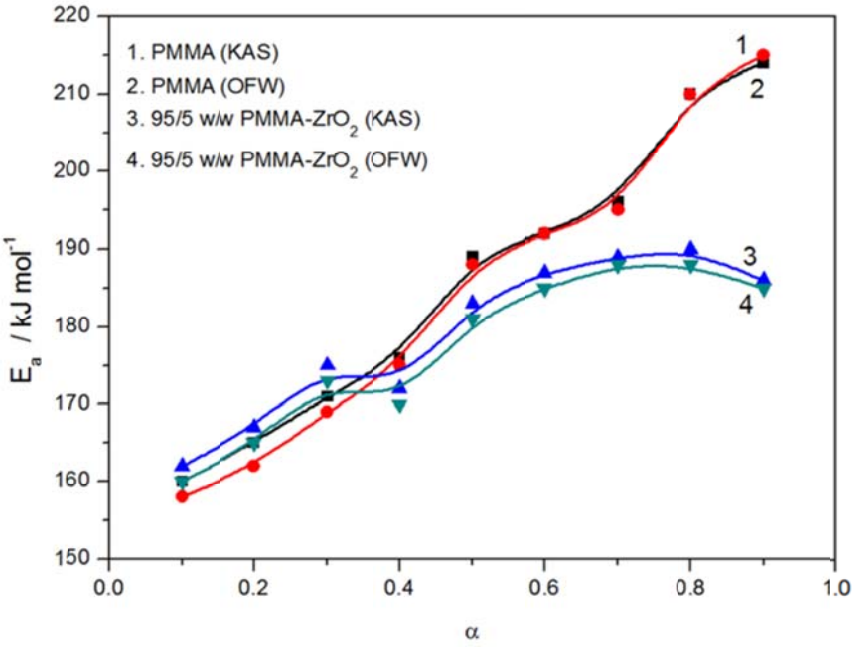

Figure 4.8 E_a values obtained by the OFW and KAS degradation kinetics methods

TGA-FTIR analyses were done to establish the nature of the degradation product(s), and to confirm the observations from the kinetic analysis of the thermal degradation of PMMA and PMMA-zirconia (5 wt.%). All the spectra almost perfectly match the known spectrum of methyl metacrylate (MMA), which confirms the primary degradation as that of de-polymerization (Figure 4.9). The peak around 2966 cm^{-1} is assigned to the CH_3 and CH_2 stretching vibrations, whereas their bending vibration appears around 1451 cm^{-1} for CH_2 and 1314 cm^{-1} for CH_3. The carbonyl absorption vibration appears around 1744 cm^{-1} and the stretching vibration for C-O is around 1167 cm^{-1}. The peak at 2336 cm^{-1} is related to the asymmetric stretching mode of CO_2. No new peaks or peak shifts were observed for the nanocomposite samples. There is a clear increase in peak intensity for all the characteristic peaks with increasing temperature, it reaches a maximum, and decreases again with further increase in temperature.

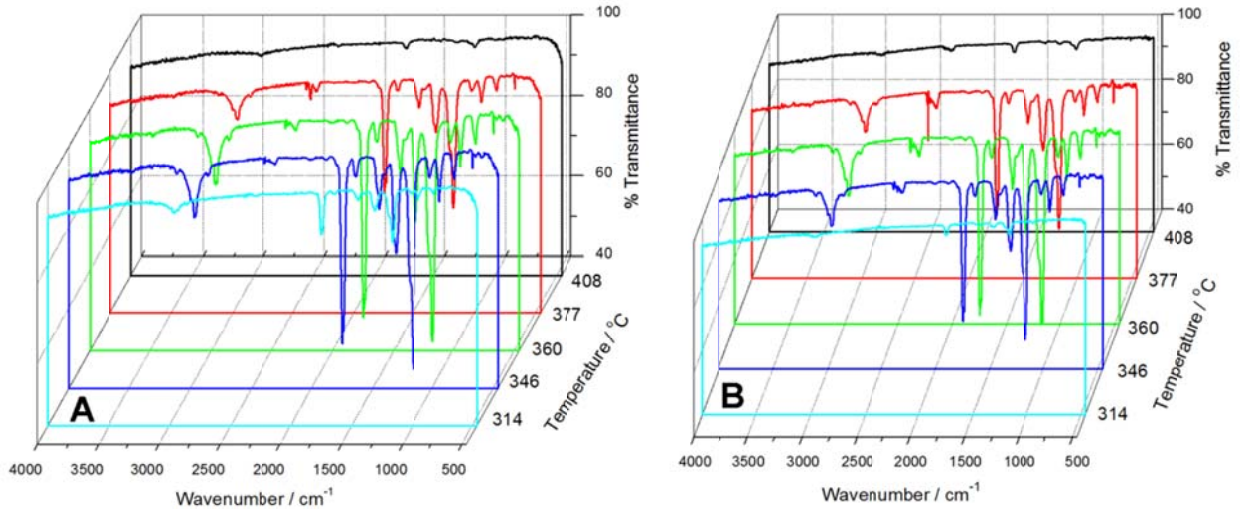

Figure 4.9 FTIR spectra at different temperatures during the thermal degradation in a TGA of (A) PMMA and (B) 95/5 w/w PMMA/ZrO_2 at a heating rate of 10 °C min^{-1}

The PMMA-zirconia (5 wt.%) sample shows the same spectra and a similar trend (Figure 4.9B). The peaks at 314 ºC for PMMA are more intense than the corresponding peaks of the PMMA nanocomposite. The intensities of the peaks for PMMA seem to reach a maximum between 346 and 360 °C, while those of the nanocomposite reach a maximum at 360 °C. This confirms that the initial release of MMA volatiles is retarded when zirconia nanoparticles are present, whether

it is because of an inhibition of the decomposition process or because of a stronger interaction between zirconia and the MMA molecules. The interaction between PMMA or MMA and the zirconia nanoparticles therefore played a significant role in modifying the degradation kinetics.

In order to investigate this aspect, solid state NMR measurements were performed. The ^{13}C {^{1}H} CP-MAS NMR spectra of PMMA and of the composite having 5% of zirconia are reported in Figure 4.10. Five peaks are present in all the spectra: peak 1 at 17 ppm is related to the methyl group, peak 2 at 45 ppm to the methylene group, peak 3 at 52 ppm to the quaternary carbon of polymeric chain, peak 4 at 56 ppm to the methoxyl group, and peak 5 at 177 ppm to the carbonyl carbon, according to literature [20]. No modification in the chemical shift and in the band shape is observed in the PMMA-ZrO_2 composite spectrum indicating that no chemical modification occurred in the polymer.

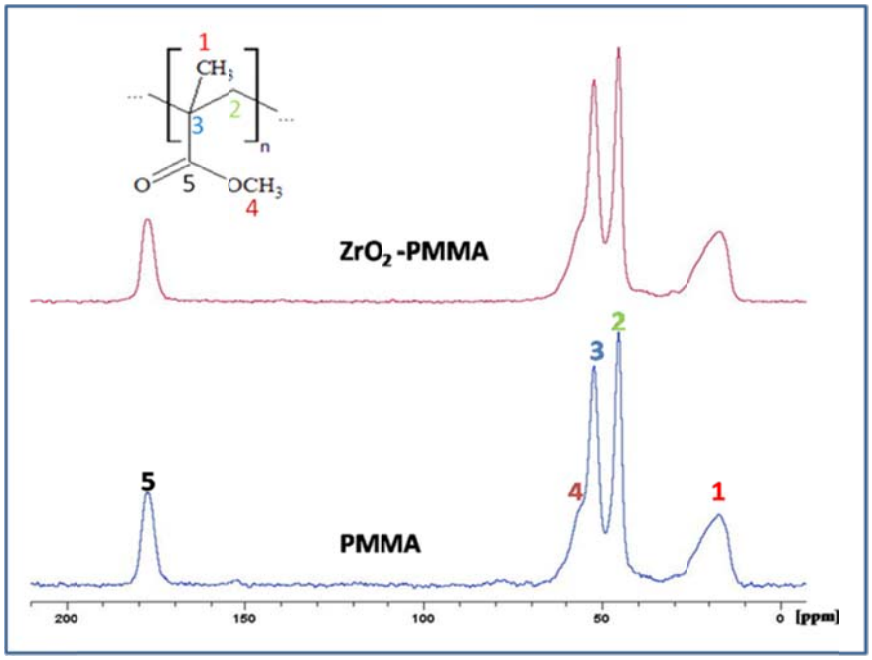

Figure 4.10 ^{13}C {^{1}H} CP-MAS NMR spectra of PMMA and the 95/5 w/w PMMA/ZrO_2 nanocomposite. Numbers on the peaks identify the carbon atoms.

The spin-lattice relaxation time in the laboratory frame $T_1(H)$, and in the rotating frame $T_{1\rho}(H)$, and the cross-polarization time T_{CH} were determined through solid-state NMR measurements in order to evaluate the dynamic modifications occurring in the polymeric chain of the PMMA

matrix after composite formation. The $T_1(H)$, $T_{1\rho}(H)$, and T_{CH} values obtained from each peak in the ^{13}C spectra of all the samples are reported in Table 4.2. The presence of the filler in the PMMA matrix did not significantly affect the $T_1(H)$ values. This indicates that the composite was dynamically homogeneous in a range from tens to hundreds of nanometres. The presence of the ZrO_2 in the PMMA causes an increase of the $T_{1\rho}(H)$ values indicating an increase in the polymer stiffness due to the presence of the filler. This effect is correlated with distances ranging from tens to hundreds of angstroms. In fact, the $T_{1\rho}(H)$ parameter is inversely proportional to the spectral density of motion in the kHz frequency region. These motions reflect the dynamic behaviour of a polymeric chain in a range of a few nanometres. Larger $T_{1\rho}(H)$ values result in an increase in the rigidity of a polymer. The T_{CH} value decrease indicates that there was an increase in the heteronuclear dipolar interactions involving the carbons and the surrounding hydrogen nuclei indicating an increase in the polymer rigidity [24,25]. It is, however, possible that the effect is not strong enough to give rise to an observable change in a macroscopic property like the T_g of a polymer.

Table 4.2 Relaxation time values for all the peaks in the ^{13}C spectra of the PMMA and the PMMA-ZrO_2 composite having the 5 wt.% of filler

ppm	T_1 (H) (s)		$T_{1\rho}$ (H) (ms)		T_{CH} (µs)	
	PMMA	**PMMA-ZrO_2**	**PMMA**	**PMMA-ZrO_2**	**PMMA**	**PMMA-ZrO_2**
178	0.70 ± 0.02	0.71 ± 0.02	18.1 ± 0.5	22.9 ± 0.9	1306 ± 167	1105 ± 126
56	0.71 ± 0.03	0.70 ± 0.03	20.4 ± 0.9	19.5 ± 0.7	254 ± 79	185 ± 26
52	0.71 ± 0.01	0.70 ± 0.01	16.2 ± 0.2	20.7 ± 0.3	339 ± 42	268 ± 22
45	0.71 ± 0.01	0.69 ± 0.01	17.0 ± 0.2	19.6 ± 0.3	614 ± 33	713 ± 41
17	0.71 ± 0.01	0.74 ± 0.02	19.3 ± 0.4	21.9 ± 0.3	320 ± 36	261 ± 21

4.4 Conclusions

Zirconia was successfully prepared by a sol-gel method and XRD analysis confirmed that the powder was composed of a mixture of tetragonal and monoclinic Baddeleyite. The elemental analysis showed evidence of the presence of carbon in the powder. PMMA-zirconia nanocomposites were prepared using a melt compounding method and were systematically investigated as a function of zirconia amount from 1 to 5 wt.%. The XRD results showed that the zirconia nanoparticles maintained their structure and did not induce orientation of the PMMA chains. TEM analysis showed that the nanoparticles were well dispersed in the PMMA matrix, with some agglomerates, especially for the highest investigated zirconia content. NMR analysis indicated that the filler increased the rigidity of the polymer.

The char content values from TGA confirmed the homogenous dispersion by zirconia nanoparticles within PMMA matrix at low zirconia contents. The degradation of the polymer and the release of volatile products occurred at higher temperatures in the presence of zirconia and an increase in zirconia content showed negligible influence on the thermal stability of PMMA. The presence of the nanoparticles also reduced the activation energy of degradation of PMMA at higher conversions.

4.5 References

1. A.Z. Muhammad, A.W. Muhammad, N. Hilal. Preparation and characterization of novel porous PMMA-SiO_2 hybrid membranes. Desalination 2006; 192:262-270. DOI: 10.1016/j.desal.2005.09.022
2. X. Sun, X. Chen, X. Liu, S. Qu. Optical properties of poly(methyl methacrylate)–titania nanostructure thin films containing ellipsoid-shaped titania nanoparticles from ex-situ sol-gel method at low growth temperature. Applied Physics B 2010; 2-8. DOI: 10.1007/s00340-010-4265-6
3. S. Ahmad, S. Ahmad, S.A. Agnihotry. Synthesis and characterization of in situ prepared poly(methyl methacrylate) nanocomposites. Bulletin of Materials Science 2007; 30:31-35. DOI: 10.1007/s12034-007-0006-9

4. X.L. Xie, Q.X. Liu, R.K.Y. Li, X.P. Zhou, Q.X. Zhang, Z.Z. Yu, Y.W. Mai. Rheological and mechanical properties of PVC/$CaCO_3$ nanocomposites prepared by *in situ* polymerization. Polymer 2004; 45:6665-6673.
DOI: 10.1016/j.polymer.2004.07.045
5. M.L. Saladino, A. Zanotto, D. Chillura Martino, A. Spinella, G. Nasillo, E. Caponetti. Ce:YAG nanoparticles embedded in a PMMA matrix: Preparation and characterization. Langmuir 2010; 26:13442-13449.
DOI: 10.1021/la9042809
6. Y. Hu, S. Zhou, L. Wu. Surface mechanical properties of transparent poly(methyl methacrylate)/zirconia nanocomposites prepared by in situ bulk polymerization. Polymer 2009; 50: 3609-3616.
DOI: 10.1016/j.polymer.2009.03.02
7. H. Wang, P. Xu, W. Zhong, L. Shen, Q. Du. Transparent poly(methyl methacrylate)/ silica/zirconia nanocomposites with excellent thermal stabilities. Polymer Degradation and Stability 2005; 87: 319-327.
DOI: 10.1016/j.polymdegradstab.2004.08.015
8. Y. Wang, D. Zhang, L. Shi, L. Li, J. Zhang. Novel transparent ternary nanocomposites films of trialkoxysilane-capped poly(methyl methacrylate)/zirconia/titania with incorporating networks. Materials Chemistry and Physics 2008; 110: 463-470.
DOI: 10.1016/jmetchemphys.2008.03.006
9. M. Atik, F.P. Luna, S.H. Messaddeq, M.A. Aegerter. Ormocer (ZrO_2-PMMA) films for stainless steel corrosion protection. Journal of Sol-Gel Science and Technology 1997; 8:517-522.
DOI: 10.1007/BF02436892
10. Y. Hu, G. Gu, S. Zhou, L. Wu. Preparation and properties of transparent PMMA/ZrO_2 nanocomposites using 2-hydroxyethyl methacraylate as a coupling agent. Polymer 2011; 52:122-129.
DOI: 101016/j.polymer.2010.11.020
11. S.H. Messaddeq, S.H. Pulcinelli, C.V. Santilli, A.C. Guastaldi, Y. Massaddeq. Macrostructure and corrosion resistance of inorganic-organic (ZrO_2-PMMA) hybrid

coating on stainless steel. Journal of Non-Crystalliane Solids 1999; 247:164-170. DOI: 10.1016/S0022-3093(99)00058-7

12. X. Wang, L. Wu, J. Li. Influence of nanozirconia on the thermal stability of poly(methyl methacrylate) prepared by in situ bulk polymerization. Journal of Applied Polymer Science 2010; 117:163-170.
DOI: 10.1002/app
13. X. Wang, L. Wu, J. Li. Synergistic flame retarded poly(methyl methacrylate) by nano-ZrO_2 and triphenylphosphate. Journal of Thermal Analysis and Calorimetry 2011; 103: 741-746.
DOI: 10.1007/s10973-010-1050-z
14. F. Bondioli, V. Cannillo, E. Fabbri, M. Messori. Preparation and characterization of epoxy resins filled with submicron spherical zirconia particles. Polimery 2006; 51:11-12.
DOI: 10.1111/j.1551-2916.2008.02666.x
15. R.A. Young (Ed.). The Rietveld Method. Oxford University Press: Oxford (1993).
16. L. Lutterotti, S. Gialanella. X-ray diffraction characterization of heavily deformed metallic specimens. Acta Metallurgica 1998; 46:101-110.
DOI: 10.1016/S1359-6454(97)00222-X
17. S.R. Hartmann, E.L. Hahn. Nuclear double resonance in the rotating frame. Physical Review Online Archive 1962; 128:2042-2053.
DOI: 10.1103/PhysRev.128.2042
18. C. Lau, Y. Mi. A study of blending and complexation of poly(acrylic acid)/poly(vinyl pyrrolidone). Polymer 2002; 43:823-829.
DOI: 10.1016/S0032-3861(01)00641-3
19. P. Conte, R. Spaccini, A. Piccolo. State of art of CPMAS ^{13}C-NMR spectroscopy applied to natural organic matter. Progress in Nuclear Magnetic Resonance Spectroscopy 2004; 44:215-223.
DOI: 10.1016/j.pnmrs.2004.02.002
20. R.G. Alamo, J.A. Blanco, I. Carrilero. Measurement of the ^{13}C spin-lattice relaxation time of the non-crystalline regions of semicrystalline polymers by a CP-MAS-based method. Polymer 2002; 43:1857-1865.
DOI: 10.1016/S0032-3861(01)00761-3

21. M.L. Saladino, T.E. Motaung, A.S. Luyt, A. Spinella, G. Nasillo, E. Caponetti. The effect of silica nanoparticles on the morphology, mechanical properties and thermal degradation kinetics of PMMA. Polymer Degradation and Stability 2012; 97:452-459.
DOI: 10.1016/j.polymdegradstab.2011.11.006

22. A.A. Vassiliou, K. Chrissafis, D.N. Bakiaris. Thermal degradation kinetics of in situ prepared PET nanocomposites with acid-treated multi-walled carbon nanotubes. Journal of Thermal Analysis and Calorimetry 2010; 100:1063-1071.
DOI: 10.1007/s10973-0090426-4

23. S. Majoni, S. Su, J.M. Hossenlopp. The effect of boron containing layered hydroxy salt (LHS) on the thermal stability and degradation kinetics of poly(methyl methacrylate). Polymer Degradation and Stability 2010; 95:1593-1604.
DOI:10.1016/j.polymdegradstab.2010.05.033

24. M. Geppi, F. Ciardelli, C.A. Veracini, C. Forte, G. Cecchin, P. Ferrari. Dynamics and morphology of polyolefinic elastomers by means of ^{13}C and ^{1}H solid- state n.m.r. Polymer 1997; 38:5713-57233.
DOI: 10.1016/S0032-3861(97)00134-1

25. J.L. Koenig (2^{nd} Ed). Spectroscopy of Polymers. Elsevier Science (1999).

Chapter 5

The effect of silica nanoparticles on the morphology, mechanical properties and thermal degradation kinetics of polycarbonate

This chapter has been accepted as a publication:
T.E. Motaung, M.L. Saladino, A.S. Luyt, D. Chillura Martino. The effect of silica nanoparticles on the morphology, mechanical properties and thermal degradation kinetics of polycarbonate. Composites Science and Technology (In press)

Abstract

Polycarbonate/silica nanocomposites with different silica quantities were prepared by a melt compounding method. The effect of silica amount, in the range 1-5 wt.%, on the morphology, mechanical properties and thermal degradation kinetics of polycarbonate (PC) was investigated. Clusters of silica nanoparticles were well dispersed in the polycarbonate whose structure remained amorphous. NMR results showed intermolecular interactions involving the carbonyl groups of different polymeric chains which did not affect the intramolecular rotational motions. The presence of the lowest silica content showed a decrease in the storage and loss moduli below the glass transition temperature, probably due to a plasticization effect. However, an increase in the amount of silica increased the moduli. The presence of silica in PC slightly increased the thermal stability, except for the highest silica content which showed a decrease. The activation energies of thermal degradation for the nanocomposites depended on the amount of silica and on the degree of conversion.

Keywords:

A. Polymer-matrix composites (PMCs); A. Nano-composites; B. Mechanical properties; B. Thermal properties.

5.1 Introduction

Polycarbonate (PC) nanocomposites are a very attractive material for a range of industrial applications due to the unique properties that can be observed when compared to conventional composites. The incorporation of small amounts of metal oxide nanoparticles into the polymer matrices was found to remarkably improve dimensional stability, and the mechanical, thermal, optical, electrical, and gas barrier properties, as well as to decrease the flammability [1-6]. PC-silica nanocomposites, prepared by various methods, attracted the attention of many institutions due to their improved transparency and mechanical properties [7,8].

The preparation of the nanocomposites by a simple one-step injection molding process showed the presence of primary silica nanopowders, together with some small nanocluster aggregates, well dispersed in the polymer matrix [7,8]. The dispersion was related to a possible chemical bonding between the organic and inorganic phases. The glass transition temperature (T_g) of the PC was found to increase with the addition of 5 wt.% silica nanopowder. The results also showed that the incorporation of silica nanopowders enhanced the thermal stability of the polymer where the chain segment motion was restricted by the interfacial-particle interactions between the surface functionalized-silica nanopowders and the polymer molecules [7].

Other studies indicated that the increase in silica content in a PC matrix prepared by sol-gel led to a decrease in both the glass transition temperature and the thermal stability. The observation was related to the presence of a steric hindrance on the formation of a silica network [9,10]. Well dispersed aggregates were observed and the size of the SiO_2 domains increased with increasing amount of TEOS in sol-gel prepared nanocomposites [9,10].

The PC-silica nanocomposites at lower loading of modified silica prepared by melt mixing showed an enhancement in thermal stability, an increase in storage modulus, scratch resistance, and hardness compared to pristine PC. This was related to the reduced particle-particle interactions dominated by hydrogen bonding ensued from the hydroxide groups on the silica surface and the carbonyl groups in the PC [8,11].

A similar reason was given for the increased storage modulus of the nanocomposites prepared by solution mixing [12]. However, the storage modulus values showed no significant difference between the samples containing unmodified and modified silica. This observation was also related to hydrogen bonding. The volumetric strain was also investigated at the cross-section where the necking dominates. The results showed that the filler brought significant differences in the onset and propagation of necking and those where related to a disrupted molecular structure of the polymer by the filler.

The aim of this work was to investigate the thermal, mechanical and degradation behavior of PC-silica nanocomposites as function of silica loading. PC-SiO_2 nanocomposites were prepared through a melt compounding method by using chemically modified SiO_2 nanoparticles. Both nanoparticles and composites were characterized using transmission electron microscopy (TEM), X-ray diffractometry (XRD), dynamic mechanical analysis (DMA), thermogravimetric analyses (TGA), and ^{13}C cross-polarization magic-angle spinning nuclear magnetic resonance ($^{13}C\{^{1}H\}$ CP-MAS NMR).

5.1.1 Experimental

5.2.1 Materials

AEROSIL® R972 (R972, Degussa, Germany) is a hydrophobic silica having chemically surface bonded methyl groups, based on a hydrophilic fumed silica with a specific surface area of 130 $m^2\ g^{-1}$ and an average primary particle size of 16 nm. The silica was dried at 120 °C under static vacuum for a minimum of 16 hours before further use. Commercial grade bisphenol-A polycarbonate (PC, Makrolon® 2407 produced by Bayer MaterialScience, Germany and having a melt flow rate at 300°C/1.2 kg of 20 g/10 min) was used in pellet form. The polymer was dried at 120 °C overnight under static vacuum before processing.

5.2.2 Composites preparation

PC was thoroughly mixed with 1, 2 and 5 wt.% silica for 10 min at 240 °C and 30 rpm in the 50 mL internal mixer of a Brabender Plastograph from Duisburg, Germany. The mixed samples were melt-pressed into 1 mm thick sheets at 200 °C for 5 min.

5.2.3 Analysis methods

TEM micrographs were acquired using a JEM-2100 (JEOL, Japan) electron microscope operating at 200 kV accelerating voltage. The obtained nanocomposites were cut into slices (thickness about 100 nm) using a Leica EM UC6 ultra-microtome. Slices were put and analysed in a 3 mm Cu grid "lacey carbon".
XRD patterns were recorded in the 2-70° 2θ range at steps of 0.05° and a counting time of 5 s/step on a Philips PW 1050 diffractometer, equipped with a Cu tube and a scintillation detector beam.

The dynamic mechanical properties of the composites were investigated from 40 to 180 ºC in the bending mode at a heating rate of 5 ºC min^{-1} and a frequency of 1 Hz using a Perkin Elmer Diamond DMA from Waltham, Massachusetts, U.S.A. The glass transition temperatures were determined from the peak maxima in the tan δ curves.

Thermogravimetric analysis (TGA) was performed in a Perkin Elmer TGA7 from Waltham, Massachusetts, U.S.A under flowing nitrogen at a constant flow rate of 20 mL min^{-1}. Samples (5-10 mg) were heated from 25 to 600 °C at different heating rates. The degradation kinetic analysis was performed using the Ozawa-Flynn-Wall (OFW) and Kissinger-Akahira-Sunose (KAS) methods, described elsewhere [13]. The % mass loss, or mass loss fraction, was used as the degree of conversion in our calculations.

The TGA-FTIR analyses were performed using a Perkin Elmer STA6000 simultaneous thermal analyzer from Waltham, Massachusetts, U.S.A, under flowing nitrogen at a constant flow rate of 20 mL min^{-1}. Samples (20-25 mg) were heated from 30 to 600 °C at 10° C min^{-1} and held for 4

min at 600 °C. The furnace was linked to a FTIR (Perkin Elmer Spectrum 100, Massachusetts, U.S.A.) with a gas transfer line. The volatiles were scanned over a 400-4000 cm^{-1} wavenumber range at a resolution of 4 cm^{-1}. The FTIR spectra were recorded in the transmittance mode at different temperatures during the thermal degradation process.

^{13}C {^{1}H} CP-MAS NMR spectra were obtained at room temperature through a Bruker Avance II 400 MHz (9.4 T) spectrometer operating at 100.63 MHz for the ^{13}C nucleus with a MAS rate of 8 kHz, 500 scans, a contact time of 1.5 ms and a repetition delay of 2 sec. The optimization of the Hartmann-Hahn condition [14] was obtained using an adamantine sample. Each sample was placed in a 4 mm zirconia rotor with KEL-F caps using silica as filler to avoid inhomogeneities inside the rotor. The proton spin–lattice relaxation time in the rotating frame $T_{1\rho}(H)$ was indirectly determined, with the variable spin lock (VSL) pulse sequence, by the carbon nucleus observation using a 90°–τ–spin-lock pulse sequence prior to cross-polarization [15]. The data acquisition was performed by ^{1}H decoupling with a delay time, τ, ranging from 0.1 to 7.5 ms and a contact time of 1.5 ms. The proton spin–lattice relaxation time in the laboratory frame $T_1(H)$ was determined, using the saturation recovery pulse sequence [16], by a carbon nucleus observation using a 90°–τ–90° pulse sequence prior to cross polarization with a delay time τ ranging from 0.01 to 3 s. The ^{13}C spin–lattice relaxation time in the rotating frame $T_{1\rho}(C)$ was determined, with the variable spin lock (VSL) pulse sequence, applying the spin-lock pulse after the cross-polarization on the carbon channel [15]. The data acquisition was performed by ^{1}H decoupling with a spin lock pulse length, τ, ranging from 0.4 to 30 ms and a contact time of 1.5 ms. The cross polarization time T_{CH} values for all the carbon signals of PC were obtained through variable contact time (VCT) experiments [17]. The contact times used in the VCT experiments were 0.05, 0.1, 0.2, 0.3, 0.4, 0.5, 0.6, 0.8, 1.0, 1.2, 1.5, 2.0, 2.5, 3.0, 3.5, 4.0, 4.5, 5.0, 6.0 and 7.0 ms.

5.3 Results and discussion

TEM micrographs of the SiO_2 powder were reported in a previous paper [13]. Silica powder shows aggregates (sizes between 1 and 3 micron) constituted of a large number of nanoparticles of ~20 nm. The TEM micrographs of the PC-silica nanocomposite having 5 wt.% of SiO2 are

shown in Figure 5.1. Agglomerated silica particles, similar in size and shape to those observed in the powder sample, are observed. Each cluster, with dimensions between 50 and 300 nm, and with a number of small nanoparticles, is well dispersed in the polymeric matrix.

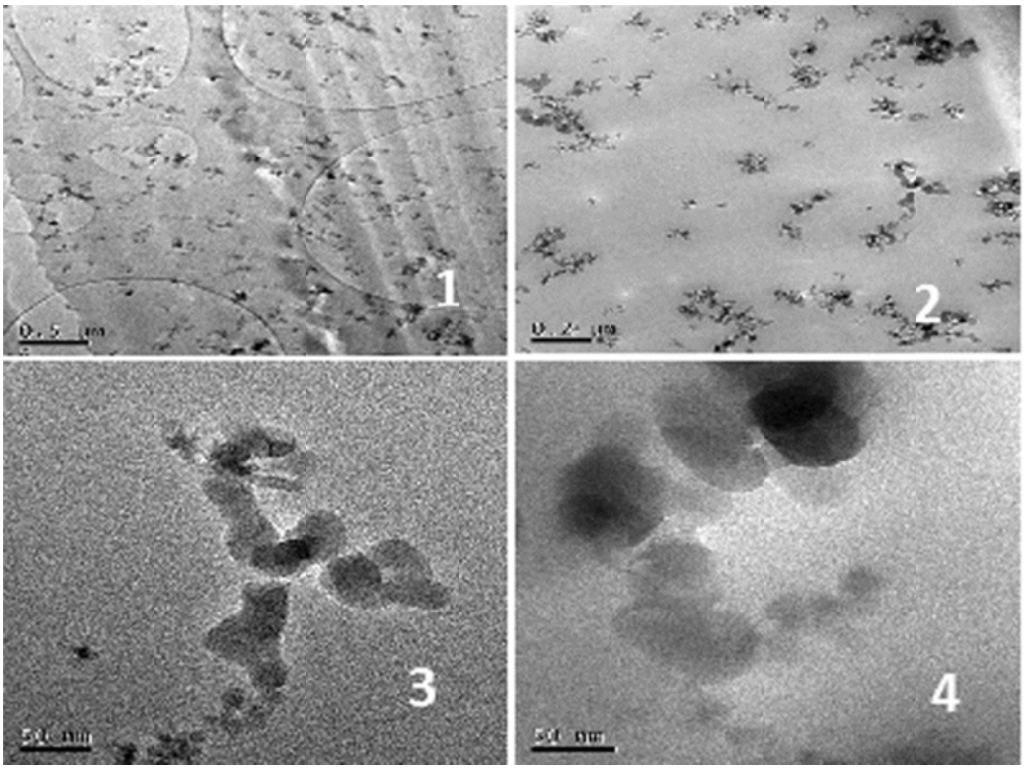

Figure 5.1 TEM micrographs of silica-PC composite having 5 wt.% of SiO_2

The XRD patterns of the SiO_2 powder and the PC-SiO_2 composites are reported in Figure 5.2. The diffraction pattern of the silica powder shows a broad band around $2\theta = 21.2$, typical of an amorphous material. The diffraction pattern of pure PC does not contain any crystalline reflection indicating that polycarbonate is also amorphous. Similar diffraction patterns were obtained for the PC-silica nanocomposites indicating that neither the orientation of the PC chains nor the amorphous structure of the silica was influenced by the presence of the filler.

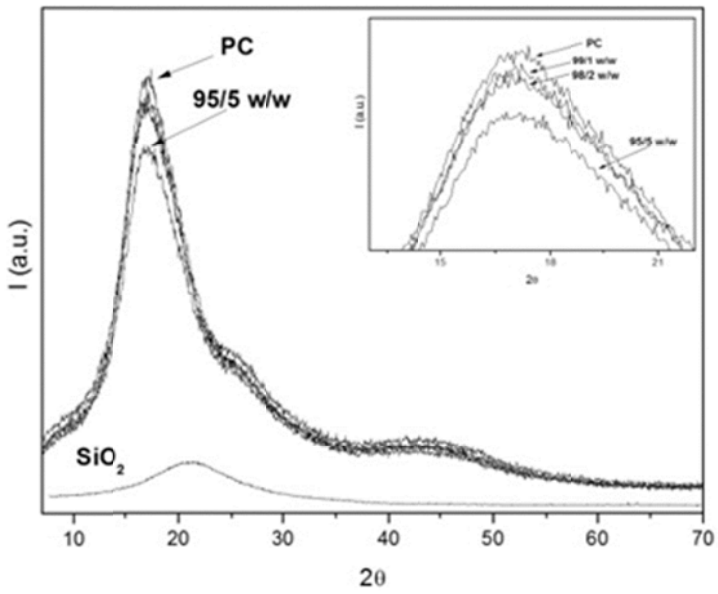

Figure 5.2 XRD patterns of silica powder, pure PC and the silica-PC nanocomposites

The storage modulus, loss modulus and tan δ of the pure PC and the PC-silica composites having 1, 2 and 5 wt.% of SiO_2 are reported in Figure 5.3. Below the glass transition temperature the storage modulus of the 1% silica containing nanocomposite is lower than that of PC, probably because of a plasticizing effect by the small amount of well dispersed silica nanoparticles on the PC matrix. Further increase in silica content increased the storage modulus over the whole temperature range. It seems as if effective immobilization of the polymer chains only takes place at higher silica contents. The loss modulus followed the same pattern as the storage modulus. The glass transition temperatures for all composites are higher than that of pure PC, indicating that effective immobilization already starts when 1% nanoparticles are introduced into the polymer.

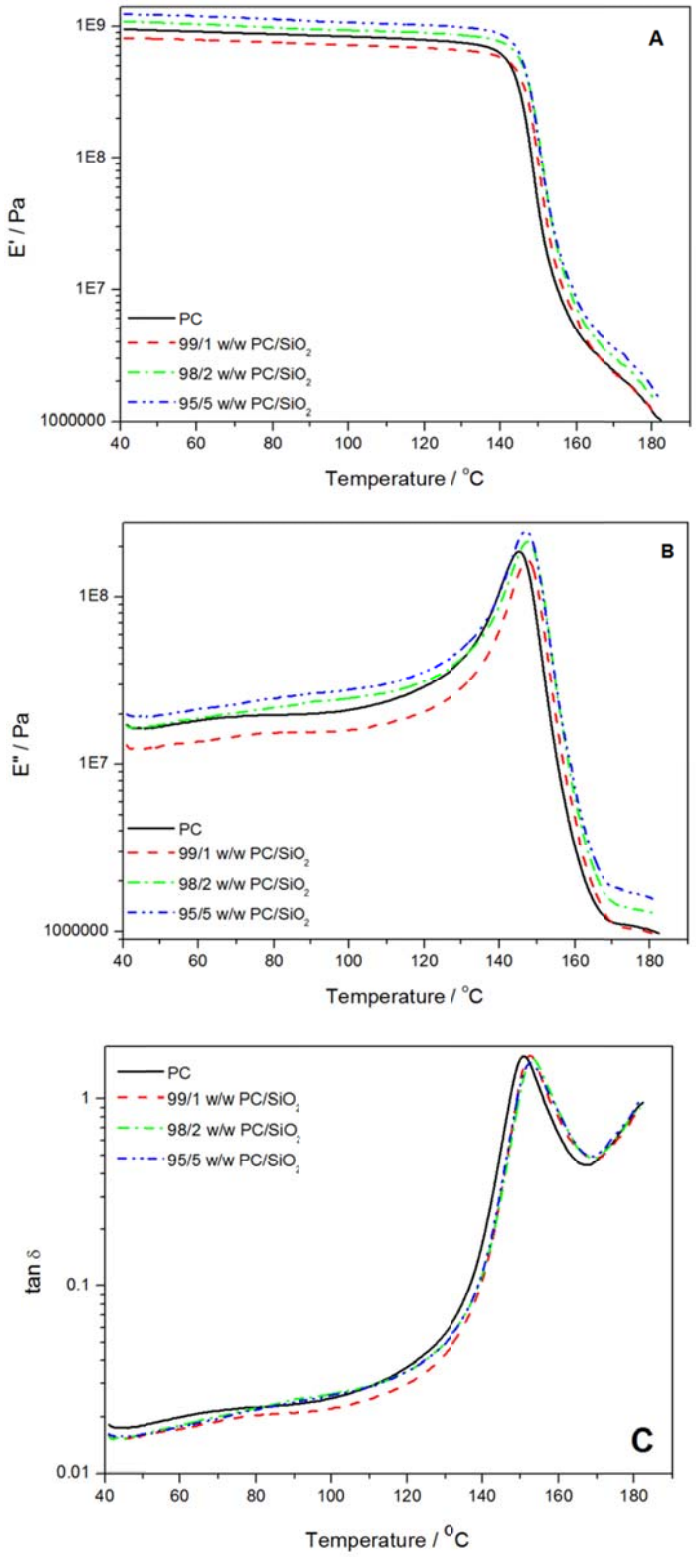

Figure 5.3 (A) Storage modulus, (B) loss modulus and (C) tan δ curves of PC and PC/silica nanocomposites

The TGA curves of the pure PC and of the PC-silica composites are reported in Figure 5.4. All the samples show single-step degradation, which very slightly moves to higher temperatures with increasing amount of silica, except for the 5% silica containing sample, which showed lower thermal stability than PC. The increase in thermal stability is not significant enough to be discussed in detail, but it could be attributed to interactions between the organically modified silica and the polymer, while the decrease for the 5% silica containing sample is probably due to a catalytic effect of the silica particles on the PC degradation, as discussed below.

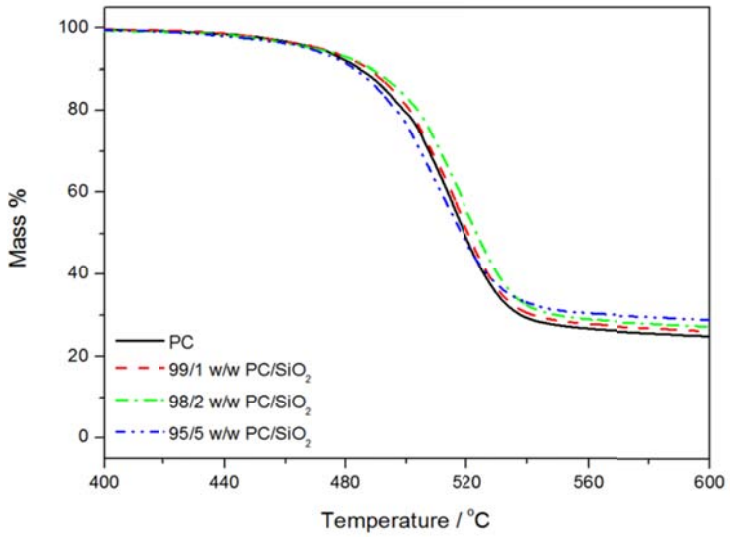

Figure 5.4 TGA curves of PC and the PC/silica nanocomposites

From the TGA curves of PC and PC-silica (2 and 5 wt.%) at heating rates of 3, 5, 7 and 9 °C min^{-1} the isoconversional graphs of ln β *versus* 1/*T* and of ln (β/T^2) *versus* 1/T were plotted, according to OFW and KAS methods, respectively [13]. The activation energy values were calculated from the slopes of the isoconversional plots. Both isoconversional methods give similar values of the activation energies within experimental uncertainty. In Figure 5.5 the relationship between the activation energy and the degree of conversion is reported.

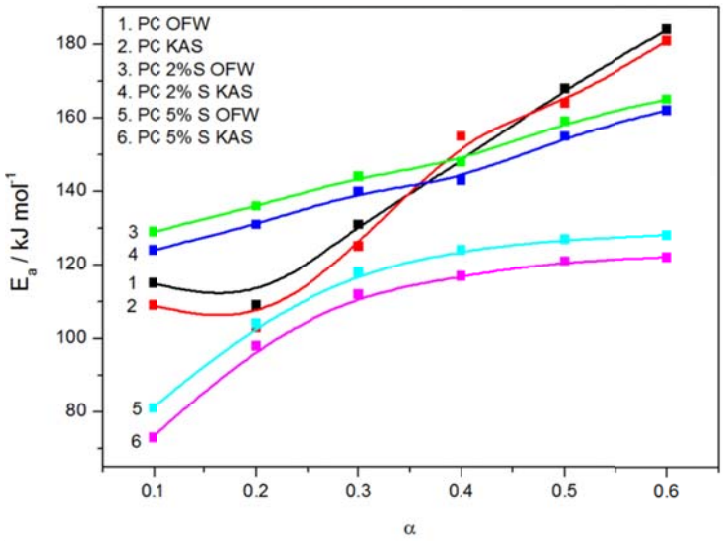

Figure 5.5 E_a values obtained by the OFW and KAS degradation kinetics methods

The activation energy values for the pure PC and its 2 wt.% silica nanocomposite increase with the degree of conversion, but those for the 5 wt.% silica nanocomposite initially increase but level off around 40% mass loss, and are lower than those of the pure polymer. The 2 wt.% silica nanocomposite shows the highest activation energy values up to 40% mass loss, while at higher degrees of conversion its activation energy values are between those of the pure polymer and the 5 wt.% silica nanocomposite.

The increase in activation energy with an increase in degree of conversion was also observed by us when investigating PMMA-SiO_2/TiO_2/ZrO_2 nanocomposites [13,18,19] and by several other authors [20-22]. It was generally explained as changes in the degradation mechanism with increasing degree of conversion. Dong *et al.* [23] investigated PC-MgO nanocomposites, and they attributed the increase in activation energy of degradation with increasing degree of conversion to the stable carbonaceous char which protects the polymer from further degradation. They also observed that an increase in MgO content shifted the TGA curves to lower temperatures, and that the initial activation energy values for the PC-MgO nanocomposites were lower than those of pristine PC. They attributed these observations to a catalytic effect the MgO nanoparticles have during the initial stages of PC degradation, which was also observed during the investigation of other, but similar, systems [19]. Their activation energy values correspond very well with the values we reported in Figure 5.5. We observed a similar change in activation

energy with increasing degree of conversion for PC-silica nanocomposites [13]. Like MgO, low quantities of silica seem to have a catalytic effect during the initial stages of the degradation. In our case, however, the protecting effect of the carbonaceous char is more dominant during the later stages of degradation. If one looks at the results of the 5% silica containing PC (Figure 5.5), it is clear that the catalytic effect is more dominant and the activation energies for this nanocomposite are clearly lower than those of the pristine PC and the 2% silica containing PC over the whole degree of conversion range. The values for the 5% silica containing PC also approach a constant value at higher degrees of conversion, which shows that the protecting effect of the carbonaceous char is less dominant in this case, despite the fact that the char content is the same than those of PC and PC-silica (2%) according to the TGA curves in Figure 5.4.

TGA-FTIR analyses were done to establish the nature of the degradation product(s) of PC and the PC-silica nanocomposites. The FTIR spectra of the degradation products of pure PC at different temperatures during the degradation process are shown in Figure 5.6A. All the spectra almost perfectly match the known spectrum of the thermal decomposition of bisphenol-A polycarbonate in which CO_2, phenol and bisphenol A are the main volatile products. The observed peaks at 3658, 2974 and 1182 cm^{-1} are assigned to free alcohols (aliphatic substituted phenol), to C-H stretching vibrations, and to the carbon hydroxyl stretching band. The peaks at 1606, 1509 and 1257 cm^{-1} are assigned to the ring stretching, to skeletal vibration of phenyl compounds, and to the aromatic ether stretch. In addition, the peak observed in the range 2388-2119 cm^{-1} and at 833 cm^{-1} are due to the symmetric stretching and the bending modes of CO_2, respectively. No new peaks or peak shifts were observed for the nanocomposite samples, the spectra of which are reported in Figure 5.6B. The peaks at 458 ºC for the PC nanocomposite are more intense than those of the PC. The intensities of the peaks for PC seem to reach a maximum between 458 and 503 °C, while those of the nanocomposite reach a maximum at 458 °C, which is in line with the lower activation energies of degradation observed for the nanocomposites.

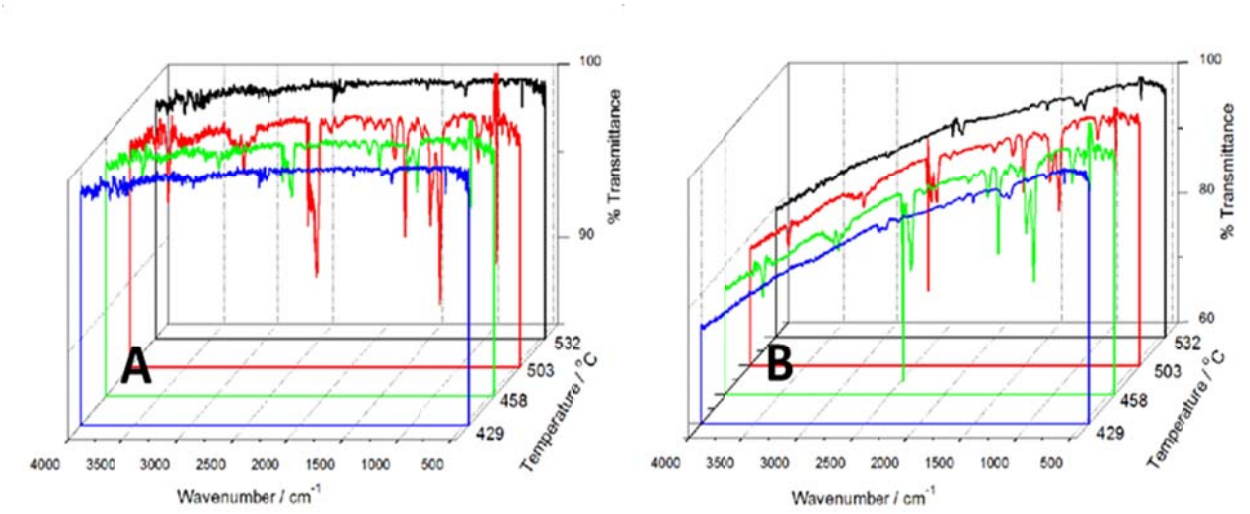

Figure 5.6 FTIR curves at different temperatures during the thermal degradation of pure PC (A) and PC with 5 wt.% (B) silica in a TGA

$^{13}C\{^{1}H\}$ CP-MAS NMR measurements were performed in order to understand the possible changes caused by the filler in the polymer and to attempt a correlation between the mechanical properties, the kinetics of degradation and the molecular structure of the polymer. The ^{13}C $\{^{1}H\}$ CP-MAS NMR spectra of the PC-SiO_2 composites having 2 and 5% of silica are reported in Figure 5.7. Five peaks are present in the spectra: peak 1 at 149 ppm is related to the quaternary carbons of the aromatic rings and to the carbonyl carbon, peak 2 at 127 ppm is related to the aromatic carbon in meta to the oxygen, peak 3 at 120 ppm is related to the aromatic carbon in ortho to the oxygen, peak 4 at 42 ppm is related to the quaternary carbon bonded to the methyl groups and peak 5 at 31 ppm is related to the methyl carbons, according to literature [24]. No modification in the chemical shift and in the band shape is observed in the PC-silica nanocomposites spectra indicating that no chemical modification occurred in the polymer. Thus, the relaxation times in the laboratory frame $T_1(H)$, in the rotating frame $T_{1\rho}(H)$, and $T_{1\rho}(C)$ and the cross-polarization time T_{CH} were determined through solid-state NMR measurements in order to evaluate the dynamic modifications occurring in the polymeric chain of the PC matrix after composite formation. The $T_1(H)$, $T_{1\rho}(H)$, $T_{1\rho}(C)$ and T_{CH} values obtained from each peak in the ^{13}C spectra of all the samples are reported in Table 5.1.

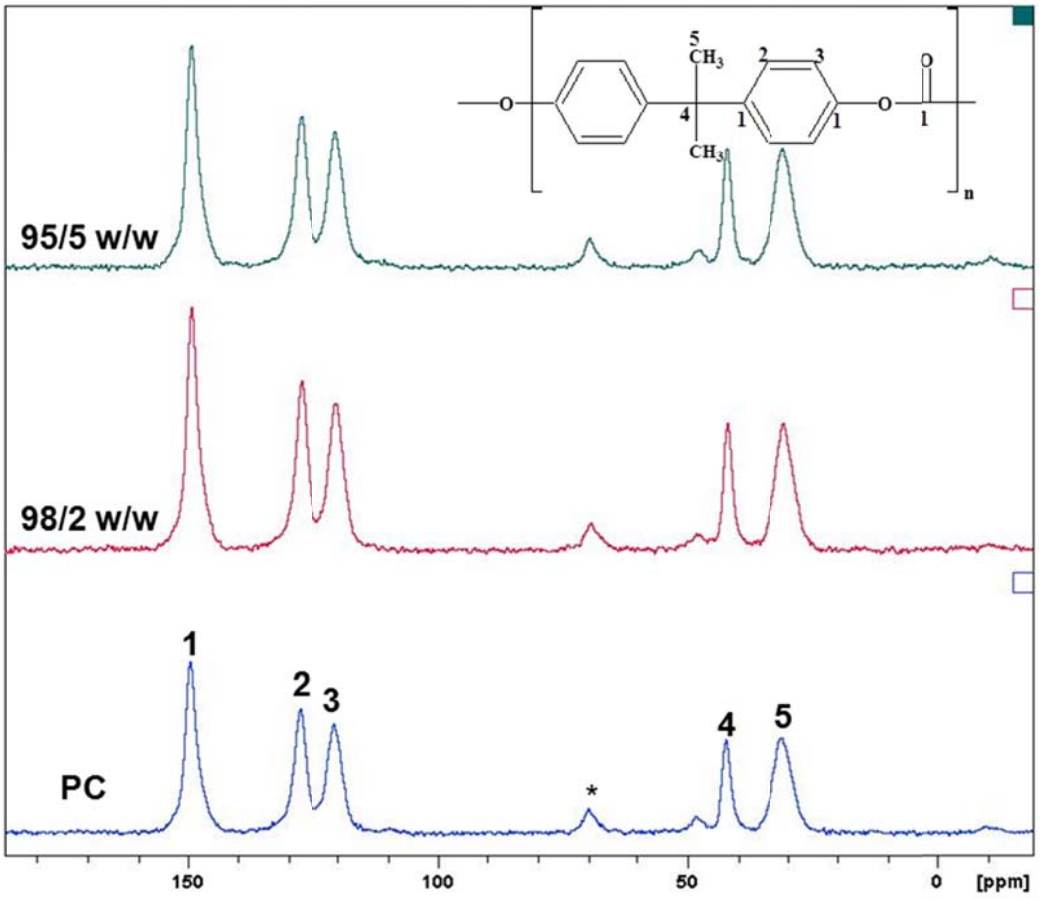

Figure 5.7 **^{13}C {^{1}H} CP-MAS NMR spectra of PC and of and silica-PC nanocomposites. Numbers on the peaks identify the carbon atoms. The * symbol indicates spinning sidebands**

The presence of the filler in the PC matrix did not significantly affect the $T_1(H)$. This indicates that the spin diffusion phenomenon averages the dynamic behavior of the polymer and that the composites are dynamically homogeneous in a range from tens to hundreds of nanometres. On the contrary, the $T_{1\rho}(H)$, $T_{1\rho}(C)$ and T_{CH} values are affected by the presence of silica. In the PC-silica composites loaded with 2% the $T_{1\rho}(H)$ values are homogenous and similar to those of pure PC, but for the PC-silica composites loaded with 5% the $T_{1\rho}(H)$ values are inhomogeneous indicating a presence of inhomogeneity in the composite. This is not a surprise considering the presence of particle aggregates and it is in agreement with the observed thermal behaviour.

Table 5.1 T_1(H), $T_{1\rho}$(H), $T_{1\rho}$(C) and T_{CH} values for all the carbons in the ^{13}C spectra of PC and the PC-SiO_2 nanocomposites having 2 and 5 wt.% of filler

		T_1 (H) (s)			$T_{1\rho}$ (H) (ms)		
Carbon	**ppm**	**PC**	**PC-SiO_2 (2%)**	**PC-SiO_2 (5%)**	**PC**	**PC-SiO_2 (2%)**	**PC-SiO_2 (5%)**
1	149	0.39 ± 0.02	0.40 ± 0.02	0.41 ± 0.03	4.9 ± 0.2	5.9 ± 0.2	5.0 ± 0.2
2	127.5	0.41 ± 0.03	0.41 ± 0.02	0.40 ± 0.05	5.4 ± 0.2	5.8 ± 0.3	6.3 ± 0.3
3	120	0.39 ± 0.01	0.41 ± 0.03	0.39 ± 0.01	5.2 ± 0.2	5.0 ± 0.3	4.8 ± 0.2
4	42	0.40 ± 0.01	0.38 ± 0.03	0.38 ± 0.01	4.8 ± 0.2	5.4 ± 0.2	6.2 ± 0.3
5	31	0.42 ± 0.01	0.38 ± 0.03	0.40 ± 0.03	4.9 ± 0.3	5.1 ± 0.3	5.3 ± 0.3
		$T_{1\rho}$ (C) (ms)			T_{CH} (ms)		
Carbon	**ppm**	**PC**	**PC-SiO_2 (2%)**	**PC-SiO_2 (5%)**	**PC**	**PC-SiO_2 (2%)**	**PC-SiO_2 (5%)**
1	149	41 ± 0.2	41.1± 0.8	53.4 ± 0.2	1328 ± 127	1009 ± 53	998 ± 50
2	127.5	10.9 ± 0.1	16.0 ± 0.3	11.5 ± 0.1	117 ± 28	127 ± 21	142 ± 14
3	120	10.2 ± 0.2	20.3 ± 0.8	15.8 ± 0.4	64 ± 12	151 ± 21	128 ± 17
4	42	18 ± 0.2	18.3 ± 0.4	23.5 ± 0.7	1059 ± 97	744 ± 51	737 ± 48
5	31	19.2 ± 0.1	23.5 ± 0.3	22.3 ± 0.2	275 ± 20	207 ± 14	231 ± 17

For each sample, the $T_{1\rho}$(C) values of the carbonyl and substituted aromatic carbons are lower than those for the protonated aromatic, methyl and quaternary carbons. This finding suggests that the fast rotational motions of the methyl group and of the phenylene rings around the 1-4 axis modulate the ^{1}H-^{13}C dipolar couplings thus providing the major contribution to the $T_{1\rho}$ relaxation. In particular, in the PC-silica composites loaded with 2% silica the $T_{1\rho}$(C) values for the peaks at 149 and 42 ppm are unchanged, but increased for the peaks resonating at 127.5, 120 and 31 ppm with respect to that of the pure PC matrix. This is evidence that the small quantity of silica slows down only the rotational motion of the phenylene rings. On the other hand, in the PC-silica composites loaded with 5% silica an increase in the $T_{1\rho}$(C) values is also observed for the peaks at 149 and 42 ppm. This implies that the main chain motions and in particular those of the carbonyl carbon are hindered by the presence of silica. In this case the rotational and

vibrational motions of the phenylene rings are slightly slowed. These observations are due to the intermolecular interactions involving the carbonyl groups of different polymeric chains which do not affect the intramolecular rotational motions. In addition, an increase in the dipolar coupling T_{CH} for the carbonyl carbons, the quaternary and the methyl carbons is observed in the PC-silica nanocomposites, while an opposite trend is observed for the protonated aromatic carbons. T_{CH} values are related to the rate at which the magnetization transfer from protons to carbons takes place. This behavior thus corroborates the hypothesis of specific intermolecular interactions caused by the silica in the composite, and may be accountable for the differences in thermal degradation and thermomechanical behavior observed between the different samples.

5.4 Conclusions

PC-silica nanocomposites, prepared by melt compounding, were systematically investigated as a function of silica quantity from 1 to 5 wt.%. The silica nanoparticles, organized in clusters uniformly dispersed into the amorphous polymer. The polymer chain immobilization, increasing with the silica amount, is due to intermolecular interactions between silica and the polymer in the composite which do not involve the protonated aromatic carbons. The composites show the same degradation mechanism as pure PC. The thermal stability and the activation energy of the degradation process also depend on the amount of silica. In fact, the nanocomposites with silica loading up to 2 wt.% have a higher thermal stability and show different degradation kinetics than the nanocomposites with 5 wt.% silica loading.

5.5 References

1. A. Lagashetty, H. Vijayanand, S. Basavaraja, M.D. Bedre, A. Venkataraman. Preparation, characteristics, and thermal studies of γ-Fe_2O_3 and CuO dispersed polycarbonate nanocomposites. Journal of Thermal Analysis and Calorimetry 2010; 99:577-581. DOI:10.1007/s10973-009-0475-8

2. F.J. Carrion, J. Sanes, M.D. Bermudez. Influence of ZnO nanoparticle filler on the properties and wear resistance of polycarbonate. Wear 2007; 262:1504-1510.
DOI:10.1016/j.wear.2007.01.016
3. F.J. Carrion, J. Sanes, M.D. Bermudez. Effect of ionic liquid on the structure and tribological properties of polycarbonate-zinc oxide nanodispersion. Materials Letters 2007; 61:4531-4535.
DOI:10.1016/j.matlet.2007.02.044
4. M.D. Bermúdez, W. Brostow, F. Carrión-Vilches, J. Sanes. Scratch resistance of polycarbonate containing ZnO nanoparticles: Effect of sliding direction. Journal of Nanoscience and Nanotechnology 2010; 10:6683-6689.
DOI:10.1166/jnn.2010.2513
5. Y. Imai, A. Terahara, Y. Hakuta, K. Matsui, H. Hayashi, N. Ueno. Transparent poly(bisphenol A carbonate)-based nanocomposites with high refractive index nanoparticles. European Polymer Journal 2009; 45:630-638.
DOI:10.1016/J.europolyj.2008.12.013
6. K. Xu, S. Zhou, L. Wu. Effect of highly dispersible zirconia nanoparticles on the properties of UV-curable poly(urethane-acrylate) coatings. Journal of Materials Science 2009; 44:1613-1621.
DOI:10.1007/s10853-008-3231-8
7. J.L.H. Chau, S.L.C. Hsu, Y.M. Chen, C.C. Yang, P.C.F. Hsu. A simple route towards polycarbonate-silica nanocomposites. Advanced Powder Technology 2010; 21:341-343.
DOI:10.1016/j.apt.2010.02.005
8. A. Christman, P. Lenny, J.C. Quantin, A.S. Caro-Bretelle, J.M.L. Cuesta. Mechanical behavior at large strain of polycarbonate nanocomposites during uniaxial tensile test. Journal of the European Ceramic Society 2011; 52:4033-4044.
DOI:10.106/j.polymer.2011.06.056

9. C.S. Tan, T.W. Kuo. Synthesis of polycarbonate-silica nanocomposites from copolymerization of CO_2 with allyl glycidyl ether, cyclohexene oxide, and sol-gel. Journal of Applied Polymer Science 2005; 98:750-757.
DOI:10.1002/app.22126
10. N. Suzuki, Y. Yamauchi. Fabrication of mesostructured silica and tatania rods on substrates by using polycarbonate membranes. Journal of Nanomaterials 2010; 2010:1-4.
DOI:10.1155/2010/382043
11. A.S. Luyt, M. Messori, P. Fabbri, J.P. Mofokeng, R. Taurion, T. Zanasi, F. Pilati. Polycarbonate reinforced with silica nanoparticles. Polymer Bulletin 2011; 66:991-1004.
DOI:10.1007/s00289-010-0408-5
12. R. Poręba, M. Špírková, Z. Hrdlička. Mechanical and thermochemical properties of polycarbonate-based polyurethane-silica nanocomposites. Processing and Application of Ceramics 2011; 5: 155-159.
DOI:10.10Sl/jp4:20030687
13. M.L. Saladino, T.E. Motaung, A.S. Luyt, A. Spinella, G. Nasillo, E. Caponetti. The effect of silica nanoparticles on the morphology, mechanical properties and thermal degradation kinetics of PMMA. Polymer Degradation and Stability 2012; 97:452-459.
DOI:10.1016/j.polymdegradstab.2011.11.006
14. S.R. Hartmann, E.L. Hahn. Nuclear double resonance in the rotating frame. Physical Reviews 1962; 128:2042-2053.
15. C. Lau, Y. Mi. A study of blending and complexation of poly(acrylic acid)/poly(vinyl pyrrolidone). Polymer 2002; 43:823-829.
DOI:org/10.1016/S0032-3861 (01)00641-3
16. R.G. Alamo, J. A. Blanco, I. Carrilero, R. Fu. Measurement of ^{13}C spin-lattice relaxation time of the non-crystalline regions of semicrystalline polymers by a CP-MAS-based method. Polymer 2002; 43:1857-1865.
DOI:10.1016/S0032-3861(01)00761-3
17. P. Conte, R. Spaccini, A. Piccolo. State of the art of CPMAS ^{13}C-NMR spectroscopy applied to natural organic matter. Progress in Nuclear Magnetic Resonance Spectroscopy 2004; 44:215–223.
DOI:10.1016/j.pnmrs.2004.02.002

18. B.J. Holland, J.N. Hay. The value and limitations of non-isothermal kinetics in the study of polymer degradation. Thermochimica Acta 2002; 253-273.
DOI:10.1016/S0040-6031(02)00034-5

19. Z. Gao, T. Kaneko, D. Hou. M. Nakada. Kinetics of thermal degradation of poly(methyl methacrylate) studied with the assistance of the fractionation conversion at the maximum reaction rate. Polymer Degradation and Stability 2004; 84: 399-403.
DOI:10.1016/j.polymdegradstab.2003.11.015.

20. S. Vyazovkin. A unified approach to kinetic processing of nonisothermal data. International Journal of Chemical kinetics 1996; 28:95-101.
DOI:10.1002/(SICI)1097-4601(1996)28:2<95::AID-KIN4>3.0.CO;2-G

21. T.E. Motaung, A.S. Luyt., F. Bondioli, M. Messori, M.L. Saladino, A. Spinella, G. Nasillo, E Caponetti. PMMA-titania nanocomposites: Properties and thermal degradation behaviour. Polymer Degradation and Stability 2012; 97:1325-1333.
DOI:10.1016/j.polymdegradstab.2012.05.022

22. T.E. Motaung, A.S. Luyt, M.L. Saladino, D. Chillura Martino, E. Caponetti. Morphology, mechanical properties and thermal degradation kinetics of PMMA-zirconia composites prepared by melt compounding. eXPRESS Polymer Letters 2012;6: 871-881.
DOI:10.3144/expresspolymlett.2012.93

23. Q. Dong, C. Gao, Y. Ding, F. Wang, B. Wen, S. Zhang, T. Wang, M. Yang. A polycarbonate/magnesium oxide nanocomposite with high flame retardancy. Journal of Applied Polymer Science 2011; 123:1085-1093.
DOI:10.1002/app.34574

24. A.P.A.M. Eijkelenboom, W.E.J.R. Maas, W.S. Veeman, G.H.W. Buning, J.M.J. Vankan. Triple-resonance fluorine-19, proton, and carbon-13 CP-MAS NMR study of the influence of PMMA tacticity on the miscibility in PMMA/poly (vinylidene fluoride) (PVF2) blends. Macromolecules 1992;25:4511-4518.
DOI:10.1021/ma00044a009

Chapter 6

Study of morphology, mechanical properties and thermal degradation of polycarbonate-titania nanocomposites as function of titania crystalline phase and content

This chapter has been accepted as a publication:
T.E. Motaung, A.S. Luyt, M.L. Saladino, E. Caponetti. Study of morphology, mechanical properties and thermal degradation of polycarbonate-titania nanocomposites as function of crystalline phase and content of titania. Polymer Composites (In press)

Abstract

Titania nanoparticles were prepared using a sol-gel method and calcination at 200 and 600 °C to obtain anatase and rutile phases, respectively. The obtained powders were used to prepare polycarbonate-titania nanocomposites by melt compounding. The effect of different crystalline phases and amounts of titania, in the range 1-5 wt.%, on the morphology, mechanical properties and thermal degradation kinetics of polycarbonate was investigated. The results show that the filler modified the plasticity or rigidity of the polymer, and influenced the degradation kinetics, in different ways depending on the type and amount of titania.

Keywords: Polycarbonate; Titania; Nanocomposites; Degradation kinetics; Interfacial interaction

6.1 Introduction

An organic-inorganic nanocomposite of engineering thermoplastics represents a unique set of mechanical, thermal and electrical properties [1-3]. Polycarbonate (PC) is an engineering plastic consumed widely to prepare composites due to its high strength, thermal stability and outstanding optical transparency. There are a number of recent papers reporting on the mechanical properties, thermal stability and flame retardancy on PC containing different clays, silica, calcium oxide, iron oxide and multi walled carbon nanotubes [4-9]. It was found that

metal oxides have a pronounced effect on the morphology, as well as mechanical and thermal behaviour, of PC. Some authors found that the well dispersed metal oxide nanoparticles in PC improved its surface and volume resistivity, mechanical properties, and increased its magnetic activity and thermal stability [4-6]. Improvements in the mechanical properties and thermal stability were also observed in PC nanocomposites with different clays [7-10]. These observations were related to the strong interaction at the polymer-filler interface.

The incorporation of titanium dioxide (TiO_2) in PC had attracted the attention of many scientists due to improved optical and mechanical properties of the final nanocomposites [11-13]. In the studies where nanocomposites were prepared by solution mixing, the results showed that TiO_2 was well dispersed inside the matrix, even at higher contents (about 6-11%). Several microscopic observations showed that the filler was not agglomerated inside the composite at all TiO_2 contents [11-14]. The refractive indices of the nanocomposites relative to that of the PC increased with increasing amounts of nanoparticles. This was attributed to the modification of the components which led to a better interfacial interaction.

Imai *et al*. [11] found that the presence of titania (up to 42% content in PC, crystalline structure not specified) deteriorated the thermal stability of the nanocomposites. The same results were found by Gupta *et al*. [14] and the behaviour was related to the dispersion of the nanoparticles in the matrix polymer. They also studied the thermal degradation kinetics of these nanocomposites. They suggested that the degradation of PC and the nanocomposites was second and first order respectively. In the case of PC the observation was related to crosslinking and branching which was formed through tertiary or peroxide free radicals during the degradation. However, in the presence of metal oxides the observation was related to the predominance of chain scission.

In a study where the nanocomposites were prepared by extrusion, the material showed areas of densification around the notch edge [15]. These areas appeared as circular crater-like areas in the scanning electron microscopy micrographs. Energy dispersive X-ray analysis of these areas showed an extremely high concentration of titanium dioxide at the centre of the crater. These observations were related to the generation of a site of nucleation for the growth of a densified

form of PC by the TiO_2 nanoparticles (fine rutile crystal grade up to 10% content). Differential scanning calorimetry results could, however, not confirm the nucleation.

Rouabah *et al.* [13] studied the effect of quenching temperature on the mechanical properties of PC-TiO_2 nanocomposies. The titania nanoparticles were fine rutile crystal grade up to 10% content. A higher TiO_2 content increased the modulus of elasticity and decreased the unnotched and notched Izod impact strengths, as well as the elongation at break. A maximum yield stress was obtained at 3% of TiO_2. Quenching at 40 °C improved the Izod impact strength and the elongation at break of samples with 3% of TiO_2, whereas the elastic modulus, density and yield stress were a minimum at this quenching temperature. The observations were related to the increase in free volume which led to higher molecular mobility.

A review paper on the photoinduced reactivity of titanium dioxide [16] discusses the differences between anatase and rutile titania, all of which may cause the respective nanoparticles to interact differently with a polymer matrix. The exposed planes of these nanoparticles are different and, although both anatase and rutile titania have tetragonal structures, anatase titania can be regarded to be built up from octahedral structures that are connected by their vertices, while in rutile titania the edges are connected. It was further found that the anatase phase has a different oxygen vacancy than the rutile phase, as well as higher electron mobility, lower dielectric constant, lower density, lower deposition temperature and lower surface energy. Both these titania phases were found to have catalytic properties.

Most of the reported studies concentrated on commercial anatase titania incorporated in PC, while little information was provided regarding the incorporation of the rutile phase into PC. No systematic comparison of the properties of PC-TiO_2 nanocomposites, containing respectively anatase and rutile titania, have been reported in literature. The purpose of this work was to prepare PC-TiO_2 nanocomposites, containing anatase and rutile titania respectively, by melt compounding, and to study the influence of the type and amount of titania on the degradation and thermomechanical behaviour of the polymer.

6.2 Experimental

6.2.1 Materials

Commercial grade bisphenol-A polycarbonate (PC, Makrolon® 2407 produced by Bayer Material Science, Germany and having a melt flow rate at 300 °C/1.2 kg of 20 g/10 min) was used in pellet form. The polymer was dried at 120 °C overnight under static vacuum before processing.

6.2.2. Titania preparation

Titania was prepared by a sol-gel combustion of aqueous solutions containing $TiO(NO_3)_2$, as precursor, and glycine as fuel [17].

6.2.3 Composites preparation

PC was thoroughly mixed with 1, 2 and 5 wt.% titania for 10 min at 240 °C and 30 rpm in the 50 mL internal mixer of a Brabender Plastograph from Duisburg, Germany. The mixed samples were melt-pressed into 1 mm thick sheets at 200 °C for 5 min.

6.2.4 Analysis methods

Transmission electron microscopy (TEM) micrographs were acquired using a JEM-2100 (JEOL, Japan) electron microscope operating at a 200 kV accelerating voltage. The nanocomposites were cut into slices (thickness about 100 nm) using a Leica EM UC6 ultra-microtome. Slices were put on a 3 mm Cu grid "lacey carbon" and analysed.

X-ray diffraction (XRD) patterns were recorded in a 2θ range of 2-70° in steps of 0.05° and a counting time of 5 s/step on a Philips PW 1050 diffractometer, equipped with a Cu tube and a scintillation detector beam. The X-ray generator worked at 40 kV and 30 mA. The instrument resolution (divergent and antiscatter slits of 0.5°) was determined using standards free from the effect of reduced crystallite size and lattice defects.

^{13}C cross polarization - magic angle spinning nuclear magnetic resonance (^{13}C {^{1}H} CP-MAS NMR) spectra were obtained at room temperature with a Bruker Avance II 400 MHz (9.4 T)

spectrometer operating at 100.63 MHz for the ^{13}C nucleus with a MAS rate of 8 kHz, 500 scans, a contact time of 1.5 ms and a repetition delay of 2 sec. The optimization of the Hartmann-Hahn condition [18] was obtained using an adamantine sample. Each sample was placed in a 4 mm zirconia rotor with KEL-F caps using silica as filler to avoid inhomogeneities inside the rotor. The proton spin–lattice relaxation time in the rotating frame $T_{1\rho}(H)$ was indirectly determined, with a variable spin lock (VSL) pulse sequence, by the carbon nucleus observation using a 90°–τ–spin-lock pulse sequence prior to cross-polarization [19]. The data acquisition was performed by ^{1}H decoupling with a delay time, τ, ranging from 0.1 to 7.5 ms and a contact time of 1.5 ms. The proton spin–lattice relaxation time in the laboratory frame $T_1(H)$ was determined, using a saturation recovery pulse sequence [20] by a carbon nucleus observation using a 90°–τ–90° pulse sequence prior to cross polarization with a delay time τ ranging from 0.01 to 3 s. The ^{13}C spin–lattice relaxation time in the rotating frame $T_{1\rho}(C)$ was determined, with the variable spin lock (VSL) pulse sequence, applying the spin-lock pulse after the cross-polarization on the carbon channel [19]. The data acquisition was performed by ^{1}H decoupling with a spin lock pulse length, τ, ranging from 0.4 to 30 ms and a contact time of 1.5 ms. The cross polarization time T_{CH} values for all the carbon signals of PC were obtained through variable contact time (VCT) experiments [21]. The contact times used in the VCT experiments were 0.05, 0.1, 0.2, 0.3, 0.4, 0.5, 0.6, 0.8, 1.0, 1.2, 1.5, 2.0, 2.5, 3.0, 3.5, 4.0, 4.5, 5.0, 6.0 and 7.0 ms.

The dynamic mechanical properties of the composites were investigated from 40 to 180 ºC in the bending mode at a heating rate of 5 ºC min^{-1} and a frequency of 1 Hz using a Perkin Elmer Diamond dynamic mechanical analyser (DMA) from Waltham, Massachusetts, U.S.A.

Thermogravimetric analysis (TGA) was performed in a Perkin Elmer TGA7 from Waltham, Massachusetts, U.S.A under flowing nitrogen at a constant flow rate of 20 mL min^{-1}. Samples (5-10 mg) were heated from 25 to 600 °C at different heating rates. The degradation kinetics analysis was performed using the Ozawa-Flynn-Wall (OFW) and Kissinger-Akahira-Sunose (KAS) methods, described elsewhere [22].

TGA combined with Fourier-transform infrared (FTIR) spectroscopy analyses were performed using a Perkin Elmer STA6000 simultaneous thermal analyzer from Waltham, Massachusetts,

U.S.A, under flowing nitrogen at a constant flow rate of 20 mL min^{-1}. Samples (20-25 mg) were heated from 30 to 600 °C at 10° C min^{-1} and held for 4 min at 600 °C. The furnace was linked to a FTIR (Perkin Elmer Spectrum 100, Massachusetts, U.S.A.) with a gas transfer line. The volatiles were scanned over a 400-4000 cm^{-1} wavenumber range at a resolution of 4 cm^{-1}. The FTIR spectra were recorded in the transmittance mode at different temperatures during the thermal degradation process.

6.3 Results and discussion

The XRD patterns of the TiO_2 powder, heated at 200°C and 600°C, pure PC, and their respective composites are reported in Figure 6.1. The pattern of titania heated at 200 °C is constituted by the anatase phase, while the powder heated at 600 °C is constituted by 99 wt.% of tetragonal rutile and 1 wt.% of orthorhombic brookite [17]. The diffraction pattern of PC shows an intense broad diffraction peak around 17° and two bands of lower intensities typical of an amorphous material. Similar diffraction patterns were obtained for all the composites indicating that the orientation of the PC chains was not influenced during the preparation process and by adding different types and amounts of titania filler. Furthermore, the intensity of the diffraction peaks for the composites decreased with increasing titania content, as expected, which is due to the increase in the amount of filler. The XRD patterns of the PC- titania (anatase) nanocomposites having 1 and 2 wt.% of filler do not show the characteristic peak of the anatase titania, while a very weak peak around 25° is present in the pattern of the nanocomposite loaded with 5 wt.% filler. The PC-titania (rutile) nanocomposites, however, clearly show the titania diffraction peaks superimposed onto the PC amorphous band, even at low titania contents, which suggests the presence of either big particles or aggregates [17].

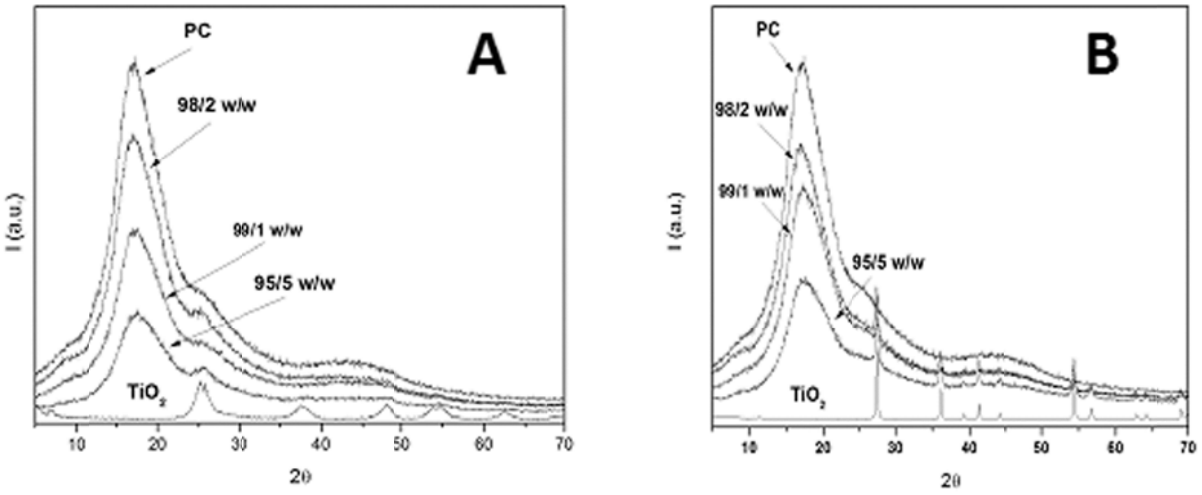

Figure 6.1 XRD patterns of titania treated at A) 200 °C and B) 600 °C, of pure PC and of the corresponding PC-TiO_2 composites

The TEM micrographs of the TiO_2 powders were reported in our previous paper [17] where it was found that anatase titania was constituted of aggregates with sizes between 0.5 and 1 micron. The aggregates were formed by several particles smaller than 5 nm diameter, very densely packed. The rutile titania was constituted of particles with sizes between 1 and 2 microns. The TEM micrographs of the PC-titania (anatase) and PC-titania (rutile) composites having 5% of filler are reported in Figure 6.2. The PC-titania (anatase) composite shows large aggregates constituted of spherical particles smaller than 5 nm in diameter, and single spherical particles near the surfaces of the aggregated particles. The PC-titania (rutile) composite shows clusters of different sizes (from 500 nm up to a few microns) composed of different numbers of nanoparticles between 20 and 60 nm in size and with irregular shapes. These results are in agreement with the XRD patterns that suggest the presence of larger aggregates.

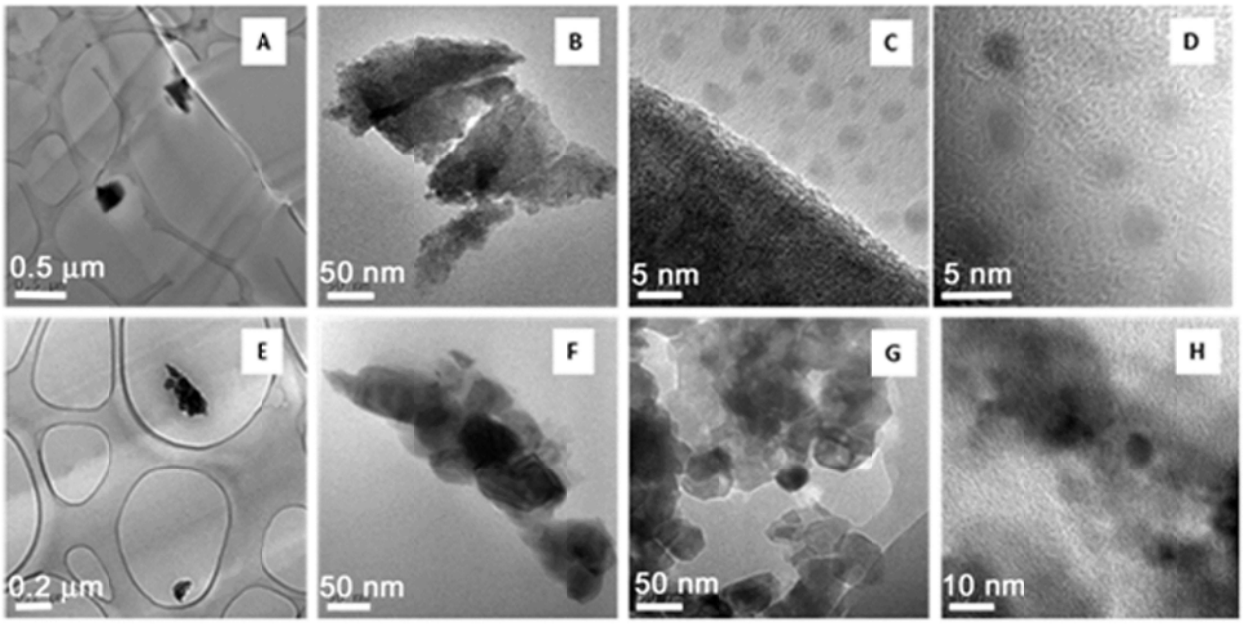

Figure 6.2 TEM micrographs of the PC-TiO_2 (anatase) (A-D) and the PC-TiO_2 (rutile) (E-H) composites

The storage modulus of the pure PC, the PC-TiO_2 (anatase) and the PC-TiO_2 (rutile) composites having 1, 2 and 5 wt.% of TiO_2 are reported in Figure 6.3 and 6.4. The presence of anatase titania (1% and 2%) shows an observable decrease in the storage and loss moduli (Figures 6.3A and 6.3B) at all temperatures, probably because of a plasticizing effect of these nanoparticles on the PC matrix [23]. However, the 5% anatase titania containing nanocomposite shows an increase in the moduli, even above the glass transition temperature. It could be due to an increase in the rigidity as a consequence of the higher filler content. However, Figure 6.4 shows a decrease in modulus only for the 1% rutile titania containing sample. The nanocomposites containing 2 and 5 wt.% of rutile titania show slightly increased moduli below the glass transition, and a negligible effect above the glass transition. The reason for this behaviour could be related to the formation of larger clusters, as shown by TEM, by the rutile titania nanoparticles in the PC matrix.

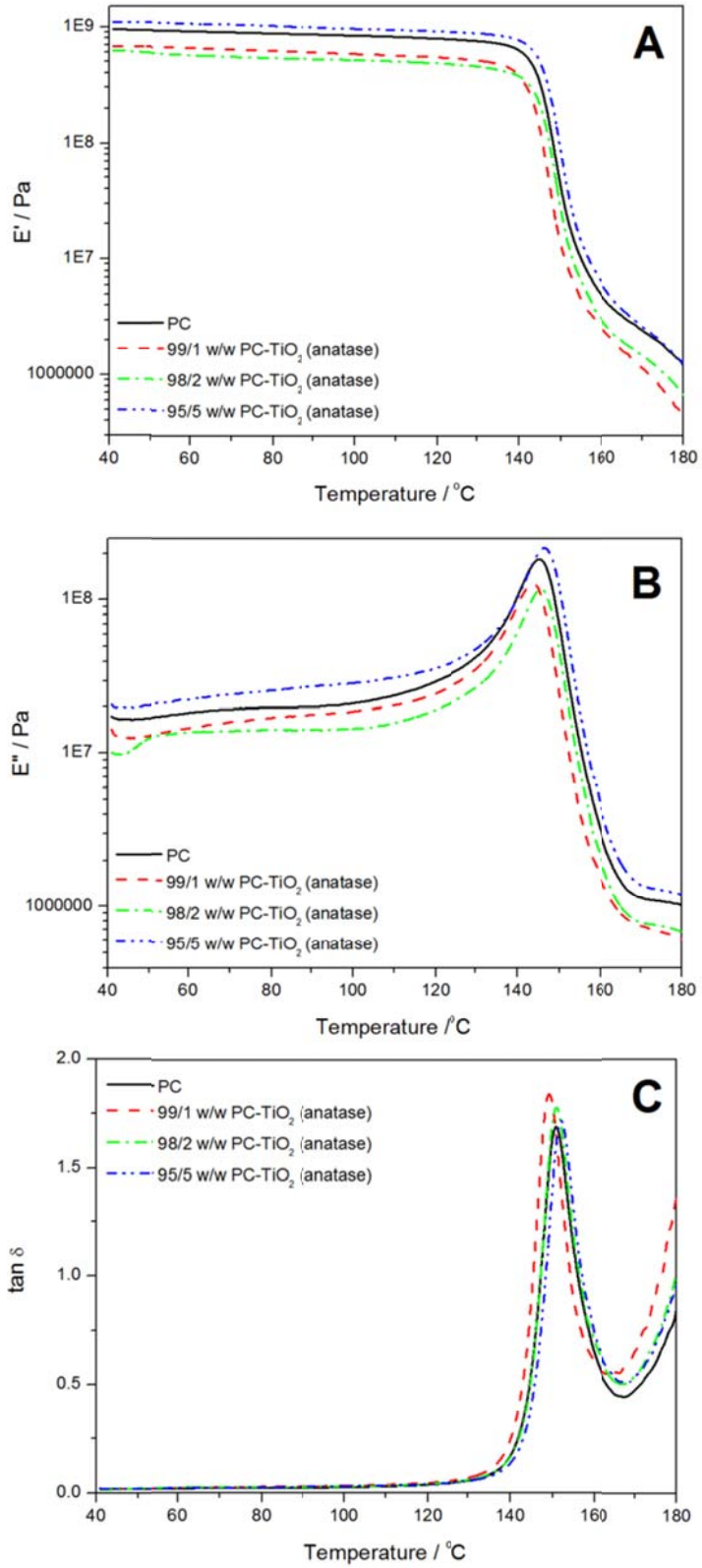

Figure 6. 3 (A) Storage modulus, (B) loss modulus and (C) tan δ curves of PC and PC-TiO_2 (anatase) nanocomposites

There is a slight decrease in glass transition temperature in the nanocomposite containing 1% anatase titania, and a slight increase in the nanocomposite containing 5% anatase titania (Figure 6.3C). The differences are fairly insignificant, but can be related to a plasticizing effect of the non-agglomerated nanoparticles in the case of 1% loading, and an immobilization effect by the larger aggregates in the case of the 5% loading. All the nanocomposites containing rutile titania show a slight increase in the glass transition temperature compared to pure PC (Figure 6.4C), which is in line with the TEM observations of higher extents of agglomeration for the PC-titania (rutile) composites.

The TGA curves of all the samples are shown in Figure 6.5. All the curves show a single-step degradation and an increase in char content for the titania containing samples. However, no correlation could be found between the amount of titania in the samples and the char contents determined at 750 °C. Unfortunately it was not possible to go to higher temperatures because of instrumental restrictions. It does, however, seem as if the titania particles size and dispersion influenced the PC degradation mechanism in a complex way, as will be seen from the rest of the discussion.

The degradation temperature for the anatase titania system increases with increasing nanoparticles content, whereas there was no significant change for the rutile titania system, except for the 5% rutile titania nanocomposite which shows increased thermal stability. Interactions between the titania particles and the polymer chains, and between the titania particles and the volatile degradation products, eventually determine the shapes of the respective TGA curves. These interactions are determined in a complex way by the titania particle sizes, the extents of agglomeration, and the crystalline structures of the particles, as will be seen in the rest of the discussion.

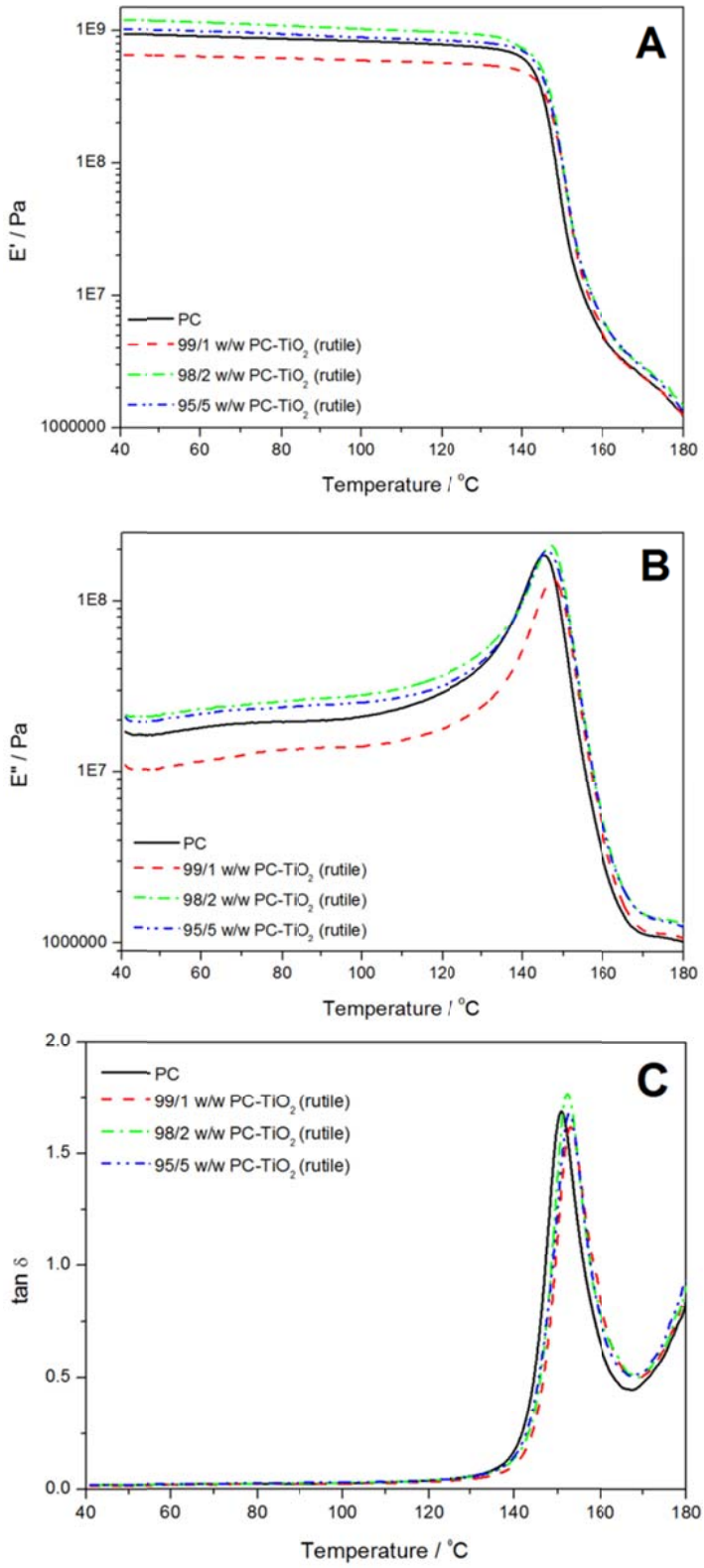

Figure 6.4 (A) Storage modulus, (B) loss modulus and (C) tan δ curves of PC and PC-TiO_2 (rutile) nanocomposites

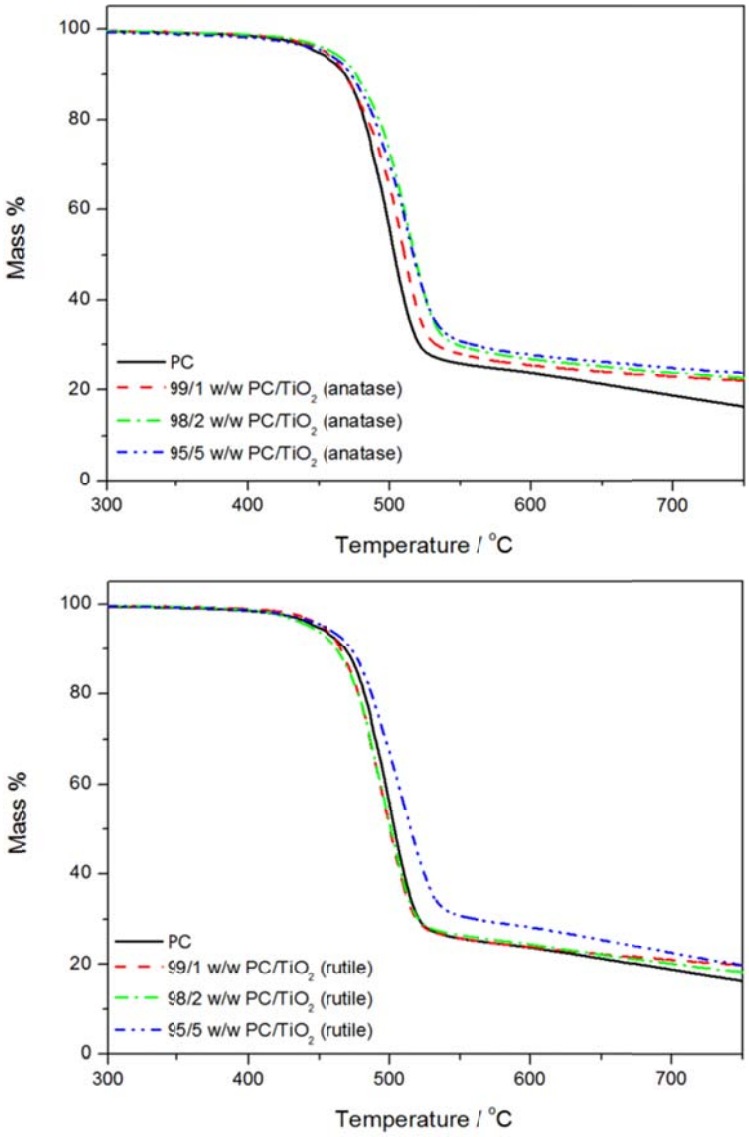

Figure 6.5 TGA curves of PC and (A) PC-TiO_2 (anatase) and (B) PC-TiO_2 (rutile) nanocomposites

From the TGA curves of PC and PC-titania (2 wt.% and 5 wt.%) at heating rates of 3, 5, 7 and 9 °C min^{-1} the isoconversional graphs of ln β *versus* 1/T and of ln (β/T^2) *versus* 1/T were plotted, according to the OFW and KAS methods, respectively [17]. The activation energy values were calculated from the slopes of the isoconversional plots. As in our previous work [17,22,28], both the isoconversional methods gave similar values of the activation energies within experimental uncertainty, and therefore only the OFW results are presented in Figure 6.6. These values fall

within the range of previously reported activation energies for PC degradation [6,24]. The activation energy values of pure PC and its nanocomposites generally show an increase with the degree of conversion. This increasing trend was observed and explained in several papers [26,27], and in our previous investigation of PMMA-SiO_2, PMMA-TiO_2 and PMMA-ZrO_2 nanocomposites [17,22,28]. It was generally explained as being the result of changes in the degradation mechanism with increasing degree of conversion. Dong *et al.* [6] gave an acceptable explanation, which could also explain our observation, for the change in activation energy with increasing degree of degradation for PC. They linked this observation to the stable carbonaceous char which protects the polymer from further degradation.

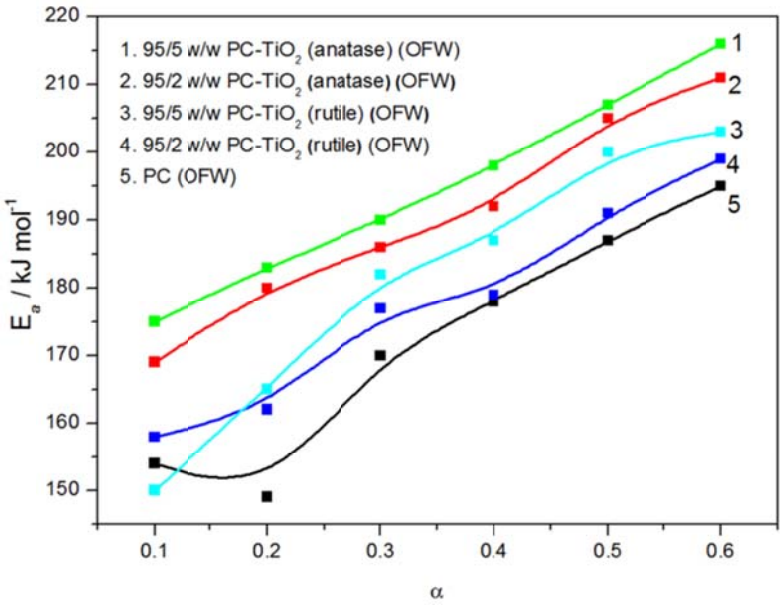

Figure 6.6 E_a values as function of extent of degradation obtained by the OFW method

The presence of a titania gives rise to higher activation energy of degradation values, and these values increase with increasing titania content. The values are also higher for the composites containing anatase titania (Figure 6.6). The degradation mechanism of PC in the presence of titania seems to be influenced in a complex way by the kind of titania and the effective particle size of the filler in the PC matrix. The already discussed XRD results indicate that the rutile titania was probably more agglomerated than the anatase titania, and this observation, together with the differences in the two kinds of titania (discussed in the 'Introduction' section), must have contributed to the differences in the interaction between the titania particles and the PC

chains, the free radicals formed during the intiation of degradation, and the volatile degradation products. The formation and distribution of char during degradation may also have been influenced by the differences between the structures and sizes of the anatase and rutile titania.

TGA-FTIR analyses were done to establish the nature of the degradation product(s) of PC and the PC-titania nanocomposites. Figure 6.7 shows the FTIR spectra of the degradation products of pure PC at different temperatures during the degradation process. All the spectra almost perfectly match the known spectrum of the thermal decomposition of bisphenol-A polycarbonate in which CO_2, phenol and bisphenol A are the main volatile products. Some band assignments are listed in Table 6.1.

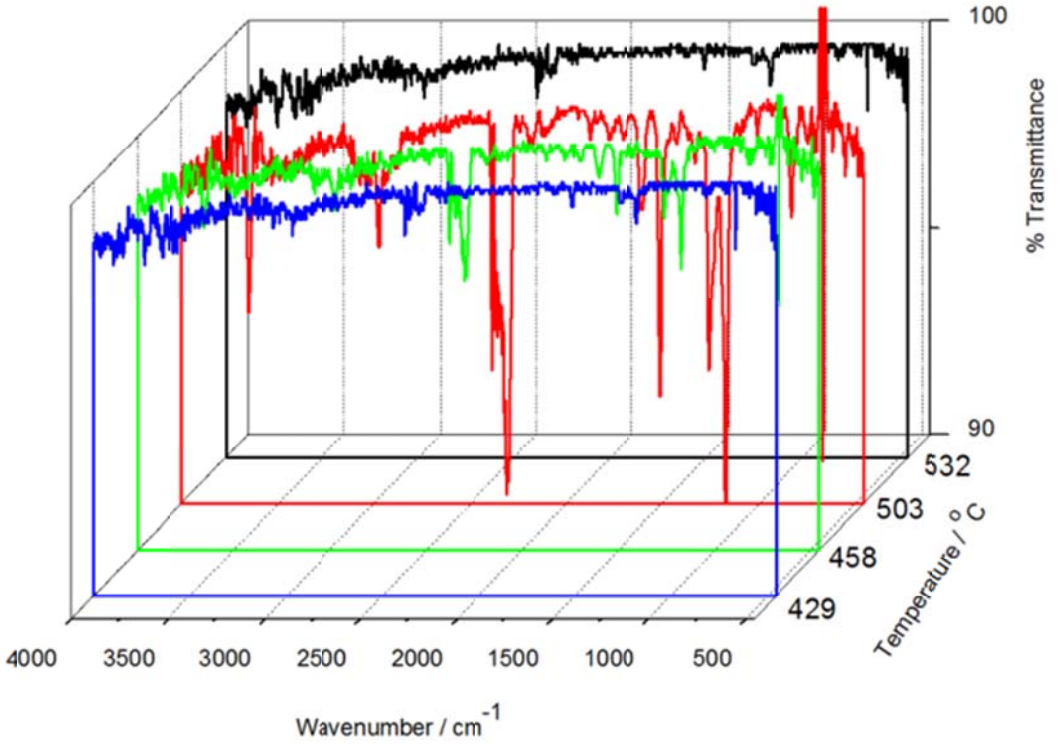

Figure 6.7 FTIR curves at different temperatures during the thermal degradation of PC in a TGA at a heating rate of 10 °C min^{-1}

Table 6.1 Band assignments in the FTIR spectra of PC

Wavenumber / cm^{-1}	Assigned vibrations
3658	Free alcohols (aliphatic substituted phenol)
2974	C-H stretching
2388-2119	Asymmetric stretching mode of CO_2
1606	Phenyl ring stretching
1509	Skeletal vibration of phenyl compounds
1257	Aromatic ether stretch
1182	Carbon hydroxyl stretching band
833	Bending mode of CO_2

No new peaks or peak shifts were observed for the nanocomposite samples (Figure 6.8 and 6.9). There is a clear increase in peak intensity for all the characteristic peaks with increasing temperature for pure PC, it reaches a maximum at around 503°C, and decreases again with further increase in temperature. It can be observed that at around 532°C the peaks of PC disappeared, while those of the PC nanocomposites are still intense. It seems as if the volatilization of the degradation products is slower for both the PC-TiO_2 nanocomposites. This is in line with the higher degradation activation energy values discussed above, and can be attributed to different interactions between the titania filler and the PC chains, the free radicals formed during degradation, and the volatile degradation products. The interactions between the PC chains and the titania particles have been investigated by NMR spectroscopy, and are described below.

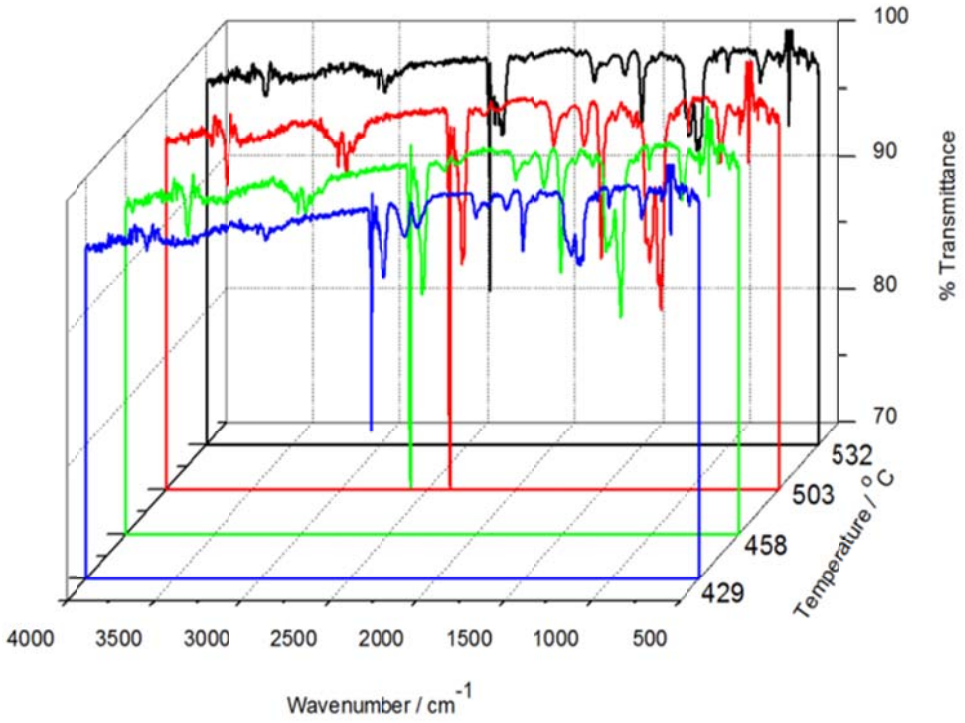

Figure 6.8 FTIR curves at different temperatures during the thermal degradation of PC with 5 wt.% anatase TiO_2 in a TGA at a heating rate of 10 °C min^{-1}

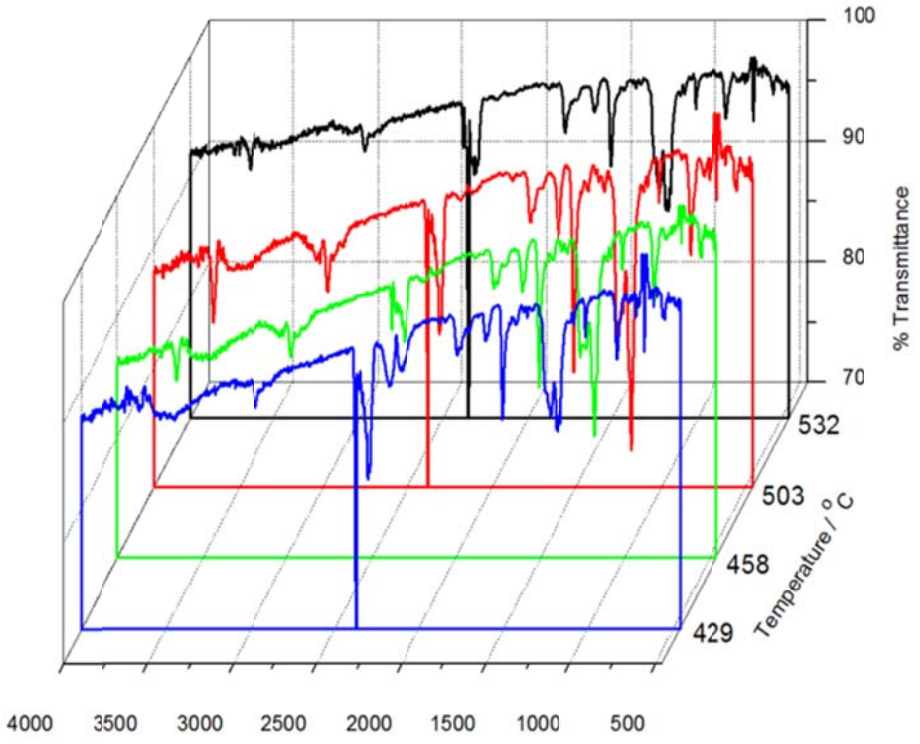

Figure 6.9 FTIR curves at different temperatures during the thermal degradation of PC with 5 wt.% rutile TiO_2 in a TGA at a heating rate of 10 °C min^{-1}

Thus, ^{13}C $\{^{1}H\}$ CP-MAS NMR measurements were performed in order to understand the possible changes caused by the filler in the polymer and to attempt a correlation between the mechanical properties, the kinetics of degradation and the molecular structure of the polymer. The ^{13}C $\{^{1}H\}$ CP-MAS NMR spectra of PC-TiO_2 composite loaded with 5% of titania are reported in Figure 6.10. Five peaks are present in the spectra: peak 1 at 149 ppm is related to the quaternary carbons of the aromatic rings and to the carbonyl carbon, peak 2 at 127 ppm is related to the aromatic carbon meta to the oxygen, peak 3 at 120 ppm is related to the aromatic carbon ortho to the oxygen, peak 4 at 42 ppm is related to the quaternary carbon bonded to the methyl groups and peak 5 at 31 ppm is related to the methyl carbons, according to literature [29]. No modification in the chemical shift and in the band shape is observed in the PC-titania nanocomposites spectra indicating that no chemical modification occurred in the polymer. Thus, the relaxation times in the laboratory frame $T_1(H)$, in the rotating frame $T_{1\rho}(H)$, and $T_{1\rho}(C)$ and the cross-polarization time T_{CH} were determined through solid-state NMR measurements in order to evaluate the dynamic modifications occurring in the polymeric chain of the PC matrix after the composite formation.

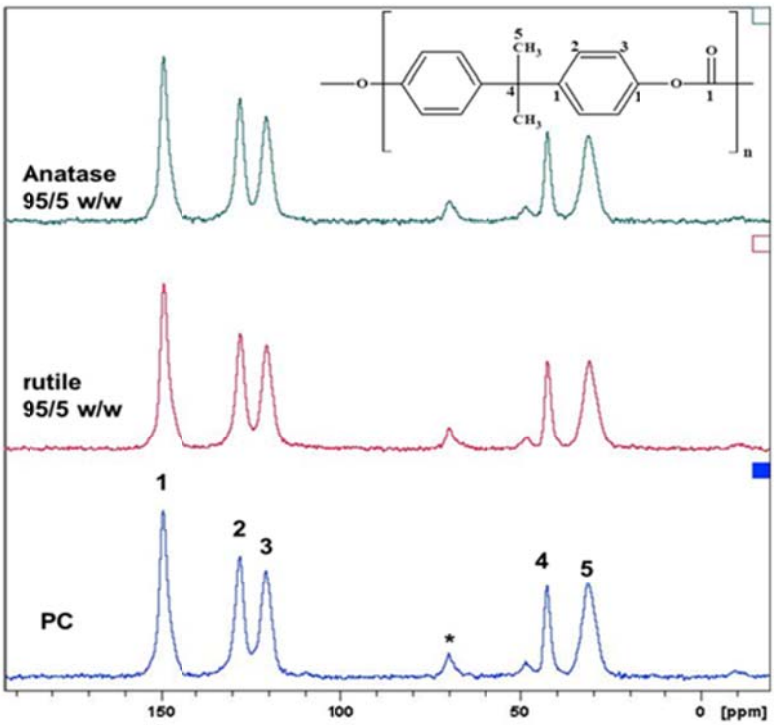

Figure 6.10 ^{13}C $\{^{1}H\}$ CP-MAS NMR spectra of PC and of and titania-PC nanocomposite loaded with 5% of titania. Number on the peak identifies the carbon atoms. The * symbol indicates spinning sidebands

The T_1(H), $T_{1\rho}$(H), $T_{1\rho}$(C) and T_{CH} values obtained from each peak in the ^{13}C spectra of all the samples are reported in Tables 6.2 and 6.3. The presence of the filler in the PC matrix did not significantly affect the T_1(H) and $T_{1\rho}$(H) values. This indicates that the spin diffusion phenomenon averages the dynamic behaviour of the polymer and that the composites are dynamically homogeneous in a range from tens to hundreds of nanometres. On the contrary, the $T_{1\rho}$(C) and T_{CH} values are affected by the presence of titania. In particular, in the PC-TiO_2 (anatase) composite, the $T_{1\rho}$(C) value of each peak and the T_{CH} value of peak 3 are higher than the ones for the pure PC. This finding indicates that the presence of anatase titania hindered the polymeric chain motions. The presence of rutile titania in PC gave rise to similar, but more intense, effects. In the PC-TiO_2 (rutile) composite an increase in $T_{1\rho}$(C) is also observed together with a significant variation in the T_{CH} values. In fact, a big decrease in the T_{CH} values of peaks 1 and 4, together with a big increase in the T_{CH} values of peaks 3 and 5, are evident. No significant variation is observed for peak 2. The significant decrease in T_{CH} values indicates that there is an increase in the heteronuclear dipolar interactions between the carbons and the surrounding hydrogen nuclei and it is connected to the increase in the rigidity of the polymer.

Table 6.2 T_1(H) and $T_{1\rho}$(H) values for all the carbons in the ^{13}C spectra of PC and the PC-TiO_2 composites having 5 wt.% of filler

		T_1 (H) (s)			$T_{1\rho}$ (H) (ms)		
Carbon	**ppm**	**PC**	**PC-TiO_2 (anatase) (5%)**	**PC-TiO_2 (rutile) (5%)**	**PC**	**PC-TiO_2 (anatase) (5%)**	**PC-TiO_2 (rutile) (5%)**
1	149	0.39 ± 0.02	0.37 ± 0.02	0.39 ± 0.03	4.9 ± 0.2	5.8 ± 0.3	5.1 ± 0.3
2	127.5	0.41 ± 0.03	0.37 ± 0.03	0.39 ± 0.02	5.4 ± 0.2	5.6 ± 0.3	5.7 ± 0.2
3	120	0.39 ± 0.01	0.37 ± 0.03	0.40 ± 0.02	5.2 ± 0.2	5.2 ± 0.2	5.0 ± 0.2
4	42	0.40 ± 0.01	0.40 ± 0.03	0.42 ± 0.02	4.8 ± 0.2	5.3 ± 0.2	5.4 ± 0.3
5	31	0.42 ± 0.01	0.38 ± 0.02	0.40 ± 0.02	4.9 ± 0.3	5.4 ± 0.3	5.8 ± 0.3

These results were unexpected compared to the DMA results, which suggested more rigid PC-TiO_2 (anatase) nanocomposites (5 wt.%). Although these results and the T_{CH} values obtained by NMR do not seem to support each other, it should be realized that the T_{CH} values reflect the

dipolar interactions within a nanometer scale and can therefore not be strictly correlated with the bulk thermomechanical properties. On the other hand, the T_{CH} relaxation time values decrease for both composites, which suggests an increase in matrix stiffness which is in line with the DMA results.

Table 6.3 $T_{1\rho}$(C) and T_{CH} values for all of the carbons in the ^{13}C spectra of PC and the PC-TiO_2 composites having 5 wt.% of filler

		$T_{1\rho}$ (C) (ms)			T_{CH} (ms)		
Carbon	**ppm**	**PC**	**PC-TiO_2 (anatase) (5%)**	**PC-TiO_2 (rutile) (5%)**	**PC**	**PC-TiO_2 (anatase) (5%)**	**PC-TiO_2 (rutile) (5%)**
1	149	41.0 ± 0.2	60.7 ± 0.2	86.7 ± 0.8	1328 ± 127	1064 ± 44	144 ± 20
2	127.5	10.9 ± 0.1	16.7 ± 0.5	10.4 ± 0.9	117 ± 28	159 ± 25	143 ± 18
3	120	10.2 ± 0.2	9.7 ± 0.2	12.7 ± 0.9	64 ± 12	151 ± 22	828 ± 41
4	42	18.0 ± 0.2	38.3 ± 0.2	22.2 ± 0.7	1059 ± 97	813 ± 69	236 ± 15
5	31	19.2 ± 0.1	28.4 ± 0.3	28.3 ± 0.4	275 ± 20	242 ± 22	1074 ± 49

6.4 Conclusions

Titania nanoparticles, with respectively anatase and rutile crystal structures and obtained through a sol-gel preparation method, were used to prepare polycarbonate (PC) based nanocomposites by melt compounding. The PC-titania nanocomposites were investigated as a function of titania content (1 to 5 wt.%) and crystal structure (anatase or rutile). TEM and XRD analyses showed that both the rutile and anatase titania were fairly well dispersed in the PC matrix, but there was more agglomeration at higher titania contents and for the rutile titania. The presence of titania did not change the amorphous structure of the PC. NMR results showed different extents of interaction between the PC and the two different types of titania. This, as well as the differences in particle crystal structure, dispersion and extent of agglomeration, had an influence on the thermomechanical properties and degradation kinetics of the composites. In this case the structure-property relationships are complex and it was difficult to directly correlate the dynamic mechanical properties and degradation kinetics with specific features like titania particle size and

crystal structure, titania particle dispersion and agglomeration in the PC matrix, and interactions between the PC matrix and the titania particles.

6.5 References

1. B.M. Dolores, B.W.C. Vilches, F.S. José. Scratch resistance of polycarbonate containing ZnO nanoparticles: Effect of sliding direction. Journal of Nanoscience and Nanotechnology 2010; 10:6683-6689.
   DOI:10.1166/jnn.2010.2513
2. M.C. Gupta, S.G. Viswanath. Role of metal oxide in the thermal degradation of bisphenol A polycarbonate. Journal of Thermal Analysis 1996; 46:1671-1679.
   DOI:10.1021/ie9700167
3. Q. Dong, C. Gao, Y. Ding, F. Wang, B. Wen, S. Zhang, T. Wang, M. Yang. A polycarbonate /magnesium oxide nanocomposite with high flame retardancy. Journal of Applied Polymer Science 2011; 123:1085-1093.
   DOI:10.1002/app.34574
4. R.M. Meri, A. Shutka, I. Zalite, A.K. Bledzki. Metal oxide mineral filler containing polymer nanocomposites. Solid State Phenomena 2009; 151:154-158.
   DOI: 10.4028/www.scientific.net/SSP.151.154
5. L. Wu, P. Chen, J. Zhang, J. He. Inhibited transesterification and enhanced fibrillation of TLCP by nano-SiO_2 in polycarbonate matrix. Polymer 2006; 47:448-456.
   DOI: 10.1016/j.polymer.2005.11.044
6. Q. Dong, C. Gao, Y. Ding, F. Wang, B. Wen, S. Zhang, T. Wang, M. Yang. A polycarbonate/magnesium oxide nanocomposite with high flame retardancy. Journal of Applied Polymer Science 2011; 123:1085-1093.
   DOI:10.1002/app.34574
7. A. Eitan, F.T. Fisher, R. Andrews, L.C. Brinson, L.S. Schadler. Reinforcement mechanisms in MWCNT-filled polycarbonate. Composites Science and Technology 2006; 66:1162-1173.
   DOI: 10.1016/j.compscitech.2005.10.004

8. J. Feng, J. Hao, J. Du, R. Yang. Effects of organoclay modifiers on the flammability, thermal and mechanical properties of polycarbonate nanocomposites filled with a phosphate and orgarnoclays. Polymer Degradation and Stability 2012; 97:108-117.
DOI: 10.1016/j.polymdegradstab.2011.09.019
9. J. Feng, J. Hao, J. Du, R. Yang. Using TGA/FTIR TGA/MS and cone calorimetry to understand thermal degradation and flame retardancy mechanism of polycarbonate filled with solid bisphenol A bis(biphenyl phosphate) and montmorillonite. Polymer Degradation and Stability 2012; 97:605-614.
DOI: 10.1016/j.polymdegradstab.2012.01.011
10. S. Wang, Y. Hu, Z. Wang, T. Yong, Z. Chen, W. Fan. Synthesis and characterization of polycarbonate/ABS/montmorillonite nanocomposites. Polymer Degradation and Stability 2003; 80:157-161.
DOI: 10.1016/S0141-3910(02)00397-X
11. Y. Imai, A. Terahara, Y. Hakuta, K. Matsui, H. Hayashi, N. Ueno. Transparent poly(bisphenol A carbonate) - based nanocomposites with high refractive index nanoparticles. European Polymer Journal 2009; 45:630-638.
DOI:10.1016/J.europolyj.2008.12.013
12. K. Xu, S. Zhou, L. Wu. Effect of highly dispersible zirconia nanoparticles on the properties of UV-curable poly(urethane-acrylate) coatings. Journal Materials Science 2009; 44:1613-1621.
DOI: 10.1007/s10853-008-3231-8
13. F. Rouabah, M. Fois, L. Ibos, A. Boudenne, D. Dadache, N. Haddaoui, P. Ausset. Mechanical and thermal properties of polycarbonate. II. Influence of titanium dioxide content and quenching on pigmented polycarbonate. Journal of Applied Polymer Science 2007; 106:2710-2717.
DOI: 10.1002/app.26807
14. M.C. Gupta, S.G. Viswanath. Role of metal oxide in the thermal degradation of bisphenol A polycarbonate. Journal of Thermal Analysis 1996; 46: 1671-1679.
DOI:10.1021/ie9700167
15. K.M. Blackwood, R.A. Pethrick, F.I. Simpson. Titanium dioxide induced failure in polycarbonate. Journal of Materials Science 1995; 30:4435-4445.

DOI:10.1007/BF00361529

16. O. Carp, C.L. Huisman, A. Reller. Photoinduced reactivity of titanium dioxide. Progress in Solid State Chemistry 2004; 32:33-177.
DOI: 10.1016/j.progsolidstchem.2004.08.001
17. T.E. Motaung, A.S. Luyt, F. Bondioli, M. Messori, M.L. Saladino, A. Spinella, G. Nasillo, E. Caponetti. PMMA-titania nanocomposites: Properties and thermal degradation behaviour. Polymer Degradation and Stability (published online).
DOI: 10.1016/j.polymdegradstab.2012.05.022
18. S.R. Hartmann, E.L. Hahn. Nuclear double resonance in the rotating frame. Physical Review Online Archive 1962; 128:2042-2053.
DOI:10.1103/PhysRev.128.2042
19. C. Lau, Y. Mi. A study of blending and complexation of poly(acrylic acid)/poly(vinyl pyrrolidone). Polymer 2002; 43:823-829.
DOI:10.1016/S0032-3861(01)00641-3
20. R.G. Alamo, J.A. Blanco, I. Carrilero. Measurement of the ^{13}C spin-lattice relaxation time of the non-crystalline regions of semicrystalline polymers by a CP-MAS-based method. Polymer 2002; 43:1857-1865.
DOI: 10.1016/S0032-3861(01)00761-3
21. P. Conte, R. Spaccini, A. Piccolo. State of art of CPMAS ^{13}C-NMR spectroscopy applied to natural organic matter. Progress in Nuclear Magnetic Resonance Spectroscopy 2004; 44:215-223.
DOI:10.1016/j.pnmrs.2004.02.002
22. M.L. Saladino, T.E. Motaung, A.S. Luyt, A. Spinella, G. Nasillo, E. Caponetti. The effect of silica nanoparticles on the morphology, mechanical properties and thermal degradation kinetics of PMMA. Polymer Degradation and Stability 2012; 97:452-459.
DOI:10.1016/j.polymdegradstab.2011.11.006
23. C. Pandis, E. Logakis, A. Kyritsis, P. Pissis, V.V. Vodnik, E. Džunuzović, J.M. Nedeljković, V. Djoković, J.C.R. Hernández, J.L.G. Ribelles. Glass transition and polymer dynamics in silver/poly(methyl methacrylate) nanocomposites. European Polymer Journal 2011; 47:1514-1525.
DOI: 10.1016/j.eurpolymj.2011.06.001

24. R. Zong, Y. Hu, S. Wang, L. Song. Thermogravimetric evaluation of PC/ABS/ montmorillonite nanocomposite. Polymer Degradation and Stability 2004; 83:423-428. DOI:10.1016/j.polymdegradstab.2003.09.004
25. B.J. Holland, J.N. Hay. The value and limitations of non-isothermal kinetics in the study of polymer degradation. Thermochimica Acta 2002; 388:253-273. DOI: 10.1016/S0040-6031(02)00034-5
26. Z. Gao, T. Kaneko, D. Hou, M. Nakada. Kinetics of thermal degradation of poly(methyl methacrylate) studied with the assistance of the fractionation conversion at the maximum reaction rate. Polymer Degradation and Stability 2004; 84:399-403. DOI:10.1016/j.polymdegradstab.2003.11.015
27. S. Vyazovkin. A unified approach to kinetic processing of nonisothermal data. International Journal of Chemical kinetics 1996; 28:95-101. DOI: 10.1002/(sici)1097-4601(1996)28:2<95::aid-kin4>3.0.co;2-g
28. T.E. Motaung, A.S. Luyt, M.L. Saladino, D.C. Martino, E. Caponetti. Morphology, mechanical properties and thermal degradation kinetics of PMMA-zirconia composites prepared by melt compounding. eXPRESS Polymer Letters (accepted for publication).
29. A.P.A.M. Eijkelenboom, W.E.J.R. Maas, W.S. Veeman, G.H.W. Buning, J.M.J. Vankan. Triple-resonance fluorine-19, proton, and carbon-13 CP-MAS NMR study of the influence of PMMA tacticity on the miscibility in PMMA/poly(vinylidene fluoride) (PVF2) blends. Macromolecules 1992; 25:4511-4518. DOI: 10.1021/ma00044a009

Chapter 7

Influence of the modification, induced by zirconia nanoparticles, on the structure and properties of polycarbonate

---

This chapter has been submitted as a publication:
T.E. Motaung, M.L. Saladino, A.S. Luyt, D. Chillura Martino. Influence of the modification, induced by zirconia nanoparticles, on the structure and properties of polycarbonate. European Polymer Journal (Under review)

Abstract

Melt compounding was used to prepare polycarbonate (PC)-zirconia nanocomposites with different amounts of zirconia. The effect of the zirconia loading, in the range of 1-5 wt.%, on the structure, mechanical properties and thermal degradation kinetics was investigated. The zirconia nanoparticle aggregates were well dispersed in the PC matrix and induced the appearance of a local lamellar order in the polycarbonate as inferred by SAXS findings. This order could be a consequence of the intermolecular interactions between zirconia and the polymer, in particular with the quaternary carbon bonded to the methyl groups and the methyl carbon as inferred from the NMR results. The presence of zirconia caused a decrease in the storage and loss moduli below the glass transition temperature. However, the highest amount of zirconia increased the modulus. The presence of zirconia in PC slightly increased the thermal stability, except for the highest zirconia content which showed a decrease. The activation energies of thermal degradation for the nanocomposites were significantly lower than that for pure PC at all degrees of conversion.

Keywords: Nanocomposites; polycarbonate; zirconia; degradation; interfacial interaction

7.1 Introduction

Polycarbonate (PC) is an amorphous and inexpensive polymer known for its excellent optical and mechanical properties. PC nanocomposites have shown potential applications in UV protecting sheets and films [1-4]. There are a number of recent papers reporting on the mechanical properties, thermal stability and flame retardancy of PC nanocomposites containing different metal oxide nanoparticles [5-10]. The results indicate that metal oxides have an effect on the morphology, as well as mechanical and thermal behaviour of PC. Some authors found that the well dispersed metal oxide nanoparticles in PC improved its surface, viscoelastic, and mechanical properties, and increased its thermal stability. They related these observations to the strong interactions at the polymer-filler interface [8-11].

PC-zirconia nanocomposites are promising materials due to the interesting optical properties of the final product [12-14]. The nanocomposites prepared by *in situ* polymerization were found to be highly transparent with up to 50 wt.% ZrO_2 nanoparticles, and exhibited good thermal stability, hardness and elastic modulus. These results were attributed to the interfacial interaction between the polymer and the nanoparticles. However, the hardness and thermal stability of the nanocomposites considerably decreased at high filler contents [12,13]. The deterioration in hardness was related to the agglomeration of the ZrO_2 nanoparticles in the polymer matrix, and the decrease in thermal stability to the evaporation of the entrapped organic solvent in ZrO_2 agglomerates and/or the unreacted monomer because of the low final conversion. Imai *et al*. [12] also modified the polycarbonate with sulphonic acid, and this was found to further reduce the thermal stability of the matrix polymer.

The purpose of this study was to obtain a deeper understanding of the interfacial interaction between zirconia nanoparticles and PC in PC-ZrO_2 nanocomposites prepared through a melt compounding method. The effect of the presence and amount of zirconia nanoparticles, prepared using a sol-gel method, on the structure, thermal and mechanical properties, as well as the thermal degradation kinetics, of the PC was investigated. The composites were characterized using transmission electron microscopy (TEM), X-ray diffractometry (XRD), Small Angle X-ray Scattering (SAXS), dynamic mechanical analysis (DMA), thermogravimetric analyses (TGA),

and ^{13}C cross-polarization magic-angle spinning nuclear magnetic resonance ($^{13}C\{^{1}H\}$ CP-MAS NMR).

7.2 Experimental

7.2.1 Materials

Tetra-*n*-propylzirconate (Aldrich), capronic acid (Aldrich), ethanol (Eurobase), ammonium hydroxide (Aldrich) were used as received without further purification. Commercial grade bisphenol-A polycarbonate (PC, Makrolon® 2407 produced by Bayer Material Science, Germany and having a melt flow rate at 300 °C/1.2 kg of 20 g/10 min) was used in pellet form. The resin was dried at 120 °C overnight under static vacuum before processing.

7.2.2 Zirconia preparation

The ZrO_2 nanoparticles were prepared according to the method reported by Bondioli *et al.* [15]. The zirconia nanoparticles was precipitated by slow addition of an alcoholic solution containing capronic acid and tetra-*n*-propylzirconate, previously reacted for 30 min at room temperature, to a mixture of ethanol and water.

7.2.3 Composites preparation

The PC pellets were thoroughly mixed with 1, 2 and 5 wt.% zirconia for 10 min at 240 °C and 30 rpm in a 50 mL internal mixer of a Brabender Plastograph (Duisburg, Germany). The mixed samples were melt-pressed into 1 mm thick sheets at 240 °C for 5 min.

7.2.4 Analysis methods

TEM micrographs were acquired using a JEM-2100 (JEOL, Japan) electron microscope operating at 200 kV accelerating voltage. The obtained nanocomposites were cut into 100 nm thick slices using a Leica EM UC6 ultra-microtome. Slices were put onto a 3 mm Cu grid "lacey carbon" for analysis.

XRD patterns were recorded in the 2-70° 2θ range at steps of 0.05° and a counting time of 5 s/step in a Philips PW 1050 diffractometer, equipped with a Cu tube and a scintillation detector

beam. The X-ray generator worked at 40 kV and 30 mA. The instrument resolution (divergent and antiscatter slits of 0.5°) was determined using standards free from the effect of reduced crystallite size and lattice defects.

SAXS measurements were taken using a Bruker AXS Nanostar-U instrument whose source was a Cu rotating anode working at 40 kV and 18 mA. The X-ray beam was monochromatized at a wavelength λ of 1.54 Å (Cu Kα) using a couple of Göbel mirrors and was collimated using a series of three pinholes with diameters of 500, 150 and 500 μm. Samples were directly mounted on the sample stage to avoid additional scattering of the holder. Data were collected at room temperature for 1000 seconds by using a two-dimensional multiwire proportional counter detector placed at 24 cm from the sample allowing the collection of data in the Q range 0.02 – 0.78 Å. The measurements were repeated in two different portions of each sample to check its homogeneity.

^{13}C cross polarization - magic angle spinning nuclear magnetic resonance (^{13}C {^{1}H} CP-MAS NMR) spectra were obtained at room temperature with a Bruker Avance II 400 MHz (9.4 T) spectrometer operating at 100.63 MHz for the ^{13}C nucleus with a MAS rate of 8 kHz, 500 scans, a contact time of 1.5 ms and a repetition delay of 2 sec. The optimization of the Hartmann-Hahn condition [9] was obtained using an adamantine sample. Each sample was placed in a 4 mm zirconia rotor with KEL-F caps using silica as filler to avoid inhomogeneities inside the rotor. The proton spin–lattice relaxation time in the rotating frame $T_{1\rho}(H)$ was indirectly determined, with the variable spin lock (VSL) pulse sequence, by the carbon nucleus observation using a 90°–τ–spin-lock pulse sequence prior to cross-polarization [10]. The data acquisition was performed by ^{1}H decoupling with a delay time, τ, ranging from 0.1 to 7.5 ms and a contact time of 1.5 ms. The proton spin–lattice relaxation time in the laboratory frame $T_1(H)$ was determined, using the saturation recovery pulse sequence [11], by the carbon nucleus observation using a 90°–τ–90° pulse sequence prior to cross polarization with a delay time τ ranging from 0.01 to 3 s. The ^{13}C spin–lattice relaxation time in the rotating frame $T_{1\rho}(C)$ was determined, with the variable spin lock (VSL) pulse sequence, applying the spin-lock pulse after the cross-polarization on the carbon channel [12]. The data acquisition was performed by ^{1}H decoupling with a spin lock pulse length, τ, ranging from 0.4 to 30 ms and a contact time of 1.5 ms. The cross

polarization time T_{CH} values for all the carbon signals of PC were obtained through variable contact time (VCT) experiments [13]. The contact times used in the VCT experiments were 0.05, 0.1, 0.2, 0.3, 0.4, 0.5, 0.6, 0.8, 1.0, 1.2, 1.5, 2.0, 2.5, 3.0, 3.5, 4.0, 4.5, 5.0, 6.0 and 7.0 ms.

The dynamic mechanical analysis of the blends and composites were performed between 40 to 180 ºC in the bending mode at a heating rate of 5 ºC min^{-1} and a frequency of 1 Hz using a Perkin Elmer Diamond DMA (Waltham, Massachusetts, U.S.A.).

Thermogravimetric analysis (TGA) was done in a Perkin Elmer TGA7 (Waltham, Massachusetts, U.S.A.) under flowing nitrogen at a constant flow rate of 20 mL min^{-1}. Samples (5-10 mg) were heated from 25 to 600 °C at different heating rates. The degradation kinetic analysis was performed using the Ozawa-Flynn-Wall (OFW) and the Kissinger-Akahira-Sunose (KAS) methods, described elsewhere [14].

TGA combined with Fourier-transform infrared (FTIR) spectroscopy (TGA-FTIR) analyses were performed using a Perkin Elmer STA6000 simultaneous thermal analyzer (Waltham, Massachusetts, U.S.A.) under flowing nitrogen at a constant flow rate of 20 mL min^{-1}. Samples (20-25 mg) were heated from 30 to 600 °C at 10° C min^{-1} and held for 4 min at 600 °C. The furnace was linked to an FTIR spectrometer (Perkin Elmer Spectrum 100, Massachusetts, U.S.A.) with a gas transfer line. The volatiles were scanned over a 400 – 4000 cm^{-1} wavenumber range at a resolution of 4 cm^{-1}. The FTIR spectra were recorded in the transmittance mode at different temperatures during the thermal degradation process.

7.3 Results and discussion

The TEM micrographs of the ZrO_2 powder, reported in the same paper, showed aggregates with a large number of particles (more than 30) of different sizes. In each aggregate the bigger, quite thick particles (around 200-400 nm) were surrounded by smaller spongy particles (50-100 nm). The TEM micrographs of the PC-ZrO_2 nanocomposite having 5 wt.% of zirconia are reported in Figure 7.1. It seems as if the aggregates are fragmented and the fragments dispersed in the polymer matrix. This could be a consequence of the interaction between nanoparticles and the

polymer matrix. At higher magnification it can be seen that the nanoparticles are constituted of several crystalline domains of about 5 nm whose atomic planes are visible in Figure 7.1F.

It is expected that if interaction occurs at the interface, the nanoparticles could induce a change in the polymer structure. For this reason, XRD patterns were registered. The pattern of the zirconia powder indicated that the zirconia consisted of 80 wt.% of tetragonal zirconia and 20 wt.% of monoclinic Baddeleyite, as reported in a previous paper [14]. The diffraction pattern of PC shows an intense broad diffraction peak around 17°, a shoulder around 26° and another broad peak at 44°. The diffraction peak is superimposable on the WAXS pattern reported in literature [15], and is typical of an amorphous material. The XRD patterns of the PC-ZrO_2 nanocomposites having 1, 2 and 5 wt.% of ZrO_2 do not show the characteristic peak of zirconia as a consequence of the low amount of small zirconia nanoparticles. The typical PC diffraction peaks do not undergo any significant change, except for a decrease in intensity with an increase in the amount of zirconia. This cannot be explained by simply considering the variation in the electron scattering density. In fact, it does not linearly change with composition. Furthermore, a broad peak appears at about 3.7°, the intensity of which increases with the amount of zirconia. It indicates the presence of a repeating distance which cannot be ascribed to either the crystalline structure of the nanoparticles or to the nanoparticle clustering. In fact, even assuming that the nanoparticles were in contact, the peak position, evaluated on the basis of the nanoparticle size from the TEM micrographs, should fall at 0.018°, which is well below the observed value. It follows that it has to be ascribed to some structure induced in the polymer by the presence of the zirconia. The peak shape is similar to that observed by SAXS on crystalline PC [23], and which was ascribed to a lamellar structure. This finding suggests that the zirconia induced a local crystallization in the polymer. It has to be noticed that the scattering peak reported in literature indicates a long period distance of about 120 Å, which is almost 4 times the distance (c.a. 30 Å) evaluated form the peak position in the diffraction data.

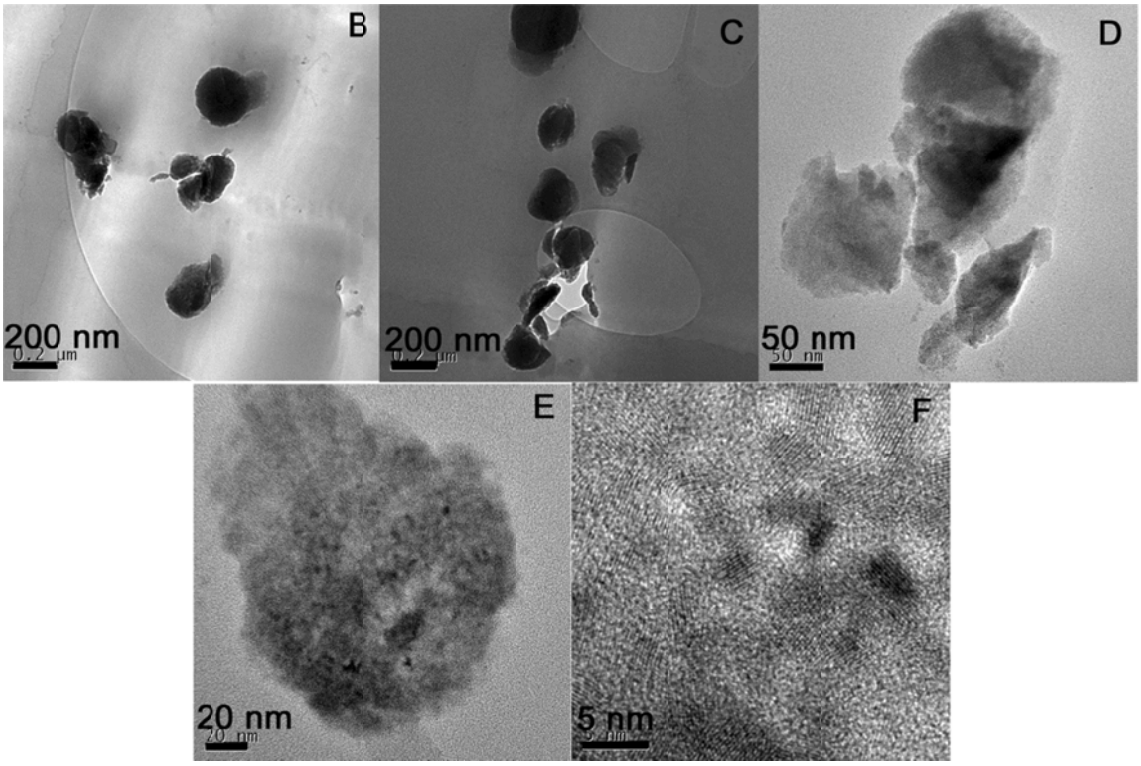

Figure 7.1 TEM micrographs of the 5 wt.% PC-ZrO_2 nanocomposite

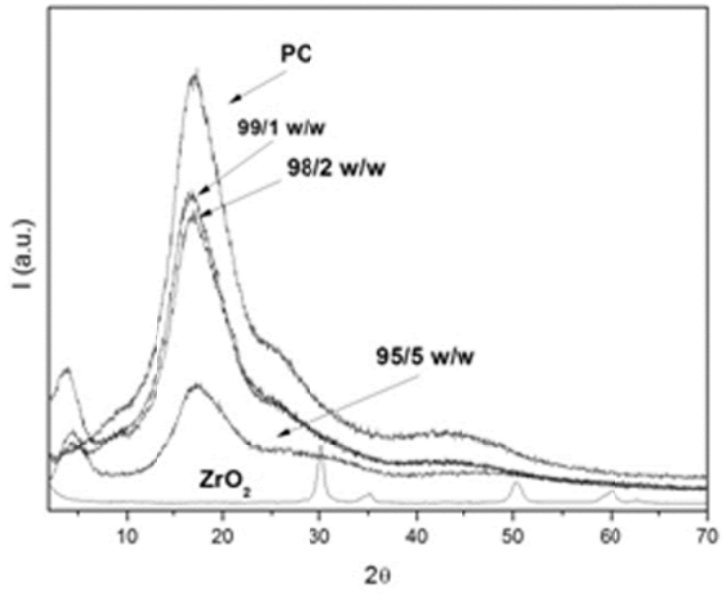

Figure 7. 2 XRD patterns of zirconia powder, pure PC and the PC-ZrO_2 composites

In order to get more clarity on this aspect, SAXS measurements were performed. The SAXS two-dimensional patterns of the nanocomposites, recorded at 24 cm sample to detector distance, displayed an isotropic halo which indicates that no preferred crystallization occurred. They were radially averaged, which gives a scattering intensity I(Q) in the 0.02-0.77 $Å^{-1}$ Q range. Q, the momentum transfer, is equal to $(4\pi \sin \theta)/\lambda$, where 2θ is the scattering angle. Measurements, carried out on different portions of the samples, were superimposable thus confirming that the samples were homogeneous. A comparison of the SAXS experimental data of the pure PC and the composite samples, after correction for the transmission, the thickness of the samples and for mylar, is shown in the Figure 7.3.

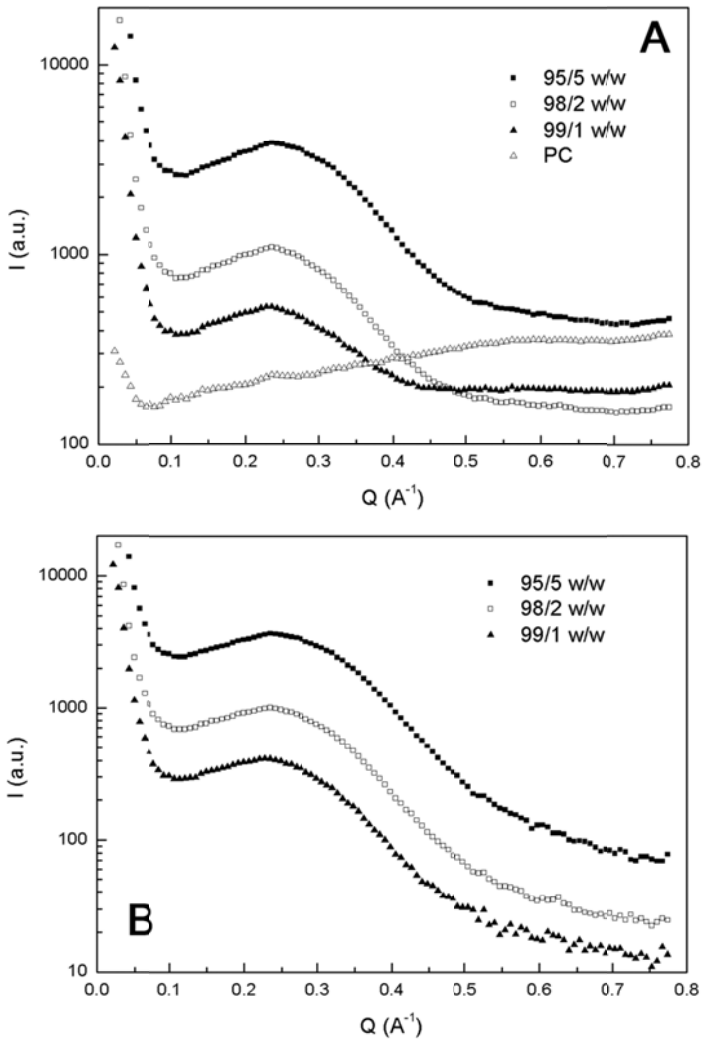

Figure 7.3 A) SAXS intensities vs. Q of PC and the composites; B) SAXS intensities vs. Q for the composites after subtracting the PC contribution

The SAXS profiles show a monotonic decrease at low Q-values followed by a peak, the intensity of which increases with the amount of zirconia nanoparticles, thus confirming the XRD data. A shoulder appears in the range 0.5-0.77 Å. It can be ascribed to some small angle scattering due to the amorphous PC. The PC intensity, properly weighted, was therefore subtracted from the ones for the composites. The corrected curves are shown in Figure 7.3B. Since the low-angle region of the pattern is dominated by a single peak, the presence of a cubic arrangement was excluded and, in agreement with literature [23], it was considered that the backbones of the polymer could arrange to form lamellae. On this basis, the model proposed by Nallet *et al.* [24] was considered.

$$I(Q) = A/(Q^2\zeta_p^2 + 1) + B/[(Q - Q_m)^2\zeta_l^2 + 1] + Bk \qquad (7.1)$$

where the first term represents the quasi-Bragg peak due to the stacking of the lamellar layers, the second the quasi-Bragg peak due to the stacking of the lamellar layers, and Bk the incoherent scattering plus the instrumental noise. A and B correspond to the scattering intensities from the diffuse scattering and the quasi-Bragg scattering, ξ_l is the spatial correlation length of the lamellar layers, and Q_{max} is the Q value corresponding to the peak intensity. The intensities for the three composites computed by means of Equation 7.1 poorly reproduce the experimental values as indicated by the dotted line reported in Figure 7.4 as an example for the 99/1 w/w PC-zirconia nanocomposite.

In our opinion the observed small-angle diffuse scattering does not depend on a density fluctuation in the polymer, but on the formation of a well-defined nanoparticle-polymer interface. On this basis, we modified the Nallet model by considering that the diffuse small-angle scattering could be described by means of a Porod contribute. The resulting equation is:

$$I(Q) = B/[(Q - Q_m)^2\zeta_l^2 + 1] + F/Q^4 + Bk \qquad (7.2)$$

where the meaning of B, ξ_l, Q_M and Bk are as described above, F is equal to $N\rho\Delta\rho^2S$ where $N\rho$ is the particle number density, $\Delta\rho^2$ is the contrast i.e. the square of the difference between the electron density of the particle and that of PC, and S is the interfacial area. The intensity

computed by this model well reproduces the experimental one for the three nanocomposites. As an example the intensity computed by means of Equation 7.2 (continuous line) is compared with the experimental one for the 99/1 w/w PC-zirconia composite in Figure 7.4. The values of the fit parameters are reported in Table 7.1. From the peak position (Q_M), using Bragg's equation, a repeat distance d of about 28 Å was determined. These results are in fairly good agreement with literature data were a cluster size of 30 Å, composed of crystalline PC in a PCL-PC blend, was detected [23]. These clusters are correlated over a length of about 8 Å. These findings confirm that the zirconia nanoparticles induce lamellar crystallization in the amorphous polymer through the formation of correlated clusters over a very small distance. These findings could explain the appearance of the peak at 3.7° in the XRD patterns. Since the shape and position of the amorphous PC peaks in the XRD patterns do not change, it indicates that the long range structure holds. The fact that the intensity does not linearly decrease with filler amount could be a consequence of both the contrast variation and the short range lamellar order which developed in the presence of the zirconia nanoparticles.

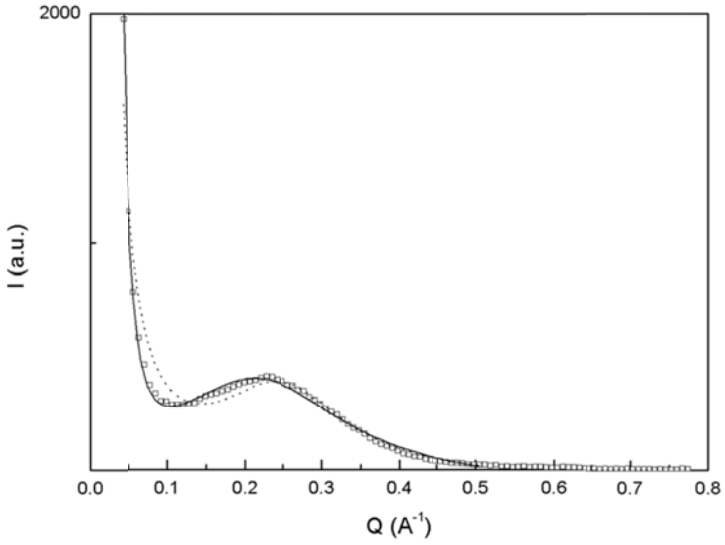

Figure 7.4 SAXS intensity vs. Q of the 99/1 w/w PC-ZrO_2 nanocomposite. Squares: experimental intensity; dotted line: fit by means of Equation 1; continuous line: fit by means of Equation 7.2

Table 7.1 The values of the fit parameters of the composites

	99/1 w/w PC-ZrO_2	98/2 w/w PC-ZrO_2	95/5 w/w PC-ZrO_2
B	420(10)	1000(20)	3660(80)
Q_M	0.223(1)	0.217(3)	0.226(2)
ξ_l	7.6(4)	8.6(3)	8.2(2)
Bk	90(10)	10(1)	10(1)
F	0.00614(3)	0.0131(2)	0.058(3)
R^2	0.998	0985	0995

The TGA curves of the pure PC and the PC-zirconia nanocomposites are shown in Figure 7.5. All the samples show single-step degradation, and the presence of the filler in PC shows a slight increase in thermal stability, except for the 5% filler containing nanocomposite which shows a significant decrease in thermal stability. The free radicals formed during degradation, and the volatile degradation products, obviously did not interact very strongly with the nanoparticles and therefore were not immobilized to a significant extent.

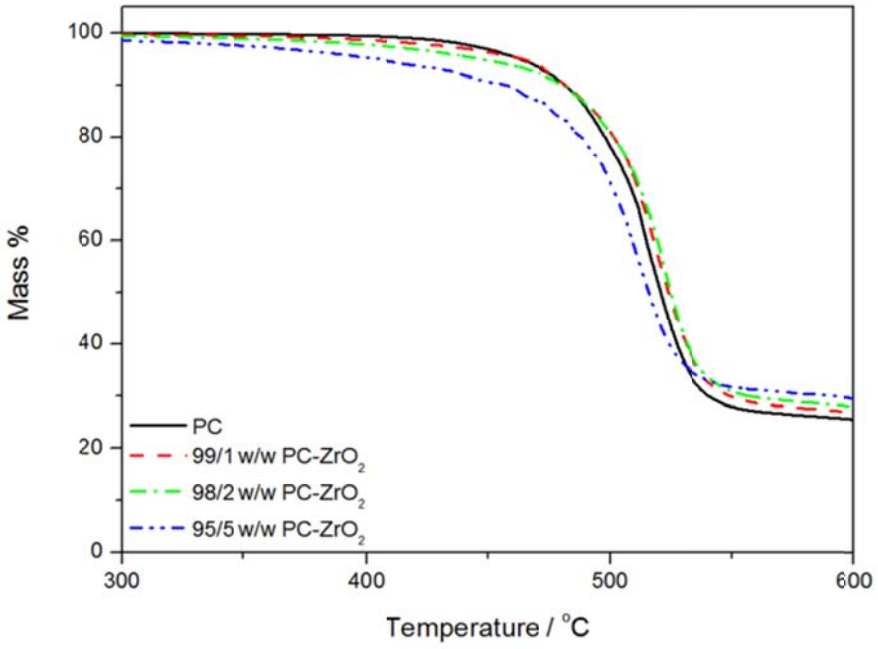

Figure 7.5 TGA curves of PC and the PC-zirconia-PC nanocomposites

The isoconversional graphs of ln β *versus* 1/*T* and of ln (β/T^2) *versus* 1/T were plotted from the TGA curves of PC, 98/2 w/w PC-zirconia and 95/5 w/w PC-zirconia at heating rates of 3, 5, 7 and 9 °C min^{-1}. The activation energy values were calculated from the slopes of the isoconversional plots. Both isoconversional methods give similar values of the activation energies within experimental uncertainty. Figure 7.6 illustrates the relationship between the activation energies and the degree of conversion. The activation energy values of pure PC and its nanocomposites generally show an increase with the degree of conversion and fall within the range of activation energies for PC degradation reported previously [25,26]. The activation energy values of the pristine PC are lower than that of the 98/2 w/w PC-zirconia nanocomposite, but they are almost the same above 40% mass loss. The 95/5 w/w PC-zirconia nanocomposite shows much lower values than the pristine PC and the 98/2 w/w PC-zirconia nanocomposite over the whole degree of conversion range. These observations can also be explained by the fact that the agglomerated zirconia particles rather acted as catalysts in the degradation process.

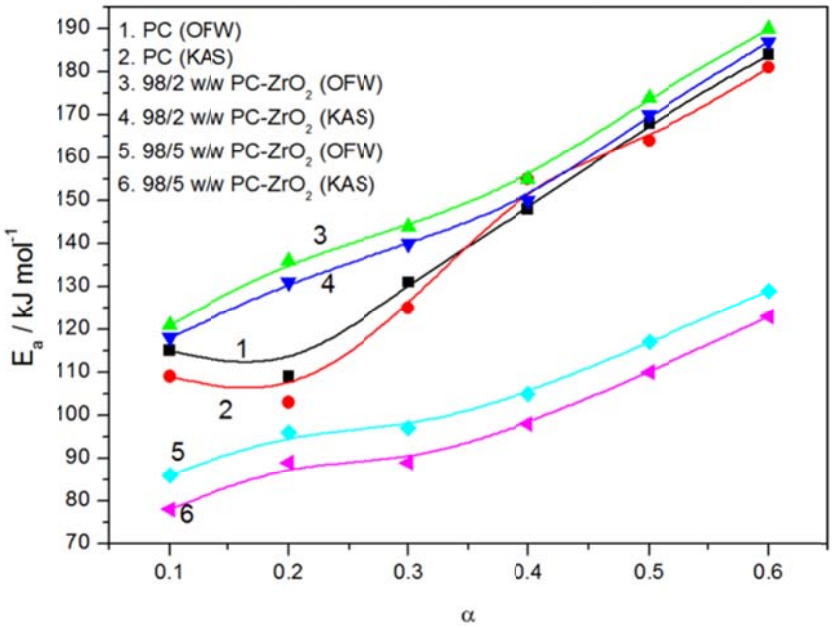

Figure 7.6 E_a values obtained by the OFW and KAS degradation kinetics methods

The increase in activation energy with an increase in degree of conversion was also observed by us when investigating PMMA-SiO_2/TiO_2/ZrO_2 nanocomposites [20,21,27] and by several other authors [26,28,29]. It was generally explained as changes in the degradation mechanism with

increasing degree of conversion. An earlier study on the thermal degradation mechanism of bisphenol-A polycarbonate reported that carbonate linkages are the major points of degradation at lower temperatures (< 400 °C), while at higher temperatures the isopropylidene group is also susceptible to loss of methyl radicals [30]. Below 500 °C, no free radical reactions were observed for the carbonate group, but rearrangement of the carbonate moiety prevailed. It is quite possible that the char formed during the degradation of PC retarded the movement of the free radicals, which led to the observed increase in activation energy with an increase in degree of conversion. The higher activation energy values for the 98/2 w/w PC-ZrO_2 can be attributed to interaction between the nanoparticles, the free radicals formed during PC degradation (which led to trapping of free radicals by the nanoparticles), and the volatile substance. The lower activation energy values for the 95/5 w/w PC-ZrO_2 nanocomposite may be related to a catalytic effect of the nanoparticles on the PC degradation. It seems as if there are two opposing effects that play a role in the degradation of PC in the presence of zirconia. More char formation leading to a retardation of the degradation process seems to be prevalent at low zirconia contents where the extent of filler agglomeration is lower, while the zirconia predominantly acts as a catalyst at higher filler contents where there are higher extents of agglomeration.

TGA-FTIR analyses were done to establish the nature of the degradation product(s), and to confirm the observations from the kinetic analysis of the thermal degradation process of PC and the PC-zirconia nanocomposites. Figure 7.7 shows the FTIR spectra of the degradation products of pure PC at different temperatures during the degradation process. All the spectra almost perfectly match the known spectrum for the thermal decomposition of bisphenol-A polycarbonate in which CO_2, phenol and bisphenol A are the main volatile products. Some band assignments are listed in Table 7.2.

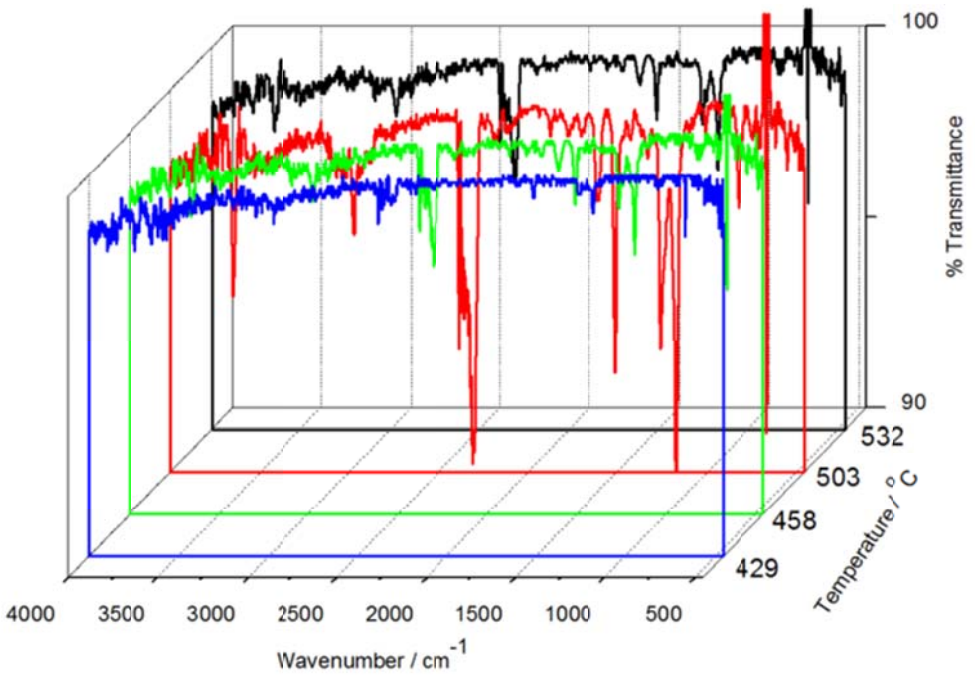

Figure 7.7 FTIR curves at different temperatures during the thermal degradation of PC in a TGA at a heating rate of 10 °C min^{-1}

Table 7.2 FTIR band assignments for PC

Wavenumber / cm^{-1}	**Assigned vibrations**
3658	Free alcohols (aliphatic substituted phenol)
2974	C-H stretching
2388-2119	Asymmetric stretching mode of CO_2
1606	Ring stretching
1509	Skeletal vibration of phenyl compounds
1257	Aromatic ether stretch
1182	Carbon hydroxyl stretching band
833	Bending mode of CO_2

No new peaks or peak shifts were observed for the nanocomposite sample. There is a clear increase in peak intensity for all the characteristic peaks with increasing temperature, it reaches a maximum, and decreases again with further increase in temperature. The 95/5 w/w PC-zirconia sample shows the same spectra and a similar trend (Figure 7.8). The peaks at 429 ºC for PC are less intense than the corresponding peaks of the PC in the nanocomposite. The intensities of the peaks for PC seem to reach a maximum between 503 and 532 °C, while the maximum position for the nanocomposite seems to occur around 458 °C. This suggests that the degradation process is accelerated when zirconia nanoparticles are present, which supports the TGA and degradation kinetics data and explanation.

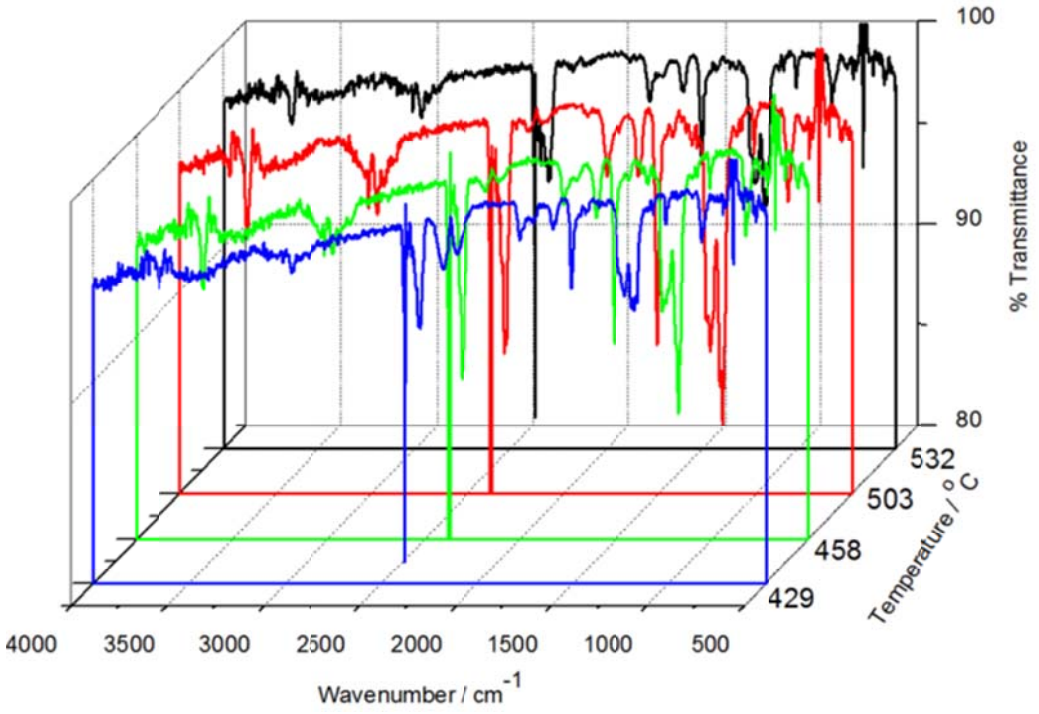

Figure 7.8 FTIR curves at different temperatures during the thermal degradation of PC with 5 wt.% zirconia in a TGA at a heating rate of 10 °C min^{-1}

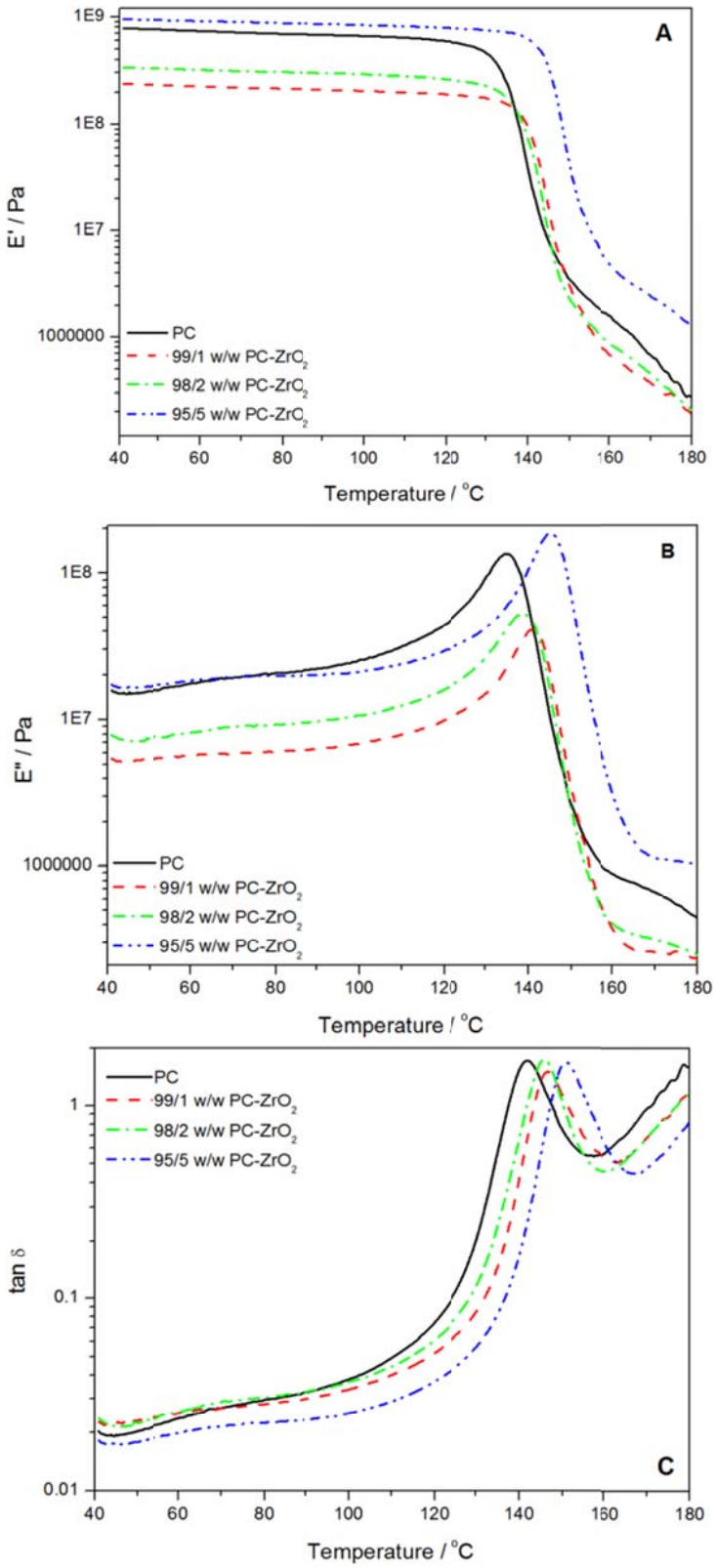

Figure 7.9 (A) Storage modulus, (B) loss modulus and (C) tan δ curves of PC and the PC-zirconia nanocomposites

The DMA curves of the pure PC, and the PC-zirconia nanocomposites having 1, 2 and 5 wt.% of zirconia are shown in Figure 7.9. Below the glass transition the storage moduli of the samples containing 1 and 2 wt.% of zirconia are lower than those of pure PC, but above the glass transition temperature the difference is negligible. The 5 wt.% zirconia containing nanocomposite has higher storage modulus values over the whole temperature range, but the difference is significant during and above the glass transition. Currently we do not have an explanation for the lower storage modulus values for the 99/1 and 98/2 w/w PC-ZrO_2 below the glass transition, and there were not enough samples to repeat these analyses to check for reproducibility. However, the formation of crystalline domains around the nanoparticles, which effectively improved the interaction between the zirconia particles and the polymer chains, is the most probable reason for the higher storage modulus values in the case of the 95/5 w/w PC-ZrO_2. Both the loss modulus and tan δ curves show an increase in the glass transition temperature with increasing zirconia content in the PC. This supports the explanation of a fairly strong interaction between the zirconia particles and the PC chains, which reduced the mobility of the polymer chains.

Since there is evidence that a local ordered structure is induced by the nanoparticles, ^{13}C $\{^1H\}$ CP-MAS NMR measurements were performed in order to understand at which molecular level the interactions occur, and to attempt to find a correlation between the mechanical properties, the kinetics of degradation and the molecular structure of the polymer. The ^{13}C $\{^1H\}$ CP-MAS NMR spectra of the PC-ZrO_2 composite loaded with 5 wt.% of zirconia are reported in Figure 7.10. Five peaks are present in the spectra: peak 1 at 149 ppm is related to the quaternary carbons of the aromatic rings and to the carbonyl carbon, peak 2 at 127 ppm to the aromatic carbon in meta to the oxygen, peak 3 at 120 ppm to the aromatic carbon ortho to the oxygen, peak 4 at 42 ppm to the quaternary carbon bonded to the methyl groups, and peak 5 at 31 ppm to the methyl carbons, according to literature [30]. No modification in the chemical shift and in the band shape is observed in the spectrum of the PC-zirconia nanocomposite, indicating that no chemical modification occurred in the polymer. Thus, the relaxation times in the laboratory frame $T_1(H)$, in the rotating frame $T_{1\rho}(H)$, and $T_{1\rho}(C)$ and the cross-polarization time T_{CH} were determined through solid-state NMR measurements in order to evaluate the dynamic modifications occurring in the polymeric chain of the PC matrix after composite formation. The $T_1(H)$, $T_{1\rho}(H)$, $T_{1\rho}(C)$

and T_{CH} values obtained from each peak in the ^{13}C spectra of all the samples are reported in Table 7.3.

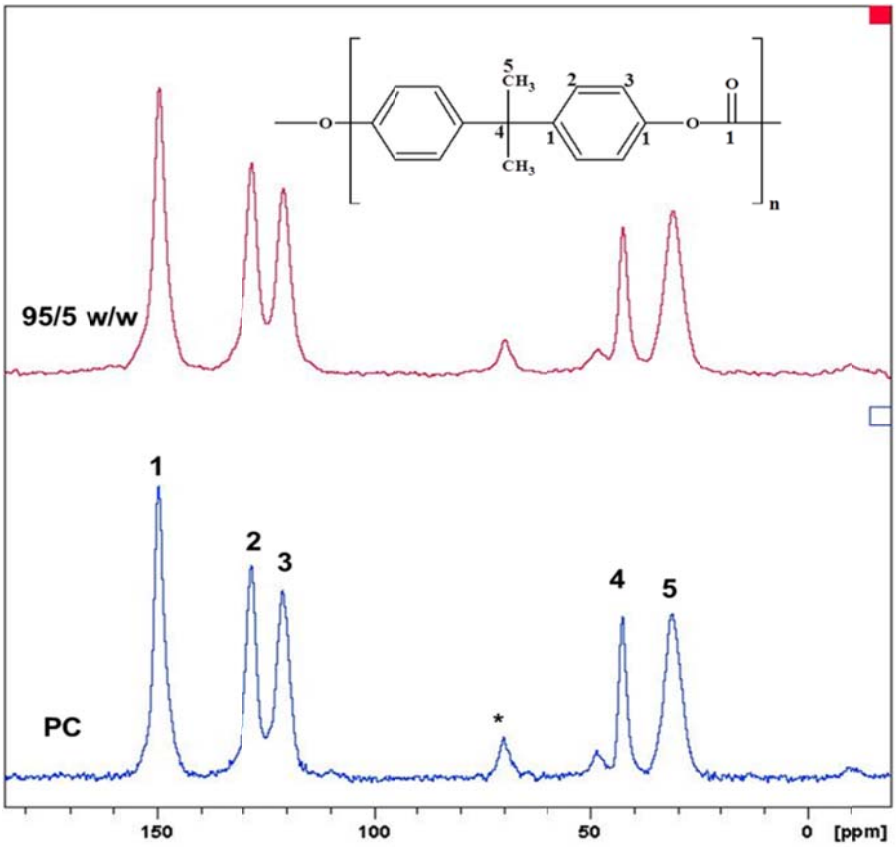

Figure 7.10 ^{13}C {^{1}H} CP-MAS NMR spectra of PC and PC-zirconia nanocomposite loaded with 5 wt.% of zirconia. Numbers on the peaks identify the carbon atoms. The * symbol indicates spinning sidebands

The presence of the filler in the PC matrix did not significantly affect the $T_1(H)$ and $T_{1\rho}(H)$ values. This indicates that the spin diffusion phenomenon averaged the dynamic behaviour of the polymer and that the composites were dynamically homogeneous in a range from tens to hundreds of nanometres. On the contrary, in the PC-zirconia nanocomposite the $T_{1\rho}(C)$ values for peaks 1, 2 and 3 were unchanged, while the values for peaks 4 and 5 relative to the quaternary carbon bonded to the methyl groups and of the methyl carbons were higher than the ones for the pure PC. In addition, an increase in the dipolar coupling T_{CH} for the protonated aromatic carbons is observed. This implies that the main motions involving this part of the

polymeric chain are hindered by the presence of zirconia, indicates specific intermolecular interactions. These interactions slightly involved the protonated aromatic carbons.

Table 7.3 T_1(H), $T_{1\rho}$(H), $T_{1\rho}$ (C) and T_{CH} values for all the carbons in the ^{13}C spectra of PC and the 95/5 w/w PC-zirconia nanocomposite

		T_1 (H) (s)		$T_{1\rho}$ (H) (ms)		$T_{1\rho}$ (C) (ms)		T_{CH} (ms)	
Carbon	**ppm**	**PC**	**95/5 w/w PC-ZrO_2**	**PC**	**95/5 w/w PC-ZrO_2**	**PC**	**95/5 w/w PC-ZrO_2**	**PC**	**95/5 w/w PC-ZrO_2**
1	149	0.39 ± 0.02	0.43 ± 0.03	4.9 ± 0.2	5.3 ± 0.3	41 ± 0.2	43.4 ± 0.8	1328 ± 127	1211 ± 92
2	127.5	0.41 ± 0.03	0.40 ± 0.02	5.4 ± 0.2	5.3 ± 0.2	10.9 ± 0.1	9.6 ± 0.9	117 ± 28	183 ± 31
3	120	0.39 ± 0.01	0.42 ± 0.02	5.2 ± 0.2	5.2 ± 0.3	10.2 ± 0.2	9.4 ± 0.9	64 ± 12	151 ± 22
4	42	0.40 ± 0.01	0.42 ± 0.01	4.8 ± 0.2	5.1 ± 0.4	18 ± 0.2	35.1 ± 0.7	1059 ± 97	831 ± 62
5	31	0.42 ± 0.01	0.41± 0.02	4.9 ± 0.3	5.0 ± 0.3	19.2 ± 0.1	33.3 ± 0.4	275 ± 20	239 16

7.4 Conclusions

The zirconia nanoparticles, organized in clusters uniformly dispersed in polycarbonate, did not change the polymer structure, but induced a modification in the organization of the PC chains. DMA showed that the polymer chain immobilization became significant at 5% zirconia content. The thermal degradation process seems to depend on the amount of zirconia, and the accompanying differences in particle size and PC-zirconia interaction. NMR analysis shows intermolecular interactions between zirconia and the polymer, in particular with the quaternary carbon bonded to the methyl groups and the methyl carbons. These interactions could be responsible for the differences in the polymer chain mobility and thermal degradation mechanism. The ordered structure induced by the nanoparticles and strong interfacial interactions between the PC and zirconia could also account for the observed differences.

7.5 References

1. A. Lagashetty, H. Vijayanand, S. Basavaraja, M.D. Bedre, A. Venkataraman. Preparation, characteristics, and thermal studies of γ-Fe_2O_3 and CuO dispersed polycarbonate nanocomposites. Journal of Thermal Analysis and Calorimetry 2010; 99:577-581.
   DOI: 10.1007/s10973-009-0475-8
2. F.J. Carrion, J. Sanes, M.D. Bermudez. Influence of ZnO nanoparticle filler on the properties and wear resistance of polycarbonate. Wear 2007; 262:1504-1510.
   DOI:10.1016/j.wear.2007.01.016
3. F.J. Carrion, J. Sanes, M.D. Bermudez. Effect of ionic liquid on the structure and tribological properties of polycarbonate- zinc oxide nanodispersion. Materials Letters 2007; 61:4531-4535.
   DOI:10.1016/j.matlet.2007.02.044
4. B.M. Dolores, B.W.C. Vilches, F.S. José. Scratch resistance of polycarbonate containing ZnO nanoparticles: Effect of sliding direction. Journal of Nanoscience and Nanotechnology 2010; 10:6683-6689.
   DOI:10.1166/jnn.2010.2513
5. R.M. Meri, A. Shutka, I. Zalite, A.K. Bledzki. Metal oxide mineral filler containing polymer nanocomposites. Solid State Phenomena 2009; 151:154-158.
   DOI: 10.4028/www.scientific.net/SSP.151.154
6. L. Wu, P. Chen, J. Zhang, J. He. Inhibited transesterification and enhanced fibrillation of TLCP by nano-SiO_2 in polycarbonate matrix. Polymer 2006; 47:448-456.
   DOI: 10.1016/j.polymer.2005.11.044
7. Q. Dong, C. Gao, Y. Ding, F. Wang, B. Wen, S. Zhang, T. Wang, M. Yang. A polycarbonate/magnesium oxide nanocomposite with high flame retardancy. Journal of Applied Polymer Science 2011; 123:1085-1093.
   DOI:10.1002/app.34574
8. A. Eitan, F.T. Fisher, R. Andrews, L.C. Brinson, L.S. Schadler. Reinforcement mechanisms in MWCNT-filled polycarbonate. Composites Science and Technology 2006; 66:1162-1173.
   DOI: 10.1016/j.compscitech.2005.10.004

9. J. Feng, J. Hao, J. Du, R. Yang. Effects of organoclay modifiers on the flammability, thermal and mechanical properties of polycarbonate nanocomposites filled with a phosphate and orgarnoclays. Polymer Degradation and Stability 2012; 97:108-117.
DOI: 10.1016/j.polymdegradstab.2011.09.019
10. J. Feng, J. Hao, J. Du, R. Yang. Using TGA/FTIR TGA/MS and cone calorimetry to understand thermal degradation and flame retardancy mechanism of polycarbonate filled with solid bisphenol A bis(biphenyl phosphate) and montmorillonite. Polymer Degradation and Stability 2012; 97:605-614.
DOI: 10.1016/j.polymdegradstab.2012.01.011
11. S. Wang, Y. Hu, Z. Wang, T. Yong, Z. Chen, W. Fan. Synthesis and characterization of polycarbonate/ABS/montmorillonite nanocomposites. Polymer Degradation and Stability 2003; 80:157-161.
DOI: 10.1016/S0141-3910(02)00397-X
12. Y. Imai, A. Terahara, Y. Hakuta, K. Matsui, H. Hayashi, N. Ueno. Transparent poly(bisphenol A carbonate)-based nanocomposites with high refractive index nanoparticles. European Polymer Journal 2009; 45:630-638.
DOI:10.1016/J.europolyj.2008.12.013
13. K. Xu, S. Zhou, L. Wu. Effect of highly dispersible zirconia nanoparticles on the properties of UV-curable poly(urethane-acrylate) coatings. Journal Materials Science 2009; 44:1613-1621.
DOI: 10.1007/s10853-008-3231-8
14. K. Luo, S. Zhou, L. Wu, B. You. Preparation and properties of cross-linked zirconia nanoparticles films on polycarbonate. Thin Solid Films 2010; 518:6804-6810.
DOI:10.1016/j.tsf.2010.06.035
15. F. Bondioli, V. Cannillo, E. Fabbri, M. Messori. Preparation and characterization of epoxy resins filled with submicron spherical zirconia particles. Polimery 2006; 51:11-12.
DOI: 10.1111/j.1551-2916.2008.02666.x
16. S.R. Hartmann, E.L. Hahn. Nuclear double resonance in the rotating frame. Physical Review Online Archive 1962; 128:2042-2053.
DOI: 10.1103/PhysRev.128.2042

17. C. Lau, Y. Mi. A study of blending and complexation of poly(acrylic acid)/poly(vinyl pyrrolidone). Polymer 2002; 43:823-829.
DOI: 10.1016/S0032-3861(01)00641-3

18. R.G. Alamo, J.A. Blanco, I. Carrilero. Measurement of the ^{13}C spin-lattice relaxation time of the non-crystalline regions of semicrystalline polymers by a CP-MAS-based method. Polymer 2002; 43:1857-1865.
DOI: 10.1016/S0032-3861(01)00761-3

19. P. Conte, R. Spaccini, A. Piccolo. State of art of CPMAS ^{13}C-NMR spectroscopy applied to natural organic matter. Progress in Nuclear Magnetic Resonance Spectroscopy 2004; 44:215-223.
DOI:10.1016/j.pnmrs.2004.02.002

20. M.L. Saladino, T.E. Motaung, A.S. Luyt, A. Spinella, G. Nasillo, E. Caponetti. The effect of silica nanoparticles on the morphology, mechanical properties and thermal degradation kinetics of PMMA. Polymer Degradation and Stability 2012; 97:452-459.
DOI:10.1016/j.polymdegradstab.2011.11.006

21. T.E. Motaung, A.S. Luyt, M.L. Saladino, D.C. Martino, E. Caponetti. Morphology, mechanical properties and thermal degradation kinetics of PMMA-zirconia composites prepared by melt compounding. eXPRESS Polymer Letters 2012; 6: 871-881.
DOI: 10.3144/expresspolymlett.2012.93

22. S. Richter, M. Saphiannikova, D. Jehnichen, M. Bierdel, G. Heinrich. Experimental and theoretical studies of agglomeration effects in multi-walled carbon nanotube-polycarbonate melts. eXPRESS Polymer Letters 2009; 3:753-768.
DOI:103144/expresspolymlett.2009.94

23. Y.W. Cheung, R.S. Stein, G.D. Wignall, H.E. Yang. Small-angle scattering investigations of poly(ε-caprolactone)/polycarbonate blends. 1. Small-angle neutron and x-ray scattering study of crystalline blend morphology. Macromolecules 1993; 26:5365-5371.
DOI: 10.1021/ma00072a012

24. F. Nallet, D. Roux, S.T.J. Milner. Small-angle scattering features of lyotropic smectics A. Journal de Physique 1990; 51:2333-2346.
DOI: 10.1051/jphys:0199000510200233300

25. R. Zong, Y. Hu, S. Wang, L. Song. Thermogravimetric evaluation of PC/ABS/ montmorillonite nanocomposite. Polymer Degradation and Stability 2004; 83:423-428. DOI:10.1016/j.polymdegradstab.2003.09.004
26. Q. Dong, C. Gao, Y. Ding, F. Wang, B. Wen, S. Zhang, T. Wang, M. Yang. A polycarbonate/magnesium oxide nanocomposite with high flame retardancy. Journal of Applied Polymer Science 2011; 123:1085-1093. DOI:10.1002/app.34574
27. T.E. Motaung, A.S. Luyt, F. Bondioli, M. Messori, M.L. Saladino, A. Spinella, G. Nasillo, E. Caponetti. PMMA-titania nanocomposites: Properties and thermal degradation behaviour. Polymer Degradation and Stability 2012; 97:1325-1333. DOI:10.1016/j.polymdegradstab.2012.05.022
28. B.J. Holland, J.N. Hay. The value and limitations of non-isothermal kinetics in the study of polymer degradation. Thermochimica Acta 2002; 388:253-273. DOI: 10.1016/S0040-6031(02)00034-5
29. Z. Gao, T. Kaneko, D. Hou, M. Nakada. Kinetics of thermal degradation of poly(methyl methacrylate) studied with the assistance of the fractionation conversion at the maximum reaction rate. Polymer Degradation and Stability 2004; 84:399-403. DOI:10.1016/j.polymdegradstab.2003.11.015
30. A.P.A.M. Eijkelenboom, W.E.J.R. Maas, W.S. Veeman, G.H.W. Buning, J.M.J. Vankan. Triple-resonance fluorine-19, proton, and carbon-13 CP-MAS NMR study of the influence of PMMA tacticity on the miscibility in PMMA/poly(vinylidene fluoride) (PVF2) blends. Macromolecules 1992; 25:4511-4518. DOI: 10.1021/ma00044a009

Chapter 8

Conclusions and recommendations

8.1 Conclusions

The nanocomposites of PMMA and PC were prepared by melt compounding and were systematically investigated as a function of silica, zirconia and titania amount at filler contents of 1, 2 and 5 wt.%. Commercial hydrophobic silica having chemically surface bonded methyl groups was used, whereas the zirconia and types of titania were prepared by a sol-gel method. The titania was annealed at two different temperatures to prepare different crystalline structures, and to remove carbon. The XRD spectra of the amorphous silica showed the expected amorphous halo, while the XRD analysis of zirconia confirmed that the powder was composed of a mixture of tetragonal and monoclinic Baddeleyite. Elemental analysis showed a marginal carbon content in the zirconia powder. The XRD analyses of titania showed that the titania powders annealed at lower and higher temperature respectively had anatase and rutile crystalline structures. The elemental analyses showed that the anatase titania had a larger amount of carbon than the rutile titania. The TEM micrographs of all the nanoparticles showed that the primary nanoparticles ranged from 10 to 30 nm, with aggregates ranging from 50 to 400 nm.

The XRD analysis of the nanocomposites showed that the polymers maintained their structure and did not induce orientation of the polymer chains. However, SAXS analysis of the PC-zirconia nanocomposites showed local orientation of the PC chains around the nanoparticles. In all the nanocomposites the nanoparticles dispersed well as primary particles and aggregates ranging from 50 to approximately 500 nm, with more aggregates at higher nanoparticles contents. The silica had observable effects on the PMMA chain mobility, but effective immobilization of the polymer chains only took place at the higher silica contents. These results are similar to the trend observed for the PC-zirconia nanocomposites, although effective immobilization of the PC chains only took place at lower zirconia contents. The DMA and NMR results show that the PC chains' immobilization was significant for the lowest silica content, and increased with increasing amounts of silica nanoparticles.

Zirconia and silica nanoparticles showed catalytic behaviour in the thermal degradation process, which decreased the activation energy of degradation, but did not change the degradation mechanism of the polymers. Only the rutile titania showed catalytic behaviour in PMMA degradation, whereas in PC both the crystal structures improved the thermal stability and increased the activation energy. The two types of titania nanoparticles had slightly different influences on the thermomechanical and thermal properties, as well as the degradation kinetics of both matrices. These results were attributed to different extents of interaction between the PC and the two different types of titania. In the PMMA-silica system the observed results were attributed to the interaction between the polymer and nanoparticles which occurred at the interface through the carbonylic groups of the polymer, whereas in the PC-silica system the results were attributed to intermolecular interactions between silica and the polymer in the composite which did not involve the protonated aromatic carbons. In the PMMA-zirconia system the results were related to an increase in the heteronuclear dipolar interactions involving the carbons and the surrounding hydrogen nuclei, while in the PC-zirconia system they were related to specific intermolecular interactions which involved the protonated aromatic carbons.

8.2 Recommendations for future work

Metal oxides are well-known to improve the morphology, thermal and mechanical properties of polymers. The particles generally interact with the matrix in various ways, depending mainly on the particles' size and modification. In this study a TGA-FTIR was *inter alia* used to follow the thermal degradation kinetics, but it will be worthwhile to also use TGA connected to gas chromatography or mass spectrometry. The study could also be extended by studying the effect of carbon content in titania at a fixed particles size, using the same preparation conditions. This would assist in clarifying whether the carbon played a role in addition to the crystalline structure in influencing the properties. The same study is recommended for the zirconia system. The effect of the bonded methyl groups on the silica surface could be crucial in improving the properties. Therefore, it is recommended to evaluate the use of silica containing modifiers with varying alkyl chain lengths.